Behaviour of Steel Bolted Connections under Extreme Actions

A Thesis Submitted for obtaining
the Scientific Title of PhD in Engineering
from
Politehnica University Timișoara
in the Field of Civil Engineering and Installations
by

Eng. Diana-Maria DUMA

PhD Committee Chair: Prof. Adrian CIUTINA
PhD Supervisor: Prof. Raul ZAHARIA
Scientific Reviewers: Prof. Marcela PRADA
Prof. Dorina ISOPESCU
Prof. Viorel UNGUREANU

Date of the PhD Thesis Defense: 17.10.2023

The PhD thesis series of UPT are:

1. Automation
2. Chemistry
3. Energetics
4. Chemical Engineering
5. Civil Engineering
6. Electrical Engineering
7. Electronic Engineering and Telecommunications
8. Industrial Engineering
9. Mechanical Engineering
10. Computer Science and Information Technology
11. Science and Material Engineering
12. Systems Engineering
13. Energy Engineering
14. Computers and Information Technology
15. Materials Engineering
16. Engineering and Management
17. Architecture
18. Civil Engineering and Installations
19. Electronics, Telecommunications and Information Technologies

Politehnica University Timișoara, Romania, initiated the above series to disseminate the expertise, knowledge and results of the research carried out within the doctoral school of the university. According to the Decision of the Executive Office of the University Senate No. 14/14.07.2006, the series includes the doctoral theses defended in the university since October 1, 2006.

Romania, 300223 Timișoara, Bd. Vasile Pârvan no. 2B
Tel./fax +40-(0)256 404677
e-mail: editura@upt.ro

Foreword

This thesis has been elaborated during my activity in the Department of Steel Structures and Structural Mechanics of the Politehnica University Timişoara, Romania.

I address my special thanks to the PhD supervisor, Prof. Raul ZAHARIA, for his guidance, motivation, and patience in assisting me to complete this research project. It has been an honour to have had Prof. Zaharia as my mentor, as his support and constructive feedback have been invaluable in the advancement of my work. His vast knowledge, keen insight, and sound advice will undoubtedly prove beneficial to me for the duration of my life.

I also want to express my appreciation to my committee members, S.L. Ioan BOTH, Prof. Florea DINU, and S.L. Ioan MARGINEAN, for their helpful discussions and assistance. They have been an excellent source of information and ideas.

I would also like to acknowledge Ovidiu ABRUDAN and Miloico UNG for their assistance in the experimental part of my work. My colleagues Anna ENE, Dominiq JAKAB, and Viorel POPA have also been kindly helpful, and I am grateful for their support.

I am also thankful for the financial support I received from the Project "Network of excellence in applied research and innovation for doctoral and postdoctoral programs / InoHubDoc", project co-funded by the European Social Fund financing agreement no. POCU/993/6/13/153437, as well as the encouragement received from the Team Manager in this project, Prof. Adrian CIUTINA.

Lastly, I want to express my utmost gratitude to my parents, remarkable sister, and close friends Liliana and Sebastian for their love, support, and motivation during my doctoral studies at Politehnica University of Timișoara.

Timişoara, October 2023 Diana DUMA

Recipients of dedication.

DUMA, Diana-Maria

Behaviour of Steel Bolted Connections under Extreme Actions

PhD theses of UPT, Series X, No. YY, Editura Politehnica, 200Z, 168 pages, 39 figures, 27 tables.

ISSN:
ISBN:

Keywords:

Grade 10.9 high strength bolt, Elevated temperature, Fire design, Strain rate, Experimental tensile tests, T-stub numerical simulations.

Abstract

The assessment of the durability of structural components at elevated temperatures is of utmost importance when designing structures under fire hazards. The capacity of multi-storey steel frame structures to withstand unforeseen events is significantly influenced by the strength of their beam-to-column joints. In instances where a column is lost due to a fire, the dynamic process can result in high strain rates, which must be taken into consideration when analysing the resistance and ductility of these connections.

The aim of this research is to enhance the fire safety of steel structures by revealing more information and understanding the behaviour of high strength bolts for steel structures, specifically grade 10.9 bolts, in fire conditions. The research work consisted of two main parts: an experimental study, concluded with a series of proposed reduction factors for bolt strength under elevated temperatures and different strain rates, and a numerical validation of the proposed factors. The research work was carried out in the laboratory of Steel Structures and Structural Mechanics Department of Politehnica University Timișoara.

In order to gain a deeper understanding of the behaviour of grade 10.9 bolts under high temperatures, an extensive study was conducted. This study examined various factors that may affect the bolts' performance, including their manufacturing process, heat treatments, surface treatments, and chemical composition. An experimental program consisting of 116 tests on grade 10.9 bolts was conducted according to EN guidelines. Tensile tests were performed at nine different temperatures (ranging from 20°C to 800°C) and nine strain rates (ranging from 0.000033 s^{-1} to 0.06 s^{-1}) to obtain stress-strain curves that describe the material behaviour. Reduction factors based on the tests were proposed to calculate the strength of grade 10.9 bolts under high temperatures. These factors depend on the strain rate that may occur in a bolt during a fire.

Additionally, numerical simulations were conducted using Abaqus software to validate the new proposed reduction factors. The simulations were based on four experimental tests from literature, which involved tension tests on T-stub specimens at normal and high temperatures. The numerical models were validated against these experiments, demonstrating a good replication of the T-stub behaviour. A comparison of the new proposed method with the EN1993-1-2 method, revealed significant differences in the estimation of the maximum force value for the T-stubs considered. These results provide important insights for the design and optimization of bolted T-stub connections when accounting for elevated temperatures.

Abstract

Evaluarea corectă a elementelor structurale la temperaturi înalte stă la baza proiectării la incendiu a unei clădiri. Capacitatea structurilor multietajate cu cadru din oțel, de a rezista la evenimente neprevăzute este influențată în mod semnificativ de rezistența îmbinărilor între grinzi și stâlpi. În cazurile în care un stâlp cedează din cauza unui incendiu, apare o încărcare dinamică ce poate duce la viteze mari de deformație. Acestea trebuie luate în considerare atunci când se analizează rezistența și ductilitatea îmbinărilor grindă-stâlp.

Scopul acestei cercetări este de a spori siguranța la foc a structurilor din oțel prin înțelegerea comportamentului șuruburilor de înaltă rezistență, în condiții de incendiu, în special șuruburile de clasă 10.9. Lucrarea de față cuprinde două părți principale: un studiu experimental privind proprietățile mecanice ale șuruburilor de înaltă rezistență la temperaturi ridicate, încheiat cu o serie de coeficienți de reducere propuși pentru rezistența șuruburilor la temperaturi ridicate și diferite viteze de deformație și validarea numerică a coeficienților propuși. Activitățile de cercetare s-a desfășurat în cadrul Departamentului de Construcții Metalice și Mecanica Construcțiilor, al Universității Politehnica Timișoara.

Pentru a obține o înțelegere mai bună a comportamentului șuruburilor de clasa 10.9 la temperaturi ridicate, cât și a ultimelor descoperiri in domeniu, a fost efectuat un studiu bazat pe literatura de specialitate. Acest studiu a examinat diverși factori care pot afecta performanța șuruburilor, inclusiv procesul lor de fabricație, tratamentele termice, tratamentele de suprafață și compoziția chimică. S-au efectuat 116 teste experimentale pe șuruburi de clasă 10.9. Testele de tracțiune au fost efectuate la nouă temperaturi diferite (între 20 °C și 800 °C) și nouă viteze de încărcare (cuprinse între 0,000033 s^{-1} și 0,06 s^{-1}) pentru a obține curbele efort-deformație care descriu comportamentul materialului. S-au propus o serie de coeficienți de reducere pentru calculul rezistenței șuruburilor de clasă 10.9 la temperaturi ridicate. Acești coeficienți depind de viteza de deformație care poate apărea într-un șurub în timpul unui incendiu.

S-au efectuat simulări numerice utilizând programul Abaqus pentru a valida coeficienții de reducere propuși. Simulările s-au bazat pe patru teste experimentale din literatură, care au implicat teste de tracțiune pe specimene T-stub la temperaturi normale și ridicate. Modelele numerice utilizate în simulări au fost validate în raport cu aceste experimente, demonstrând o replicare bună a comportamentului îmbinărilor T-stub. În plus, studiul a comparat metoda recent propusă pentru comportamentul materialului șuruburilor la temperaturi ridicate cu metoda din EN1993-1-2, dezvăluind diferențe semnificative în estimarea forței maxime pentru T-stub-urile considerate. Aceste rezultate oferă informații importante pentru proiectarea și optimizarea îmbinărilor cu șuruburi de tip T-stub la temperaturi ridicate.

Table of contents

List of Notations

b_p =flange width.
c = distance between bolts.
d = bolt diameter.
d_0 = diameter of the machined specimen.
d_s = thread diameter.
e = position of holes from the edge on z-axis.
$\dot{\varepsilon}$ = strain rate.
E = modulus of elasticity at normal temperature.
E_θ = modulus of elasticity at temperature θ.
f_y = yield stress at normal temperature.
$f_{y,\theta}$ = yield stress at temperature θ.
$f_{p\theta}$ = proof value at temperature θ.
f_{ub} = ultimate tensile strength at normal temperature.
$f_{u,\theta}$ = ultimate tensile strength at temperature θ.
$f_{u,\theta,exp}$ = tensile strength at temperature θ, obtained experimentally.
$f_{u,\theta,\dot{\varepsilon}}$ = tensile strength at temperature θ, under strain rate $\dot{\varepsilon}$.
$f_{u,20}$ = tensile strength at normal temperature, under 0.00033 s^{-1} strain rate.
$f_{u,20,\dot{\varepsilon}}$ = tensile strength at normal temperature, under strain rate $\dot{\varepsilon}$.
$f_{0.5\%,\theta,\dot{\varepsilon}}$ = yield stress at 0.5% strain, at temperature θ, under strain rate $\dot{\varepsilon}$.
$f_{0.5\%,20,\dot{\varepsilon}}$ = yield stress at 0.5% strain, at normal temperature, under strain rate $\dot{\varepsilon}$.
$F_{y,0.5\%}$ = yield stress at 0.5% strain.
F_{max} = maximum force.
h = grip length.
k_b = reduction factor defined by Kirby (1995).
$k_{b,u}$ = reduction factor defined as $f_{u,\theta,\dot{\varepsilon}} / f_{u,20,\dot{\varepsilon}}$.
$k_{b,u,min}$ = reduction factor defined as $f_{u,\theta,\dot{\varepsilon}} / f_{u,20}$, for $\dot{\varepsilon}$ = 0.00033 s^{-1}.
$k_{b,u,max}$ = reduction factor defined as $f_{u,\theta,\dot{\varepsilon}} / f_{u,20}$, for $\dot{\varepsilon}$ = 0.02 s^{-1}.
$k_{b,u,new}$ = reduction factor defined as $f_{u,\theta,\dot{\varepsilon}} / f_{u,20}$.
$k_{b,0.5\%}$ = reduction factor defined as $f_{0.5\%,\theta,\dot{\varepsilon}} / f_{0.5\%,20,\dot{\varepsilon}}$.
$k_{b,\theta}$ = reduction factor defined in EN1993-1-2 (2005) for bolt strength.
$k_{E,\theta}$ = reduction factor for modulus of elasticity.
L_0 = initial gauge length.
L_p = flange length.
L_t = total length of the specimen.
m_x = position of holes from the edge on y-axis.
R_m = tensile strength.
t_p = flange thickness.

Greek symbols

ε = strain.
$\varepsilon_{engineering}$ = engineering strain.
ε_y = yield strain at normal temperature.
$\varepsilon_{y,\theta}$ = yield strain at temperature θ.
ε_{true} = true strain.
ε_0 = strain due to slippage in the experimental curve.
η_{fi} = the reduction factor for load combination in fire situation.
θ = temperature.
σ = stress.
$\sigma_{engineering}$ = engineering stress.
σ_{true} = true stress.

List of Tables

List of Figures

1 Introduction

1.1 Thesis Motivation

The design of structures to withstand fire involves analysing the strength and stability of structural elements when exposed to high temperatures. This field of research is vast and involves studying the behaviour of materials and the response of different structural systems, as well as modelling the fire action.

Since the 1980s, engineers have been able to use computer programs to analyse structural elements at high temperatures using numerical methods. The most complex buildings can nowadays be modelled and analysed in the event of a fire (Jelenewicz, 2019). While these programs are useful, they can be time-consuming and expensive. For simpler structures, such as buildings with regular architecture, semi-structures, or isolated elements, the Eurocodes offer simplified or tabular methods that are easier to apply. However, these methods are limited in their scope of application, demonstrating that more research is needed in this field.

The capacity of multi-storey steel frame structures to withstand unforeseen events is significantly influenced by the strength of their beam-to-column joints (Izzuddin et al., 2008). In instances where a column is lost due to a fire, the dynamic process can result in high strain rates, which must be taken into consideration when appraising the resistance and ductility of these connections (Evans et al., 1997; Delia et al., 2005; Pantousa & Mistakidis, 2016; Zaharia & Pintea, 2009; Sun et al., 2012).

End plate bolted connections are commonly utilized in steel-framed structures. To accurately evaluate the risk of progressive collapse during a fire, it is crucial to consider the strength reduction factors of bolts in relation to both temperature and strain rate. This information is critical for obtaining realistic results from structural assessments.

The thesis primarily focuses on the bolted connections of steel members, when exposed to high temperatures. Traditionally, the joints between steel structural elements have been considered to have sufficient fire resistance, remaining able to transmit stresses due to lower temperatures than in the joined elements, if the following conditions are fulfilled (EN 1993-1-2, 2005):

- the thermal resistance of the joint's fire protection is at least equal to, or greater than, the minimum value of thermal resistance of fire protection applied to any of the jointed members.
- the utilization of the joint should not exceed the maximum value of utilization of any of the connected members.
- the resistance of the joint at ambient temperature should adhere to the guidelines provided in EN 1993-1-8 (2005).

During a fire, the stresses and movements affecting joints may differ significantly from those considered in regular temperature design. As a result, joints may be more susceptible to damage than previously thought, particularly under extreme circumstances. Specifically, compressive forces arise due to expansion,

followed by tension caused by significant displacements of structural components (Usmani et al., 2001). This means that the joints normally designed to withstand bending and shear forces may be vulnerable in the event of a fire.

The elevated temperatures have a negative impact on the bolt's mechanical properties. Consequently, it's essential to understand how bolts behave at high temperatures, to ensure the safety and reliability of structures that rely on them for structural integrity. If a bolt fails to withstand high temperatures, it can compromise the overall structural integrity of the system in fire conditions.

The specific Eurocode for the fire design of steel structures, EN 1993-1-2 (2005) offers a simplified method for the verification of the joints under elevated temperatures. This method involves calculating the strength of bolts based on the temperature they will be exposed to. The bolt's strength decreases at a specific temperature, and this reduction is accounted for by a reduction factor, $k_{b,\theta}$. These reduction factors were developed based on experimental tests realized only on grade 8.8 bolts (Kirby, 1995), although the simplified method is used today in practice for other bolts type as well. Moreover, this method does not count for the extreme loading conditions that might appear in fire scenarios, like higher strain rates in the bolts. Although no specific research was published so far to quantify the influence of strain rate, this aspect is clearly observed by others (Bull et al., 2015; Both et al., 2021) and is also mentioned in ISO 6892-2 (2011).

The main goal of this thesis is to conduct an in-depth investigation into the behaviour of grade 10.9 high-strength bolts when subjected to high temperatures and various strain rates. These specific bolts are widely employed in bolted joint frameworks, thus making it crucial to study their performance under different conditions.

1.2 Thesis Objectives

The thesis aims to gain an understanding of how grade 10.9 bolts behave in fire situations, considering also the influence of the strain rate. To achieve this, the following objectives have been set:

- Compile a literature review and state of the art of the knowledge in the field to support the thesis motivation;
- Conduct experiments to determine the mechanical properties of the material, especially the tensile strength;
- Observe how tensile strength varies with temperature and strain rate;
- Determine whether the strain rate affects the tensile strength of grade 10.9 bolts;

- Propose new reduction factors for tensile strength of grade 10.9 bolts under various temperatures and strain rates;

- Validate the new reduction factors through numerical simulations on T-stub connections, in comparison with available experimental data.

1.3 Thesis Outline

This thesis consists of six chapters, as introduced below.

Chapter 1, *Introduction*, of the thesis offers an overview of the studied subject, the research motivation, and its importance. Additionally, it presents a synopsis of the study's objectives. The goal of this research is to gain a more profound comprehension of the behaviour of grade 10.9 bolts when subjected to elevated temperatures.

The second chapter, *Literature Review and State of the Art*, delves into bolts utilized in construction and their various types, as well as their manufacturing processes, treatment methods, testing protocols, existing fire design methods and parameters, and performance under fire conditions. Particular attention is given to the reduction factors of bolt strength proposed by EN1993-1-2 (2005), in terms of their availability regarding the grade 10.9 bolts. Moreover, this chapter covers the latest advancements regarding the high strength bolt behaviour in extreme settings, as subjected to high strain rate in fire situations. It is highlighted that the strain rate influence is not considered by the existing fire design methods. Although the influence of this parameter was acknowledged, no quantification method is available in the literature.

Chapter 3, *Laboratory Equipment and Experimental Procedure*, presents a detailed account of the experimental setup and test program employed during the study, in the laboratory of Steel Structures and Structural Mechanics Department of Politehnica University Timișoara. The program consists of 106 tensile tests, which were conducted using the 250 kN Instron universal testing machine. The machined specimens were subjected to tension until failure, under 9 temperatures, ranging from 20 ^{o}C to 800 ^{o}C, and 9 strain rates, ranging from 0.000033 s^{-1} to 0.06 s^{-1}. The information provided therein elucidates the laboratory equipment utilized in the research, as well as the procedures implemented during the experiment. This section aims to provide a comprehensive understanding of the methodology used.

Chapter 4, *Experimental Results*, describes the experimental data, and the assessment of the studied parameters in the bolt behaviour. It outlines the primary findings derived from the experimental tests and proposes new equations function of the strain rate, for determination of the reduction factor of grade 10.9 bolt strength

under elevated temperatures. Further, a table of coefficients, $k_{b,\theta,min}$ and $k_{b,\theta,max}$ are proposed to be used for the computation of reduction factor, under quasi-static strain rate, and high strain rate, respectively. The tabular approach can simplify the process and provide accurate results for the intended application. The new reduction factors, for quasi-static strain rate are with 10% smaller than the reduction factors proposed by Eurocode (EN1993-1-2, 2005) for temperature of 400 ^{o}C, and with more than 40% smaller for higher temperatures. In contrast, the new reduction factors for high strain rate are with 13% higher than the reduction factors proposed by Eurocode (En1993-1-2, 2005) for temperature of 500 ^{o}C, and with more than 40% higher for higher temperatures. This proves the importance of this study and quantify the impact of strain rate in the behaviour of the bolt material.

Chapter 5, *Numerical Simulations*, presents the numerical simulations on T-stub connections to validate the proposed reduction factors. Finite element analysis was performed using Abaqus software and compared to four available experimental tests from literature. The models accurately replicated T-stub behaviour and emphasized the significance of considering loading conditions, specifically the strain rate.

Chapter 6, *Conclusions and Personal Contributions*, presents a summary of the research and the main outcomes, highlighting the personal contribution. The proposed equations for the new reduction factors are showed, and the scope of application is explained. Several research perspectives that might be derived further are mentioned as well.

2 Literature Review and State of the Art

2.1 General Aspects: Bolts used in Construction

Structural elements in construction require bolts with a grade ranging from 4.6 to 10.9, as specified by Eurocode EN1993-1-8 (2005). Additionally, it is required by the Romanian standard P100-1/2013 and Eurocode EN1998-1 (2004) that grade 8.8 or 10.9 high strength bolts are considered for connections of primary seismic members of a building. Moreover, for preloaded bolts, often used in steel elements connections, it's important that they meet the requirements set forth in both Group 4 (standards for bolts, nuts, and washers) and Group 7 (standards for execution of steel structures) of the Reference Standards outlined in EN1993-1-8 (2005) and presented in Table 2. 1.

Table 2. 1. Reference Standard (EN1993-1-8, 2005).

Group of Reference Standards	Reference Standards
Group 4 - Bolts, nuts and washers	EN 14399-1: 2002 High strength structural bolting for preloading Part 1: General Requirements
	EN 14399-2: 2002 High strength structural bolting for preloading Part 2: Suitability Test for preloading
	EN 14399-3: 2002 High strength structural bolting for preloading Part 3: System HR -Hexagon bolt and nut assemblies
	EN 14399-4: 2002 High strength structural bolting for preloading - Part 4: System HV -Hexagon bolt and nut assemblies
	EN 14399-5:2002 High strength structural bolting for preloading - Part 5: Plain washers for system HR
	EN 14399-6:2002 High strength structural bolting for preloading - Part 6: Plain chamfered washers for systems HR and HV
	EN ISO 898-1: 1999 Mechanical properties of fasteners made of carbon steel and alloy steel Part 1: Bolts, screws and studs (ISO 898-1: 1999)
	EN 20898-2: 1993 Mechanical properties of fasteners - Part 2: Nuts with special proof load values. Coarse thread (ISO 898-2: 1992)
	EN ISO 2320: 1997 Prevailing torque type steel hexagon nuts Mechanical and performance requirements (ISO 2320: 1997)

	EN ISO 4014:2000 Hexagon head bolts Product grades A and B (ISO 4014:1999)
	EN ISO 4016:2000 Hexagon head bolts Product grade C (ISO 4016: 1999)
	EN ISO 4017:2000 Hexagon head screws - Product A and B (ISO 4017: 1999)
	EN ISO 4018:2000 Hexagon head screws - Product C (ISO 4018: 1999)
	EN IS0 4032:2000 Hexagon nuts, style 1 - Product grades A and B (ISO 4032: 1999)
	EN ISO 4033:2000 Hexagon nuts, style 2 - Product grades A and B (ISO 4033: 1999)
	EN ISO 4034:2000 Hexagon nuts - Product C (ISO 4034: 1999)
	EN ISO 7040:1997 Prevailing torque nuts (with non-metallic insert), style 1 - Property classes 5, 8 and 10
	EN ISO 7042: 1997 Prevailing torque all-metal hexagon nuts, 2 - Property classes 5, 8, 10 and 12
	EN ISO 7719:1997 Prevailing torque type all-metal hexagon nuts, style 1 - Property classes 5, 8 and 10
	ISO 286- 2: 1988 ISO system of limits and fits Part 2: Tables of standard tolerance grades and limit deviations for hole and shafts
	ISO 1891:1979 Bolts, screws, nuts and accessories Terminology and nomenclature Trilingual edition
	EN ISO 7089:2000 Plain washers- Nominal series- Product grade A
	EN ISO 7090:2000 Plain washers, chamfered Normal series - Product grade A
	EN ISO 7091 :2000 Plain washers - Normal series - Product grade C
	EN ISO 10511: 1997 Prevailing torque hexagon thin nuts (with non-metallic insert)
	EN ISO 10512:1997 Prevailing torque type hexagon nuts thin nuts, style 1, with metric fine pitch thread - Property classes 6, 8 and 10
	EN ISO 10513: 1997 Prevailing torque type all-metal Hexagon nuts, style 2, with metric fine pitch thread - Property classes 8, 10 and 12
Group 7 - Execution of steel structures	EN 1090-2 Requirements for the execution of steel structures

When it comes to bolt assembly solutions in Europe, there are a few options available (EN 14399-1, 2005) that meet the necessary standards outlined in Table 2. 1. and provide the required ductility (EN 14399-2, 2015). Two common assemblies are the HR and HV assemblies. The term *assembly* is used in the literature for the bolt and nut pair, which are often required to be bought together from the same producer. The HR assembly (EN 14399-3, 2005) includes bolt grades 8.8 and 10.9, while the HV assembly (EN 14399-4: 2005) only includes bolt grade 10.9.

Following EN 14399-3 (2005), commonly used by British/French engineers, the HR system involves using thick nuts and bolts with extended thread lengths. This approach is aimed at achieving greater ductility by allowing for plastic elongation of the bolt. Longer thread lengths are necessary to prevent localized strain, and these bolts are less vulnerable to damage caused by overtightening during preloading. However, it is important to exercise proper control to avoid overtightening, as this can lead to the ductile failure mode of bolt breakage, which is easily detectable.

In accordance with EN 14399-4 (2005), the German method involves utilizing thinner nuts and shorter thread lengths to achieve the necessary ductility through the plastic deformation of the threads inside the nut. The HV bolt assembly is employed for both preloaded and non-preloaded applications in Germany, and it can be argued that in the event of thread plastic deformation, the assembly still functions as a non-preloaded assembly. When assembling these parts, it's important to exercise caution as they are prone to over-tightening during preloading. This means that stronger site control is necessary. If the parts are overly tightened during preloading, the bolt assembly's thread may undergo plastic deformation, which may not necessarily indicate that failure is imminent.

Comparing the characteristics of the two systems, HR and HV assemblies, it can be noticed that they cover different quality grades, 10.9 for HV system, as HR systems are applicable for quality grades 8.8, as well as 10.9. Both systems are similar and should comply with the same standards in terms of manufacturing, surface treatment and testing. The main difference remains in the geometry of the assembly (see Figure 2. 1. and Figure 2. 2.). Both systems will be found for a range of bolts with dimeter between M12 and M36. For HR system, the nut should be of type 1 (IS0 4032, 2000) and a thread length according to ISO 888 (2012), to ensure the proper ductility through the plastic bolt elongation. The geometrical properties of the bolts are presented in Figure 2. 1.a. (EN 14399-3, 2005) and the geometrical properties of the nuts are presented in Figure 2. 2.a. (EN 14399-3, 2005). HR bolts which are too short threaded to meet the requirements for a minimum of four thread pitches under the nut in the bolting assembly according to EN 1090-2 (2011) shall be fully threaded. For the HV system, the nut height should be approximately 0.8d (d is the bolt diameter) and the bolt has a short thread length, to ensure the proper ductility through the engaged threads. The geometrical properties of the bolts are presented in Figure 2. 1.b. (EN 14399-4, 2005), as the geometrical properties of the nuts are presented in Figure 2. 1.b. (EN 14399-4, 2005).

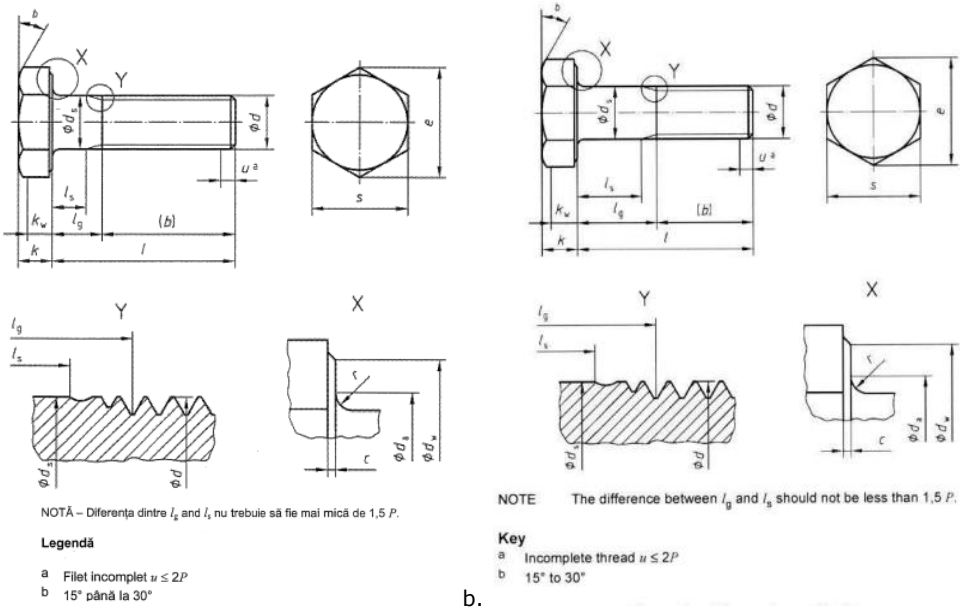

a. b.

Figure 2. 1. Bolt geometry: a. HR system (EN 14399-3, 2005); b. HV system (EN 14399-4, 2005).

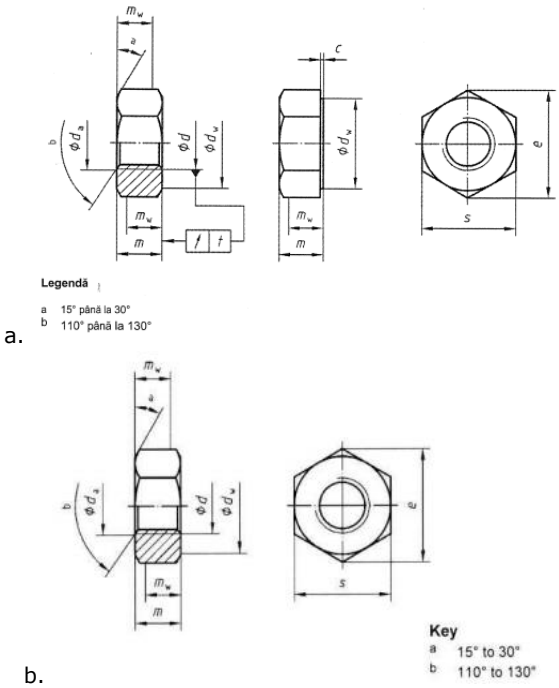

a.

b.

Figure 2. 2. Nuts geometry: a. HR system (EN 14399-3, 2005); b. HV system (EN 14399-4, 2005).

The bolt assemblies shown above need to have a metric screw thread (M profile) with a basic profile following ISO 68-1 (1998). The necessary tolerance is 6g6H or 6g6AZ (EN 14399-3, 2005; EN 14399-4, 2005), which is a typical tolerance utilized in the construction industry.

D'Aniello et al. (2016) showed that the HR assembly and HV assembly behave similarly, when the thread stripping mode of failure is prevented by adding a second nut.

2.2 Bolts Material

The chemical composition of steel is very important as this will influence the material behaviour.

Steel products are found in the form of steel or cast iron, depending on the amount of carbon. Therefore, steel products are the ones that contain less than 1.7% carbon, while cast iron products contain between 1.6% and 6.67% carbon. There are also alloys in the steel products, which contain other metallic chemical elements. But these chemical elements can be found in very small quantities, so they are considered impurities and the accepted quantities are: Manganese (Mn <0.6%), Silicon (Si <0.35%), Sulphur (S <0.06%), Phosphorus (P <0.05%), Chromium (Cr), Copper (Cu), Nickel (Ni), Oxygen (O <0.05%), Nitrogen (N), Molybdenum (Mo) [17].

Although the literature gives the values presented above, the standards require clear quantities of chemical elements in the component of a grade 10.9 bolt. Therefore, the bolts should be manufactured (EN 14399-4, 2005) with a chemical composition and a tempering temperature according to ISO 898-1 (1999) (see Table 2. 2.).

Table 2. 2. Steel chemical composition and the heat treatment in function of the bolt grade (ISO 898-1, 1999).

Property class	Material and treatment	Chemical composition limits (check analysis) % (m/m)					Tempering temperature
		C		P	S	B [a]	°C
		min.	max.	max.	max.	max.	min.
8.8 [c]	Carbon steel with additives (e.g. B, Mn or Cr) quenched and tempered	0,15 [d]	0,40	0,035	0,035	0,003	425
	Carbon steel quenched and tempered	0,25	0,55	0,035	0,035		
9.8	Carbon steel with additives (e.g. B, Mn or Cr) quenched and tempered	0,15 [d]	0,35	0,035	0,035	0,003	425
	Carbon steel quenched and tempered	0,25	0,55	0,035	0,035		
10.9 [e f]	Carbon steel with additives (e.g. B, Mn or Cr) quenched and tempered	0,15 [d]	0,35	0,035	0,035	0,003	340
10.9 [f]	Carbon steel quenched and tempered	0,25	0,55	0,035	0,035	0,003	425
	Carbon steel with additives (e.g. B, Mn or Cr) quenched and tempered	0,20 [d]	0,55	0,035	0,035		
	Alloy steel quenched and tempered [g]	0,20	0,55	0,035	0,035		
12.9 [f h i]	Alloy steel quenched and tempered [g]	0,28	0,50	0,035	0,035	0,003	380

[a] Boron content can reach 0,005 % provided that non-effective boron is controlled by addition of titanium and/or aluminium.

[b] Free cutting steel is allowed for these property classes with the following maximum sulfur, phosphorus and lead contents: sulfur 0,34 %; phosphorus 0,11 %; lead 0,35 %.

[c] For nominal diameters above 20 mm the steels specified for property classe 10.9 may be necessary in order to achieve sufficient hardenability.

[d] In case of plain carbon boron steel with a carbon content below 0,25 % (ladle analysis), the minimum manganese content shall be 0,6 % for property class 8.8 and 0,7 % for 9.8, 10.9 and 10.9.

[e] Products shall be additionally identified by underlining the symbol of the property class (see clause 9). All properties of 10.9 as specified in table 3 shall be met by 10.9, however, its lower tempering temperature gives it different stress relaxation characteristics at elevated temperatures (see annex A).

[f] For the materials of these property classes, it is intended that there should be a sufficient hardenability to ensure a structure consisting of approximately 90 % martensite in the core of the threaded sections for the fasteners in the "as-hardened" condition before tempering.

[g] This alloy steel shall contain at least one of the following elements in the minimum quantity given: chromium 0,30 %, nickel 0,30 %, molybdenum 0,20 %, vanadium 0,10 %. Where elements are specified in combinations of two, three or four and have alloy contents less than those given above, the limit value to be applied for class determination is 70 % of the sum of the individual limit values shown above for the two, three or four elements concerned.

[h] A metallographically detectable white phosphorous enriched layer is not permitted for property class 12.9 on surfaces subjected to tensile stress.

[i] The chemical composition and tempering temperature are under investigation.

The presence of other metallic chemical elements will influence the material properties of final steel product, as Gadeanu et al. (1989) explains in their book:

- The Manganese favourably influences the increase of mechanical strengths and its deformability, if it appears in quantities of 0.85 - 1.6% (above these values, it hardens the areas close to the weld;
- The Silicon increases the breaking strength and yield strength of steel but reduces ductility and promotes the formation of brittle constituents that reduce weldability and corrosion resistance, if found in quantities greater than 0.35%;

- The small quantities of Phosphorus, 0.1%, leads to brittleness, i.e., the steel material becomes brittle at low temperatures;
- The Sulphur reacts chemically with iron and forms inclusions that reduce mechanical strength and lead to decreased bearing capacity. Hot embrittlement also occurs since iron sulphide melts at lower temperatures than steel;
- The Oxygen forms with iron oxides that remain in the form of inclusions in the metal mass, leading to decreases in the strength of the material.
- The Nitrogen in steels reduces the weldability and aging of the material;
- The Copper and Chromium increase the breaking strength and corrosion resistance, without affecting the deformability characteristics of the steel;
- The Nickel increases the strength of steel and ensures its good behaviour at low temperatures;
- The Molybdenum increases mechanical and corrosion resistance. It ensures good behaviour at high temperatures.

2.3 Bolts Manufacturing

Bolts manufacturing processes are differentiated as shown in Figure 2. 3., into bolts formed without cutting and ones formed by machining. With forming without cutting there is a further classification between cold and hot forming.

The controlled removal of material to achieve a desired shape and size is known as *machining*. In the manufacturing of bolts, machining is involved in several steps such as turning, milling, grinding, and reaming. Turning is the most used method for fasteners, although it has become less important due to the advancements in cold pressing technology. During the turning process, a turning tool is used to cut the required shape of the component from the input material, which is typically a bar up to 6 meters in length. Unlike cold or hot forming, the chamfer course of the input material is destroyed. This method is used when the production run is small or when the part geometry cannot be achieved through cold or hot forming due to sharp edges, small radius, or nominal sizes (Wuerth-Industrie, 2023).

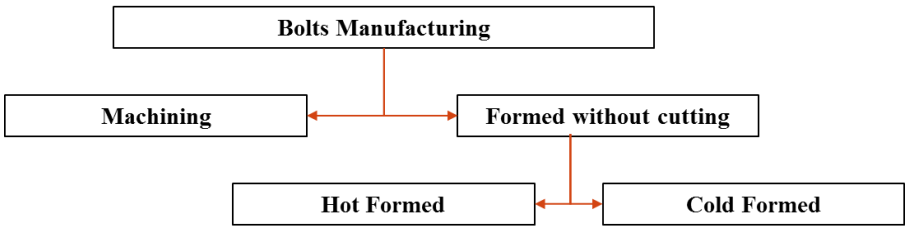

Figure 2. 3. Classification of Bolts Manufacturing Processes - (Wuerth-Industrie, 2023).

In the modern era, the preferred method for creating most fasteners is *cold forming*. This process involves pressure forging, cold extrusion, and reducing the fastener through multiple stages. It is often chosen for large quantities due to its economic benefits. The selection of the appropriate forming machine depends on the size and degree of forming required for the fastener. Sharp-edged transitions or thin profiles are not ideal for cold forming, as they can increase tool wear. The quality of the input material, such as wire, is critical to ensuring the final product's quality. Cold forming offers numerous benefits, including optimal material usage, high output, precise dimensions, and surface quality. Additionally, strain hardening can increase the strength properties of the product, and chamfers can be run in press parts in accordance with the load (Wuerth-Industrie, 2023).

The *hot forming* production method is utilized for the production of sizable components that are typically larger than M27 and longer than 300 mm. This method is also employed for the manufacture of parts that cannot be produced through cold forming due to their smaller volumes or high degree of forming required. The process involves heating the input material, usually bars, at forging temperature either wholly or partially. This enables the production of even the most intricate geometry or high degrees of forming. It is noteworthy that hot-formed components possess a raw surface structure and are not strain-hardened during the hot-forming process. The hot forming process presents several advantages, including the ability to produce intricate geometries, accommodate low production runs, and produce large diameters and lengths (Wuerth-Industrie, 2023).

The process of forming or rolling a thread involves passing the screw between two flat dies, one of which is stationary while the other moves. This process creates the thread and allows to produce a large quantity of fasteners. Typically, the thread is applied before the hardening and tempering process, but in some cases, it may be applied afterwards, which is known as *finally rolled* thread (Wuerth-Industrie, 2023).

2.3.1 Heat Treatment: quenching and tempering, and annealing

The combination of hardening and tempering is made according to ISO 898-1 (1999), and EN 20898-2 (1993).

The process of *bolt hardening* involves increasing the hardness and strength of bolts or fasteners to enhance their resistance to deformation, wear, and breakage in high-load or demanding operating conditions. Various methods can be used to achieve bolt hardening, including *heat treatment* and *surface coating*.

Heat treatment is a popular method for hardening bolts. It involves heating the bolt to a specific temperature and then quickly cooling it to alter its microstructure and improve its mechanical properties. The two primary heat treatment processes for bolt hardening are *quenching and tempering* (Gadeanu et al., 1989).

Quenching involves heating the bolt to a high temperature and then rapidly cooling it by immersing it in a quenching medium such as water, oil, or polymer solution. The rapid cooling rate during quenching results in the transformation of the

material's microstructure, leading to increased hardness and strength. The quenching process typically involves the following steps:

- Heating: The material is heated to a temperature above its critical transformation temperature, depending on the specific material and is usually determined based on its phase diagram or known metallurgical properties.
- Soaking: After reaching the desired temperature, it is held at that temperature for a specific duration to ensure uniform heating and allow for complete transformation of the microstructure.
- Quenching: Once the material has been soaked, it is rapidly cooled by being submerged in a quenching substance. The choice of quenching substance relies on elements such as the type of material being processed, the level of hardness desired, and the required rate of cooling.

After quenching, the bolt may be too hard and brittle for certain applications. *Tempering* is a process that involves reheating the bolt to a lower temperature, below its critical transformation temperature. Following the bolt is held there for a specific duration, and finally, it is cooled in a controlled manner. This allows for the reduction of excessive hardness and the adjustment of mechanical properties, such as toughness and ductility, to make the bolt more suitable for its intended use. The tempering process brings several improvements to the material's properties:

- Toughness: When a material is quenched, it can become brittle. To counteract this, tempering is used to convert the brittle martensite into a more flexible microstructure. This can lead to increased toughness and a lower risk of fracture.
- Ductility: The process of tempering holds significant importance in enhancing the ductility of a material. This, in turn, enables it to undergo plastic deformation without fracturing, making it ideal for applications that involve shaping or forming processes.
- Reduction of Residual Stresses: After quenching, residual stresses can form and cause issues such as distortion or cracking. Tempering can reduce these effects by relieving those stresses.

Annealing is a process used to change the properties of materials, particularly metals or alloys, by heating them to a specific temperature and then gradually cooling them. Its main purpose is to reduce internal stresses, increase ductility, and refine the material's microstructure (Gadeanu et al., 1989).

During the annealing process, the material is heated to a temperature above its recrystallization temperature. This is the temperature at which new grains form in the material and can vary depending on the specific type of material. Once the desired temperature is reached, the material is held at that temperature for a specific time to allow for the recrystallization process to occur.

After the heating phase, the material is slowly cooled down, which helps to minimize the formation of new stresses and distortion in the material. This phase is

known as the cooling cycle and can be done naturally in a furnace or in a controlled environment.

Annealing has several effects on the material, including stress relief, softening, improved ductility, and homogenization. It helps to reduce internal stresses caused by processes such as machining, cold working, or welding, making the material less likely to crack, warp, or distort. The process also softens the material by refining its grain structure, reducing the presence of dislocations, and making it more ductile. Finally, annealing promotes the uniform distribution of alloying elements within the material, resulting in improved consistency and properties.

2.3.1.1 Carbon-Steel Diagram

The carbon steel diagram (also known as iron-carbon phase diagram) is the graphical representation that show the relationship between the temperature, carbon content, and carbon steel phase (Figure 2. 4.). It provides valuable information on the changes and microstructures of these materials under different conditions. The diagram is divided into regions that correspond to different phases and phase mixtures. The most common phases depicted in the diagram are:

- Ferrite (α-iron): A carbon steel with a low melting point and a small amount of carbon in the ferrite phase. Ferrite is a relatively simple material with a body-centred cubic (BCC) crystalline structure.
- Austenite (γ-steel): At high temperature and high carbon content, carbon steel is converted to austenite. Austenite has a face-centred cubic (FCC) crystal structure and is relatively ductile. It can dissolve a significant amount of carbon in its structure.
- Cementite (iron carbide): Cementite, also known as iron carbide (Fe3C), is a hard and brittle alloy containing about 6.7% carbon. Carbon usually occurs as a secondary element in steel, especially at high carbon concentrations.

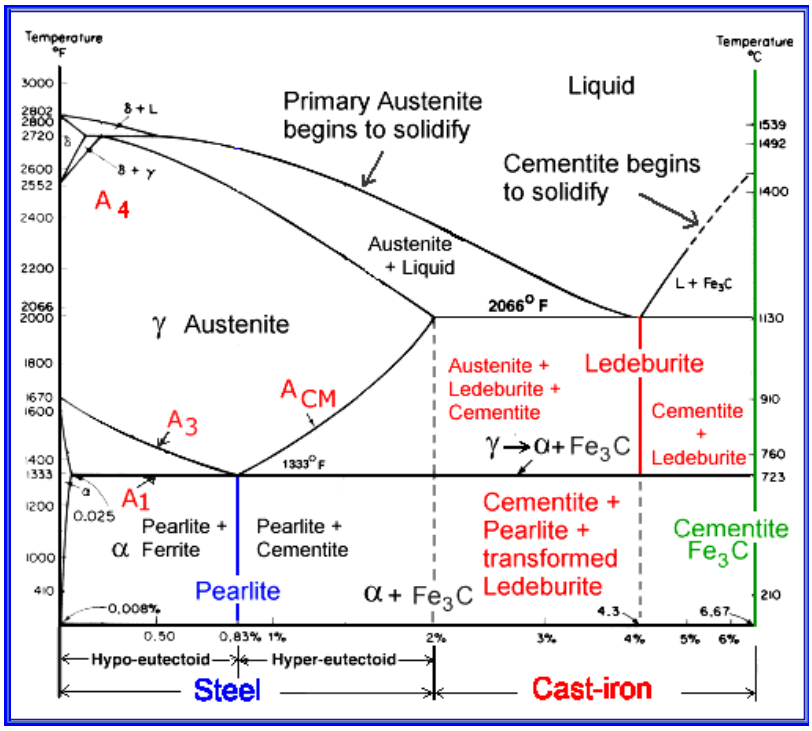

Figure 2. 4. Iron-carbon phase Diagram (Uni-kiel.de, 2023).

By studying carbon steel models, engineers and metallurgists can predict the microstructure that will form in a given steel alloy under specific heat treatment conditions. To be more specific, function of the carbon content in the steel, the temperature reached during quenching and tempering processes varies, as it is shown in Figure 2. 5. (Gadeanu et al., 1989).

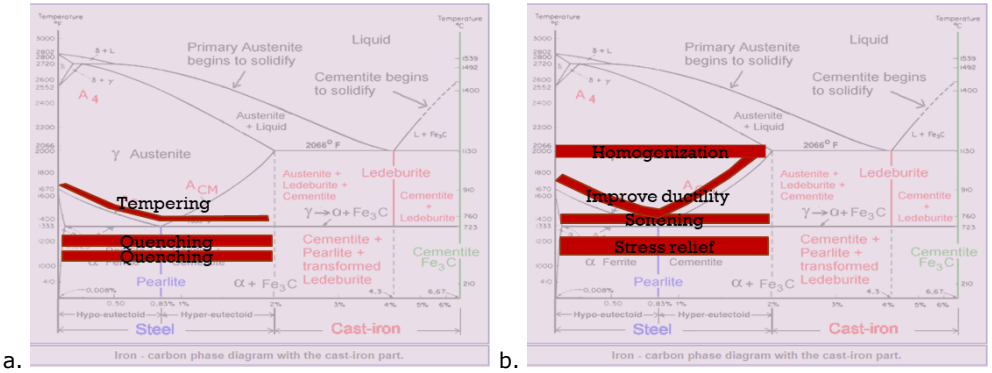

a. b.

Figure 2. 5. Iron-carbon phase Diagram showing the temperature for: a. quenching and tempering; b. annealing processes.

2.3.2 Bolts Surface Treatment

The corrosion protection of steel structures, including fasteners, is given by the metal coating, which provides primary protection during construction, but not only, as it will contribute to the overall corrosion protection during building lifetime. Function of elements exposure, they might be painted or treated additionally. According to EN 14399-3 (2005) and EN 14399-4 (2005), respectively, the surface treatment is done by *hot dip galvanizing*.

Other treatments are accepted providing that they do not affect the mechanical or functional characteristics. It is important to note that coatings containing cadmium or alloys are not permissible due to the potential toxicity they may emit when vaporized, for example during welding. Anodizing, on the other hand, creates an oxide layer that seamlessly integrates with the substrate and does not pill. For indoor use, black oxide is a suitable option that does not corrode. Black phosphate, which replaces a microscopic layer of iron with a thinner layer of zinc or manganese dioxide, is not recommended for use on steel containing large amounts of nickel. Although chrome provides notable corrosion resistance, it should be noted that it is generally more expensive than zinc plating (Aspen, 2023).

The most often used method for surface treatment is zinc coating. There are 4 methods to apply a zinc coating to fasteners, as electroplating (electrolysis of a watery solution of zinc salt), sherardizing (diffusion process in which the elements are heated in close contact with zinc dust), hot dip galvanizing (HDG) (dipped in molten zinc bath), and thermo-chemical surface modification (TCSM) (diffusion process with zinc aluminium polymetallic coating) (SCI, 2015).

2.3.2.1 Hot Dip Galvanization

The process of galvanization results in the formation of a metallurgical bond between the zinc coating and the underlying steel, producing a complex series of zinc-iron alloy layers. This protective coating exhibits varying levels of both hardness and ductility, rendering it highly effective at preventing damage to the steel material from the core element.

Figure 2. 6. shows the layers formed during the Hot Dip Galvanizing process. The hardness of each layer is determined by a Diamond Pyramid Number (DPN), which is a measure of hardness. Typically, the Gamma, Delta, and Zeta layers are harder than the underlying steel, while the Eta layer is more ductile, providing the coating with some degree of impact resistance. The combination of hardness, ductility, and adherence provides the galvanized coating with unparalleled protection against damage caused by rough handling during transportation and in service (Galvanizeit, 2023).

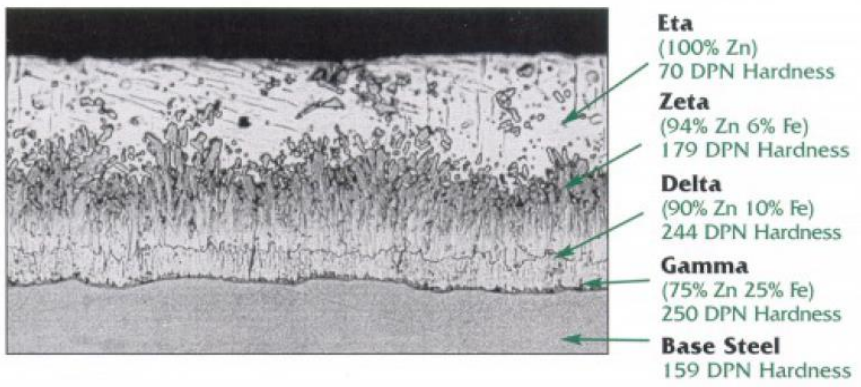

Figure 2. 6. Layers formed during Hot Dip Galvanizing process (Galvanizeit, 2023).

2.4 Bolts under Fire

High temperatures that arise in case of a fire can cause bolts to expand, soften or damage their integrity.

When designing bolts to withstand fire incidents, several factors should be considered to ensure their performance and reliability, such as:

- evolution of the material properties depending on bolt sizes and grades, ensuring that the bolts are designed to withstand the anticipated loads and stresses during a fire event;
- the applied specialized coatings or treatments;
- the thermal expansion, which may induce different internal forces in the structure, in comparison with the normal temperature situation.

Understanding the bolts behaviour for fire resistance requires a multidisciplinary approach involving structural engineers, materials experts, and fire design specialists. The fire-resistant bolt design should ensure compliance with applicable codes and standards and to optimize the performance and safety of the bolted assembly under fire conditions.

The standards, as well as the literature, offer knowledge about the bolts' behaviour under fire conditions, how to approach a given situation, or to realize a test on bolt material, as described in the following sections. However, the latest research showed that the understanding of this matter is far from being complete. In the last two decades, tests on bolt materials, connections or joints highlighted certain gaps and questioned the applicability of simplified methods when analysing the bolt behaviour under elevated temperatures.

2.4.1 Testing Procedure

One of the most accurate options to understand how a structural element behaves under elevated temperatures is through experimental testing.

According to EN 14399-4 (2005), the mechanical properties of high strength bolts is required to be determined according to European Standard ISO 898-1 (2009). This document should be approached in close corelation with ISO 6892-1 (2009) for the method for tensile testing of metallic materials to define their mechanical properties at normal temperature, and with ISO 6892-2 (2011) for tensile testing under elevated temperatures, respectively.

In testing standards, for tests on specimen subjected to high temperatures, a distinction is made between two main groups of tests: steady-state tests and transient tests, latter being closer to real conditions of structures subjected to fire. A decision should be made when choosing the method, as the material properties measured are closely related to the test method used. Steady-state tests are characterized by a heating period and a soaking period during which the desired temperature is uniformly reached over the entire volume of the tested piece. After the specimen's temperature is stabilized, the load is applied until failure occurs. The strain measured before the load is applied corresponds to the thermal expansion. This method is used to obtain a stress-strain relationship at a given temperature, to establish tensile strength, modulus of elasticity, and ultimate strain. The test procedures for steady-state tests are presented in the standards ISO 6892-1 (2009) and ISO 6892-2 (2011).

On the other hand, the transient temperature tests are characterized by an increasing temperature, while the specimen is loaded before heating with a constant load. This method is used in order to obtain the failure temperature. For transient tests, no standardized procedure exists.

Further, the attention is focused on steady-state tests, with a strain rate loading procedure, according to the standards ISO 6892-1 (2009) and ISO 6892-2 (2011), as it is the procedure implemented in the experimental tests realized in this work and described in Chapter 3 of this thesis.

Thus, to prepare a tensile test on metallic material under elevated temperature, the specimen should be machined in accordance with the requirements of Annex D of ISO 6892-1 (2009). Further, the test piece must be heated to the specified temperature, with a heating rate of 10 K/min, and maintained at that temperature for at least 10 min before loading (Kirby, 1995; ISO 6892-2, 2011). This is known as the soaking period. The loading shall only be started after the output of the extensometer has stabilized. When the gauge length is less than 50 mm, one temperature sensor shall measure the temperature at each end of the parallel length directly. When the gauge length is equal to or greater than 50 mm, a third temperature sensor shall measure near the centre of the parallel length (ISO 6892-2, 2011).

There are 2 methods described by ISO 6892-2 (2011) for measuring the material properties, under strain rate control:

- Method A, based on strain rate control, which intended to minimize the variation of the test rates during the moment when strain rate sensitive parameters are determined and to minimize the measurement uncertainty of the test results. The strain rates proposed for this method are presented in Table 2. 3.

- Method B, based on expanded strain rate ranges. The proposed strain rates are presented in Table 2. 3.

Table 2. 3. Strain rate ranges (ISO 6892-1, 2009; ISO 6892-2, 2011).

	Property	COLD testing Strain Rate [s^{-1}]	HOT testing Strain Rate [s^{-1}]	Observation
Method A	Upper yield strength Proof strength	R1: 0.00007 +/- 20% R2: 0.00025 +/- 20%	R1: 0.00007 +/- 20% R2: 0.00025 +/- 20%	R1 = range 1 R2 = range 2
	Lower yield strength Percentage yield point extension	R1: 0.00007 +/- 20% R2: 0.00025 +/- 20%	R2: 0.00025 +/- 20% R3: 0.002 +/- 20%	R1 = range 1 R2 = range 2 R3 = range 3
	Tensile strength (R_m) Percentage elongation after fracture Percentage reduction area Percentage total extension at the maximum force Percentage plastic extension at maximum force	R1: 0.00007 +/- 20% R2: 0.00025 +/- 20% R3: 0.0014 +/- 20% R4: 0.0067 +/- 20%	R2: 0.00025 +/- 20% R3: 0.002 +/- 20% R4: 0.0067 +/- 20%	R1 = range 1 R2 = range 2 R3 = range 3 R4 = range 4 R3 is to be used throughout entire test if only R_m to determine
Method B	Upper yield strength Lower yield strength	0.0000167 - 0.0000833	0.00025 - 0.0025	
	Proof strength	0.0000167 - 0.0000833	up to 0.0025	
	Tensile strength	0.00033 - 0.0033	up to 0.008	
	Percentage elongation after fracture Percentage reduction area Percentage total extension at the maximum force Percentage plastic extension at maximum force		up to 0.008	

The values of the material properties are very sensitive to the strain rate at elevated temperatures, as Annex B of ISO 6892-2 (2011) points out. Therefore, attention must be made during the testing.

Method A relies on narrow tolerance strain rates, while Method B uses conventional strain rate ranges and tolerances. Method A is designed to minimize the variation in test rates during the determination of strain rate sensitive parameters and reduce uncertainty in test results. The standard ISO 6892 -2 (2011) does not recommend a specific method among the two, but allows the producer to make his own choice. Typically, tensile tests at high temperatures are carried out at slower strain rates than at normal temperature. The standard ISO 6892 -2 (2011) suggests using slow strain rates, but higher strain rates are allowed for specific applications, such as comparing properties at normal temperature and the same strain rate.

2.4.2 Fire Resistance Design

The experimental procedure may offer the best understanding of a structural element behaviour and evolution of material properties with the increase in temperatures, but it remains the most expensive one and difficult to be accessed by most engineers. Therefore, the simplified methods provided by the Eurocodes (for steel structures EN1993-1-2, 2005) or literature remain the preferred approach for design, as they are cheaper, more accessible and time saving techniques.

To analyze a steel connection subjected to fire, the assessment may be done in two steps:

- a thermal analysis, which offers information about the temperature in the joint, and its components, respectively;
- a mechanical analysis, which describes the efforts and the deformations of the joint.

The mechanical properties, like strength and deformation of steel, are affected by the elevated temperature. The Eurocode EN1993-1-2 (2005) offers the stress-strain curve as shown in Figure 2. 7. This curve might present a strain-hardening behaviour when tested below 500 ^{o}C, for which the Annex A of the Eurocode EN1993-1-2 (2005) offers an alternative (Figure 2. 8.).

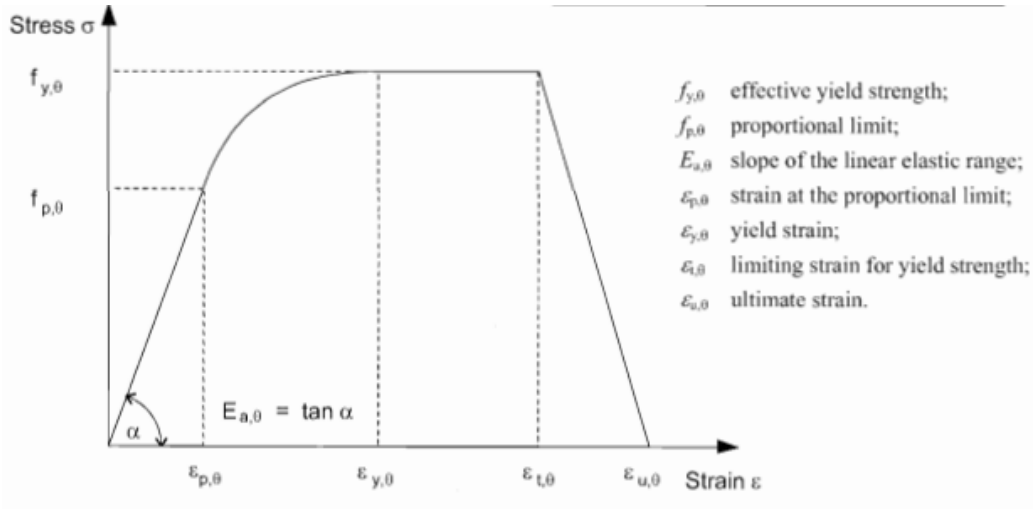

Figure 2. 7. Stress-strain curve for steel at elevated temperature (EN1993-1-2, 2005).

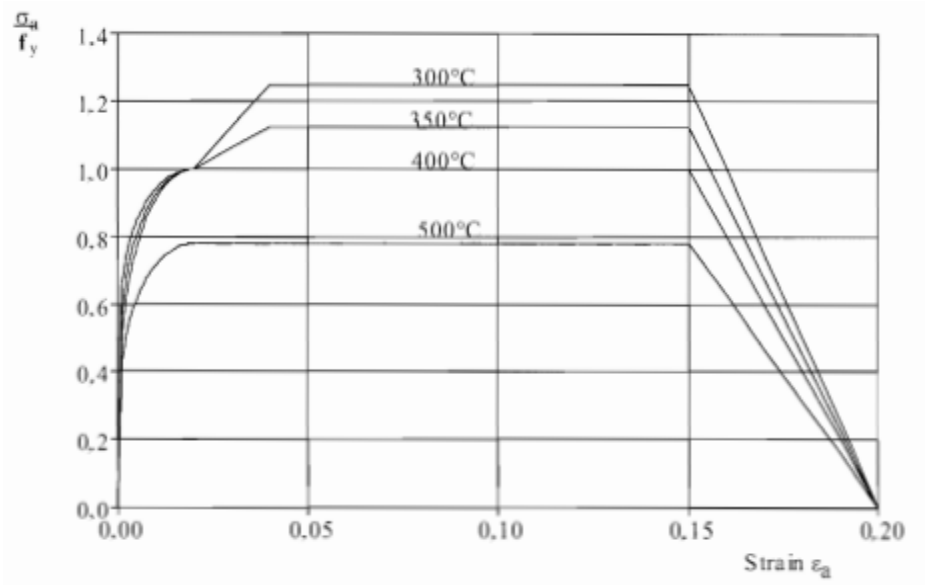

Figure 2. 8. Alternative stress-strain relationships for steel at elevated temperatures, allowing for strain hardening (EN1993-1-2, 2005).

The simplified method for designing steel elements under fire conditions, presented by the Eurocode EN1993-1-2 (2005) allows to determine the stress-stain curve, but also to compute the key mechanical properties of steel. There are proposed reduction factors for the yield strength, proportionality limit, and modulus of elasticity for steel material under high temperature. Annex D of the same Eurocode (EN1993-1-2, 2005), offers reduction factors for bolts and welding material, loaded in tension or shear, which are different from the reduction factors for steel material. These

factors presented in Table 2. 4. were experimentally determined by Kirby (1995), which studied grade 8.8 bolts subjected to tension and shear.

Table 2. 4. Strength Reduction Factors for Bolts and Welds (EN1993-1-2, 2005).

Temperature θ	Reduction factor for bolts, $k_{b,\theta}$ (Tension and shear)	Reduction factor for welds, $k_{w,\theta}$
20	1	1
100	0.968	1
150	0.952	1
200	0.935	1
300	0.903	1
400	0.775	0.876
500	0.550	0.627
600	0.220	0.378
700	0.100	0.130
800	0.067	0.074
900	0.033	0.018
1000	0	0

2.5 Studies on Bolts exposed to Fire: a State of the Art

Under fire conditions, the Eurocode EN1993-1-2 (2005), Chapter 4.2, presents the assumption that the overall temperature in the joints is lower than the temperature in the adjacent steel elements. This assumption is based on the consideration that the temperature in the joints increases slower due to a higher concentration of material. For steel members, EN1993-1-2 (2005) provides a simple method to compute the temperature within the cross-section, based on its section factor, which is described as the ratio between the volume and the surface exposed to fire (perimeter over area). This method is also used to compute the temperature in the joints (EN1993-1-2, 2005, Annex D-D.3). In this case, the Eurocode EN1993-1-2 (2005) states that the net section does not need to be computed, if a fastener is present in each hole. Therefore, the gross section should be used in computation of the temperature.

Nevertheless, Franssen (2004) showed that this method is not valid after an important duration of exposure to fire, as the temperature becomes uniform over the joint. More than that, the authors showed that the method gives unsafe results when the diameter of the bolt is smaller than the total thickness of the connected plates. In these cases, the bolt becomes a "hot spot", because its temperature increases faster than the temperature in the connected plates, and so a heat transfer from the bolt to the plates appears (Franssen, 2004).

On the other hand, for a more thorough assessment of a connection, one can study the bolt resistance. Hence, the Eurocode EN1993-1-2 (2005) offers a series of reduction factors for bolt strength under elevated temperature. These factors, denoted $k_{b,\theta}$, are to be used for strength reduction of bolts under both, tension or

shear stresses. Therefore, $k_{b,\theta}$ represents the ratio between ultimate tensile strength (Kirby, 1995) at elevated temperature, $f_{u,\theta}$, and ultimate tensile strength at normal temperature, f_{ub}:

$$k_{b,\theta}=f_{u,\theta}/f_{ub} \quad \text{– reduction factor for bolts' strength} \qquad [2.1]$$

Attention should be made at the fact that the reduction factors for bolt strength refers to the tensile strength, i.e., the maximum stress reached on the stress-strain material's curve. While referring to the steel material, Eurocode EN1993-1-2 (2005) uses the terminology of the yield strength reduction factors, which is also the maximum stress reached, according to the stress-strain curve (see Figure 2. 7.), in comparison with the yield stress, f_y, which is different from the maximum stress reached on the stress-strain curve of steel material under normal temperature.

This simplified method was developed following Kirby's experimental research realized in 1995 (Kirby, 1995). The authors tested diameter M20 Grade 8.8 bolts assemblies in pure tension and pure shear, under different temperatures between 20 °C and 800 °C. The experimental procedure was supplemented with tensile tests on bolt material. The bolts were manufactured by either hot forging, quenched from 900 °C and tempered at a temperature of 600-620 °C, either by cold forging, quenched from 850 °C and tempered at a temperature of 450-500 °C. Each bolt assembly had an 8g7H tolerance, as at the time no requirements regarding matching nuts and bolts were in place. For each test, the specimen was heated at a rate of 5-10 °C and stabilized for 15 min. The control of the displacement, in the tests on assemblies, was realized at a strain rate of 0.002 min^{-1} (0.000033 s^{-1}) measured in the elastic region and maintained until the ultimate capacity (i.e. ultimate force) was exceeded. The tests on material were realized over the temperature range of 20-800 °C, with a pace of 50 °C, at a strain rate of 0.002 min^{-1} (0.000033 s^{-1}) to provide proof stress value, $f_{p\theta}$, up to 5%, beyond which the strain rate was raised to 0.1 min^{-1} (0.00166 s^{-1}) until rupture.

Following the experimental program, Kirby (1995) concluded that parameters such as the heating rate or the soaking time are not influencing the results. In contrast, the manufacturing and treatment processes applied to the bolts can affect the failure mode of the assemblies, i.e. the cold forged ones are more predisposed to thread stripping rather than the hot forged ones, especially for temperatures below 400 °C. This phenomenon was quantified in a lower reduction coefficient with 20%. Above 400 °C, the different manufacturing and treatment processes did not affect the assemblies' behaviour. The main results of Kirby's work consist in the reduction factor for ultimate capacity of Grade 8.8 bolts, acting in shear and tension, as a tri-linear relationship (Kirby, 1995):

$k_b = 1$, for $\theta \leq 300$ ℃ [2.2.]

$k_b = 1-(\theta-300)*0.2128*10^{(-2)}$, for 300 ℃ $< \theta \leq 680$ ℃ [2.3.]

$k_b = 0.17-(\theta-680)*0.5312*10^{(-3)}$, for 680 ℃ $< \theta \leq 1000$ ℃ [2.4.]

Since Kirby's research (Kirby, 1995), different authors presented results on bolts, trying to establish the limits of the above method, to validate it for other ranges or to improve it.

Although Kirby (1995) mentioned that a tighter tolerance of the assembly might reduce the chances of failure through thread stripping, Bull et al. (2015) and Lange and Gonzalez (2012) obtained the same mode of failure (thread stripping) for tighter assemblies with tolerance class of 6H6g, as required by EN 14399-4 (2005). Therefore, both research (Bull et al., 2015; Lange & Gonzalez, 2012) concluded that the thread tolerance has small impact on the failure mode of the assembly.

The microstructure of the element material obtained through the heat treatment and surface treatment during the manufacturing process, rather plays a more important role. Bull et al. (2015) realised tensile tests on assemblies and material of grade 8.8 bolts under elevated temperatures and obtained only thread stripping failure mode. He suggests that the failure mode might be influenced by the microstructure at the ambient temperature, with tempered martensite leading to thread-stripping, and bainite and pearlite leading to necking at significantly lower force levels. Remembering the carbon-steel diagram presented in Chapter 2.3.1.1 of this work, it can be concluded that a lower tempering temperature will bring a higher strength and less ductility to the bolt. If a failure through necking is desired, then a higher tempering temperature should be considered to obtain a more ductile steel at the expense of strength. This conclusion is consistent with the observations of Kirby (1995), where the assemblies with a lower tempering temperature (i.e. lower ductility) failed through thread stripping.

As the material properties are in discussion, no influence of the bolt diameter should be found in the tensile testing. Hanus et al. (2011) confirmed that the diameter of the bolt has not a major influence on tests results.

Different research has been conducted to confirm the applicability of the existing reduction factors for bolts exposed to fire and to make necessary corrections. The strain rate parameter seems to be one which influence the most the results, among others. Kirby's work (Kirby, 1995) on M20 grade 8.8 bolts serves as the basis for the current reduction factors from Eurocode EN1993-1-2 (2005). But these tests were not corelated with different strain rates, they were only made under a strain rate of 0.002 min^{-1} (0.000033 s^{-1}). In addition to the mode of failure of bolt assemblies, Bull et al. (2015) observed that at ambient temperature, the effect of strain rate is negligible. However, at elevated temperatures, of 550 °C (Bull et al., 2015), both strength and ductility were found to be strain rate dependent. The authors' findings (Bull et al., 2015) regarding reduction factors for grade 8.8 bolts are consistent with Eurocode EN1993-1-2 (2005) when a strain rate of 0.02 min^{-1} (0.00033 s^{-1}) is applied during testing. However, for smaller strain rates, he obtained smaller reduction factors than the values from Eurocode EN1993-1-2 (2005). As mentioned previously, Bull et al. (2015) explained this difference through the microstructure of the material, which was tempered at higher temperatures. Hanus et al. (2012) studied the material behaviour of all the components in a connection,

including Grade 8.8 bolts, during both the heating and cooling phase, and he obtained similar reduction factors as the ones provided by the Eurocode EN1993-1-2 (2005).

Research has been conducted on grade 10.9 bolts, revealing distinct differences in behaviour when compared to grade 8.8 bolts. This raises concerns regarding the applicability of reduction coefficient factors provided by the Eurocode EN1993-1-2 (2005). For instance, Mushahary et al. (2022) has analysed the tensile and shear capacity of 10.9 grade bolts in heating and cooling fires and proposed tensile and shear reduction factors during the cooling phase. The author observed that the material's tension resistance is more affected by temperature changes than its shear resistance, as evidenced by the higher reduction factors for shear resistance compared to tension. The findings indicate a notable difference in the behaviour of grade 8.8 and grade 10.9 bolts, respectively. In comparison to the cooling phase results of the grade 8.8 bolts, the strength regain is higher in grade 10.9 bolts up to 400 °C. However, if the specimen is heated to 600 °C, the grade 10.9 regains lower strength than the grade 8.8 bolt in post-fire phase (Mushahary et al., 2022). Lu et al. (2022) has also conducted research on the mechanical and fracture properties of grade 10.9 high-strength bolts throughout the entire fire process (heating, heating-cooling, and post-fire stage), and proposed reduction factors of mechanical properties for each stage (see Table 2. 5.).

Lange and Gonzalez (2012) showed that the ultimate load of a bolt depends on the material as well as on the geometry of the threads and that the reduction factors of EN 1993-1-2 (2005), Annex D, are not safe. Therefore, he proposed a series of new reduction factors for grade 10.9 bolts (see Table 2. 5.). Lange and Gonzalez (2012) tested machined specimens from gr 10.9 M16 bolts cold forged, quenched and tempered (no tempering temperature is given), under elevated temperature. The temperature was reached in the oven and the specimen was kept for 30 minutes before being tested to a strain rate of 0.001 min^{-1} until a 0.2% proof stress, followed by 0.025 min^{-1} until rupture. The reduction factors for ultimate tensile strength obtained on material tests were in accordance with EN1993-1-2 (2005) ones. In contrast, the authors (Lange & Gonzalez, 2012) concluded from the tests on HV assemblies, that the reduction factors of ultimate tensile strength from EN1993-1-2 (2005) are unsafe, as they depend on the material and on the thread geometry.

Kawohl and Lange (2016) tested HV assemblies in tension of grade 10.9 bolts, subjected to a similar strain rate as Kirby (1995), i.e. 0.015 min^{-1}. He concluded that the reduction factors are slightly smaller than the ones from EN1993-1-2 (2005), due to fact that the failure was produced through thread stripping. But the results were superior to the ones of Lange and Gonzalez. (2012) obtained on HV assemblies. This can be explained through the strain rate higher than the one used by Lange and Gonzalez (2012) (0.0001-0.005 min^{-1} on assemblies). Therefore, the smaller strain rate conduct to a smaller reduction factor.

An analysis conducted by Kodur et al. (2012) studied the thermal and mechanical properties of high-strength steel utilized in Grade A325 and A490 steel bolts. It was determined that the yield strength of high-strength steel bolts remains unaffected up to 400 °C, which is different from the provisions of EN1993-1-2 (2005).

The reason for the high strength retention of A325 and A490 bolt steel, when compared to conventional steel, is attributed to the manufacturing process adopted for the steel used in these bolts. High-strength steel experiences a significant reduction in strength beyond 450 °C compared to conventional steel. Additionally, when high-strength steel bolts are exposed to temperatures beyond 800 °C, they lose approximately 95% of their strength, which is a more significant percentage loss than conventional steel.

Dwiputra et al. (2016) tested the material of grade 10.9 bolts at two different strain rates: 0.003 min^{-1} until 0.05 strain (5% strain) and 0.043 min^{-1} (0.0007 s^{-1}) in the plastic region. They found that the reduction factor was smaller than the values offered by EN1993-1-2 (2005) for the smaller strain rate, but similar to EN1993-1-2 (2005) for the high strain rate.

The Table 2. 5. presents a state of the art of the reduction factors found in the literature, developed in the last two decades. The data are also displayed in a graphical manner in the Figure 2. 8. for comparison. In the Figure 2. 9., the strength reduction factors, $k_{b,\theta}$, are defined as the ratio between the ultimate tensile strength of the material obtained from the tests at high temperature and the nominal ultimate tensile strength of the material tested at normal temperature.

These proposed coefficients vary with more than +/- 20% compared with the reduction factors from the EN1993-1-2 (2005), especially for temperature higher than 400 °C. It is difficult to conclude over the strain rate influence on bolt behaviour, as the tests were realised under different situations, as stress control (Kodur et al., 2012), strain control (Lange & Gonzalez, 2012), and displacement control (Lu et al., 2022; Mushahary et al., 2022).

Therefore, this thesis proposes to realize a first step into better understanding the grade 10.9 bolts behaviour, by quantifying the strain rate influence over the grade 10.9 bolt material, through a large series of tests on machined specimens, as described in the following chapters.

Table 2. 5. Strength Reduction Factors for Bolts - Literature

Author		EN 1993-1-2 (2005)	Lange and Gonzalez (2012)	Lu et al. (2022)	Mushahary et al. (2022)	Kodur et al. (2012)
Specimen			Grade 10.9	Grade 10.9	Grade 10.9	A490
Strain rate			0.025 min^{-1}	0.3 mm/min	0.5 mm/min	150 kN/min
Temperature	20	1	1	1	1	1
	100	0.968			0.95	1
	150	0.952				1
	200	0.935	0.97	0.99	0.94	1
	300	0.903	0.95		0.93	1
	400	0.775	0.79	0.73	0.83	0.85
	450		0.67			
	500	0.550	0.49		0.56	0.45
	550		0.28			
	600	0.220	0.16	0.23	0.25	0.17
	650		0.09			
	700	0.100	0.05		0.11	0.01
	800	0.067			0.07	0.04
	900	0.033			0.05	
	1000	0				

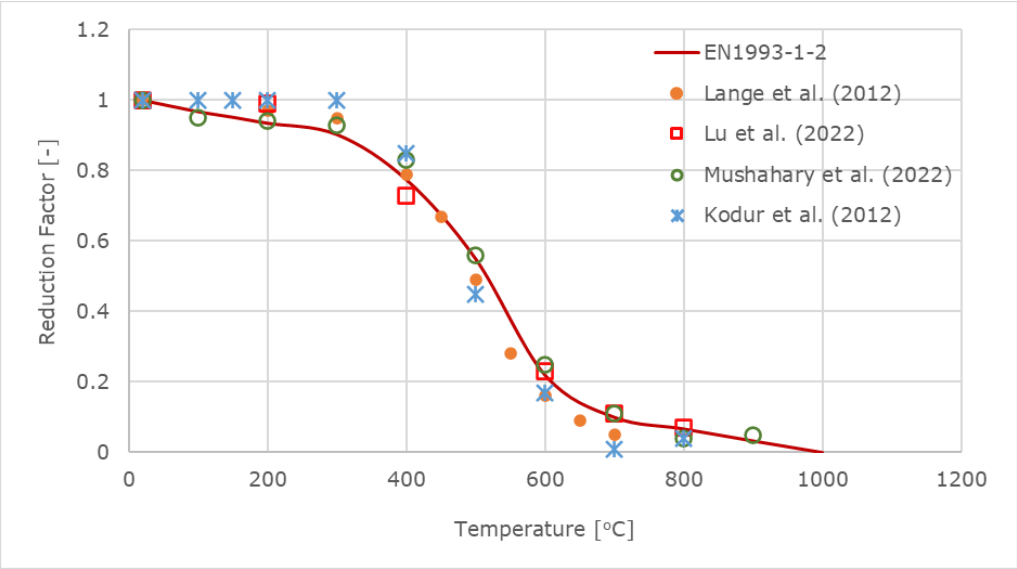

Figure 2. 9. Comparison of Strength Reduction Factors for Bolts.

2.6 Concluding Remarks

The steel structures require bolts with a grade ranging from 4.6 to 10.9, as specified by Eurocode EN1993-1-8 (2005). Additionally, the Eurocode EN1998-1 (2004) mandates the use of high strength bolts with bolt grade 8.8 or 10.9 in bolted connections of primary seismic members of a building. The commonly used high strength bolts assemblies are the type of HR (EN 14399-3, 2005) or HV (EN 14399-3, 2005). Nowadays, the bolts are mainly cold formed manufactured due to reduced time and cost of production. Only the larger diameters, greater than M27, will be hot formed manufactured. They are subjected to heat treatment and surface treatment, which will alter the bolt behaviour.

Understanding the bolts behaviour for fire resistance requires a multidisciplinary approach involving structural engineers, materials experts, and fire design specialists. The fire-resistant bolt design should ensure compliance with applicable codes and standards and to optimize the performance and safety of the bolted assembly under fire conditions.

The standards, as well as the literature, offer knowledge about the bolts' behaviour under fire conditions, how to approach a given situation, or to realize a test on bolt material.

However, the latest research showed that the understanding of bolts' behaviour presents certain gaps, especially the influence of strain rate, discussed in the previous section. The strain rate parameter gives important differences in the results of tensile tests, and it cannot be accounted as an accepted variability value. This aspect is highlighted in the ISO 6892-2 (2011), Annex B, as one of the important measurement uncertainties impossible, at this time, to be quantified without a tensile test on material. The scope of application of the reduction factors for bolts, in tension and in shear, under elevated temperatures, given by the Eurocode EN1993-1-2 (2005), remains another open question.

Therefore, this thesis intends to expand the existing knowledge, by offering a corelation between the strain rate and the reduction factor for grade 10.9 bolts material under temperatures from 20 ^{o}C until 800 ^{o}C.

3 Laboratory Equipment and Experimental Procedure

The experimental part, consisting in the bolt's material tensile tests under different temperatures, ranging from 20 °C to 800 °C, was undertaken in the laboratory of the Steel Structures and Structural Mechanics Department of Politehnica University Timișoara. This chapter describes the experimental set-up, and the tests program and procedure.

3.1 Experimental Set-up

The tensile tests were realized in the Instron universal testing machine of 250 kN, as shown in Figure 3. 1. Both ends of the specimen were fixed in the machine's crossheads by screwing. During the test, the bottom part remains in the initial position, while the upper part is mobile on the vertical axis. All the tests were realized in compliance with test standards ISO 6892-2 (2011).

Figure 3. 1. Experimental set-up.

3.1.1 Devices and Machines

Furnace – MAYTEC HTO-08/01, Round Furnace up to 1000 °C.

The furnace is a round cylinder split in two halves, as shown in Figure 3. 2. Both halves of the furnace are hinged on a common axis. The furnace casing is covered, at the top and at the bottom, with a stainless-steel sheet. Three temperature controller thermos-elements are mounted on the furnace right hand half. One is

placed in the middle of the furnace and the other two are 25 mm above and below the middle one.

The furnace diameter is 275 mm, measured on the exterior, and 405 mm in height. The heated area has an inner diameter of 100 mm and 300 mm in height. The temperature can reach 1000 °C in the heating space.

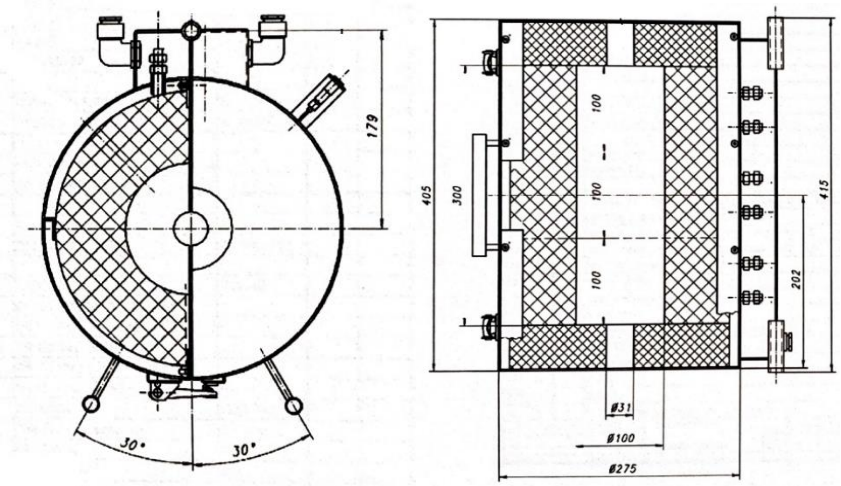

Figure 3. 2. The MAYTEC HTO-08/1 Furnace: top view (left), vertical cross section (right) (MAYTEC HTO-08/1, 2023).

The temperature inside the furnace is controlled through a separated unit shown in the Figure 3. 3. The temperature is controlled in three zones of heated area corresponding to the position of the three thermo-elements.

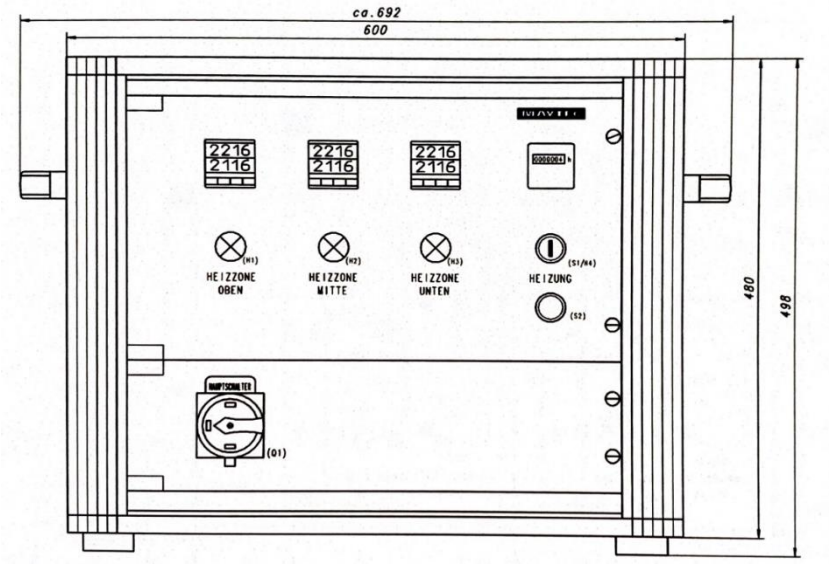

Figure 3. 3. The temperature control unit (MAYTEC HTO-08/1, 2023).

Extensometer – MAYTEC PMA-12/V7-1, HT-Extensometer up to 1500 °C

The extensometer used in the experimental part of this work is presented in Figure 3. 4. It consists of three components: the base plate, the casing containing the mechanism and the measurement system, and the sensor arms. The base plate is a carrier for all components, which allows for position adjustment. The sensor arms allow to set the initial gauge length, i.e. the distance of the sensor arms in relation to one another. They are manufactured from ceramics, having a round cross section, with the knife edge shape on their tip, to ensure a good contact with the specimen. These sensor arms are introduced in the furnace through a slot to enter in contact with the heated specimen.

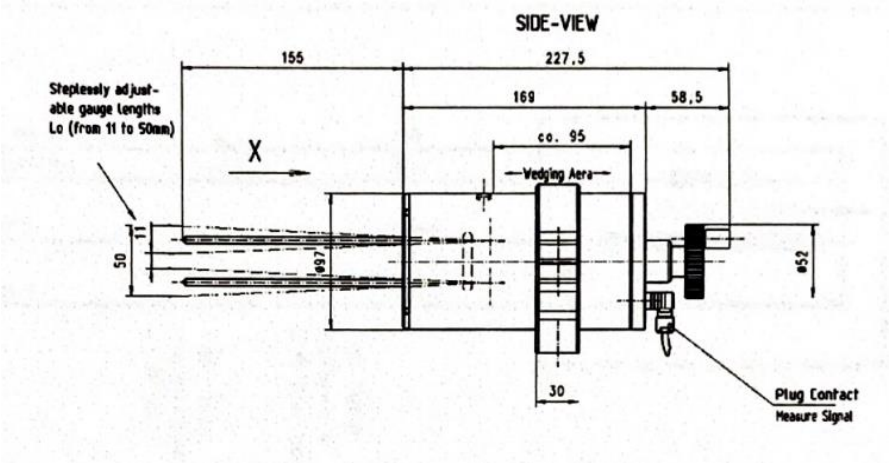

Figure 3. 4. MAYTEC PMA-12/V7-1, HT-Extensometer up to 1500 °C sensor arms (MAYTEC PMA-12/V7-1, 2023).

3.1.2 Machined Specimens

The specimens used for the tensile tests were extracted from diameter M12 bolts of grade 10.9, with bolt's length of 80 mm (EN14399-4 (2005) M12*80 10.9 ZNT). The bolts were all acquired from the same batch, manufactured in accordance with EN14399-4 (2005) standard requirements. Although their surface was treated by hot dip galvanization, as required for these bolts, this parameter has no influence in the tensile testing since the zinc layer was removed from the bolt during the machined process of the specimen.

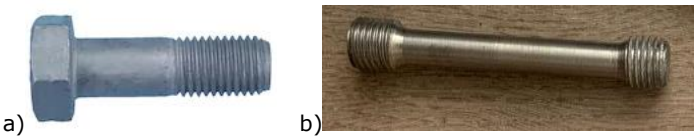

Figure 3. 5. Tested specimen: a) bolt type M12*80 10.9 ZNT (EN14399-4, 2005); b) machined specimen.

The dimensions of the machined pieces were chosen in accordance with the international standard ISO 6892-2 (2011), Annex A, which describes the test pieces with diameter equal to or greater than 4 mm (Figure 3. 6.). Figure 3. 7. presents a sketch with dimensions: the total length L_t is 80 mm, the original gauge length L_0 is 40 mm, the diameter between the gripped ends d_0 is 8 mm, the gripped end h is 12 mm, the metric ISO thread d_s is 12 mm.

Dimensions in millimetres

d_o	L_o	d_1	r min.	h min.	L_c min.	L_t min.[a]
4	20	M6	3	6	24	41
5	25	M8	4	7	30	51
6	30	M10	5	8	36	60
8	40	M12	6	10	48	77
10	50	M16	8	12	60	97
12	60	M18	9	15	72	116
14	70	M20	11	17	84	134
16	80	M24	12	20	96	154
18	90	M27	14	22	108	173
20	100	M30	15	24	120	191
25	125	M33	20	30	150	234

[a] The minimum value is only sufficient when the transition radius r, the length of the gripped ends h and the parallel length L_c are minimum values.

d_o original diameter of the parallel length
d_1 metric ISO-thread
r transition radius
h length of the gripped ends
L_o original gauge length ($L_o = 5d_o$)
L_c parallel length ($L_c \geqslant L_o + d_o$)
L_t total length of test piece

Figure 3. 6. Table of dimensions for the machined specimen (up) and sketch of the machined specimen (down) according to ISO 6892-2 (2011).

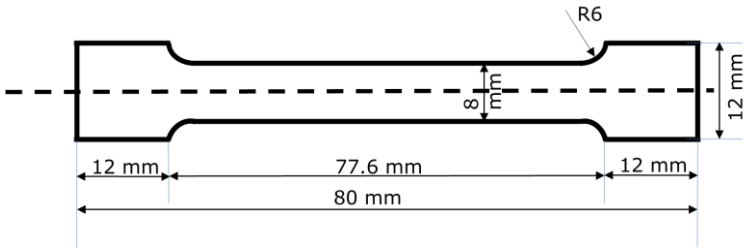

Figure 3. 7. Tested specimen: the machined specimen with dimensions.

3.2 Experimental Program

The experimental program was conceived for 81 configurations to describe the material behaviour under 9 different temperatures and 9 different strain rates. A steady-state procedure was implemented. As the experimental tests under elevated temperature can be very time consuming, the focus was mainly on the key strain rates: 0.000033 s^{-1}, 0.00033 s^{-1}, 0.0033 s^{-1}, 0.02 s^{-1}. For other strain rates values, tests were supplemented to ensure an accurate trend of the results. Where necessary, the tests were repeated 2, 3 or even 4 times in order to prove the results accuracy, leading to a final number of 116 tests for the experimental program. Table 3. 1. describes the main parameters for each test. The name of the test was marked to

show the temperature (e.g. T400S1R2 – shows a test under temperature of 400 °C), the strain rate (e.g. T400S1R2 – shows a test under 0.000033 s^{-1} strain rate), and the repetition (e.g. T400S1R2 – shows a second repetition of the test).

Table 3. 1. The tests configurations and repetitions.

Total no. of tests = 116		Number of tests per configuration								
		20 [°C]	150 [°C]	300 [°C]	400 [°C]	500 [°C]	542 [°C]	600 [°C]	700 [°C]	800 [°C]
S1	0.000033 [s^{-1}]	2	1	2	2	3	2	3	2	2
S2	0.00033 [s^{-1}]	3	1	2	3	3	0	3	3	3
S3	0.002 [s^{-1}]	1	0	1	1	1	0	1	1	0
S4	0.0033 [s^{-1}]	2	1	2	2	2	2	1	1	2
S5	0.008 [s^{-1}]	1	0	1	1	2	0	1	1	0
S6	0.01 [s^{-1}]	1	0	1	1	1	0	2	1	0
S7	0.02 [s^{-1}]	3	1	3	3	3	2	4	3	3
S8	0.04 [s^{-1}]	1	0	1	1	1	0	3	1	0
S9	0.06 [s^{-1}]	1	0	1	1	2	0	1	1	1

As Table 3. 1. shows, the tests were undertaken under 9 values of temperature: normal temperature of 20 °C, and elevated temperature, at 150 °C and from 300 °C until 800 °C, with a step of 100 °C degrees. An additional temperature was considered, of 542 °C. This temperature represents the corresponding temperature at which the steel yield strength decreases to $0.65f_y$. The value 0.65 represents the η_{fi} factor, the reduction factor for load combinations in fire situation, from EN1993-1-2 (2005), which is recommended to be used conservatively, in a simplified manner.

For each tested temperature, the specimens were subjected to 9 different values of strain rate, from 0.000033 s^{-1} to 0.06 s^{-1}, as listed in Table 3. 1. The strain rate was kept constant during the test, until the failure of the specimen.

Thermal protocol

One geometry, as described above, has been used for all tests. The furnace – MAYTEC HTO-08/01 (2023), Round Furnace up to 1000 °C, was set up in the test machine to heat the sample at the required level of temperature. The temperature is regulated by the exterior unit linked to the furnace and is based on the measurements of three thermocouples placed inside the furnace.

The test procedure consists of heating the sample in a first step until the required test temperature, with a heating rate of 10 K/min, and keeping the temperature constant for 10 min, so called the soaking period (ISO 6892-2, 2011). Further the tensile test starts, with a given strain rate until fracture, while the sample temperature remains the same.

Mechanical protocol

A steady-state procedure was used in all tests. The loading can be accomplished by either controlling the strain rate or the stress rate, named by EN ISO 6892-1 (2009). In EN ISO 6892-2 (2011), it is clearly mentioned that the stress rate method is not recommended under elevated temperature. Therefore, a strain rate method of loading, according to EN ISO 6892-2 (2011) was implemented in the 250 kN Instron testing machine. Loads and displacements are measured by the test machines. Elongations have been measured with the extensometer – MAYTEC PMA-12/V7-1, HT-Extensometer up to 1500 ^{o}C.

The strain rate control is based on the machine's displacement, reported to the calibrated length of the sample. The mechanical test starts after the soaking period. The strain rate was kept constant until the end of the test, marked by the failure of the specimen, in order to determine the tensile strength R_m, according to ISO 6892-2 (2011).

3.3 Conclusions

The experimental tests were undertaken in the laboratory of the Steel Structures and Structural Mechanics Department of Politehnica University Timișoara. The entire program comprises 81 configurations of tensile testing. Machined specimens were subjected to tension until failure, under 9 temperatures and 9 strain rates. Where necessary, repetitions of tests were realized to prove the accuracy of the measurements.

4 Experimental Results

This chapter presents the experimental results obtained in tensile tests made on grade 10.9 bolt material. The study intends to add over a hundred stress-strain curves to the existing literature database. The material curves describe the mechanical properties of this grade of steel under different temperatures (between 20 ^{o}C and 800 ^{o}C), and strain rates (between $3*10^{-5}$ s^{-1} and 0.06 s^{-1}).

Each stress-strain characteristic was attentively observed and corrected for equipment or human errors that might have affected the results. Details about this procedure are presented in Chapter 4.1. Each test configuration was repeated, to ensure the accuracy and the repetitiveness of the results obtained. A sensitivity analysis is shown in Chapter 4.6.

The yield strength, the modulus of elasticity, tensile strength, and the strain rate taken from the experimental obtained curves are given in Chapters 4.2, 4.3, 4.4, and 4.5, respectively. These values are also compared with the values provided by EN1993-1-2 (2005).

Chapters 4.7 and 4.8 provides a simplified method for the computation of the tensile strength reduction factors for grade 10.9 bolts, dependent on the strain rate. This method is proposed under a series of equations, but also in tabular form.

4.1 Treatment of the Raw Data

The machined specimens were tested for 9 different temperatures, including the normal temperature of 20 ^{o}C. For each temperature, nine tests were carried under the same conditions, excepting for the strain rate. A given test was repeated, to ensure the accuracy and the repetitiveness of the results obtained. The raw data obtained from the laboratory measurements and their treatment is discussed in this section.

The data recorded consists in the stress-strain curve (σ-ε curve). A test report was created for each test realized in the Laboratory of Steel Structures and Structural Mechanics of the Politehnica University Timișoara. Each report was realized considering the template required by ISO 6892-2 (2011). A couple of representative examples are showed in Figures 4. 1. And 4. 2.: the report of the test T20S7R1 (temperature of 20 ^{o}C, strain rate of 0.02 s^{-1}, 1st repetition) and the test T500S4R1 (temperature of 600 ^{o}C, strain rate of 0.0033 s^{-1}, 1st repetition).

Test Name: (*as required by ISO 6892-2*)	• (*larger strain rate*)
Identification of the test piece: (Test Name *as defined in this thesis*)	**T20S7R1**
Specified material:	Bolt EN14399-4 M12*80 10.9 ZNT
Type of test piece:	Machined specimen from bolt M12
Testing control mode:	Strain rate control
Testing rate [s^{-1}]:	0.02
Soaking time [minutes]:	0
Test temperature [°C]:	20
Method of establishing the extensometer gauge length L_e:	Method 2a - The extensometer is set on the test piece at the test temperature with nominal gauge length before mechanical loading. L_e = 40 mm.
Test Results: (*excel file's name*)	T-P3-7-20

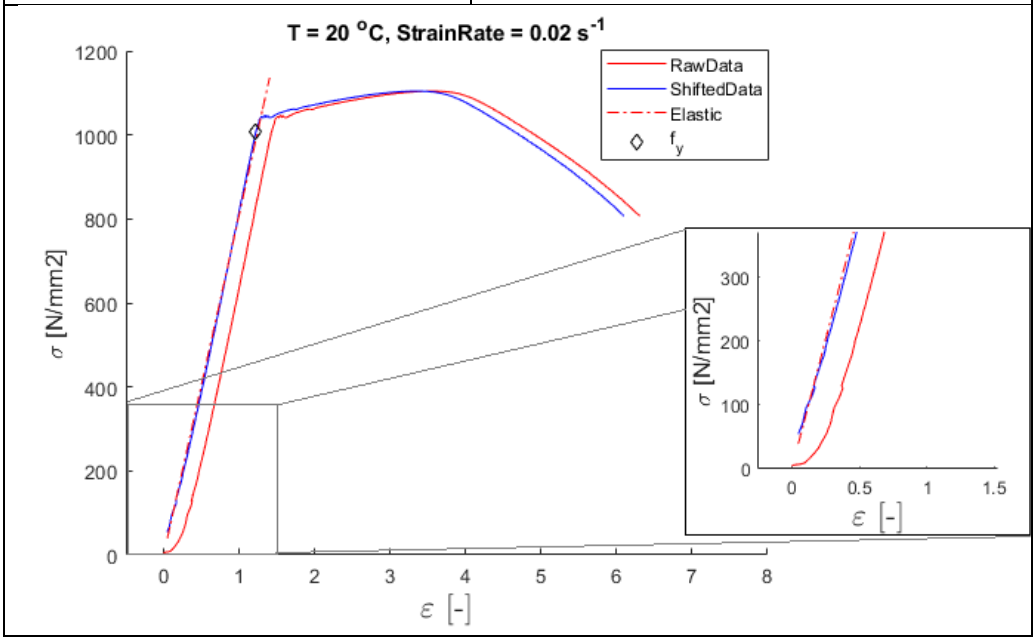

Figure 4. 1. Stress-strain curve.

All the recorded curves presented a sliding segment at the beginning of the loading procedure, a phenomenon which is very well known. The ISO 6892-1 (2009) recommends treating the results by correcting this range of the stress-strain curve, through the most convenient method. Therefore, according to Annex A of ISO 6892-

1 (2009), the elastic range was found through an iterative process, using a MatLAb (2021) algorithm (see Annex B of this thesis). The values considered to be part of the elastic range were those whose slope was fulfilling the following conditions:

- constant throughout the segment;
- representative selected range.

Test Name: (as required by ISO 6892-2)	ISO 6892-2 B
Identification of the test piece: (Test Name as defined in this thesis)	**T500S4R1**
Specified material:	Bolt EN14399-4 M12*80 10.9 ZNT
Type of test piece:	Machined specimen from bolt M12
Testing control mode:	Strain rate control
Testing rate [s-1]:	0.0033
Soaking time [minutes]:	10
Test temperature [oC]:	500
Method of establishing the extensometer gauge length Le:	Method 2a - The extensometer is set on the test piece at the test temperature with nominal gauge length before mechanical loading. Le = 40 mm.
Test Results: (excel file's name)	T-P3-4-500

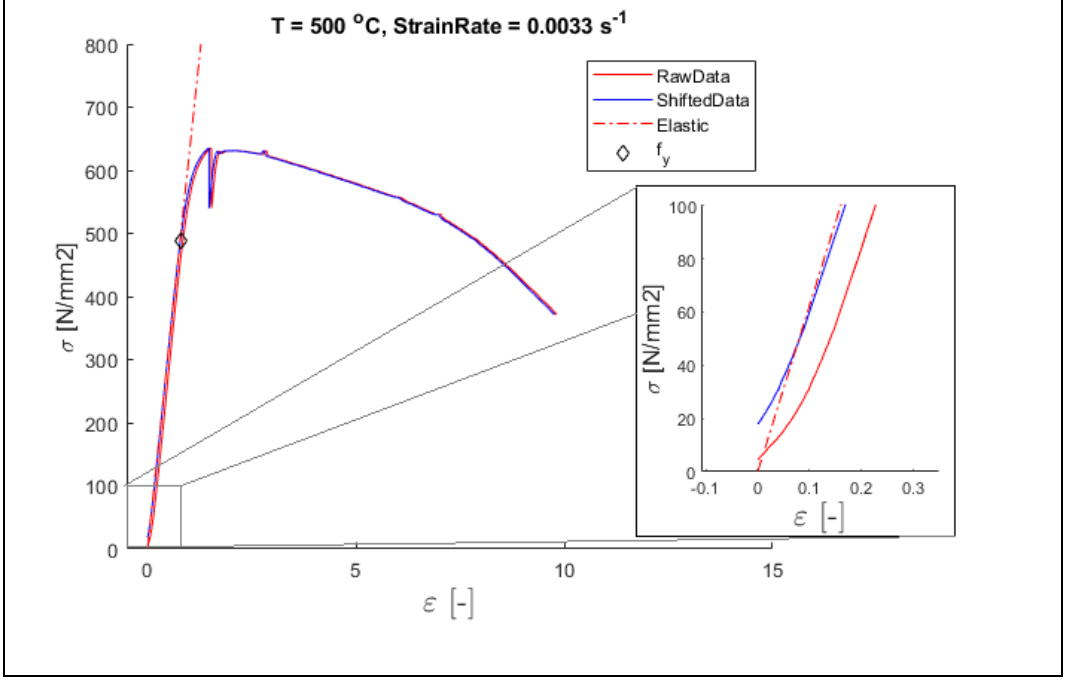

Figure 4. 2. Stress-strain curve.

The last value added to this straight segment of the stress-strain curve, was considered to be the yielding point, f_y. Further, the equation of the elastic range was

obtained and represented in the Figure 4. 1. And Figure 4. 2. with a dotted red line. In order to complete the correction of the raw data, the curve was shifted in the left side with a value ε_0. This value (ε_0) was found at the intersection of red line (the elastic range) with the horizontal axis (the strain), in the Figure 4. 1. and Figure 4. 2.

4.2 Yield Strength

The theory defines the yield strength, f_y, as the value of the material stress-strain curve that indicates the boundary between the elastic domain and the plastic domain. If stressed before the yield strength, the material will behave elastically, which means that the deformations reached while the specimen is loaded will return to zero, when unloaded. On the other hand, if the stress increases above the yield strength value, part of the deformation will remain permanent (the literature refers to it as plastic deformation).

The yield strength is defined by the ISO 6892-1 (2009) as the stress on the stress-strain curve, corresponding to the point reached during the test at which plastic deformation occurs without any increase in the force.

The Eurocode EN1993-1-1 (2005) in the Chapter 3 defines the yield strength as:

$$f_y = \varepsilon_y * E \qquad [4.1]$$

Where: ε_y is the yield strain

and E is the modulus of elasticity.

Meanwhile, Chapter 3 of EN1993-1-2 (2005) offers a method to obtain the strength and deformation properties of steel at elevated temperatures from the stress-strain relationship where the yield strength is considered to be at the strain of 2%.

In ASTM E21 (2020), yield strength is defined as the stress at 0.2% strain on the stress–strain curve, for brittle steels which do not develop a yield plateau. Kirby (1995) used the same definition of yield strength in his study in order to develop the reduction factors k_b.

Other common values for the yield strength are taken at 0.5%, 1% and 5% (Riaux, 1980; Kirby, 1995).

Therefore, in this work the yield strength was assessed at 0.2%, 0.5%, 1%, 2%, and 5% respectively, for all the stress-stain curves obtained. The last value of the elastic range is also shown in the figures below. The elastic range was assessed for each measured curve, according to the method described in the Chapter 4.1.

The stress-strain curves recorded at different temperatures under the recommended strain rate interval (0.00033 s^{-1} until 0.0033 s^{-1}) according to the tensile testing standard (ISO 6892-2, 2011) are presented in Figure 4. 3. - Figure 4. 10. The stress-strain curves obtained experimentally at normal temperature and 150 ^oC under the two strain rates show a yield strength at 0.5% strain in Figure 4. 3. and Figure 4. 4. At temperatures between 300 ^oC and 542 ^oC, the yield strength seems to be more accurate at 1% strain for both considered strain rates, as shown in Figure

4. 5. - Figure 4. 7., and Figure 4. 8.b. For temperatures of 600 °C and above, the yield strength is more appropriately taken at 2% strain, as shown in Figure 4. 8.a, Figure 4. 9., and Figure 4. 10. This observation is consistent with the EN1993-1-2 (2005), which considers the steel modulus of elasticity to decrease as the temperature of the material increases.

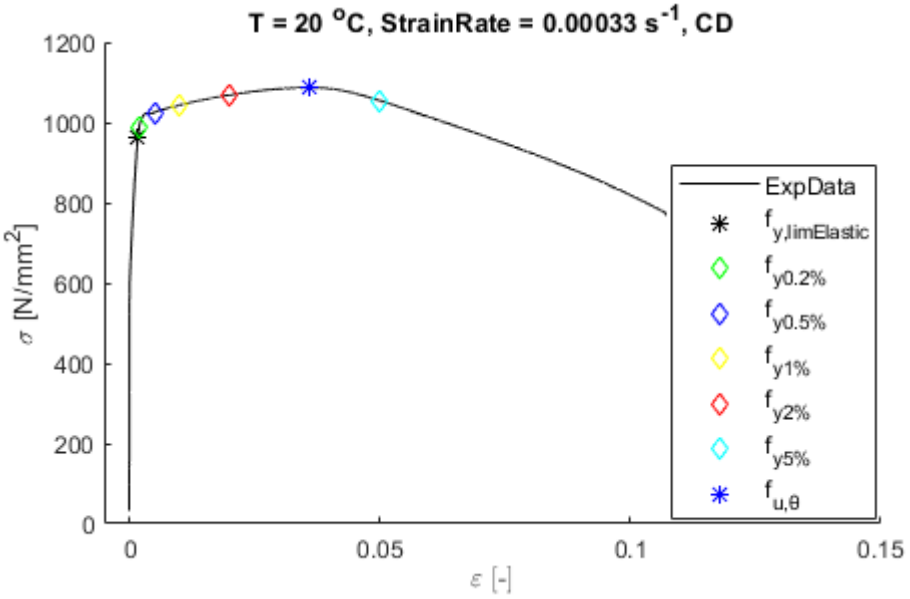

a.

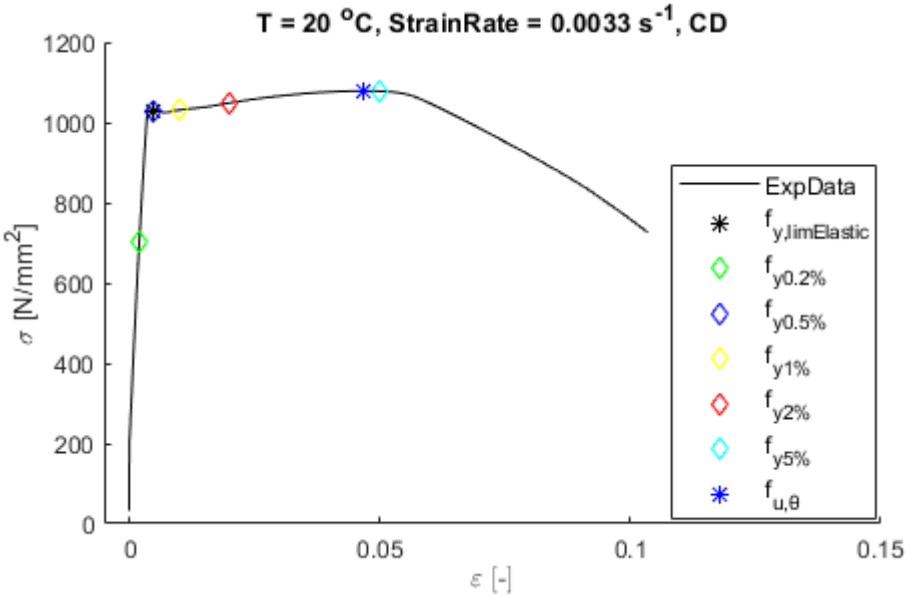

b.

Figure 4. 3. The stress-strain curve at normal temperature under: a. 0.00033 s^{-1} strain rate; b. 0.0033 s^{-1} strain rate.

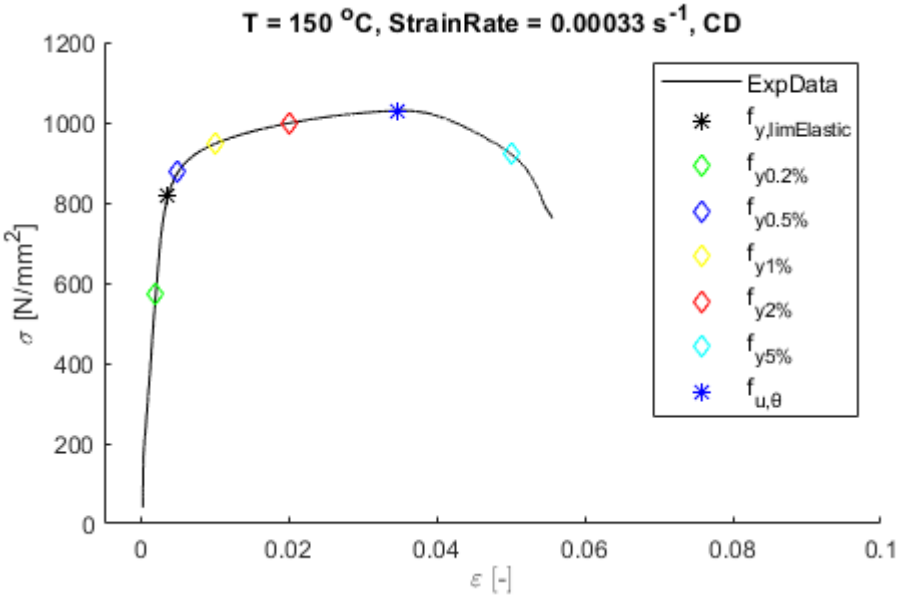

a.

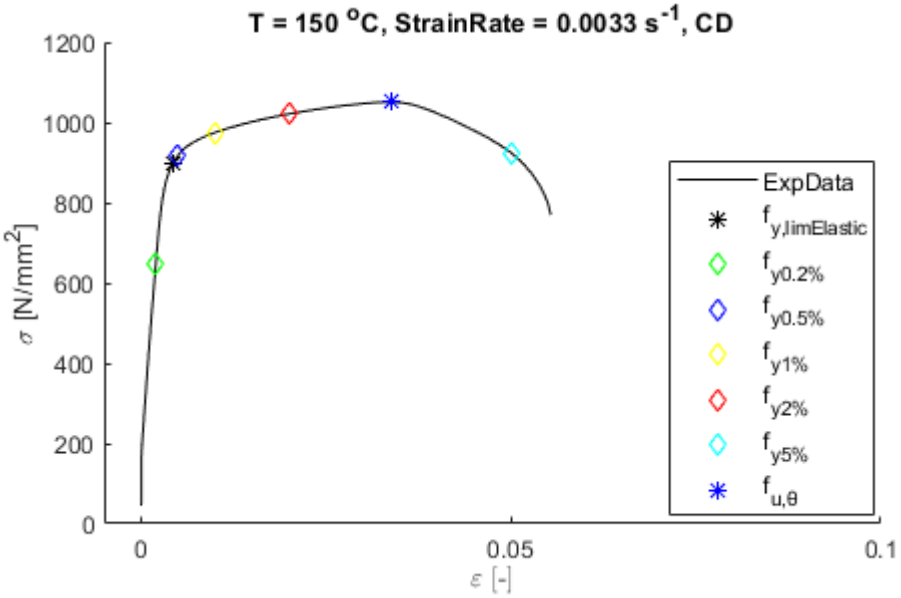

b.

Figure 4. 4. The stress-strain curve at 150 °C under: a. 0.00033 s^{-1} strain rate; b. 0.0033 s^{-1} strain rate.

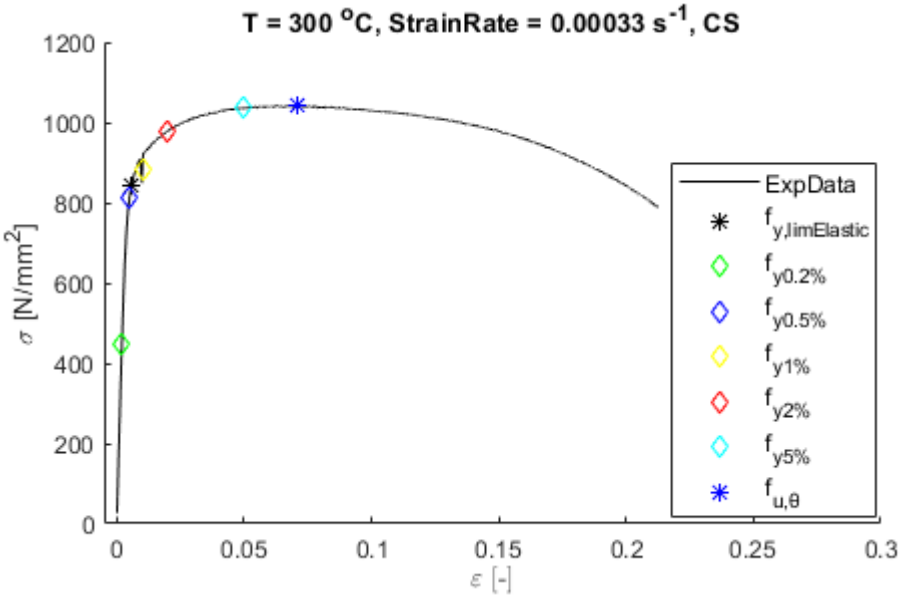

a.

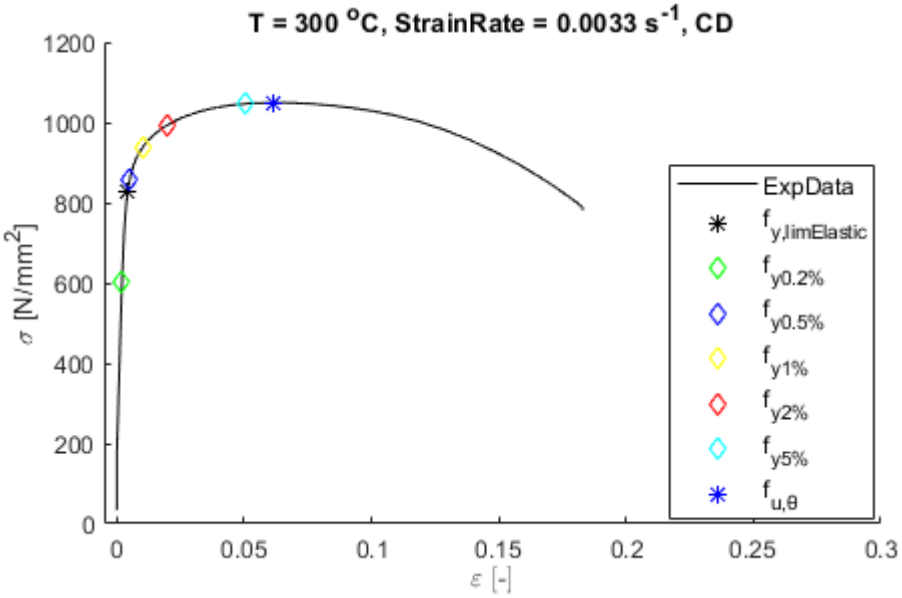

b.

Figure 4. 5. The stress-strain curve at 300 °C under: a. 0.00033 s^{-1} strain rate; b. 0.0033 s^{-1} strain rate.

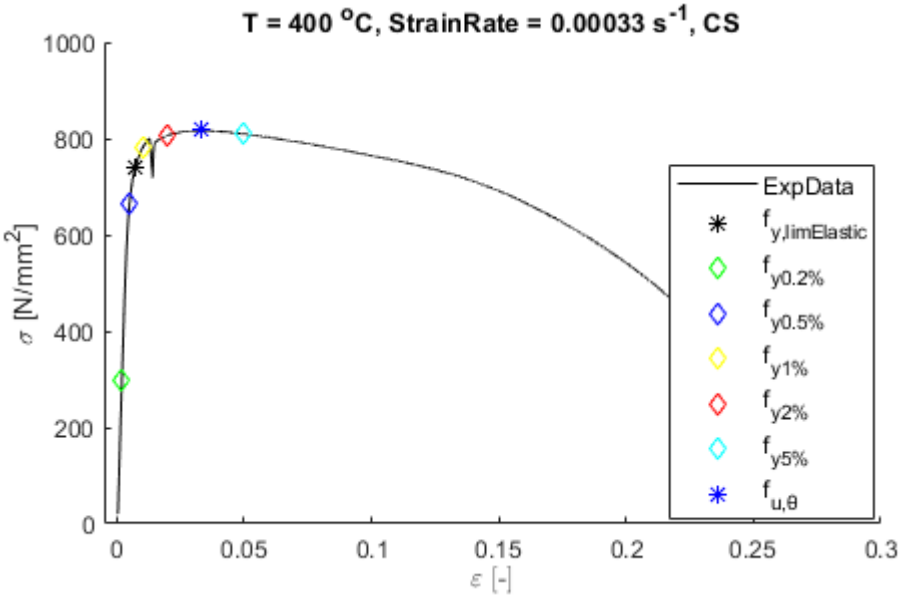

a.

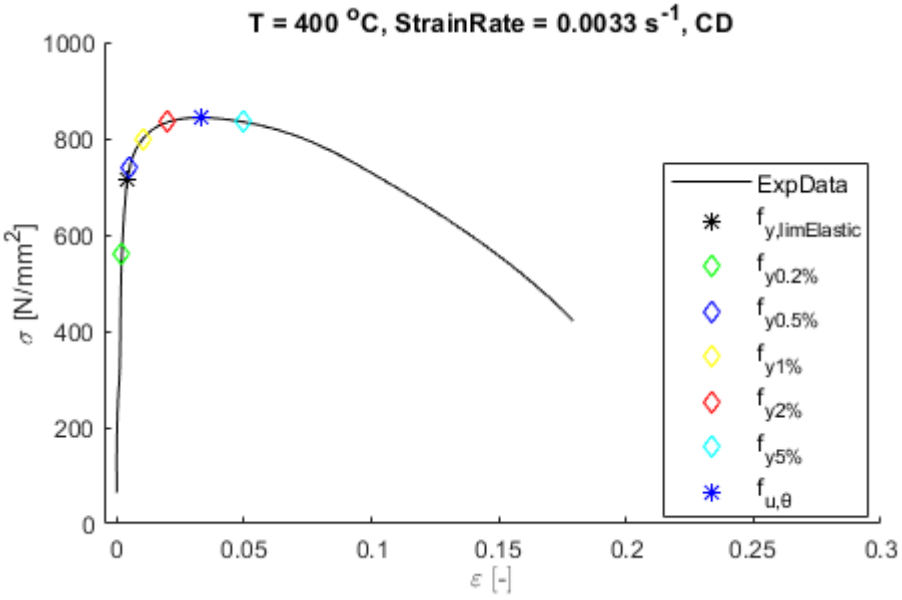

b.

Figure 4. 6. The stress-strain curve at 400 °C under: a. 0.00033 s^{-1} strain rate; b. 0.0033 s^{-1} strain rate.

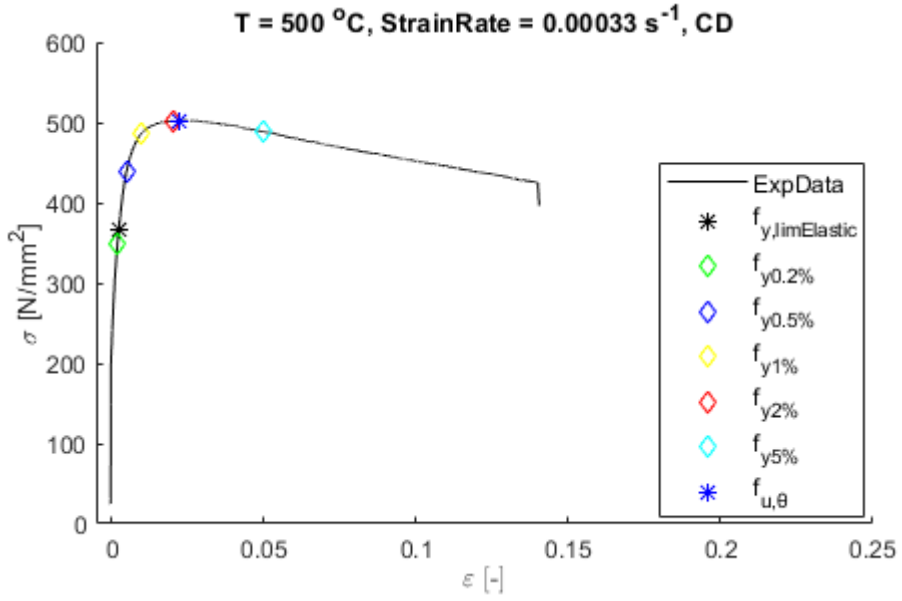

a.

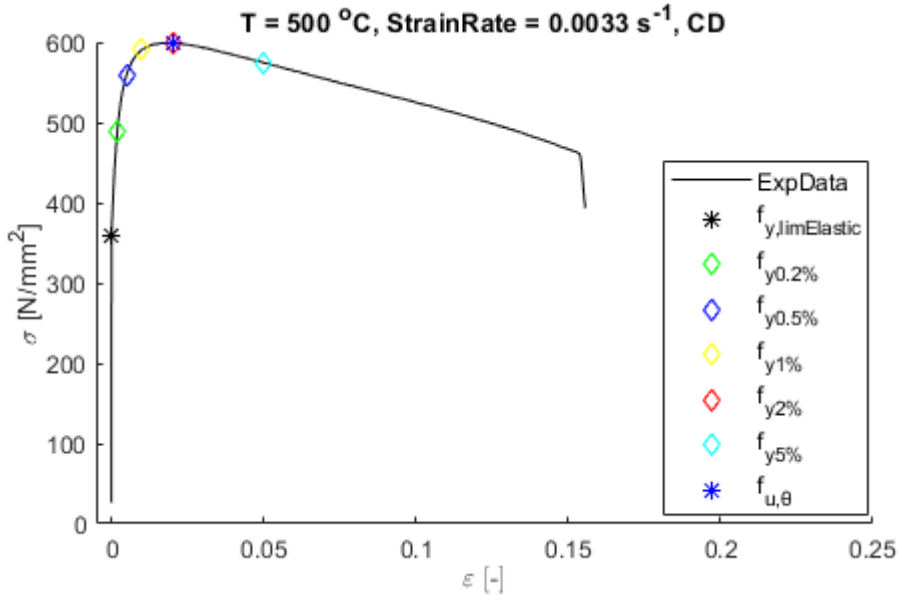

b.

Figure 4. 7. The stress-strain curve at 500 °C under: a. 0.00033 s^{-1} strain rate; b. 0.0033 s^{-1} strain rate.

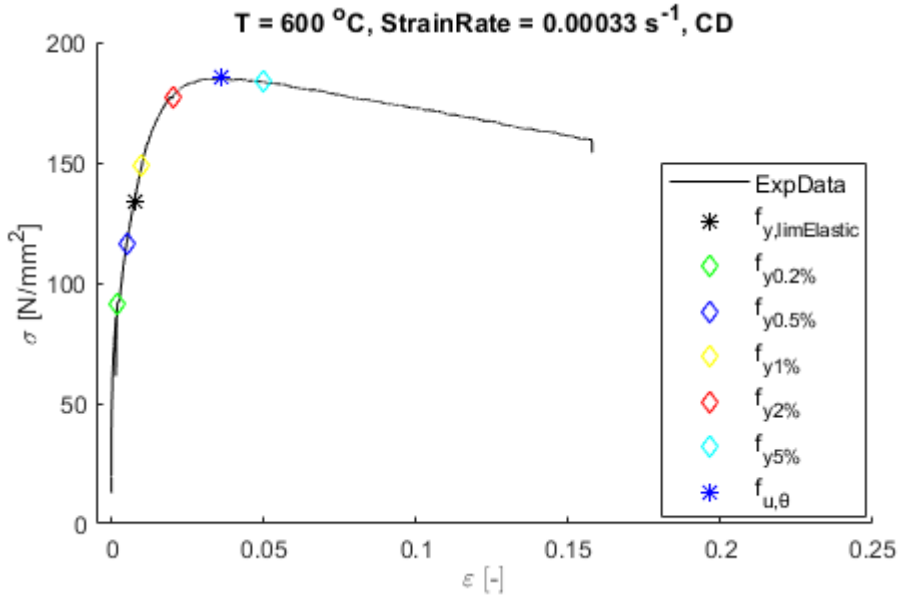

a.

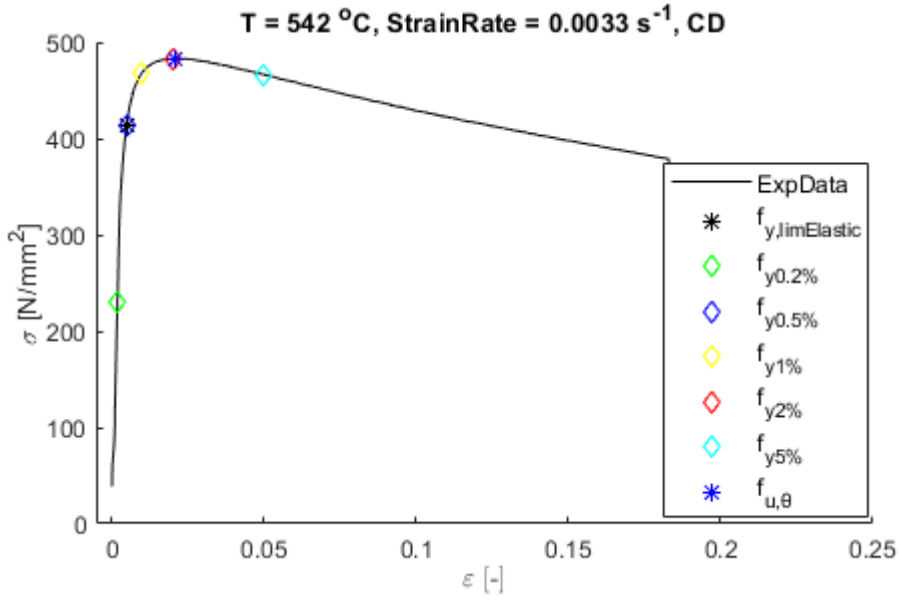

b.

Figure 4. 8. The stress-strain curve at: a. 600 °C under 0.00033 s^{-1} strain rate; b. 542 °C under 0.0033 s^{-1} strain rate.

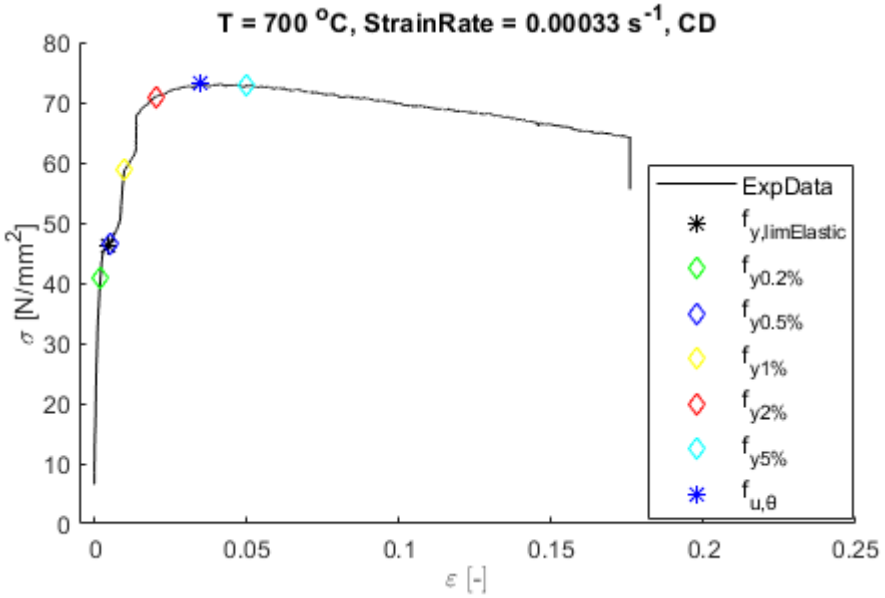

a.

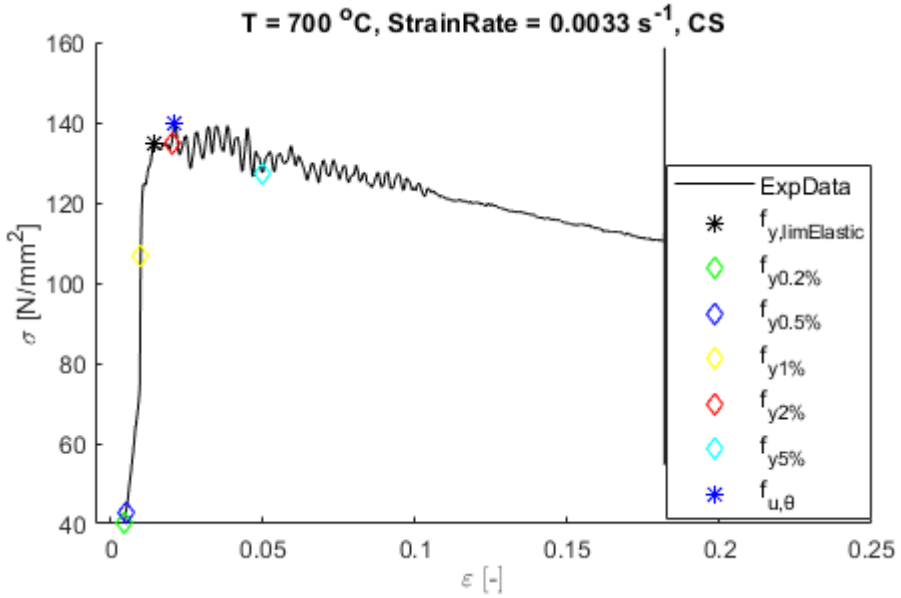

b.

Figure 4. 9. The stress-strain curve at 700 °C under: a. 0.00033 s^{-1} strain rate; b. 0.0033 s^{-1} strain rate.

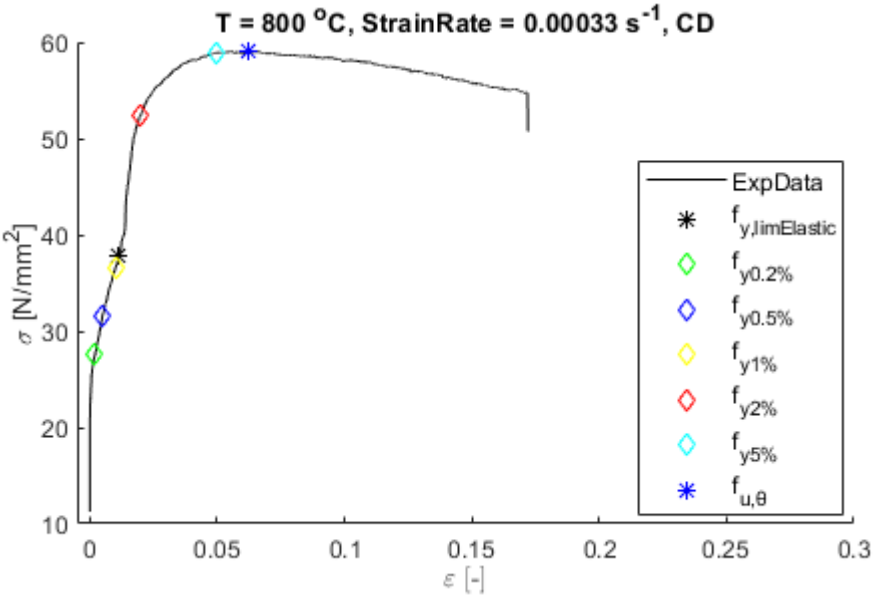

a.

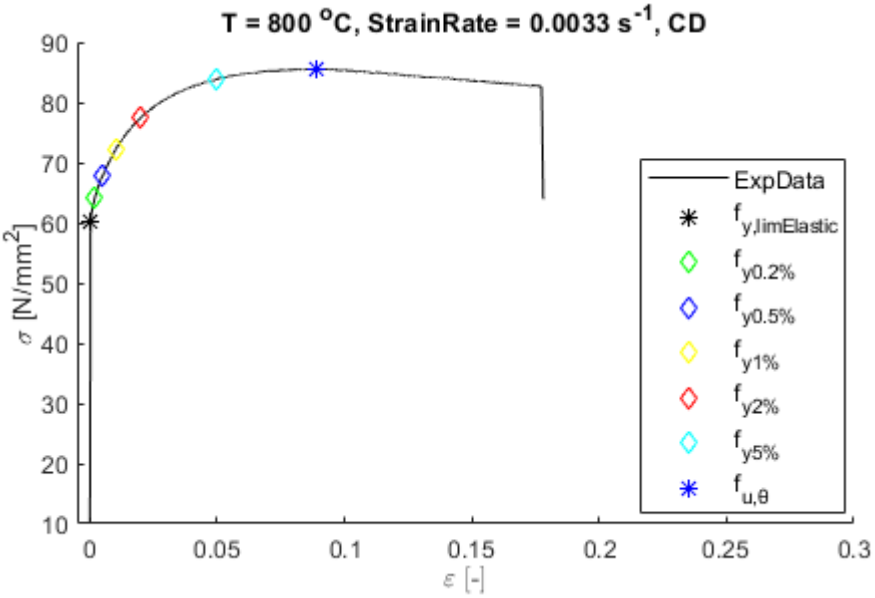

b.

Figure 4. 10. The stress-strain curve at 800 °C under: a. 0.00033 s^{-1} strain rate; b. 0.0033 s^{-1} strain rate.

The stress-strain curves recorded for each temperature, with a slow strain rate of 0.000033 s^{-1} and a high strain rate of 0.02 s^{-1}, respectively, are shown in Figure 4. 11– Figure 4. 19. For tests realized at normal temperature and at 150 °C, the yield strength remains consistent at 0.5% strain, so the strain rate has no

influence at these temperatures. The same observation related to little connection between the strain rate and yield strength was made for temperatures between 300 °C and 500 °C, where the yield strength can be considered at 1% strain. In contrast, the strain rate influences the yield strength for temperatures of 600 °C and above. Especially for higher strain rates, the material becomes more brittle and tensile strength is reached before the 2% strain is developed. Therefore, the yield strength is better to be considered at 0.5% for high strain rate, and at 1% for low strain rate.

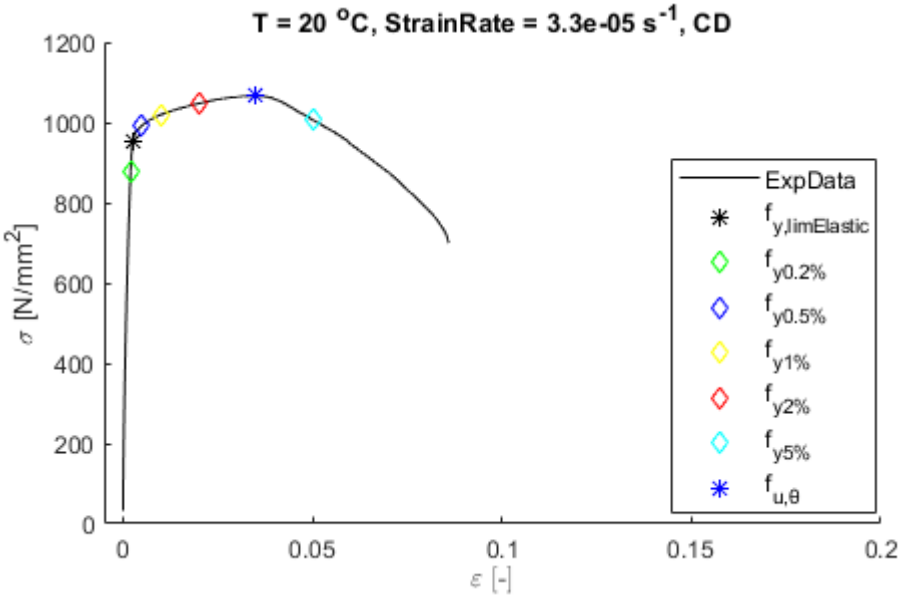

a.

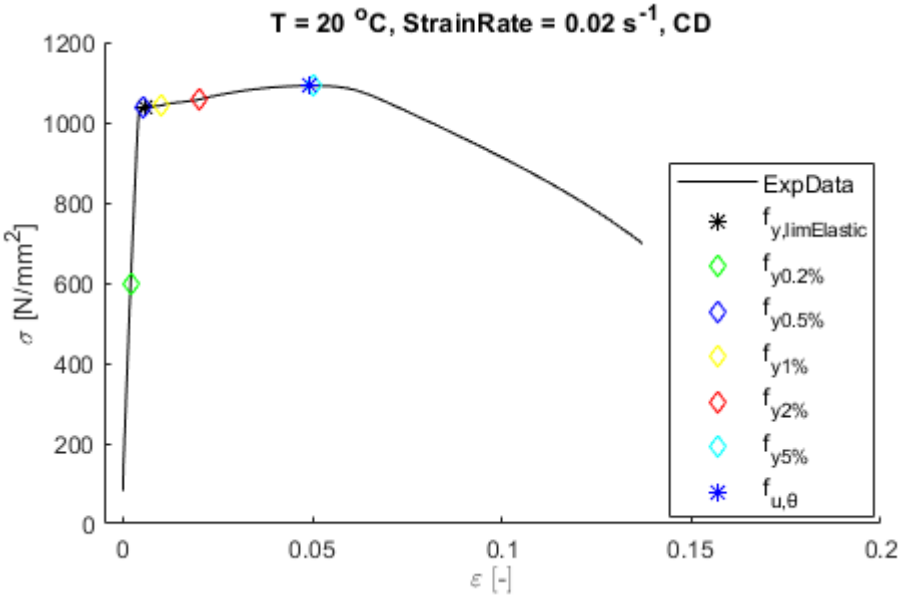

b.

Figure 4. 11. The stress-strain curve at 20 °C under: a. 0.000033 s^{-1} strain rate; b. 0.02 s^{-1} strain rate.

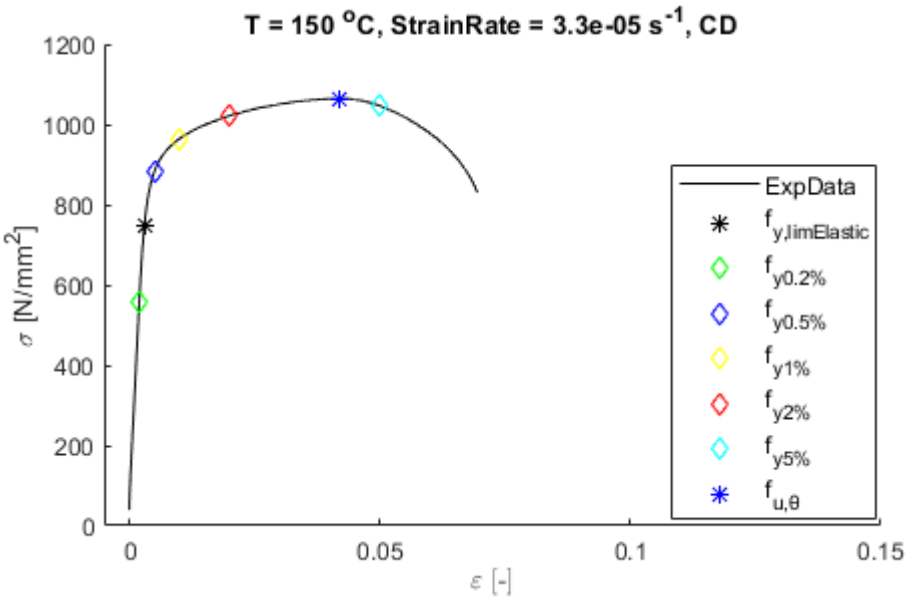

a.

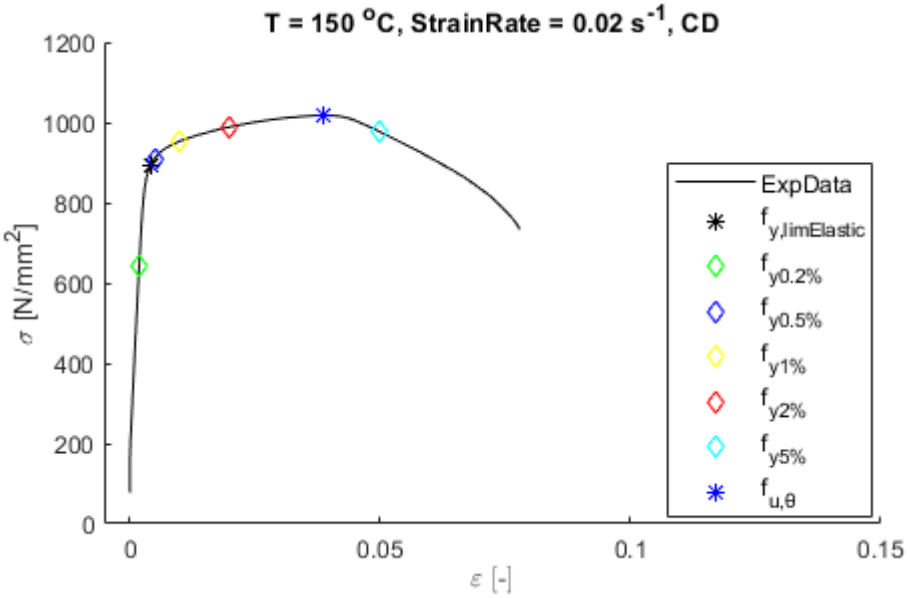

b.

Figure 4. 12. The stress-strain curve at 150 °C under: a. 0.000033 s^{-1} strain rate; b. 0.02 s^{-1} strain rate.

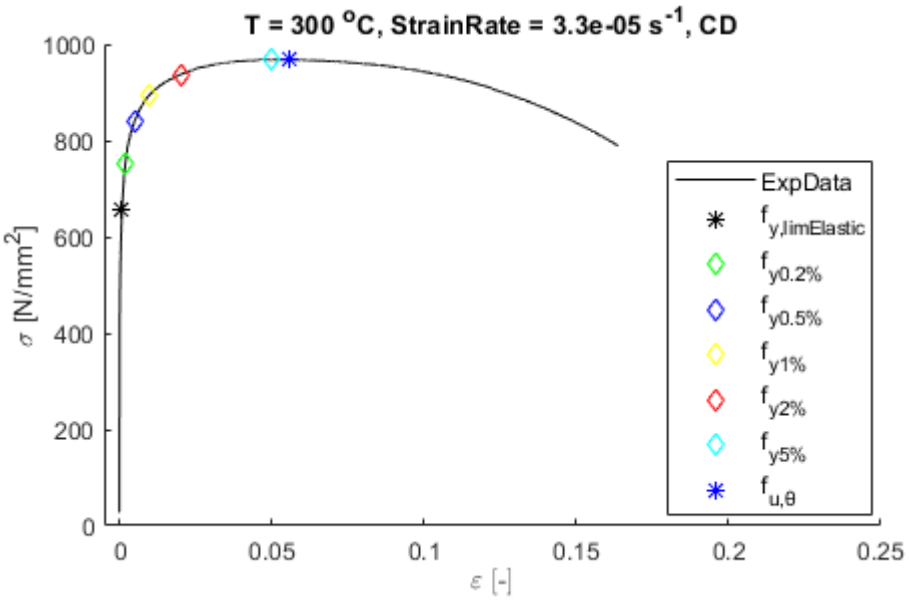

a.

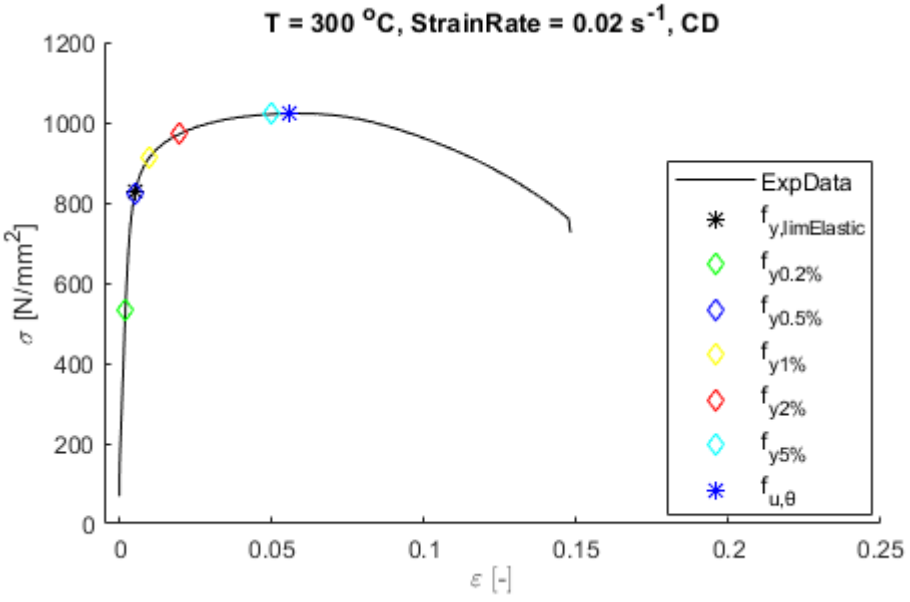

b.

Figure 4. 13. The stress-strain curve at 300 °C under: a. 0.000033 s^{-1} strain rate; b. 0.02 s^{-1} strain rate.

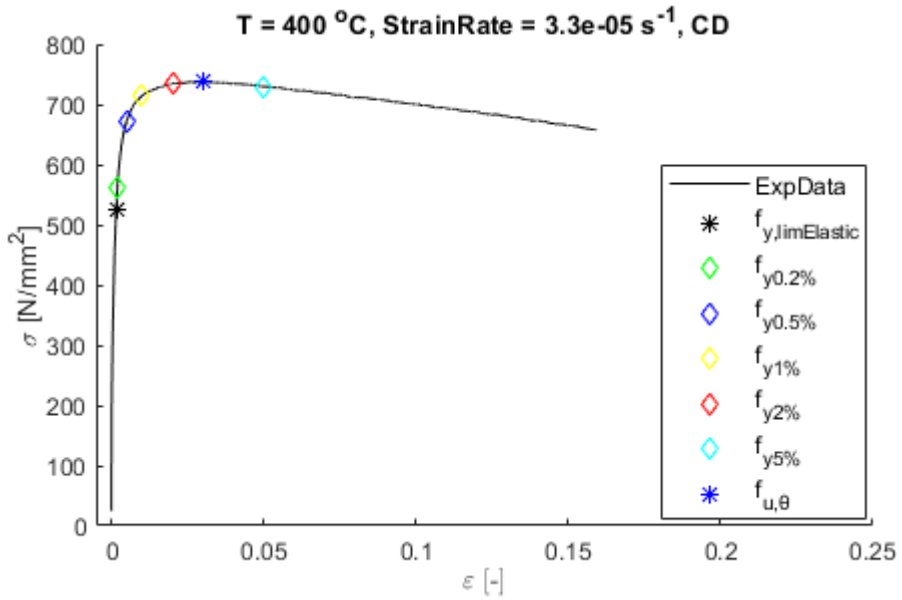

a.

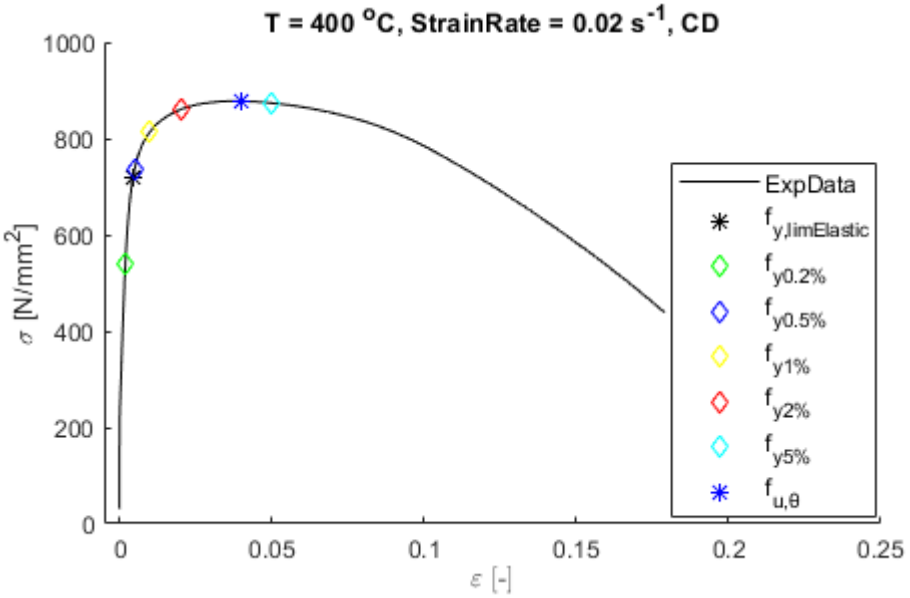

b.

Figure 4. 14. The stress-strain curve at 400 °C under: a. 0.000033 s^{-1} strain rate; b. 0.02 s^{-1} strain rate.

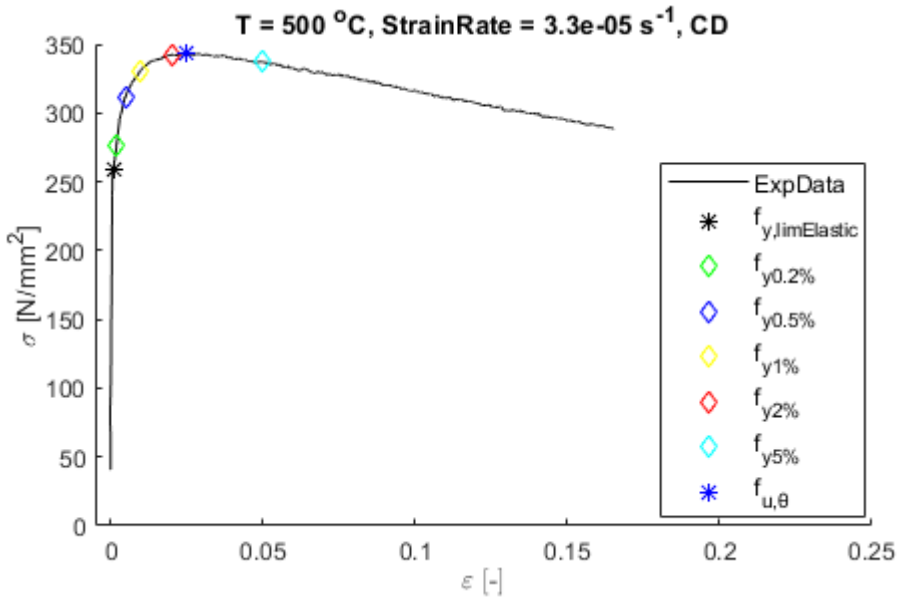

a.

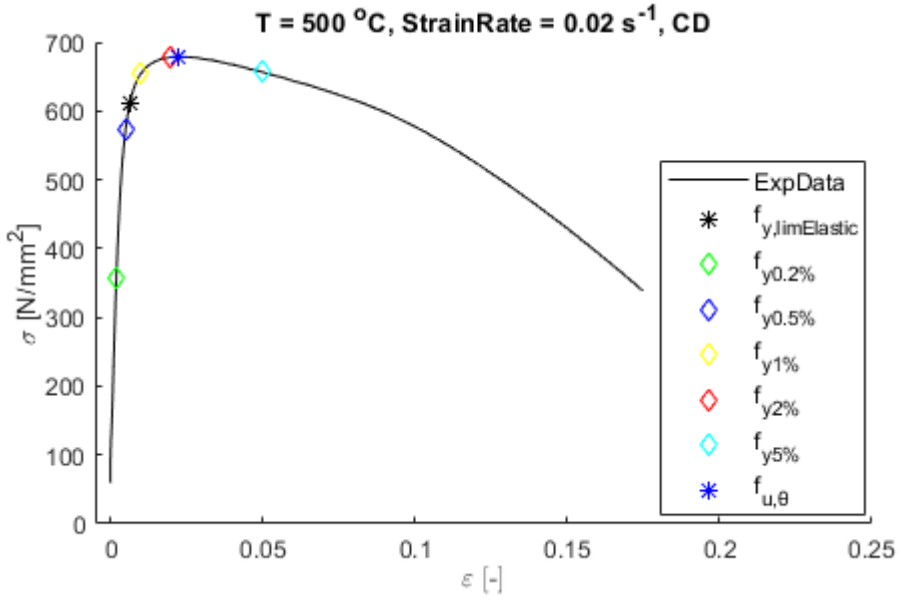

b.

Figure 4. 15. The stress-strain curve at 500 °C under: a. 0.000033 s^{-1} strain rate; b. 0.02 s^{-1} strain rate.

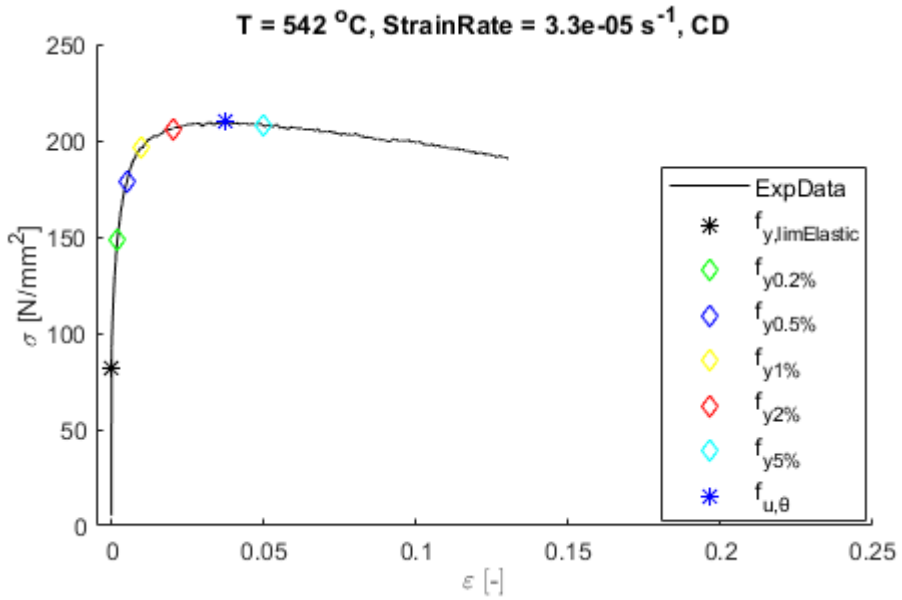

a.

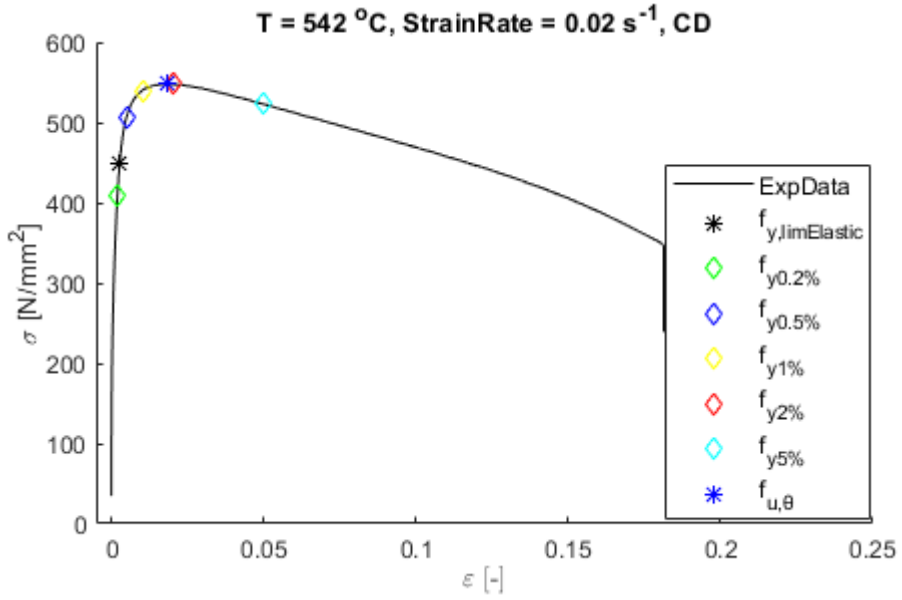

b.

Figure 4. 16. The stress-strain curve at 542 °C under: a. 0.000033 s^{-1} strain rate; b. 0.02 s^{-1} strain rate.

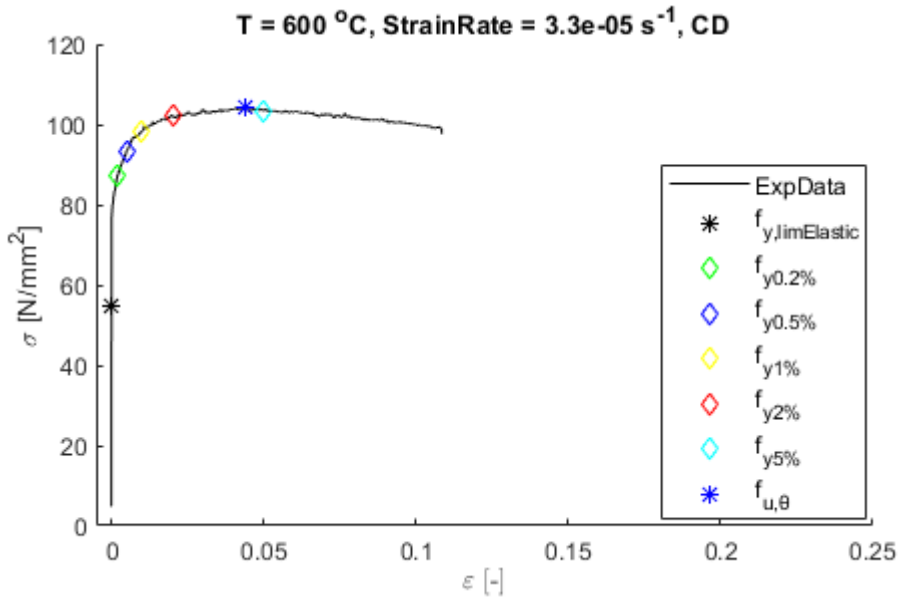

a.

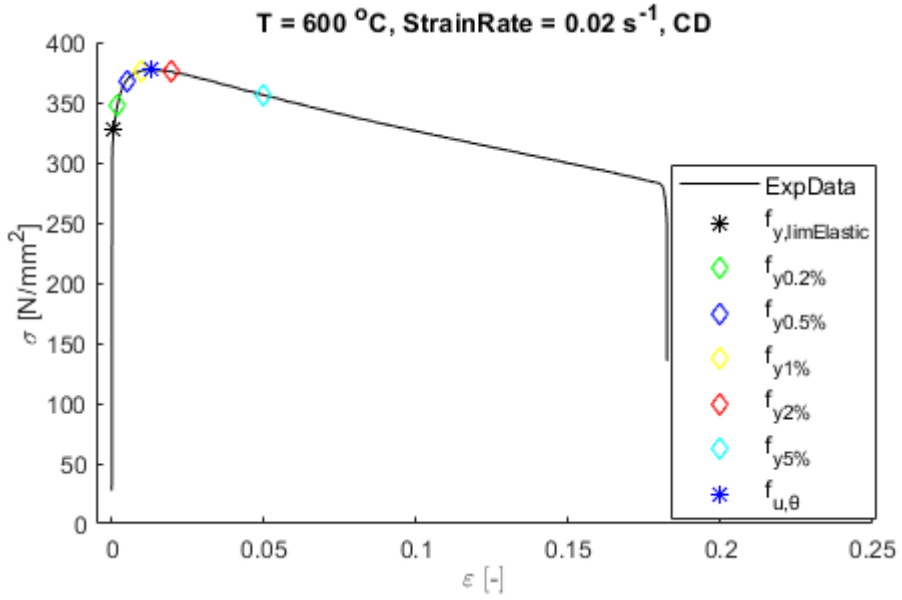

b.

Figure 4. 17. The stress-strain curve at 600 °C under: a. 0.000033 s^{-1} strain rate; b. 0.02 s^{-1} strain rate.

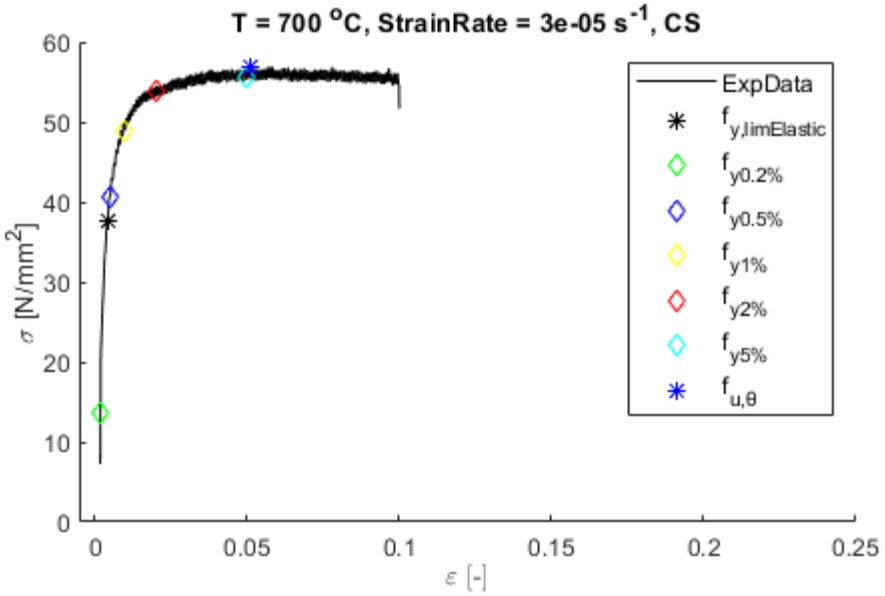

a.

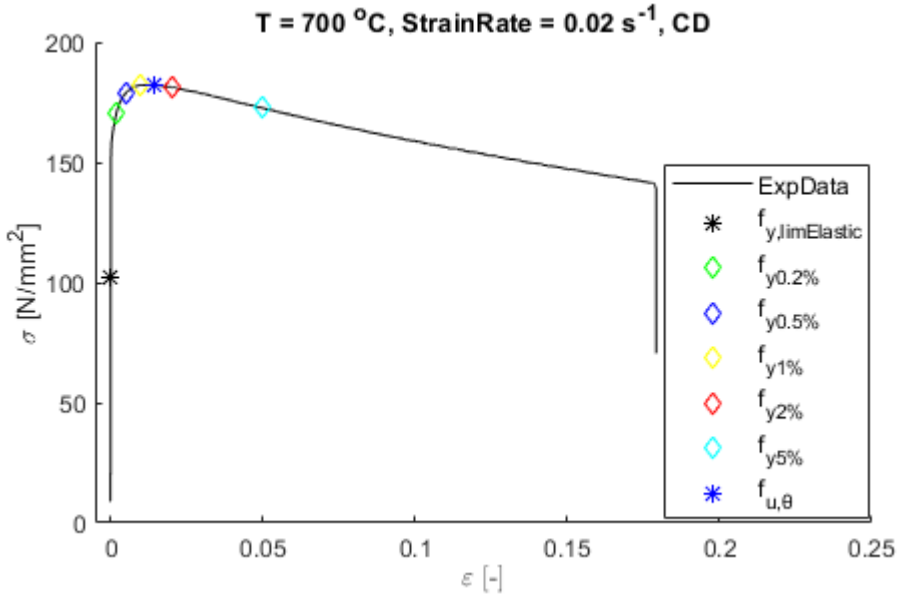

b.

Figure 4. 18. The stress-strain curve at 700 °C under: a. 0.000033 s^{-1} strain rate; b. 0.02 s^{-1} strain rate.

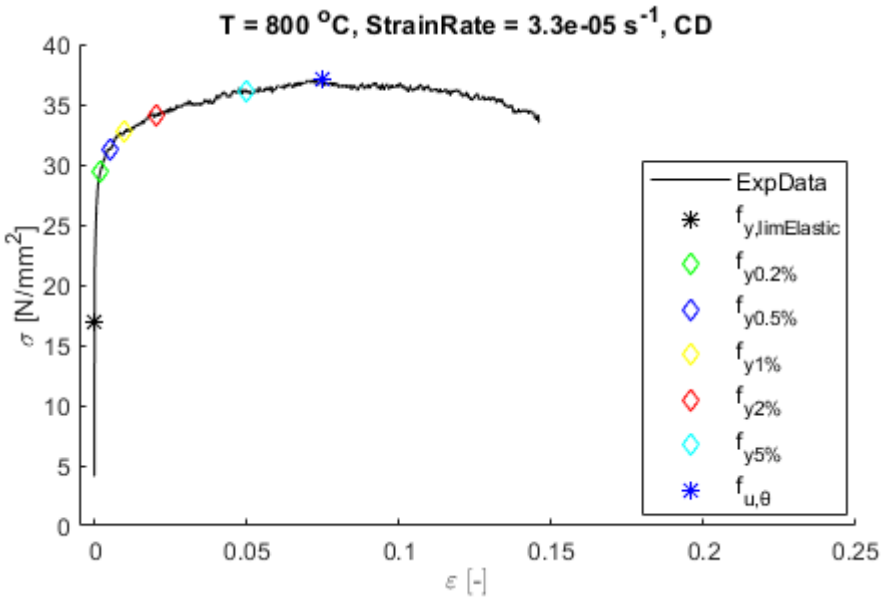

a.

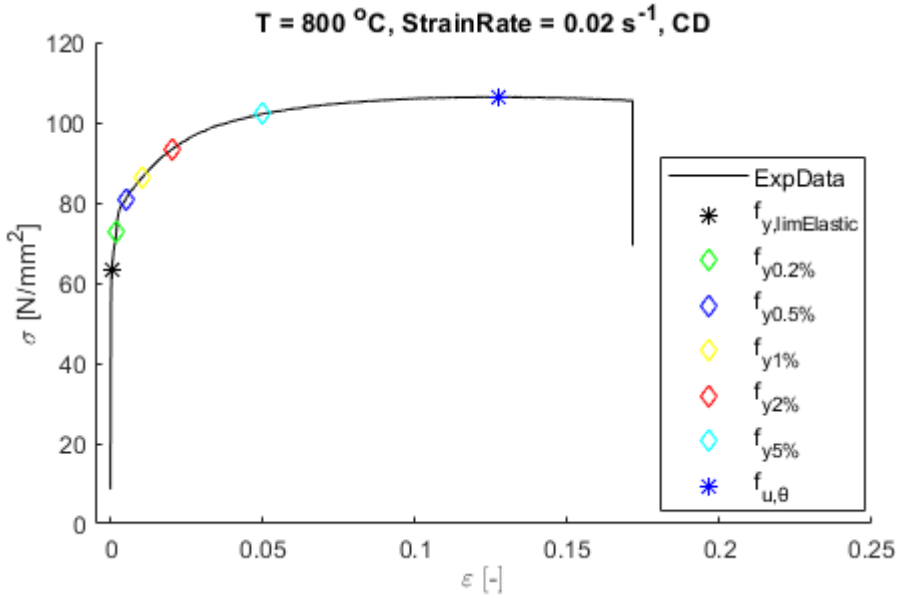

b.

Figure 4. 19. The stress-strain curve at 800 °C under: a. 0.000033 s^{-1} strain rate; b. 0.02 s^{-1} strain rate.

On the other hand, the value of yield strength taken at 5% is not realistic for the present study, as the strain of 5% is larger than the strain at tensile strength in most of the configurations tested.

Table 4. 1. shows a summary of visual observations conducted above on stress-strain curves to identify the optimal position of the yield strength. However, to achieve greater accuracy, a more precise approach will be discussed in the subsequent chapter, where a calculation of the modulus of elasticity at various positions of yield strength will be presented.

Table 4. 1. The position of yield strength function of temperature and strain rate

Temperature [°C]	20 - 150	300 - 542	600 - 800	Strain Rate [s^{-1}]
x% strain for considering f_y	0.5%	1%	2%	0.00033 – 0.0033
	0.5%	1%	1%	0.000033
	0.5%	1%	0.5%	0.02

4.3 Modulus of Elasticity

The modulus of elasticity is defined as the slope of the linear elastic range (EN1933-1-2, 2005). As the yield strength is defined as the boundary value between the elastic and plastic range, then we can assume that the modulus of elasticity can be computed as:

$E=f_y/\varepsilon_y$ for 20 °C, [4.2]

and $E_\theta=f_{y,\theta}/\varepsilon_{y,\theta}$ for elevated temperature [4.3]

Chapter 3 of EN1993-1-2 (2005) provides the reduction factors, $k_{E,\theta}$, for the computation of modulus of elasticity for steel material (Table 4. 2.).

Table 4. 2. The reduction factors for modulus of elasticity (EN1993-1-2, 2005) and the computed modulus of elasticity

Temperature [°C]	$k_{E,\theta}$	E_θ
20	1	210000
100	1	210000
200	0.9	189000
300	0.8	168000
400	0.7	147000
500	0.6	126000
600	0.31	65100
700	0.13	27300
800	0.09	18900

Within the current research, the modulus of elasticity was computed from the experimentally obtained curves, for different points on the stress-strain curve, and

compared with the reduced modulus of elasticity using the reduction factors from EN1993-1-2 (2005) (Table 4. 2.).

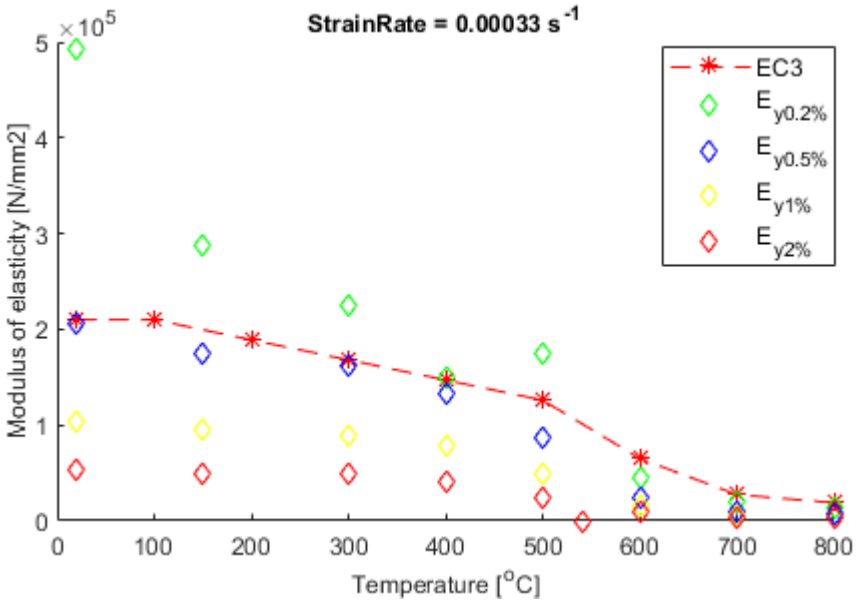

Figure 4. 20. The modulus of elasticity with temperature, for tests realized under 0.00033 s^{-1} strain rate.

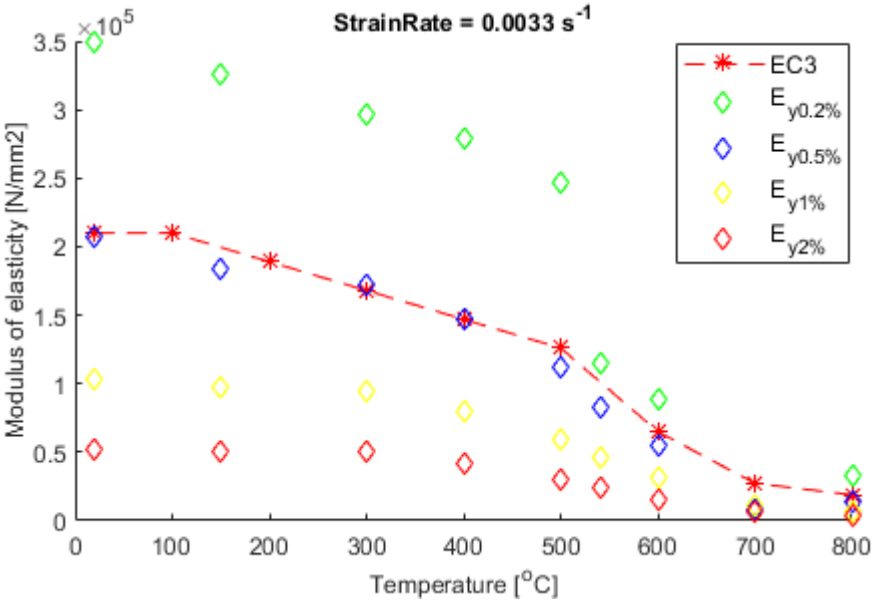

Figure 4. 21. The modulus of elasticity with temperature, for tests realized under 0.0033 s^{-1} strain rate.

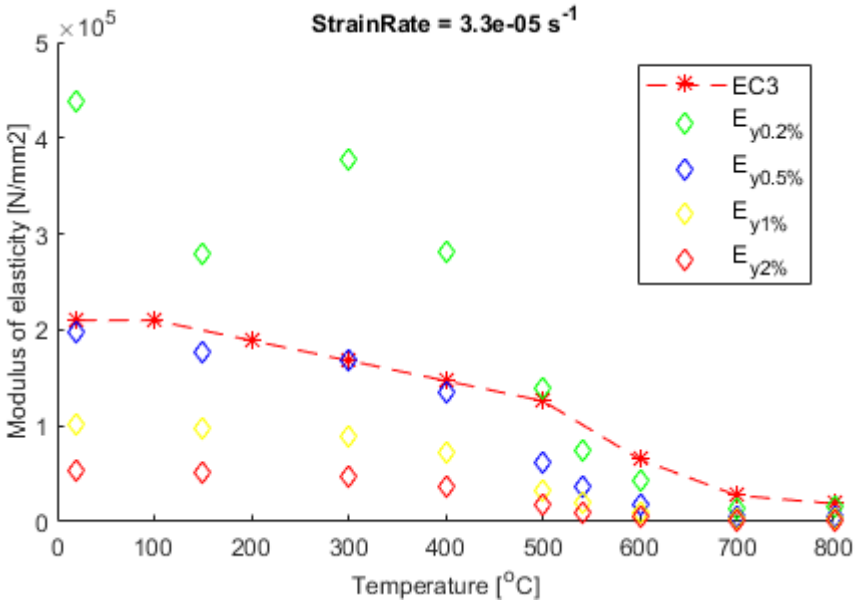

Figure 4. 22. The modulus of elasticity with temperature, for tests realized under 0.000033 s^{-1} strain rate.

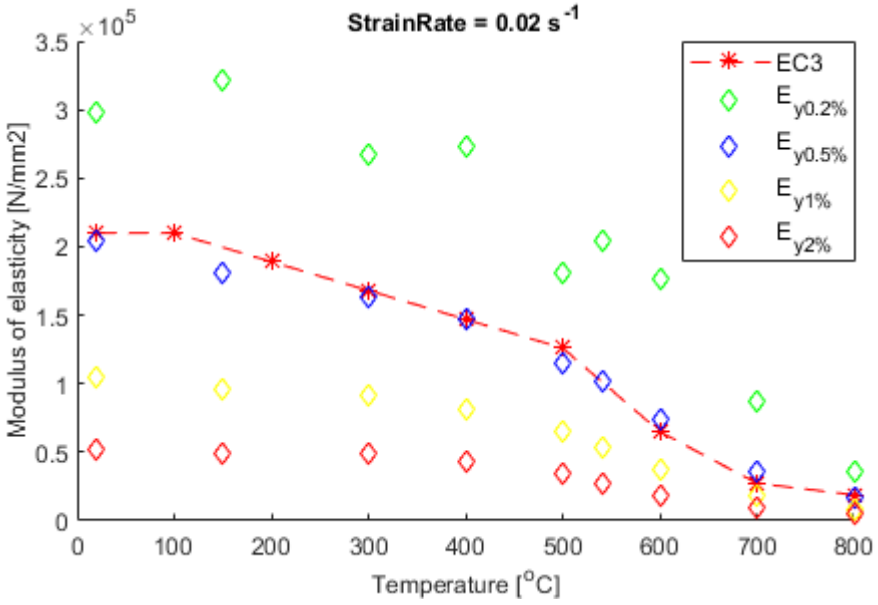

Figure 4. 23. The modulus of elasticity with temperature, for tests realized under 0.02 s^{-1} strain rate.

Figure 4. 20. and Figure 4. 21. show a good agreement between the modulus of elasticity computed by considering the yield strength at 0.5% strain and the values computed with the reduction factors from EN1993-1-2 (2005). As well, the tests were

conducted under a higher strain rate, of 0.02 s^{-1}, the yield strength should be considered at 0.5%, as shown in Figure 4. 23. The only difference observed is in Figure 4. 22., where the modulus of elasticity presents better agreement with the Eurocode when computed at 0.2% strain, for temperatures equal with 500 °C and higher.

Therefore, the yield strength will be used further taken at 0.5% strain. Even for the tests at very low strain rate, of 0.000033 s^{-1}, the yield stress is taken at 0.5% strain, in order to be constant in the results assessment. This assumption is possible as the results are in the safe side, i.e. the yield strength at 500 °C and above are underestimated when the strain rate is 0.000033 s^{-1} (Figure 4. 22.).

4.4 Tensile Strength

The tensile strength, $f_{u,\theta}$, is defined by the ISO 6892-2 (2011) as the stress corresponding to the maximum force.

Figure 4. 24. until Figure 4. 32. present the stress-strain curves recorded at normal temperature and elevated temperatures, under different strain rates between 0.000033 s^{-1} until 0.06 s^{-1}. As expected, for all strain rates, the temperature has a large impact over the specimen behaviour. With the increase of the temperature the tensile strength decreases, while the material softens.

EN1993-1-2 (2005) provides a model for the stress-strain curve of steel under elevated temperatures, with a yielding plateau, in which the yield limit and the tensile strength have the same value.

As shown in Figure 4. 24. until Figure 4. 32., the experimental data shows a clear plateau only for the curves recorded at 600 °C or above, for strain rates up to 0.0033 s^{-1}, and at 700 °C or above, for strain rates higher than 0.0033 s^{-1}.

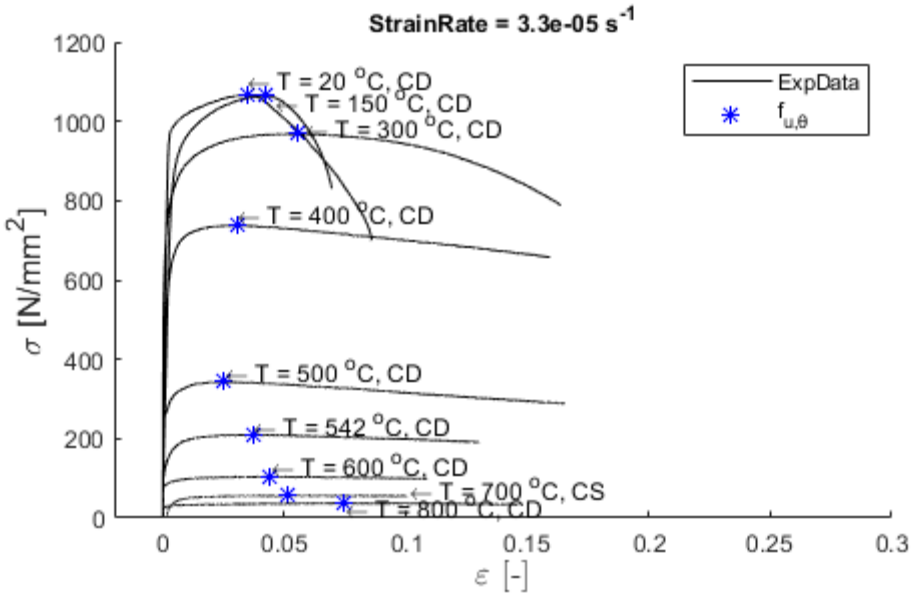

Figure 4. 24. The stress-strain curves at different temperatures, under 0.000033 s^{-1} strain rate.

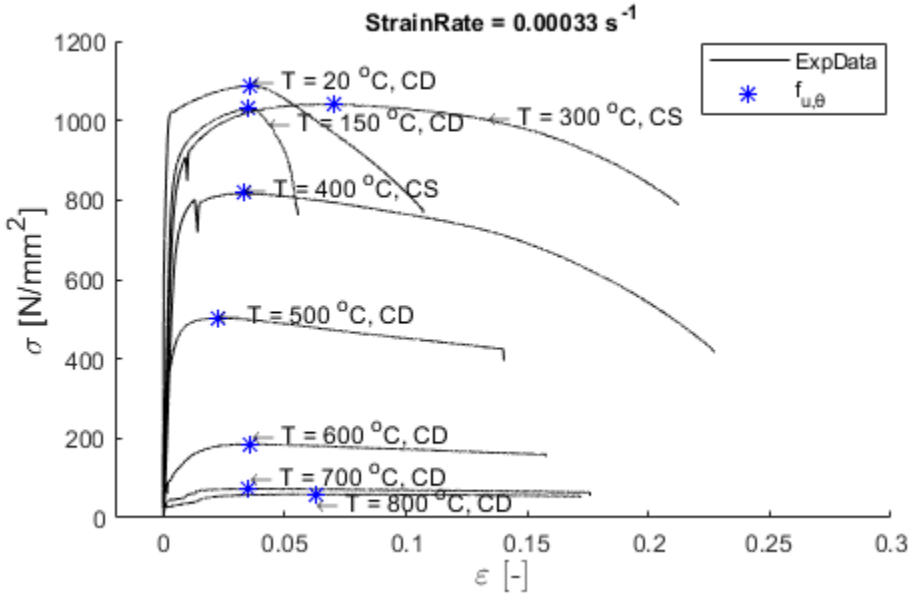

Figure 4. 25. The stress-strain curves at different temperatures, under 0.00033 s^{-1} strain rate.

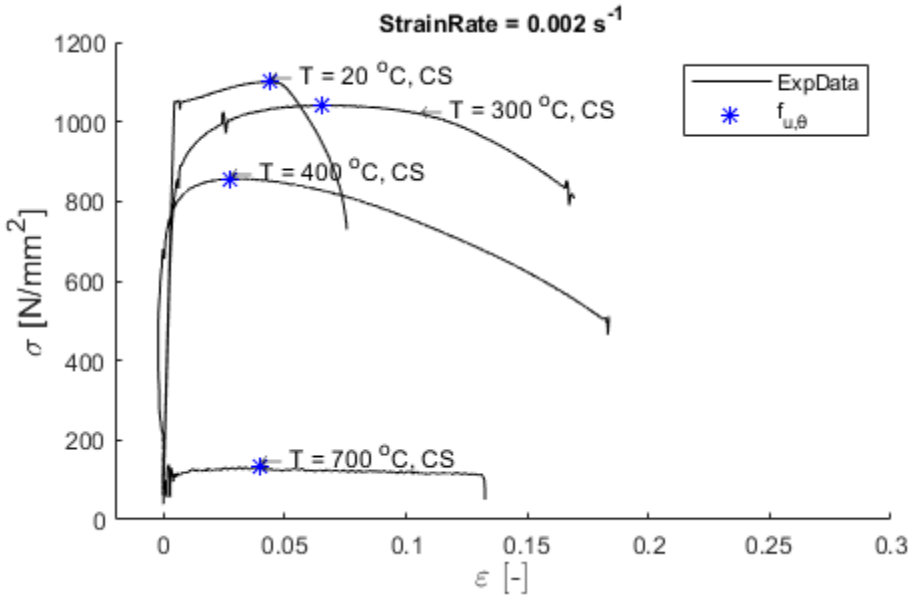

Figure 4. 26. The stress-strain curves at different temperatures, under 0.002 s^{-1} strain rate.

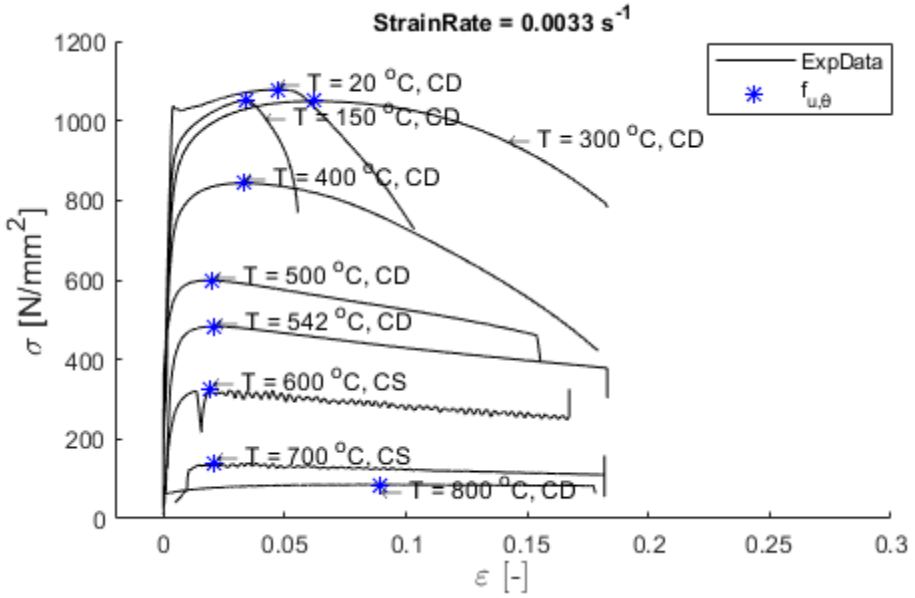

Figure 4. 27. The stress-strain curves at different temperatures, under 0.0033 s^{-1} strain rate.

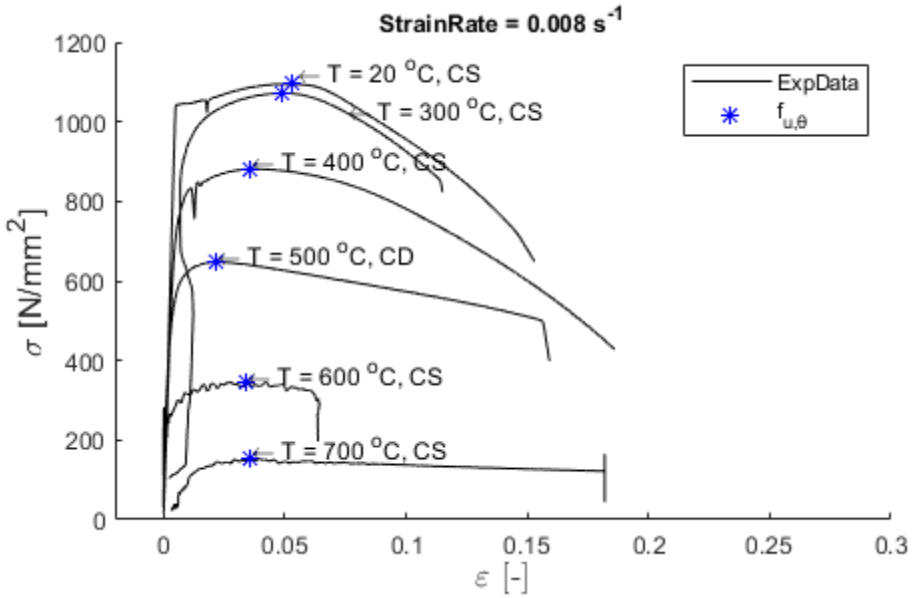

Figure 4. 28. The stress-strain curves at different temperatures, under 0.008 s^{-1} strain rate.

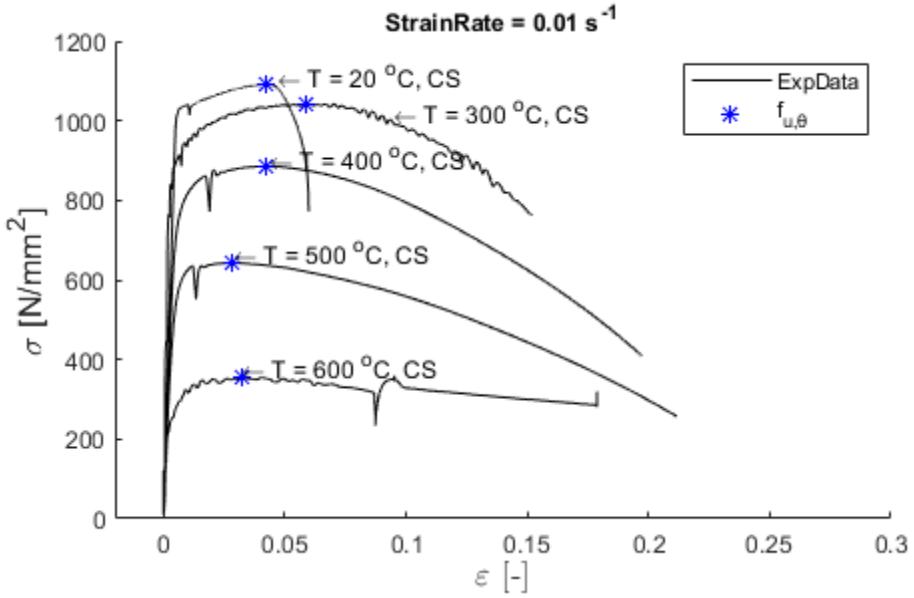

Figure 4. 29. The stress-strain curves at different temperatures, under 0.01 s^{-1} strain rate.

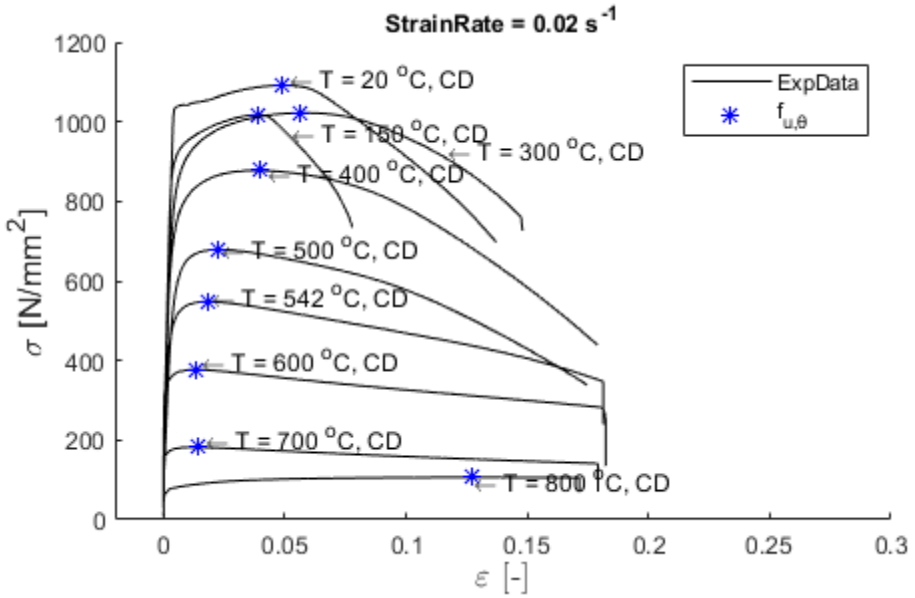

Figure 4. 30. The stress-strain curves at different temperatures, under 0.02 s^{-1} strain rate.

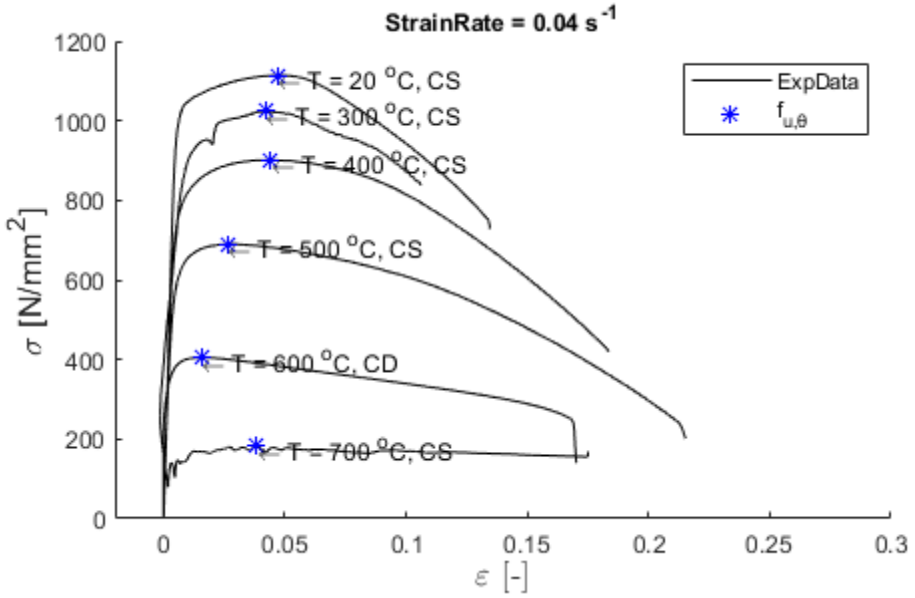

Figure 4. 31. The stress-strain curves at different temperatures, under 0.04 s^{-1} strain rate.

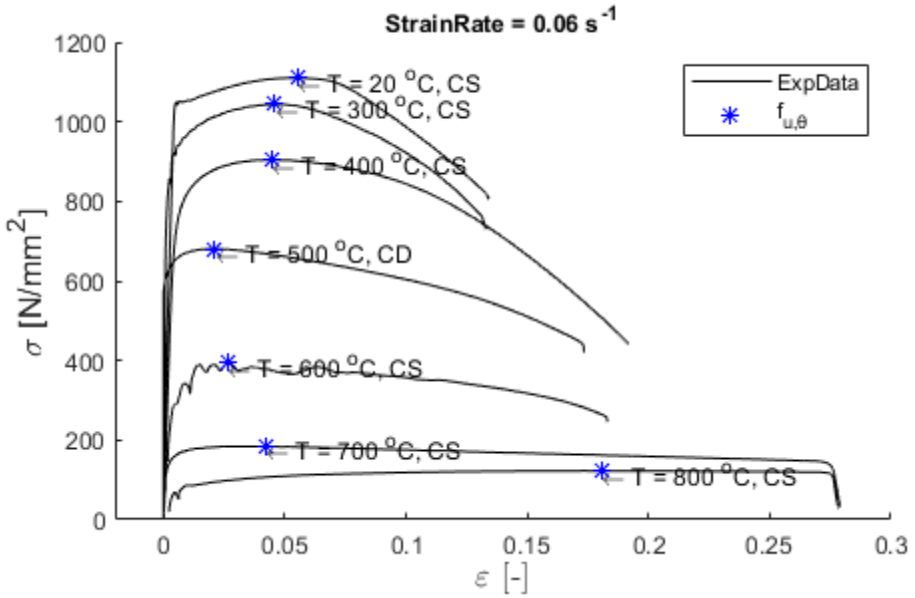

Figure 4. 32. The stress-strain curves at different temperatures, under 0.06 s^{-1} strain rate.

The impact of strain rate over the material behaviour is highlighted in Figure 4. 33. until Figure 4. 41. For the entire range of strain rate values considered, the stress-strain curves show little difference in terms of tensile strength, when tested at temperatures below 400 °C. On the other hand, the tensile strength varies due to the strain rate considered during the experimental tests with 20% for a temperature of 500 °C, and between 35% and 43%, for higher temperatures.

Table 4. 3. shows the variation in percentage of the value of tensile strength, obtained for each temperature, with different strain rates. The variation was computed as the difference between the tensile strength obtained in a test under a certain strain rate, and the mean value of tensile strength obtained in all the tests under different strain rates, for one given temperature.

Table 4. 3. The variation of tensile strength with the strain rate.

Temperature [°C]	20	150	300	400	500	542	600	700	800
Variation [%]	1.35	2.03	2.76	6.15	20.0	43.4	34.8	40.8	42.2

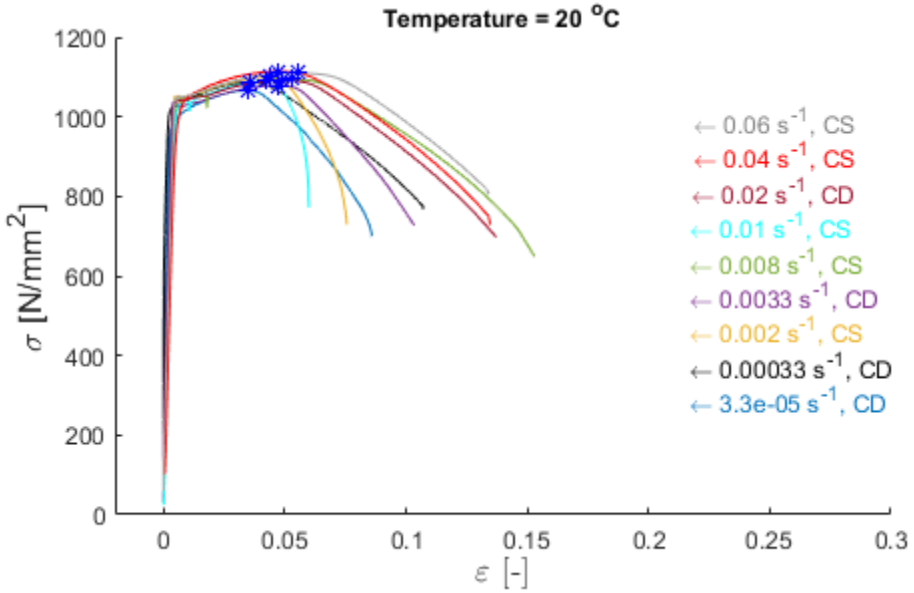

Figure 4. 33. The stress-strain curves under different strain rates, at 20 °C.

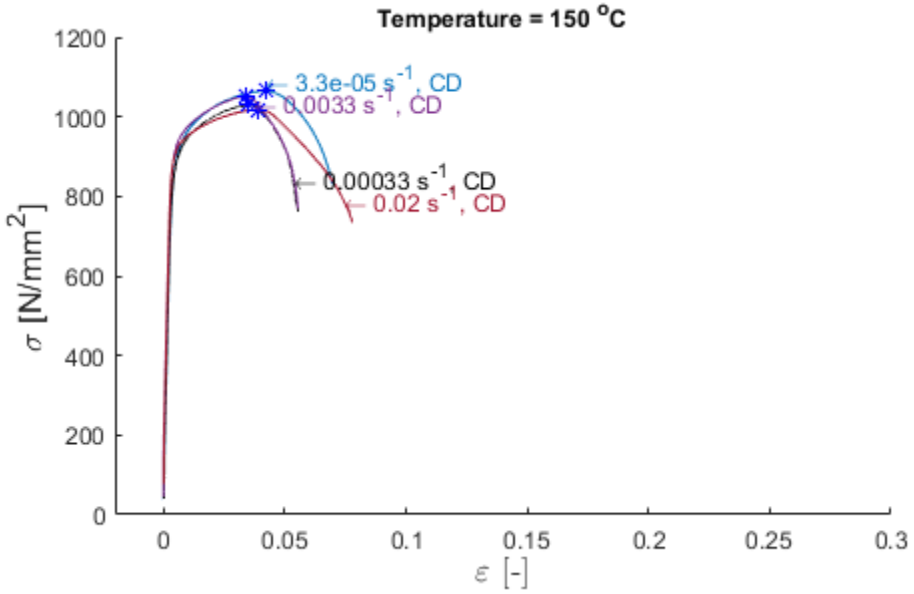

Figure 4. 34. The stress-strain curves under different strain rates, at 150 °C.

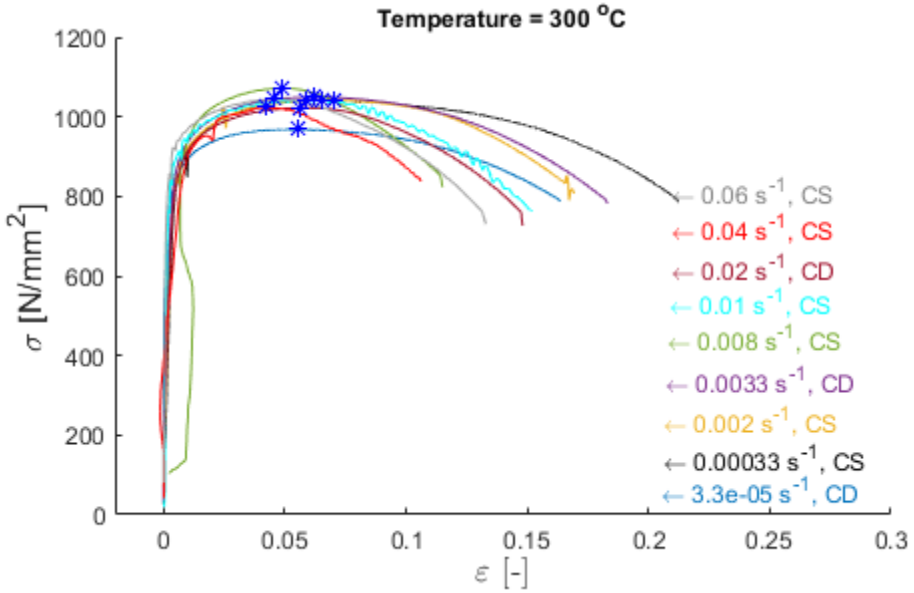

Figure 4. 35. The stress-strain curves under different strain rates, at 300 °C.

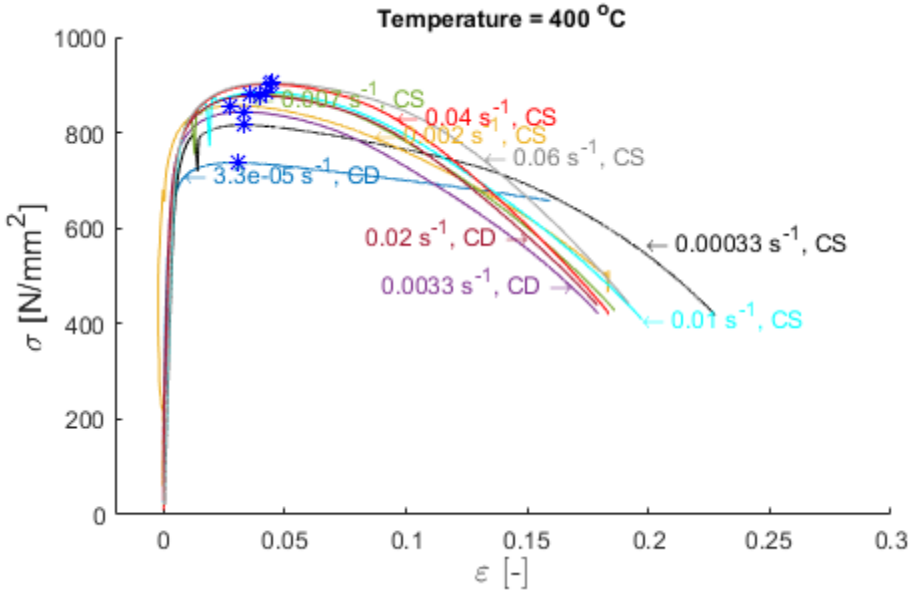

Figure 4. 36. The stress-strain curves under different strain rates, at 400 °C.

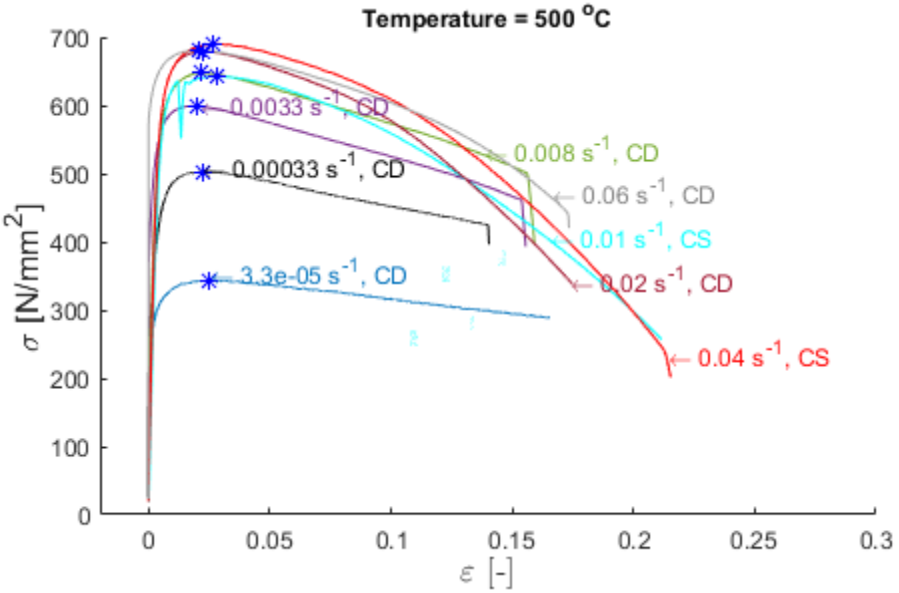

Figure 4. 37. The stress-strain curves under different strain rates, at 500 °C.

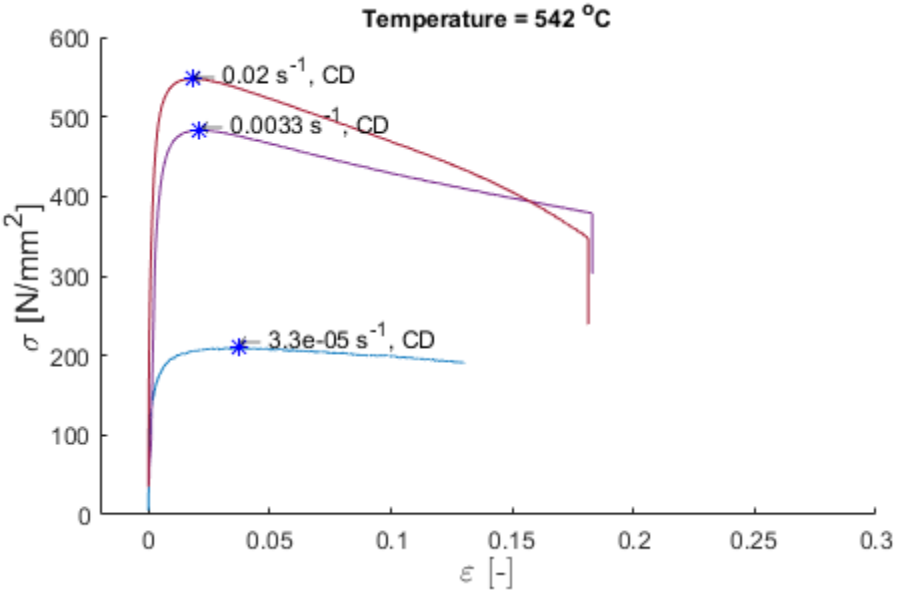

Figure 4. 38. The stress-strain curves under different strain rates, at 542 °C.

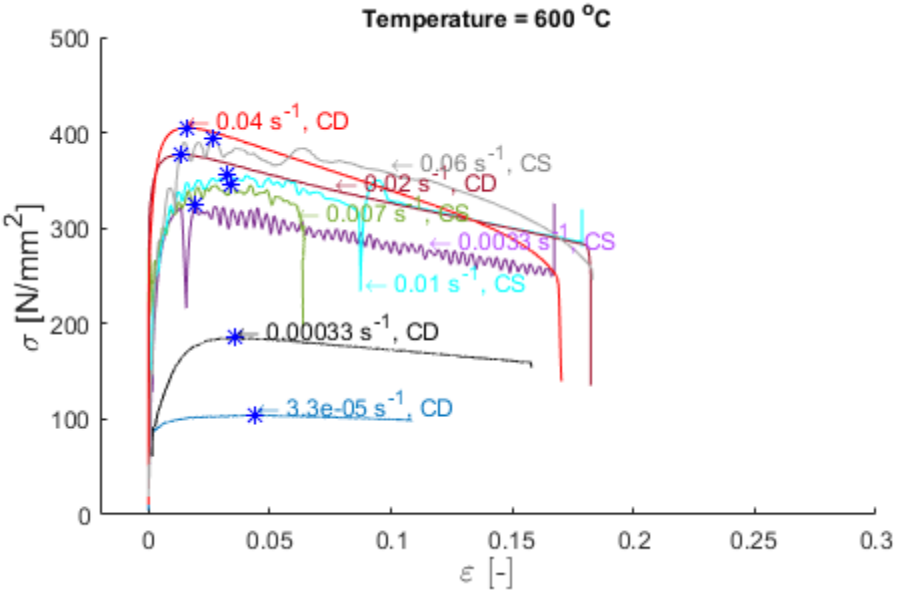

Figure 4. 39. The stress-strain curves under different strain rates, at 600 °C.

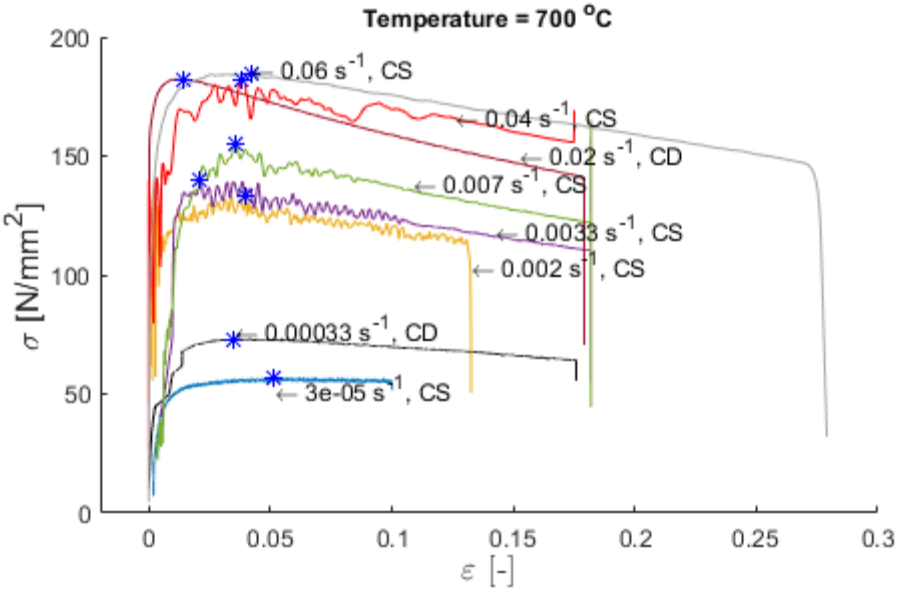

Figure 4. 40. The stress-strain curves under different strain rates, at 700 °C.

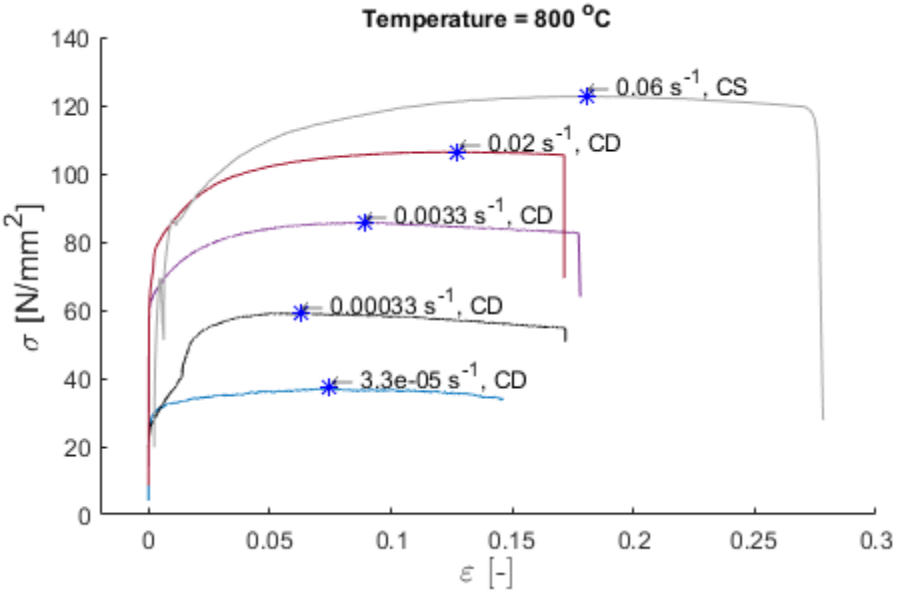

Figure 4. 41. The stress-strain curves under different strain rates, at 800 °C.

4.5 Strain Rate

The Eurocode EN1993-1-2 (2005) does not provide a straight corelation between the stress-strain curve and the strain rate. Annex B of ISO 6892-2 (2011) only mentions that relevant uncertainties might be induced in the measurements due to the strain rate considered, without quantifying them.

EN1993-1-2 (2005) provides a model to develop the stress-strain curve at elevated temperatures for mild steels and the reduction factors, k_b, for the computation of bolt strength, $f_{u,\theta}$. Both simplified methods (presented in Chapter 2.4.2) are not dependent on the strain rates. Therefore, one can obtain the material characteristics at elevated temperatures of steel, or the bolt strength, completely ignoring the strain rate that will be induced in the element during the large displacements produced under fire conditions.

Table 4. 4. presents a comparison between the tensile strength of the bolt material computed by the EN1993-1-2 (2005), $f_{u,\theta}$, and the tensile strength obtained from experimental tests, $f_{u\theta,exp}$, under different strain rates, for a given temperature.

Table 4. 4. Tensile strength of bolt material – Comparison with EN1993-1-2 (2005)

Temperature [°C]	20	150	300	400	500	542	600	700	800
$f_{u,\theta}$ [N/mm^2]	1040	990	939	806	572	428	229	104	70
$f_{u\theta,exp}$ [N/mm^2] at 0.000033 [s^{-1}]	1066	1064	968	737	344	210	104	56	37
$f_{u\theta,exp}$ [N/mm^2] at 0.00033 [s^{-1}]	1087	1029	1041	817	502	-	185	73	59
$f_{u\theta,exp}$ [N/mm^2] at 0.002 [s^{-1}]	1100	-	1042	857	-	-	-	133	-
$f_{u\theta,exp}$ [N/mm^2] at 0.0033 [s^{-1}]	1078	1051	1049	843	599	483	325	140	86
$f_{u\theta,exp}$ [N/mm^2] at 0.008 [s^{-1}]	1095	-	1072	882	648	-	346	155	-
$f_{u\theta,exp}$ [N/mm^2] at 0.01 [s^{-1}]	1091	-	1042	885	643	-	357	-	-
$f_{u\theta,exp}$ [N/mm^2] at 0.02 [s^{-1}]	1091	1017	1022	878	679	548	377	182	106
$f_{u\theta,exp}$ [N/mm^2] at 0.04 [s^{-1}]	1114	-	1024	901	690	-	405	182	-
$f_{u\theta,exp}$ [N/mm^2] at 0.06 [s^{-1}]	1110	-	1044	904	681	-	394	185	123

4.6 Sensitivity Analysis

This section presents a sensitivity analysis regarding the results obtained from repetitions of one configuration.

Figure 4. 42. until Figure 4. 49. show some examples of stress-strain curves obtained for the same configuration. The rest of the figures can be found in the Annex A of this work.

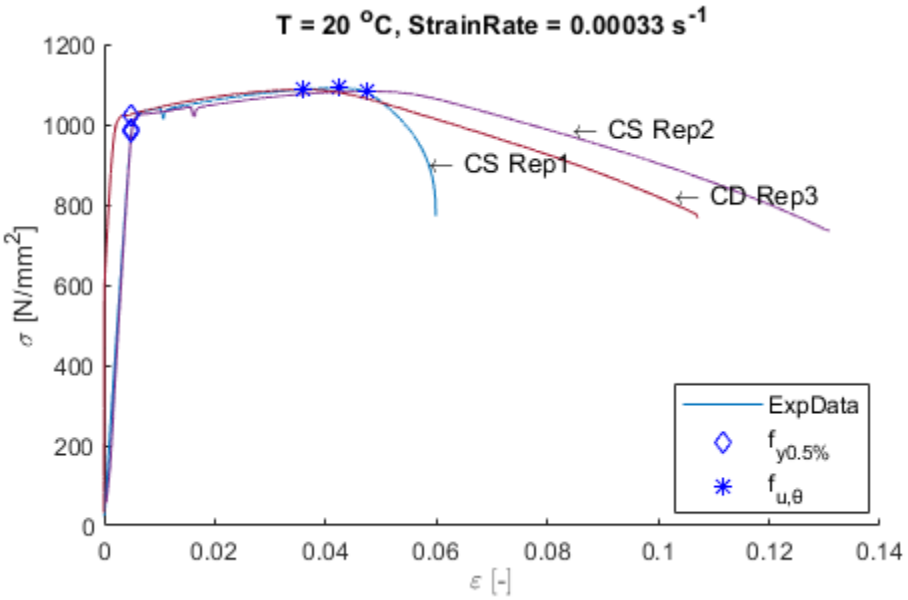

Figure 4. 42. The stress-strain curves obtained for the same configuration: 20 °C, 0.00033 s^{-1}.

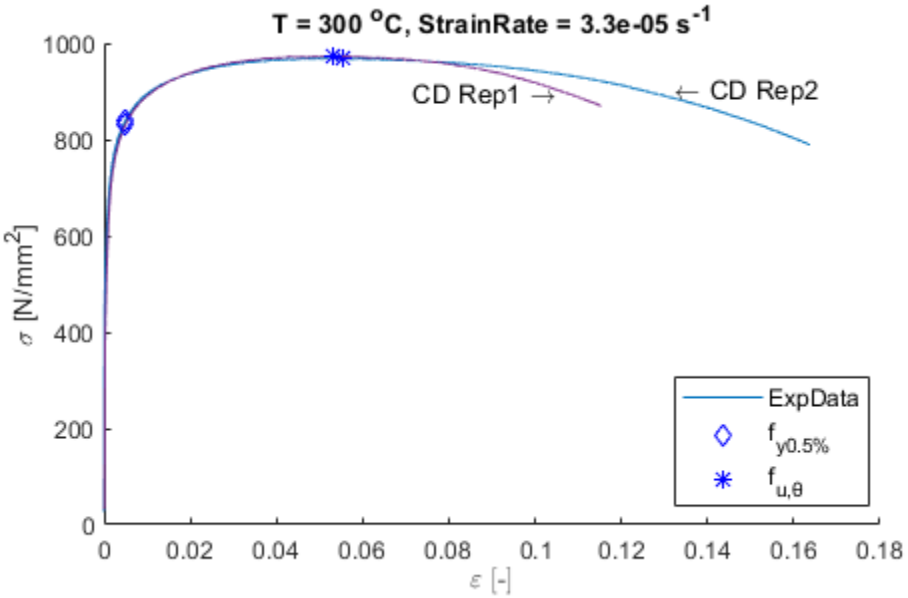

Figure 4. 43. The stress-strain curves obtained for the same configuration: 300 °C, 0.000033 s^{-1}.

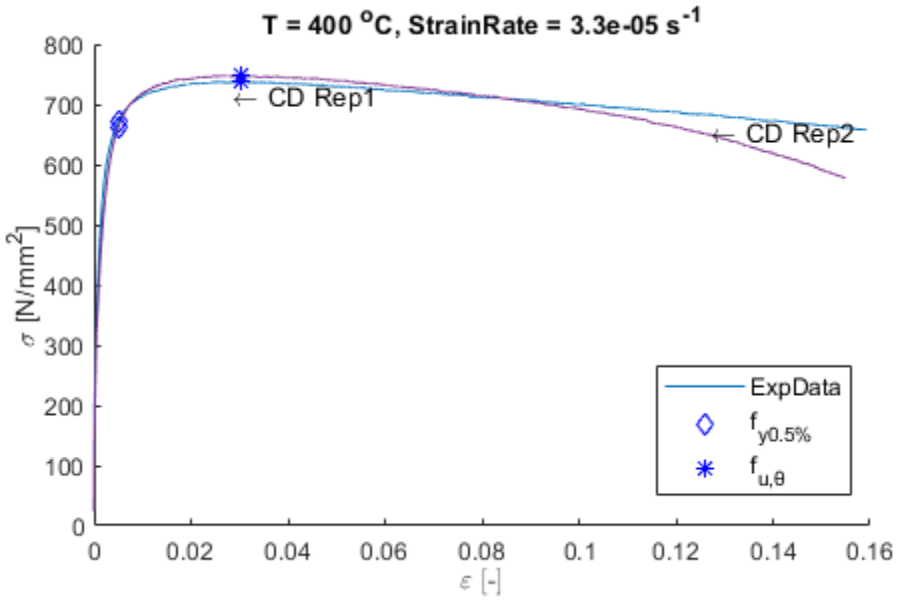

Figure 4. 44. The stress-strain curves obtained for the same configuration: 400 °C, 0.000033 s^{-1}.

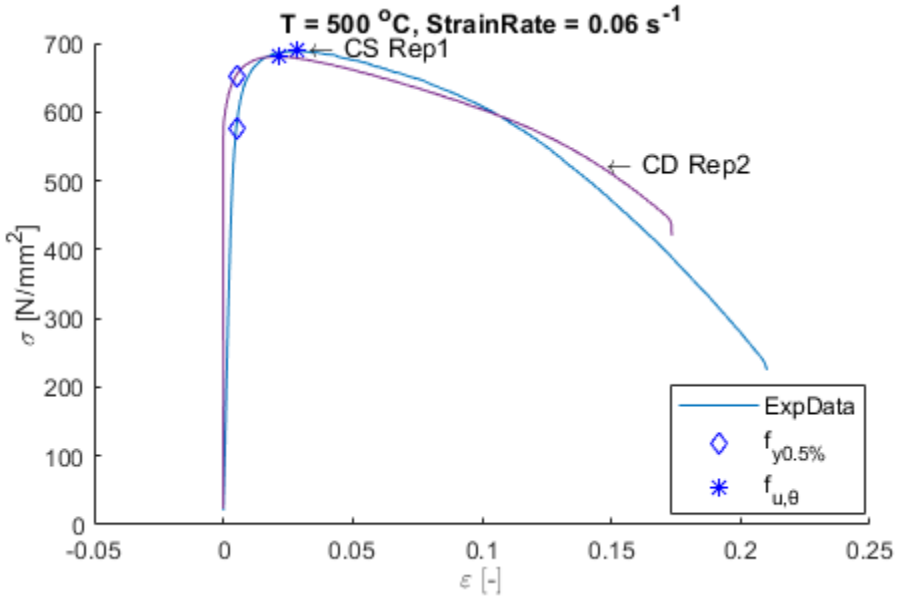

Figure 4. 45. The stress-strain curves obtained for the same configuration: 500 °C, 0.06 s^{-1}.

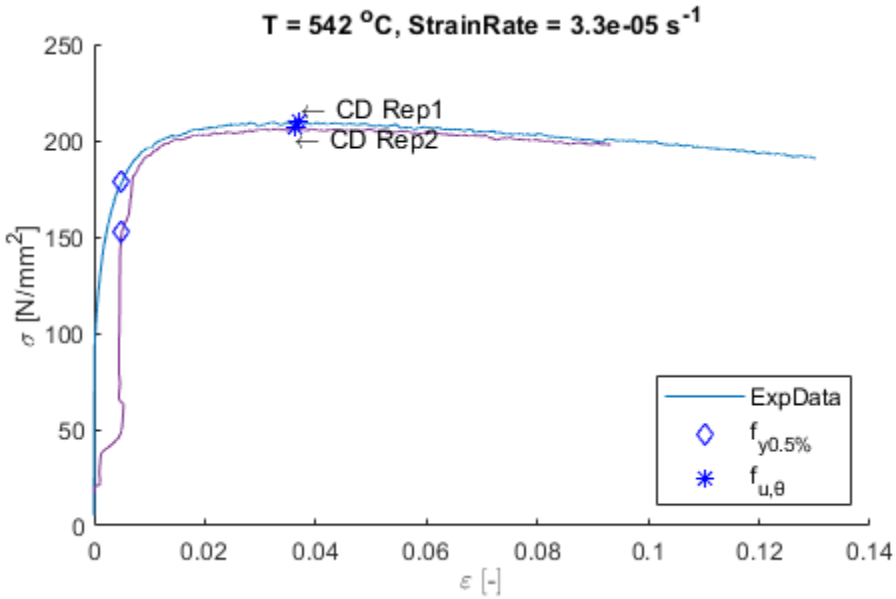

Figure 4. 46. The stress-strain curves obtained for the same configuration: 542 °C, 0.000033 s^{-1}.

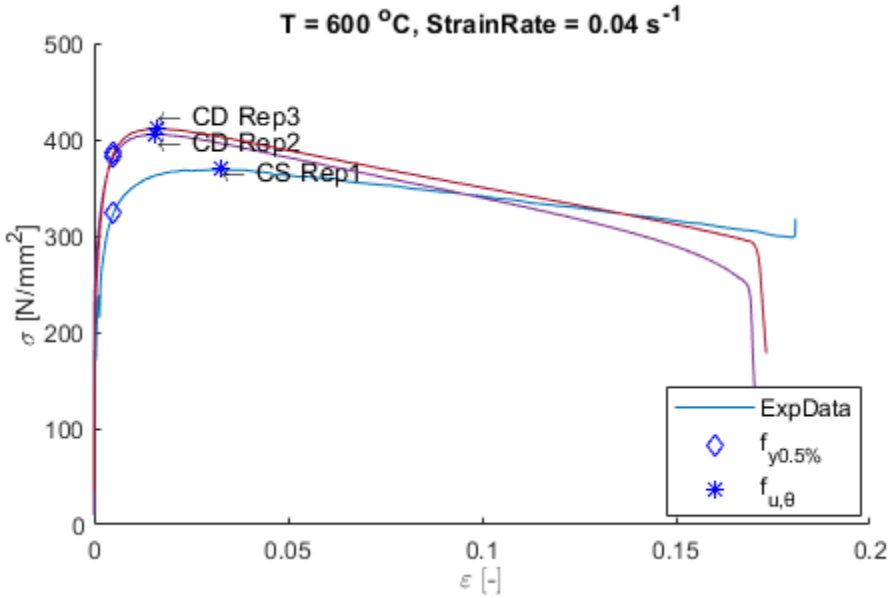

Figure 4. 47. The stress-strain curves obtained for the same configuration: 600 °C, 0.04 s^{-1}.

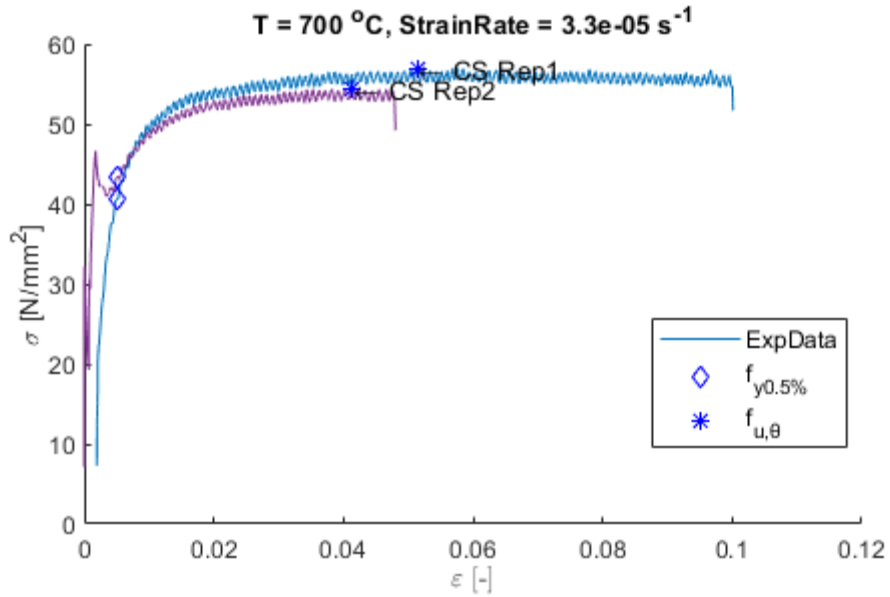

Figure 4. 48. The stress-strain curves obtained for the same configuration: 700 °C, 0.000033 s^{-1}.

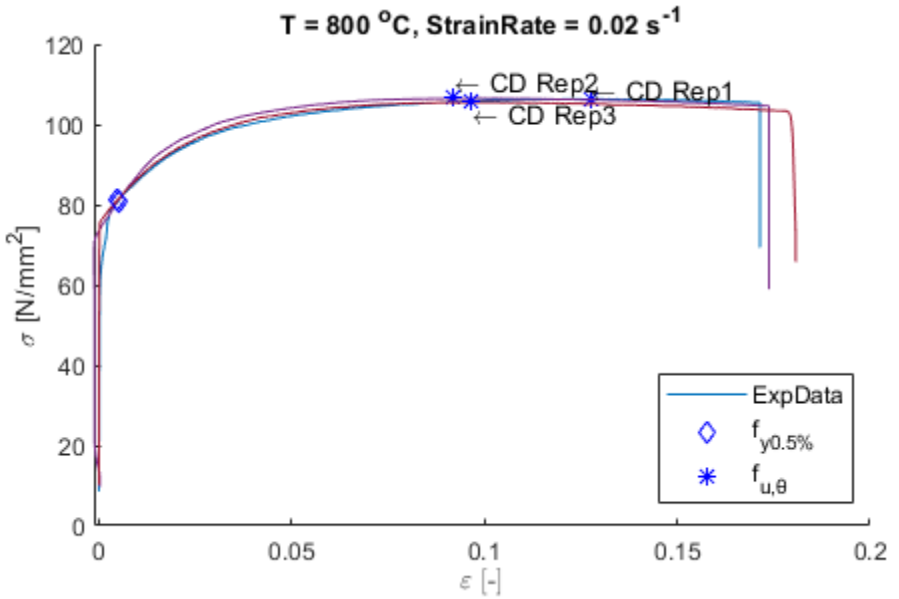

Figure 4. 49. The stress-strain curves obtained for the same configuration: 800 °C, 0.02 s^{-1}.

Each configuration was repeated 2 or 3 times to verify the accuracy of the data recorded. Some configurations offered a variability below 1%, therefore a 3rd repetition was not considered to be necessary. Table 4. 5. shows the variability of

tensile strength per configuration. In all cases, this value is under 5%. The variability was computed as the percentage of standard deviation from the mean value of the tensile strength.

As it was concluded from the sections 4.2 and 4.3 of this chapter, the yield strength is considered as the strength recorded at 0.5% strain. For that reason, the variability of yield strength $F_{y0.5\%}$ per configuration is shown in Table 4. 6. The values show a good accuracy of the measurements as the variability is below 5% for most of the configurations. Although, some configurations (6 of them) present a variation of about 10%, two configurations show 43%, and in one case it was observed 50%.

It is clear that more attention should be paid for the measurement of the yield strength. This analysis is realized here only in an estimative purpose, as the strain rate recommended by the ISO 6892-2 (2011) for the yield strength measurements was not respected.

Table 4. 5. The variability of tensile strength per configuration.

	Temperature [°C]								
Strain rate	20	150	300	400	500	542	600	700	800
0.000033 [s^{-1}]	0.12	-	0.34	0.98	2.46	1.20	2.00	3.16	1.67
0.00033 [s^{-1}]	0.39	-	0.66	0.23	2.60	-	4.98	-	2.89
0.002 [s^{-1}]	-	-	-	-	-	-	-	-	-
0.0033 [s^{-1}]	1.08	-	0.67	1.72	4.10	3.29	-	-	0.47
0.008 [s^{-1}]	-	-	-	-	0.34	-	-	-	-
0.01 [s^{-1}]	-	-	-	-	-	-	-	-	-
0.02 [s^{-1}]	0.83	-	2.33	1.39	3.42	0.85	1.12	2.22	0.49
0.04 [s^{-1}]	-	-	-	-	-	-	5.80	-	-
0.06 [s^{-1}]	-	-	-	-	0.83	-	-	-	-

Table 4. 6. The variability of yield strength per configuration.

	Temperature [°C]								
Strain rate	20	150	300	400	500	542	600	700	800
0.000033 [s^{-1}]	0.10	-	0.66	0.95	1.58	10.9	10.6	4.57	0.25
0.00033 [s^{-1}]	2.44	-	7.37	2.49	3.60	-	43.9	-	43.4
0.002 [s^{-1}]	-	-	-	-	-	-	-	-	-
0.0033 [s^{-1}]	1.76	-	0.31	5.22	1.28	0.44	-	-	0.26
0.008 [s^{-1}]	-	-	-	-	1.27	-	-	-	-
0.01 [s^{-1}]	-	-	-	-	-	-	-	-	-
0.02 [s^{-1}]	0.94	-	5.73	2.32	2.30	3.37	54	12.0	0.35
0.04 [s^{-1}]	-	-	-	-	-	-	9.69	-	-
0.06 [s^{-1}]	-	-	-	-	8.89	-	-	-	-

When a test under a certain configuration was repeated, the results had a variation below 2.5% in terms of tensile strength, for 75% of the tests. Figure 4. 50.

shows a boxplot of the values computed for all the tested configurations. The central mark indicates the median, and the bottom and top edges of the box indicate the 25th and 75th percentiles, respectively. The whiskers extend to the most extreme data points not considered outliers, and the outliers are plotted individually using the '+' marker symbol (MatLab, 2021). It can be seen that, almost all tests present a variability in repetition of maximum 5%, except one which is close to 6%. This is due to the procedure implemented, i.e., one of the tests was realized under strain rate control, while the others under displacement control (see Figure 4. 47.).

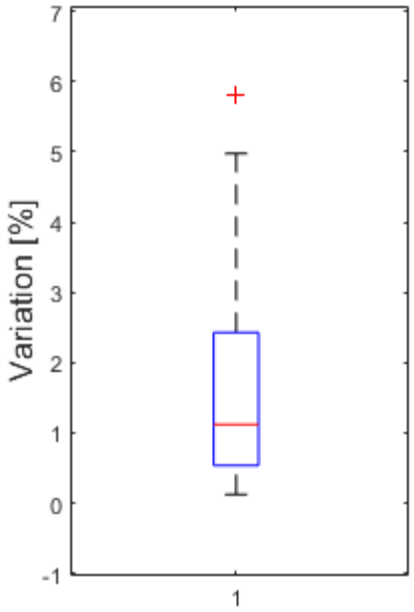

Figure 4. 50. Variation computed for all the tested configurations, in terms of tensile strength.

4.7 Reduction Factors

This section presents the reduction factors for 0.5% yield strength and for tensile strength computed based on the experimental tests. Similar with the definition from the literature, presented in the previous chapters, these factors are defined as:

- The 0.5% yield strength reduction factor, depending on the strain rate, represents the ration between the 0.5% yield strength at elevated temperature, under a certain strain rate, and 0.5% yield strength at normal temperature, under the same strain rate:

$$k_{b,0.5\%} = f_{0.5\%,\theta,\dot{e}} / f_{0.5\%,20,\dot{e}} \quad [4.4]$$

- the reduction factor $k_{b,u}$, depending on the strain rate, represents the ratio between tensile strength at elevated temperature under a

certain strain rate, and tensile strength at normal temperature under same strain rate:

$$k_{b,u} = f_{u,\theta,\dot{e}} / f_{u,20,\dot{e}} \quad [4.5]$$

Function of the strain rate, a comparison is shown in Figure 4. 51. until Figure 4. 59., between the reduction factors for bolts strength provided by EN1993-1-2 (2005), $k_{b,\theta}$, and the values of 0.5% yield strength reduction factors obtained in this study.

It can be seen that, for slow strain rates (and even for 0.00033 s^{-1}, which is the low limit recommended by ISO 6892-2 (2011), EN1993-1-2 (2005) overestimates the 0.5% yield strength by 6 % when the temperature is below 400 °C, by more than 10% for 400 °C, and by over 40% for higher temperatures. For strain rates between 0.00033 - 0.0033 s^{-1}, the 0.5% yield strength reduction factors obtain in this study are consistent with the ones provided by EN1993-1-2 (2005). For a strain rate of 0.02 s^{-1} and above, EN1993-1-2 (2005) overestimates the 0.5% yield strength by 13% for temperatures below 500 °C, and underestimates it by over 40% for temperatures higher than 500 °C.

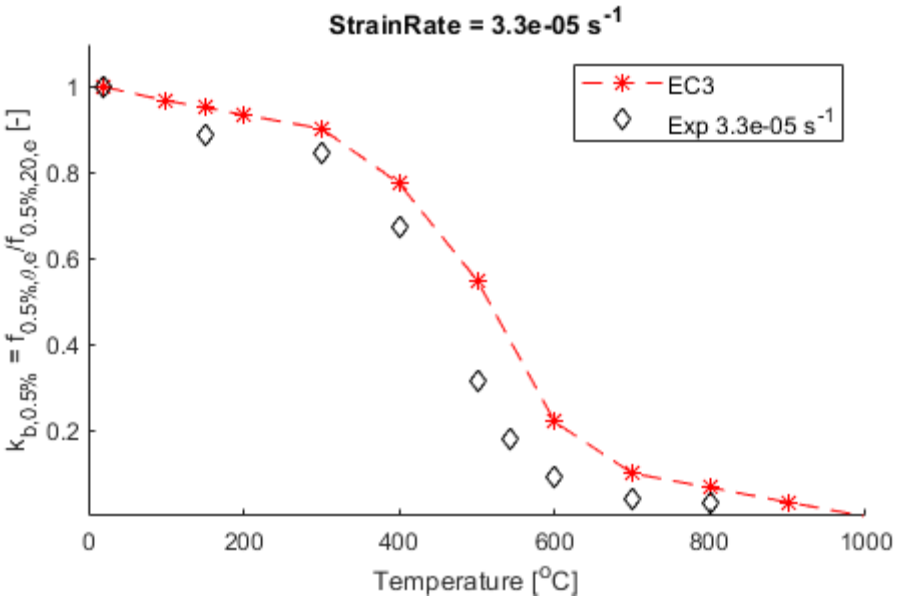

Figure 4. 51. Reduction factor for 0.5% yield strength with temperature, for grade 10.9 bolts, obtained under 0.000033 s^{-1} strain rate.

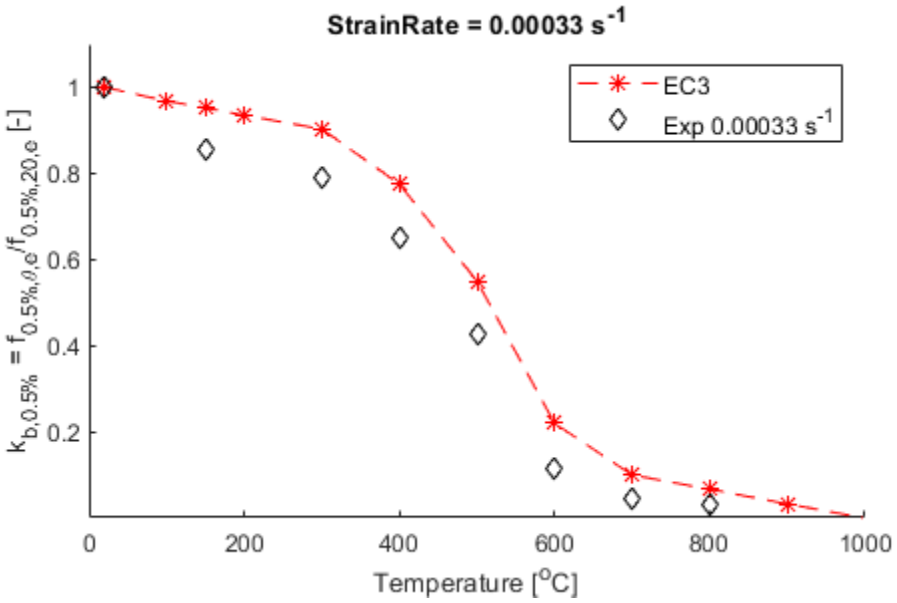

Figure 4. 52. Reduction factor for 0.5% yield strength with temperature, for grade 10.9 bolts, obtained under 0.00033 s^{-1} strain rate.

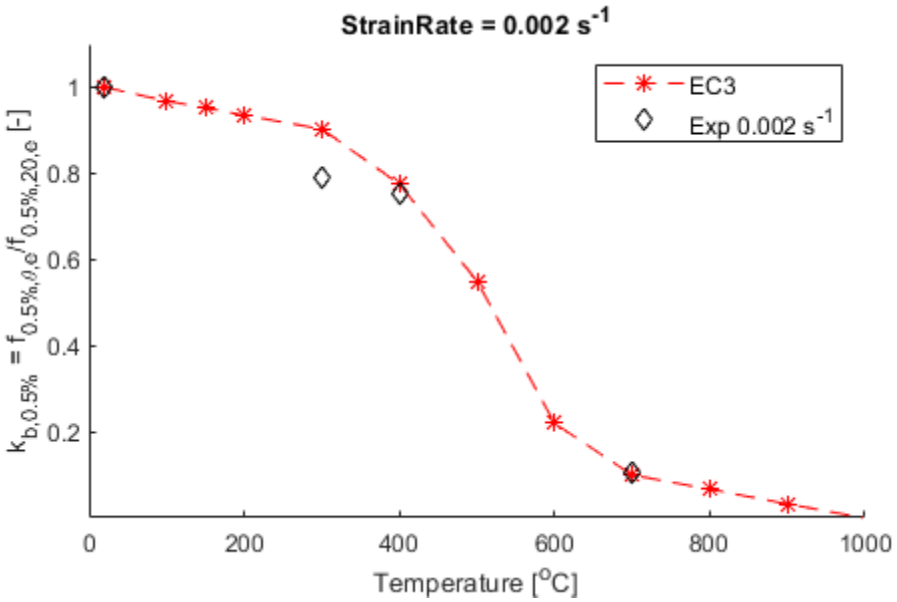

Figure 4. 53. Reduction factor for 0.5% yield strength with temperature, for grade 10.9 bolts, obtained under 0.002 s^{-1} strain rate.

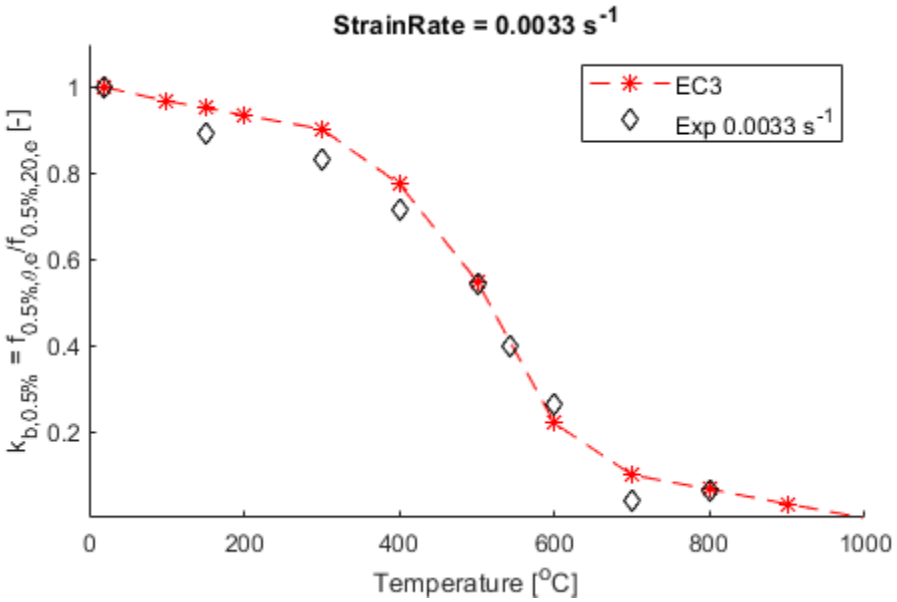

Figure 4. 54. Reduction factor for 0.5% yield strength with temperature, for grade 10.9 bolts, obtained under 0.0033 s^{-1} strain rate.

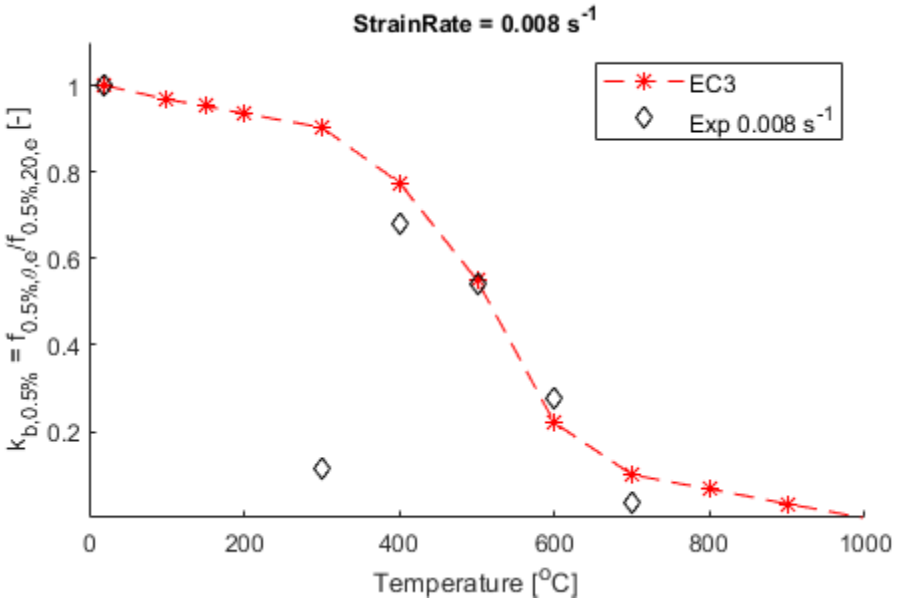

Figure 4. 55. Reduction factor for 0.5% yield strength with temperature, for grade 10.9 bolts, obtained under 0.008 s^{-1} strain rate.

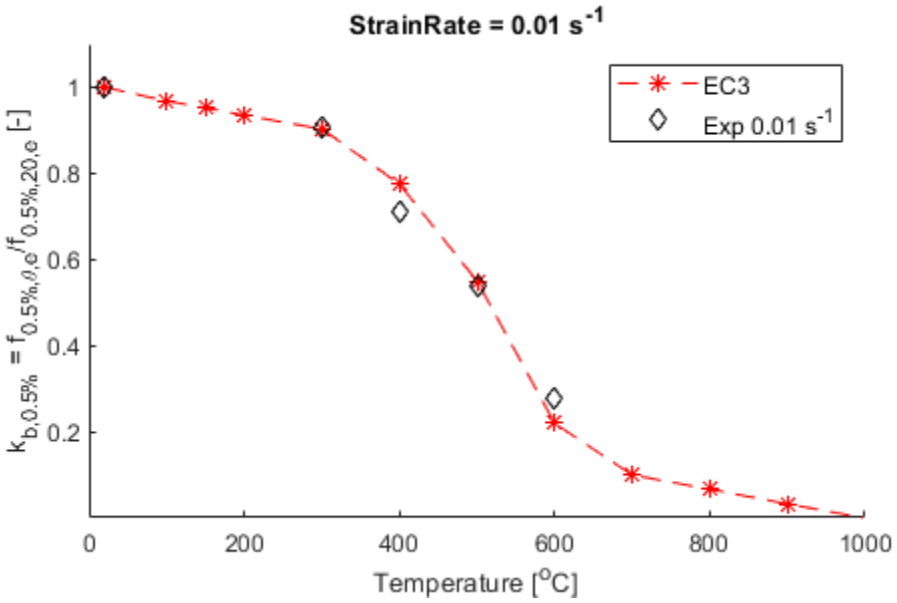

Figure 4. 56. Reduction factor for 0.5% yield strength with temperature, for grade 10.9 bolts, obtained under 0.01 s^{-1} strain rate.

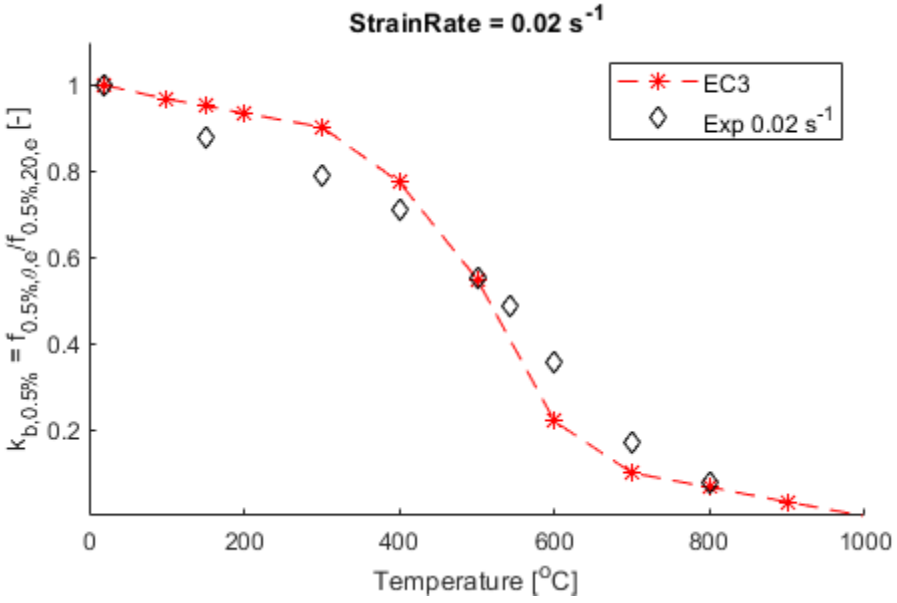

Figure 4. 57. Reduction factor for 0.5% yield strength with temperature, for grade 10.9 bolts, obtained under 0.02 s^{-1} strain rate.

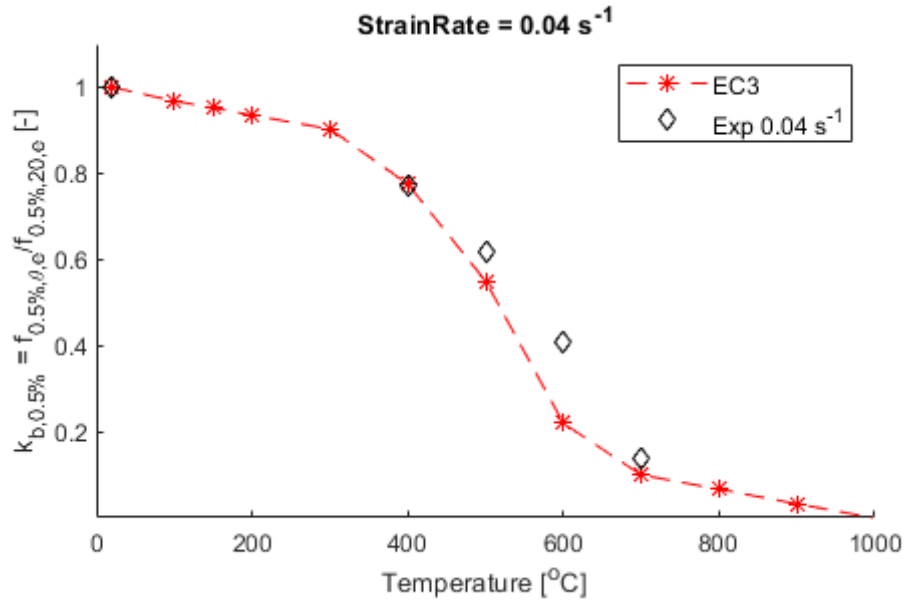

Figure 4. 58. Reduction factor for 0.5% yield strength with temperature, for grade 10.9 bolts, obtained under 0.04 s^{-1} strain rate.

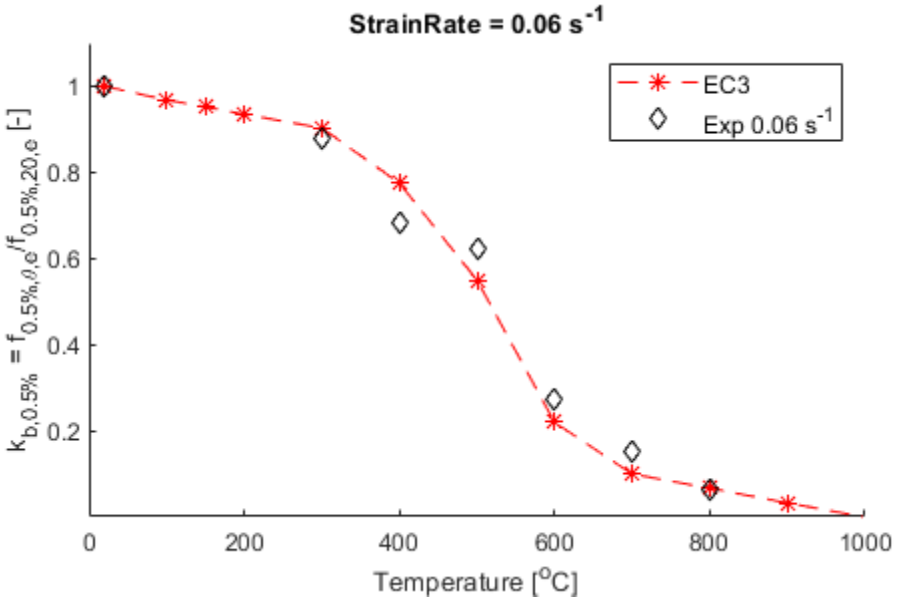

Figure 4. 59. Reduction factor for 0.5% yield strength with temperature, for grade 10.9 bolts, obtained under 0.06 s^{-1} strain rate.

Further the reduction factor for tensile strength, $k_{b,u}$, is assessed. Function of the strain rate, a comparison is shown in Figure 4. 60. until Figure 4. 68., between the reduction factors for bolts strength provided by EN1993-1-2 (2005) and the values obtained in this study. For a very slow strain rate, EN1993-1-2 (2005) overestimates the tensile strength by 10% when the temperature is 400 °C, and by more than 40% for higher temperatures. For strain rates between 0.00033 s^{-1} and 0.0033 s^{-1} (even for 0.008 s^{-1} as recommended by ISO 6892-2 (2011)), the tensile strength reduction factors obtained in this study are consistent with the ones provided by EN1993-1-2 (2005). For a strain rate of 0.02 s^{-1} and above, EN1993-1-2 (2005) underestimates the tensile strength by 13% for 500 °C and by over 40% for higher temperatures.

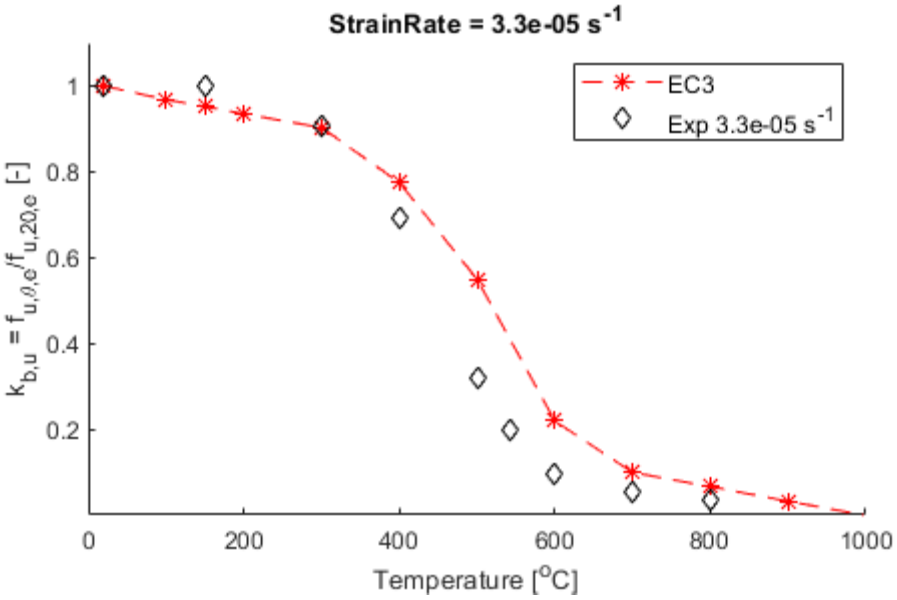

Figure 4. 60. Reduction factor of tensile strength with temperature, for grade 10.9 bolts, obtained under 0.000033 s^{-1} strain rate.

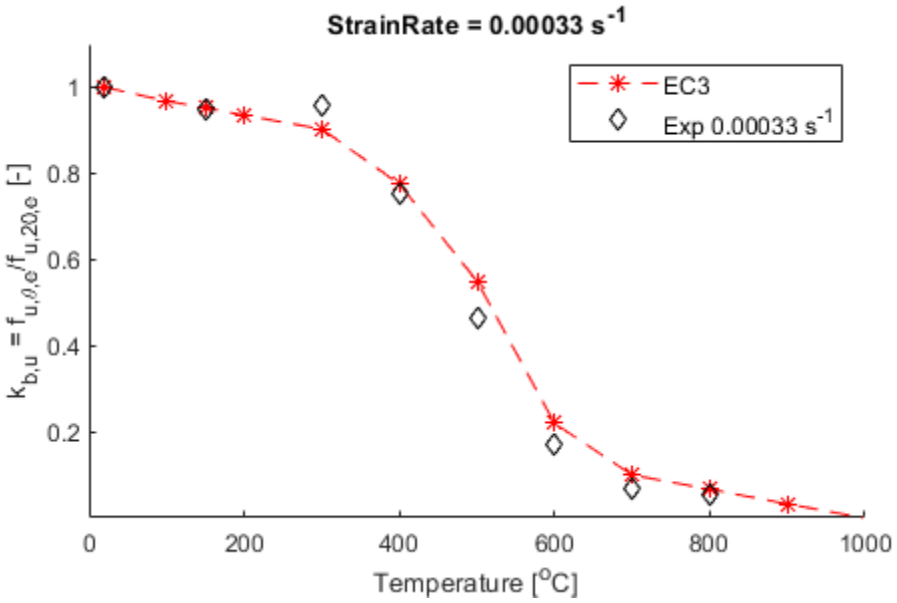

Figure 4. 61. Reduction factor of tensile strength with temperature, for grade 10.9 bolts, obtained under 0.00033 s^{-1} strain rate.

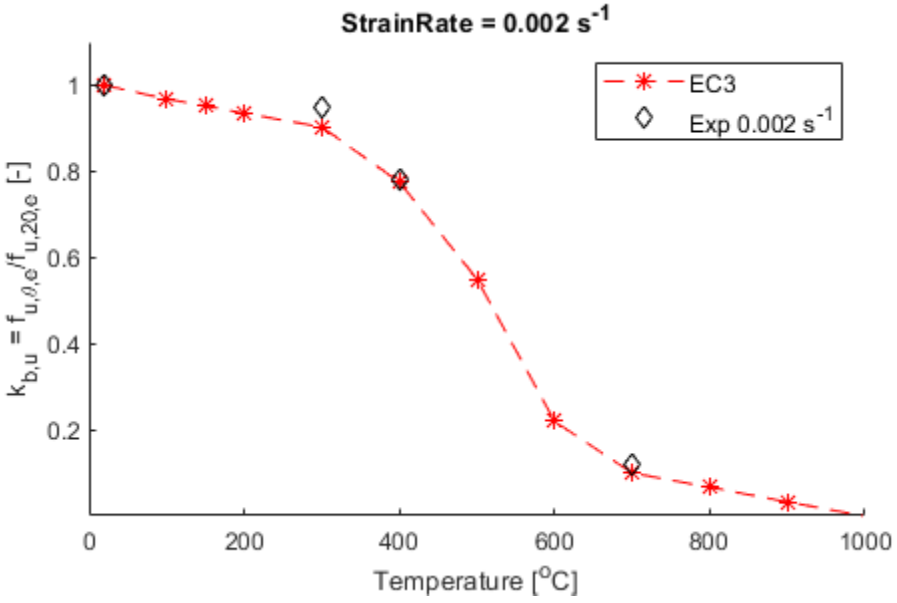

Figure 4. 62. Reduction factor of tensile strength with temperature, for grade 10.9 bolts, obtained under 0.002 s^{-1} strain rate.

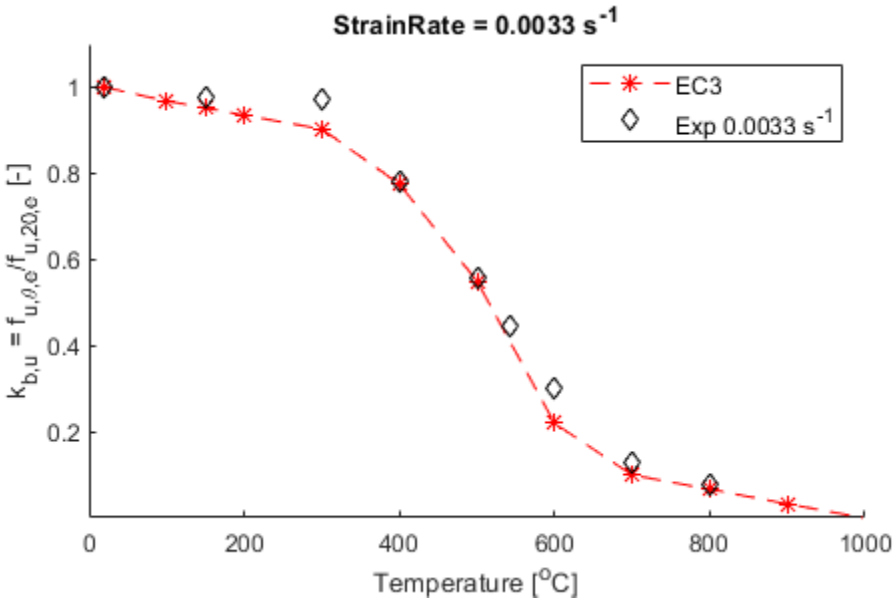

Figure 4. 63. Reduction factor of tensile strength with temperature, for grade 10.9 bolts, obtained under 0.0033 s^{-1} strain rate.

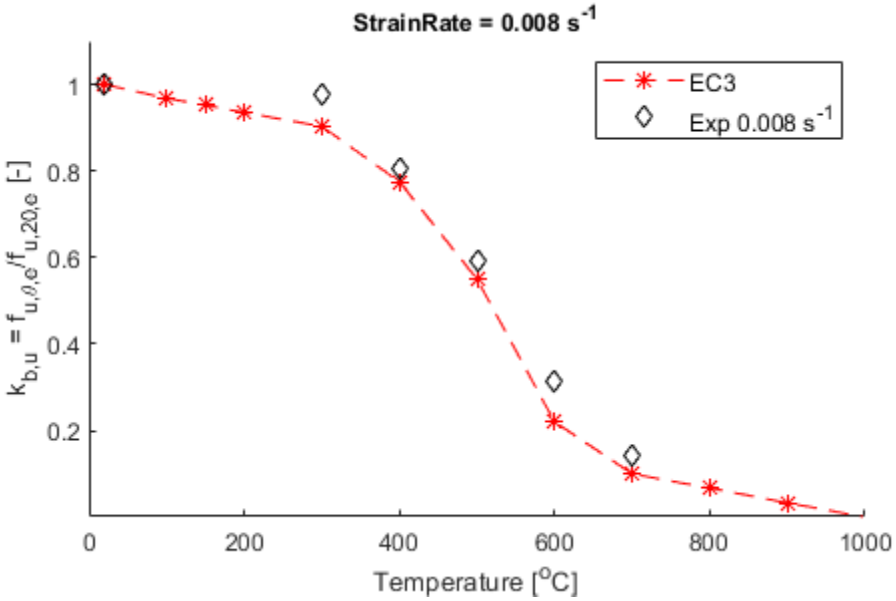

Figure 4. 64. Reduction factor of tensile strength with temperature, for grade 10.9 bolts, obtained under 0.008 s^{-1} strain rate.

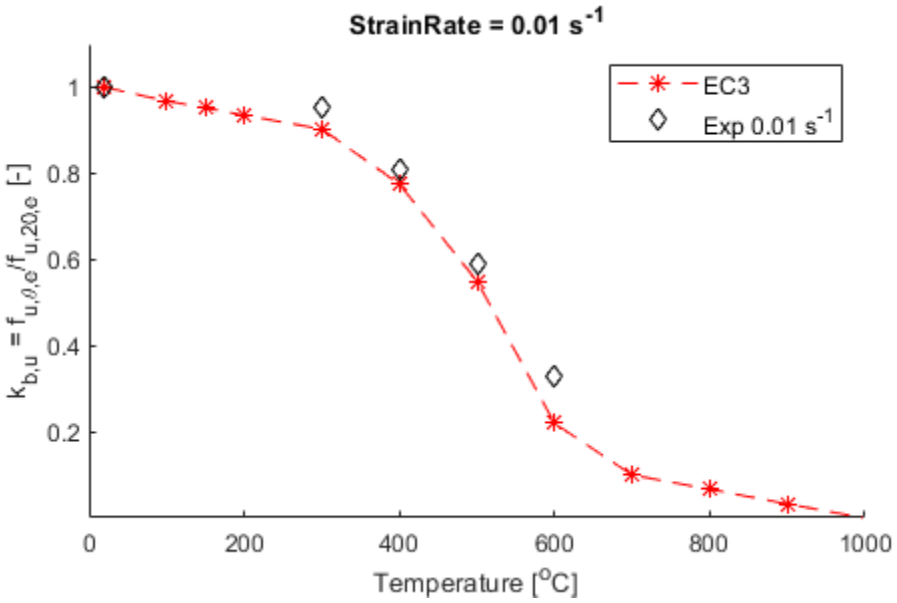

Figure 4. 65. Reduction factor of tensile strength with temperature, for grade 10.9 bolts, obtained under 0.01 s^{-1} strain rate.

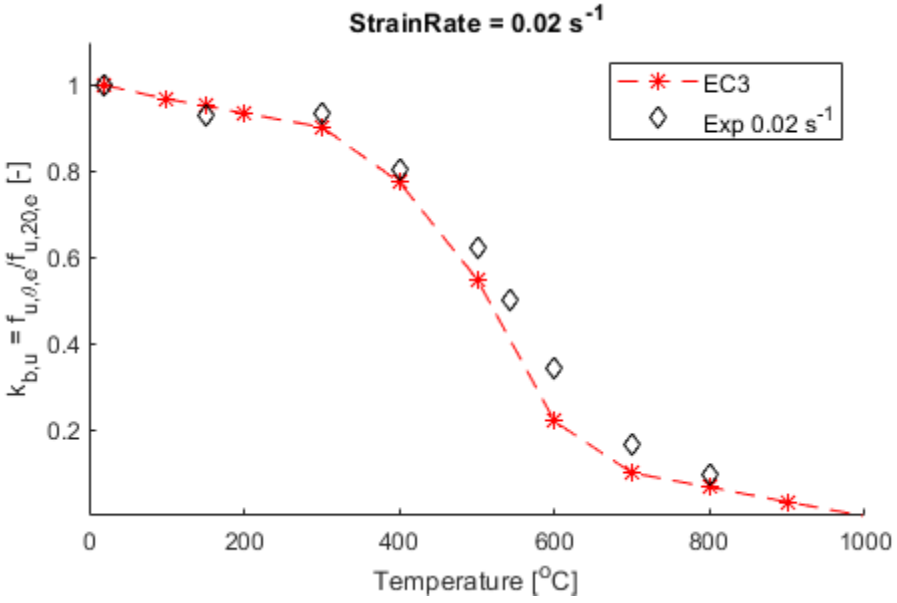

Figure 4. 66. Reduction factor of tensile strength with temperature, for grade 10.9 bolts, obtained under 0.02 s^{-1} strain rate.

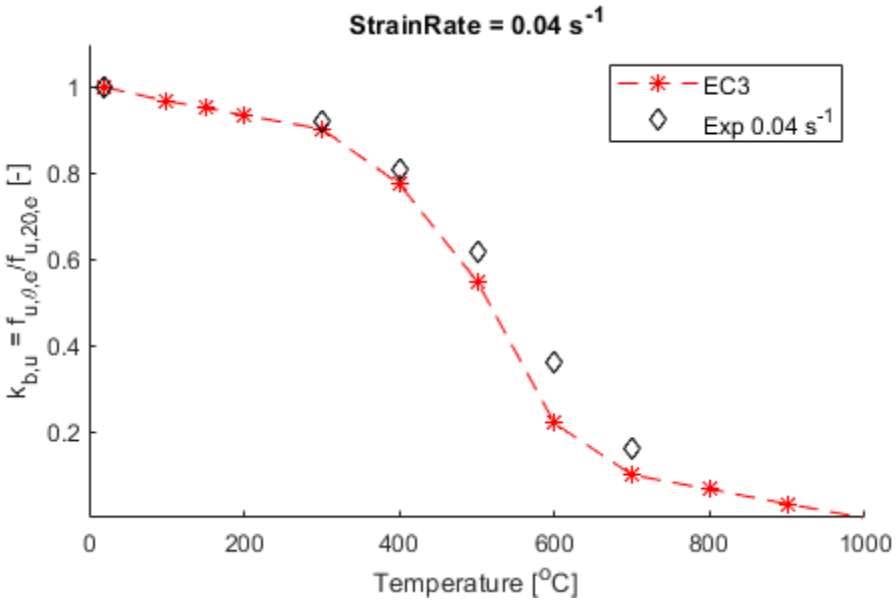

Figure 4. 67. Reduction factor of tensile strength with temperature, for grade 10.9 bolts, obtained under 0.04 s^{-1} strain rate.

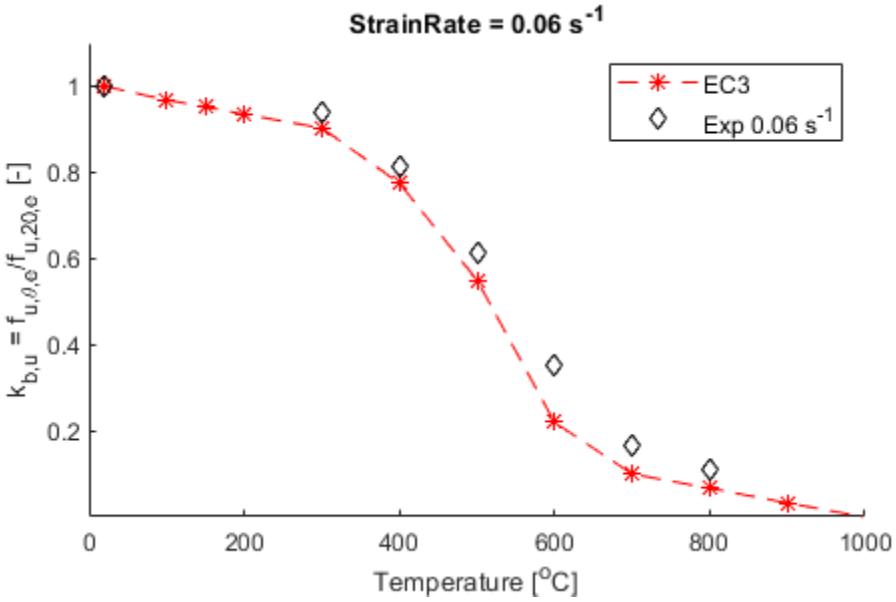

Figure 4. 68. Reduction factor of tensile strength with temperature, for grade 10.9 bolts, obtained under 0.06 s^{-1} strain rate.

A summary of the influence of strain rate over the 0.5% yield strength reduction factor and tensile strength reduction factor, respectively, is shown in Figure

4. 69. and Figure 4. 70, for each tested temperature. Figure 4. 69.a. and Figure 4. 70.a. show a linear plot of data, whereby the logarithmic tendency of the correlation can easily be noticed. Figure 4. 69.b. and Figure 4. 70.b. show a logarithmic plot of data. These figures prove the strong influence of the strain rate on the material strength, especially for temperatures above 300 °C. Even in the recommended interval for strain rate, 0.0000333 s^{-1} and 0.0033 s^{-1} (acc. 6892-2 (2011)), the reduction factor varies with 20% for 400 °C, and with more than 50% for higher temperatures.

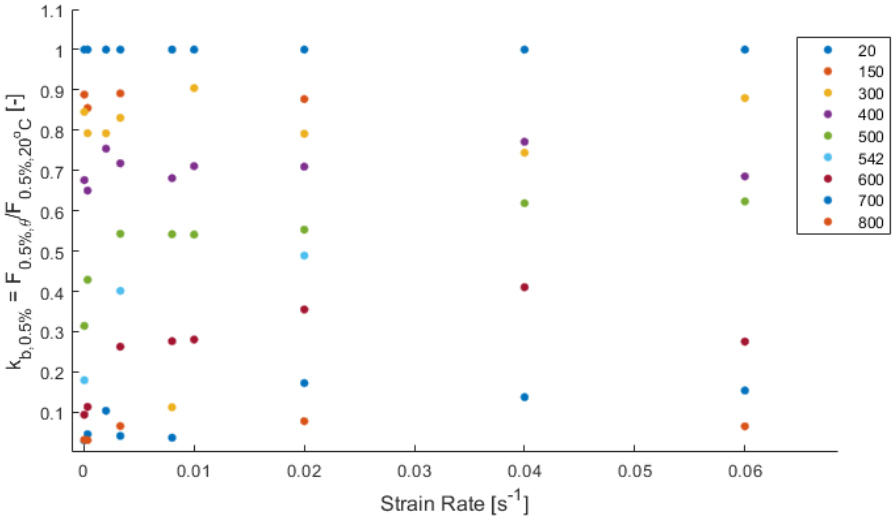

a.

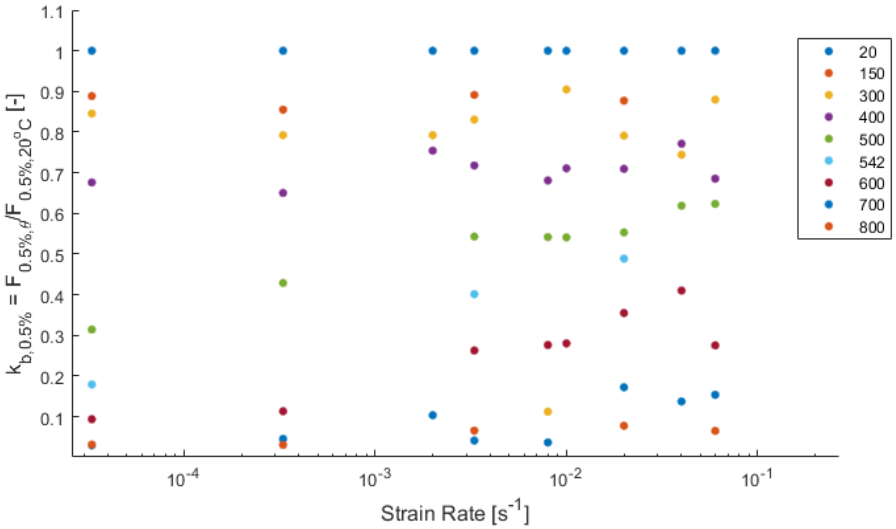

b.

Figure 4. 69. Reduction factors for 0.5% yield strength, with strain rate: a. linear plot; b. logarithmic plot.

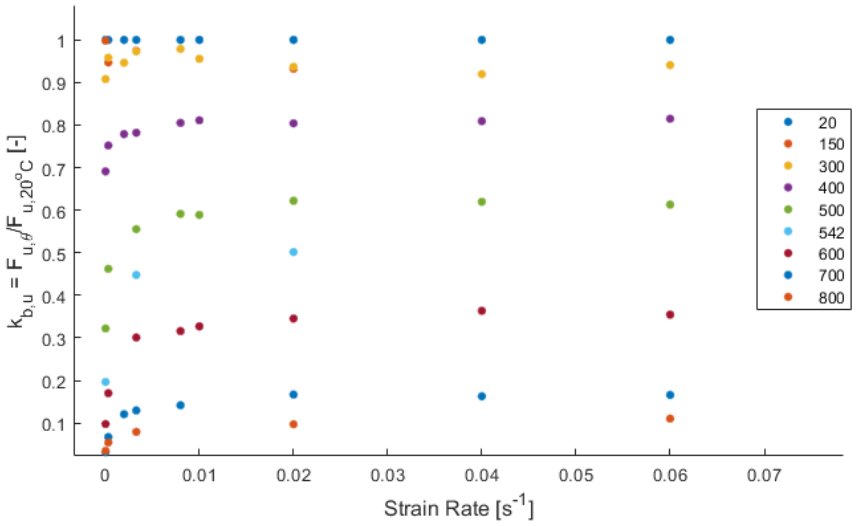

a)

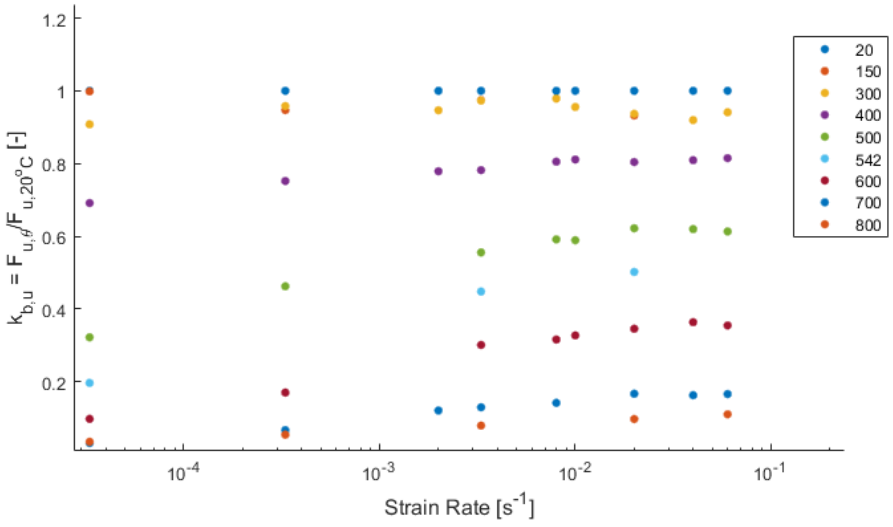

b)

Figure 4. 70. Reduction factors for tensile strength, with strain rate: a. linear plot; b. logarithmic plot.

A series of equations were developed (see Figure 4. 71. until Figure 4. 76.) for the computation of tensile strength reduction factors, $k_{b,u}$, function of the strain rate, for each temperature tested. It was observed that for temperatures below 400 °C, the reduction factors are not influenced by the strain rate.

$$k_{b,u} = 0.016 \ln(\dot{\varepsilon}) + 0.8716 \qquad \text{for } \theta = 400\ ^oC \qquad [4.6]$$

$k_{b,u}$ = 0.0399 ln(ė) + 0.7635 for θ = 500 °C [4.7]

$k_{b,u}$ = 0.049 ln(ė) + 0.708 for θ = 542 °C [4.8]

$k_{b,u}$ = 0.0374 ln(ė) + 0.4874 for θ = 600 °C [4.9]

$k_{b,u}$ = 0.0169 ln(ė) + 0.2216 for θ = 700 °C [4.10]

$k_{b,u}$ = 0.0101 ln(ė) + 0.1376 for θ = 800 °C, [4.11]

Where ė = the strain rate [s^{-1}]

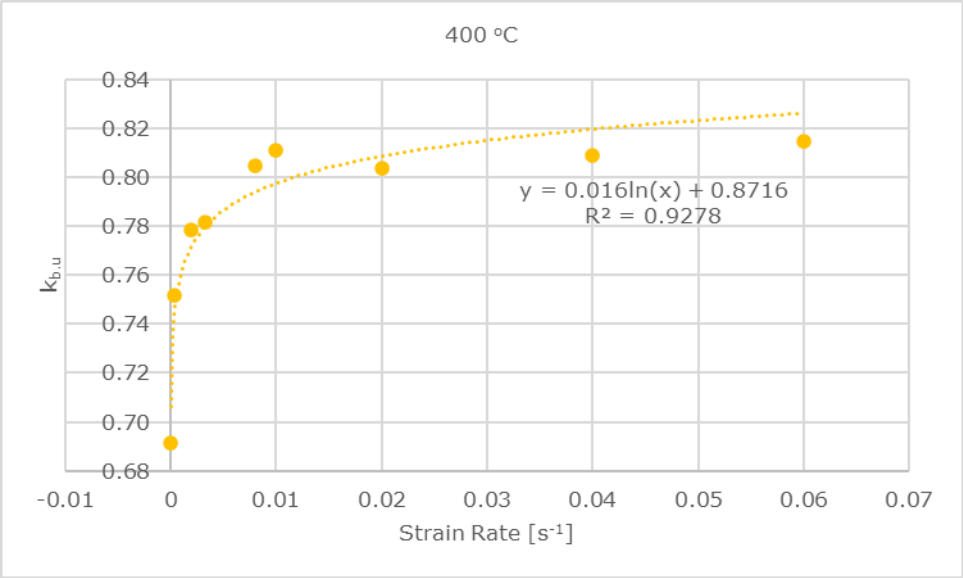

Figure 4. 71. Reduction factors for tensile strength, with strain rate: for 400 °C.

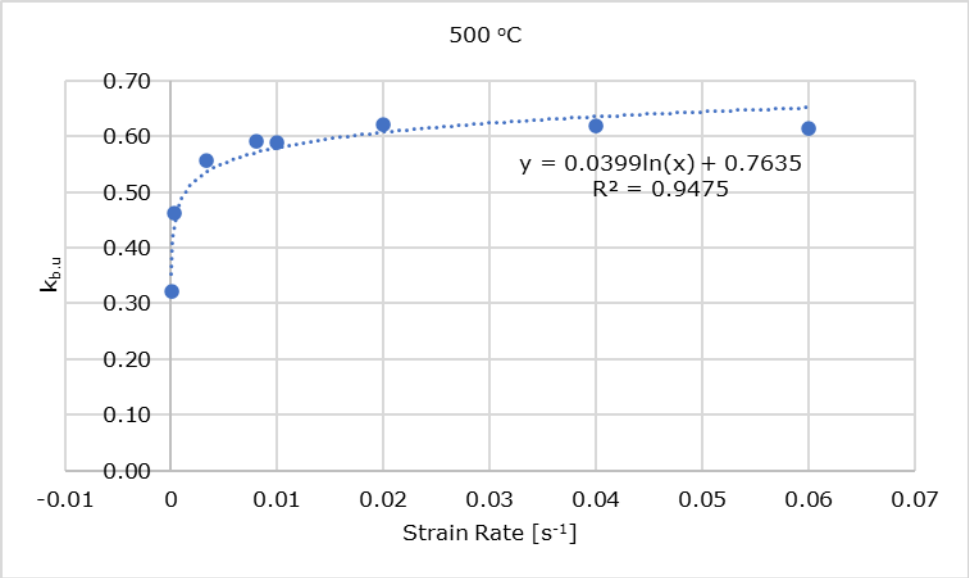

Figure 4. 72. Reduction factors for tensile strength, with strain rate: for 500 °C.

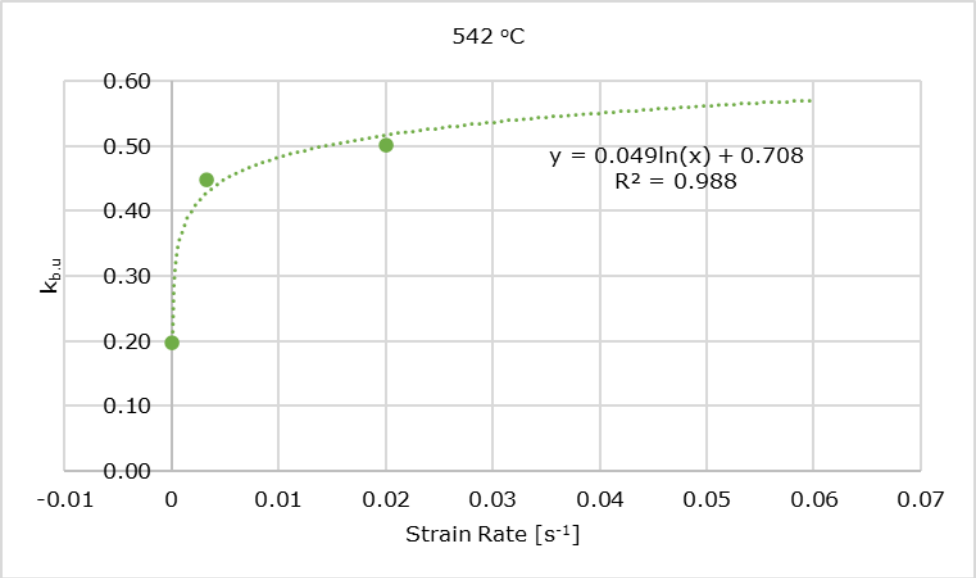

Figure 4. 73. Reduction factors for tensile strength, with strain rate: for 542 °C.

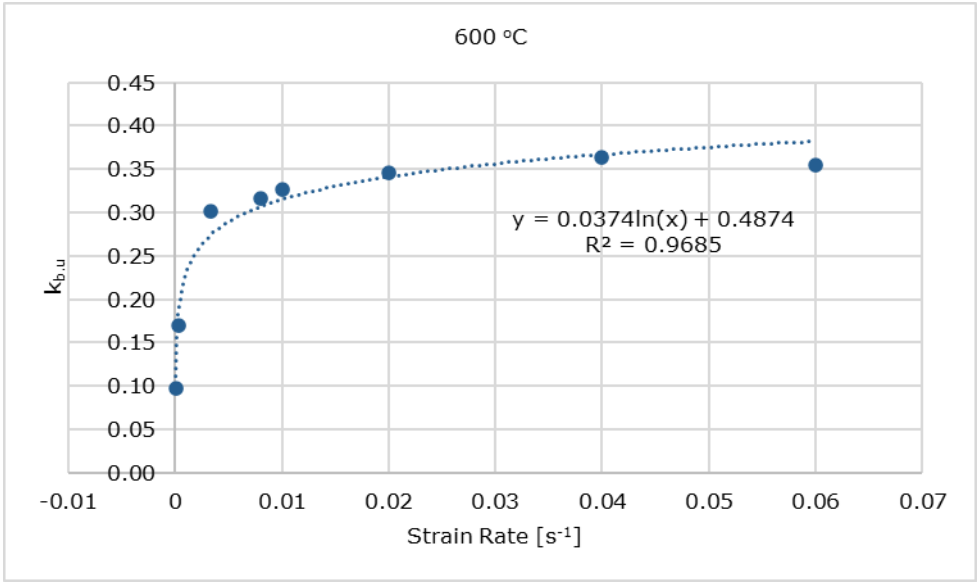

Figure 4. 74. Reduction factors for tensile strength, with strain rate: for 600 °C.

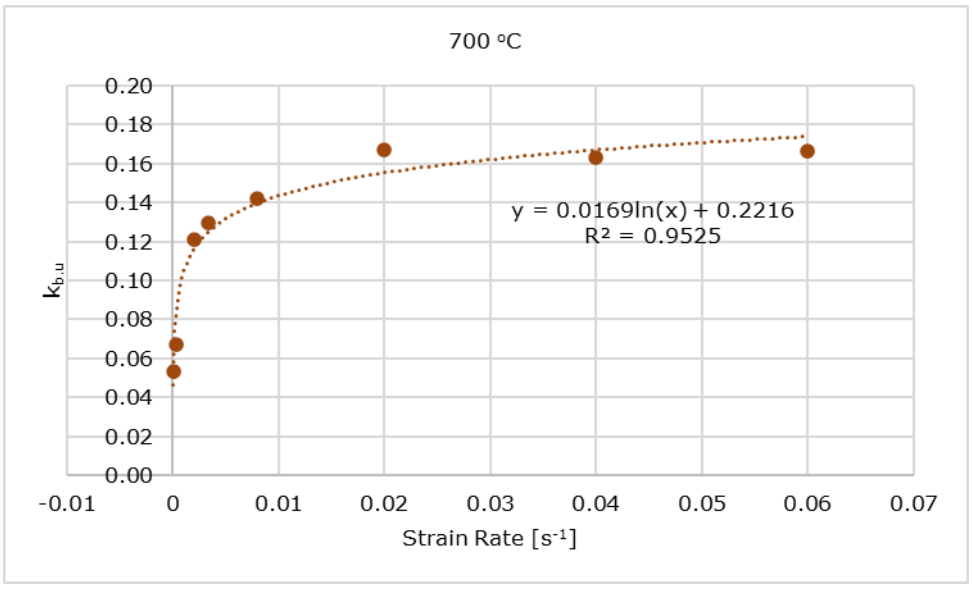

Figure 4. 75. Reduction factors for tensile strength, with strain rate: for 700 °C.

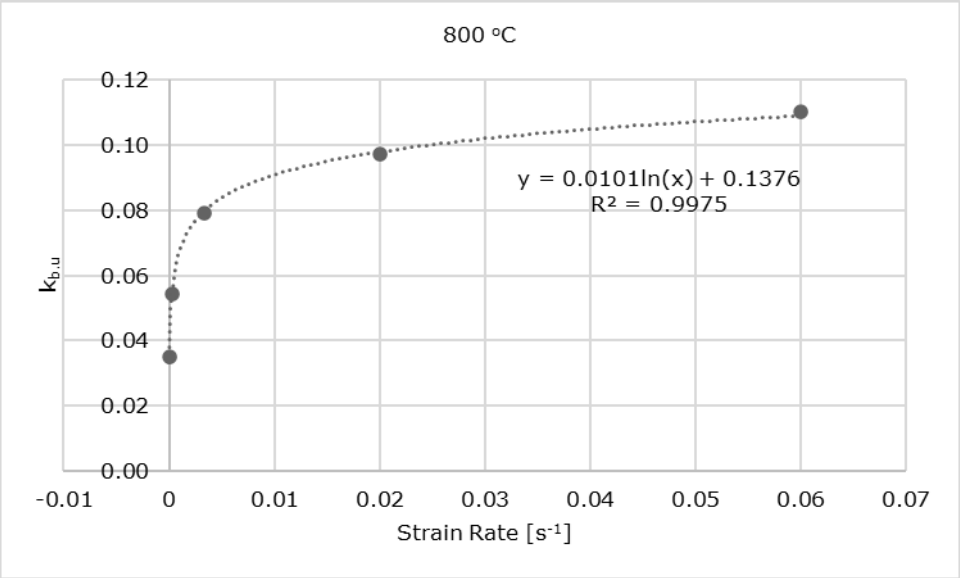

Figure 4. 76. Reduction factors for tensile strength, with strain rate: for 800 °C.

4.8 Proposed Reduction Factors

The previous section presented a series of empirical equations to compute the tensile strength, more specifically the reduction coefficient for tensile strength at different temperatures, if the strain rate is known, particularly if the tensile strength at normal temperature for a chosen strain rate is known. Usually, the engineers do not have at hand this last information, i.e., the strain rate which appears during a fire scenario, or is nearly impossible to be predicted without an experimental test. Hence, in this section, the aim is to define a tensile strength reduction factor which provides a range of values function of the strain rate.

Therefore, the tensile strength reduction factor, $k_{b,u,new}$, is defined as the ratio between the tensile strength at elevated temperature under a certain strain rate, and the tensile strength at normal temperature, under a strain rate of 0.00033 s^{-1}.

$$k_{b,u,new} = f_{u,\theta,\dot{e}} / f_{u,20} \quad [4.12]$$

The value of the fixed tensile strength, $f_{u,20}$, was chosen as it offers close results of $k_{b,u}$, as seen in the chapter 4.7 of this work. So, one can easily find this value, by the technical sheet of a grade 10.9 bolt.

Figure 4. 77. presents the influence of the strain rate over the new tensile strength reduction factor, $k_{b,u,new}$, in a linear plot and a logarithmic plot, respectively. These figures prove the strong influence of the strain rate on the material strength, especially for temperatures above 300 °C. Even in the recommended interval of strain rates, 0.00033 s^{-1} until 0.0033 s^{-1} (acc. to 6892-2 (2011)), the reduction factor varies.

A difference between the new factor and the factors provided by the EN1993-1-2 (2005) is presented in Figure 4. 78. until Figure 4. 80., for different values of strain rate.

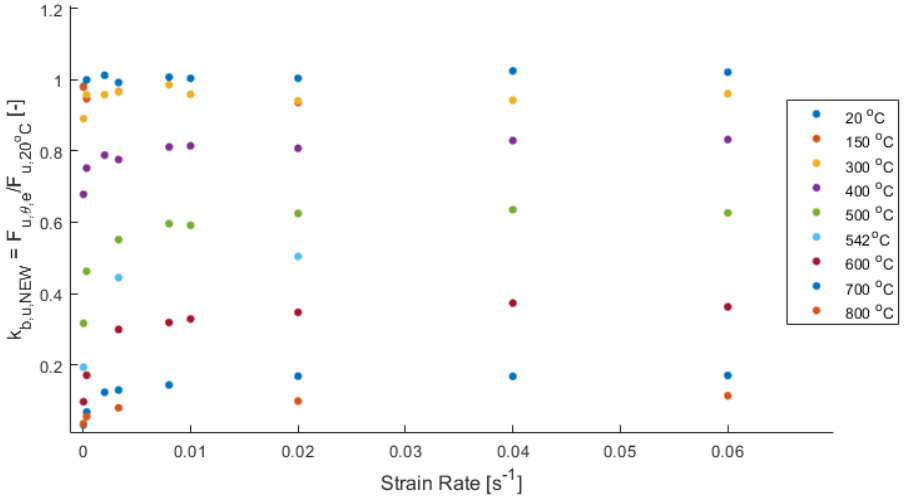

a)

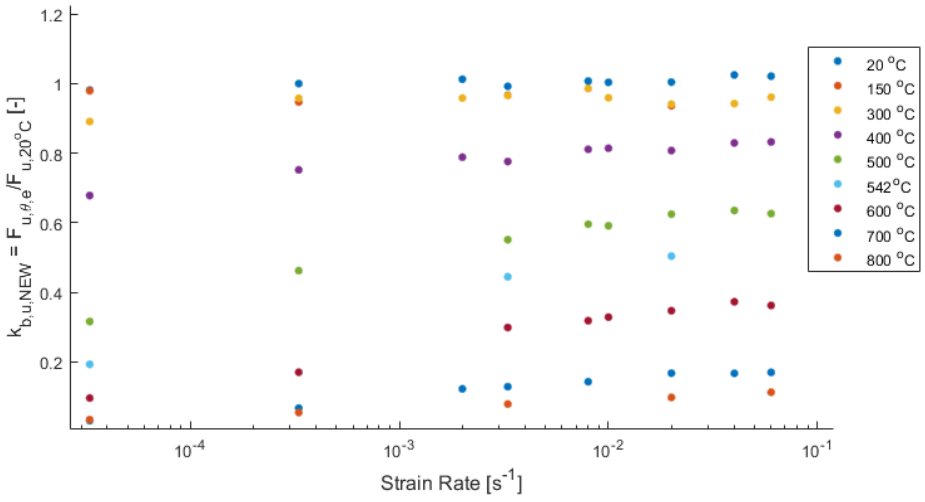

b)

Figure 4. 77. The new reduction factors for tensile strength with strain rate: a) linear plot, b) logarithmic plot.

In Figure 4.78. it can be observed that the yellow dots (0.00033 s^{-1}) and blue dots (0.0033 s^{-1}) are closer to the values of $k_{b,\theta}$ from EN1993-1-2 (2005). These values were obtained by using the tests strain rate according to the interval recommended by ISO 6892-2 (2011). The variation is in-between +/- 30%.

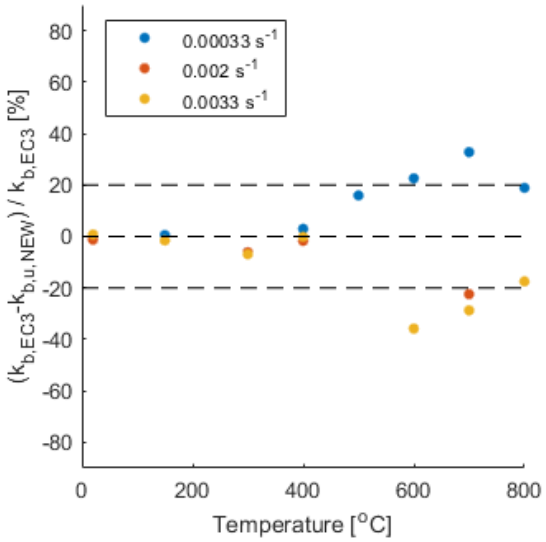

Figure 4. 78. The difference between the new reduction factor and reduction factor from EN1993-1-2 (2005).

As shown in Figure 4. 79., the blue dots (0.000033 s^{-1}) are below the values from the EN1993-1-2 (2005). Therefore, it can be concluded that a lower strain rate will conduct to a bolt failure under a smaller force that EN1993-1-2 (2005) estimates. So, the Eurocode values overestimate the reduction coefficient $k_{b,\theta}$, especially for temperatures above 400 °C, where the difference is in between 40-80%.

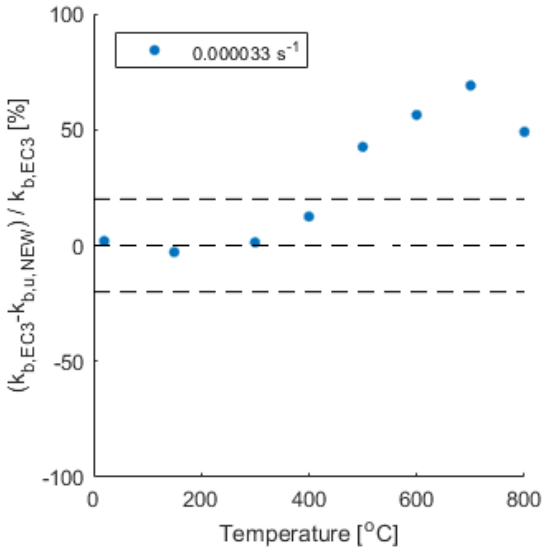

Figure 4. 79. The difference between the new reduction factor and reduction factor from EN1993-1-2 (2005).

The rest of the dots, which represent different strain rate values, above 0.0033 s^{-1} until 0.06 s^{-1}, offer a higher value of k_b than the ones estimated by the Eurocode. As it can be observed in Figure 4. 80., especially for temperatures above 500 °C, the Eurocode underestimates the reduction factor values.

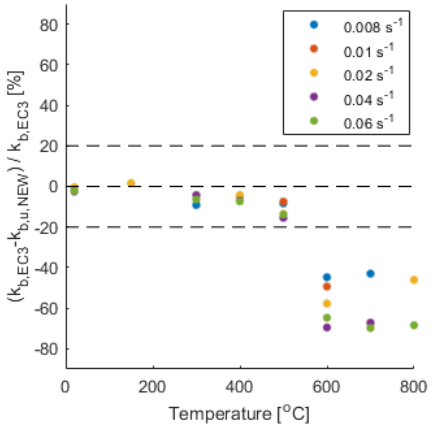

Figure 4. 80. The difference between the new reduction factor and reduction factor from EN1993-1-2 (2005).

4.8.1 Proposed Equations for the tensile strength - new reduction factors

A series of equations were developed (see Figure 4. 81. until Figure 4. 86.) for the computation of the tensile strength new reduction factors, $k_{b,u,new}$, function of the strain rate, for a given temperature. It was observed that the strain rate has a negligible influence over the bolt strength, for temperatures below 400 °C.

$$k_{b,u,new} = 0.0195 \ln(\dot{\varepsilon}) + 0.8955 \quad \text{for } \theta = 400\ ^{o}C \quad [4.13]$$

$$k_{b,u,new} = 0.0422 \ln(\dot{\varepsilon}) + 0.7797 \quad \text{for } \theta = 500\ ^{o}C \quad [4.14]$$

$$k_{b,u,new} = 0.0461 \ln(\dot{\varepsilon}) + 0.6804 \quad \text{for } \theta = 542\ ^{o}C \quad [4.15]$$

$$k_{b,u,new} = 0.0385 \ln(\dot{\varepsilon}) + 0.496 \quad \text{for } \theta = 600\ ^{o}C \quad [4.16]$$

$$k_{b,u,new} = 0.0200 \ln(\dot{\varepsilon}) + 0.2462 \quad \text{for } \theta = 700\ ^{o}C \quad [4.17]$$

$$k_{b,u,new} = 0.0104 \ln(\dot{\varepsilon}) + 0.1397 \quad \text{for } \theta = 800\ ^{o}C \quad [4.18]$$

Where $\dot{\varepsilon}$ = the strain rate [s^{-1}].

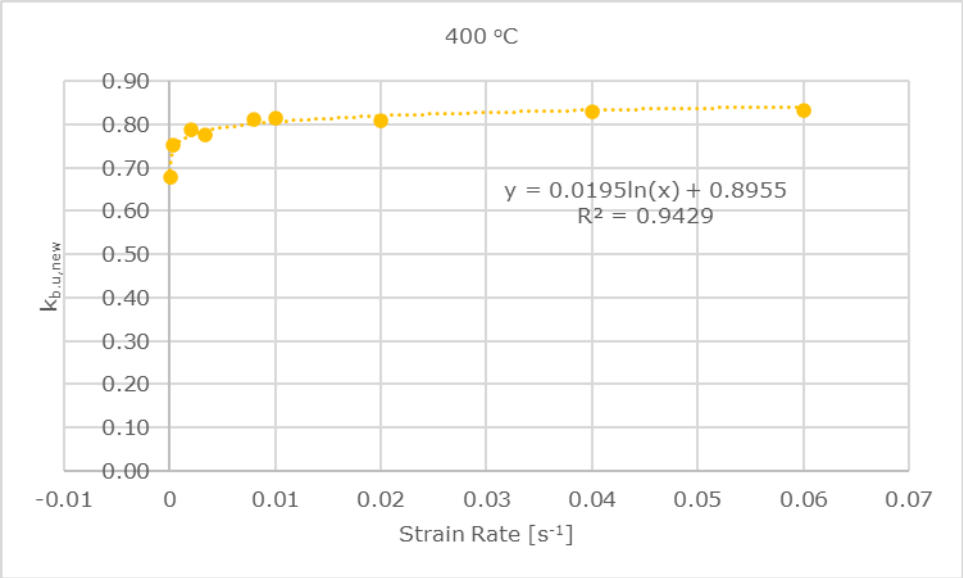

Figure 4. 81. New reduction factors for tensile strength with strain rate: for 400 °C.

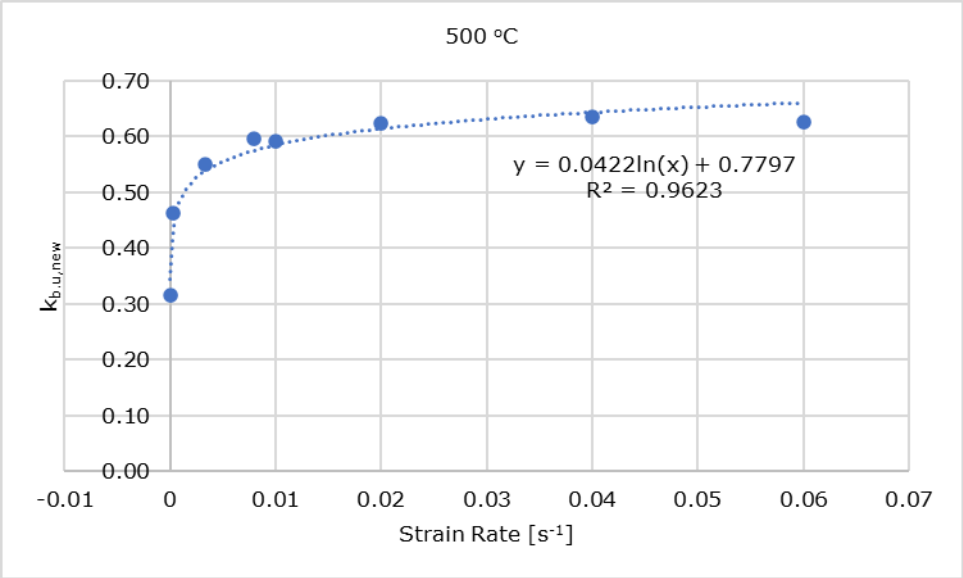

Figure 4. 82. New reduction factors for tensile strength with strain rate: for 500 °C.

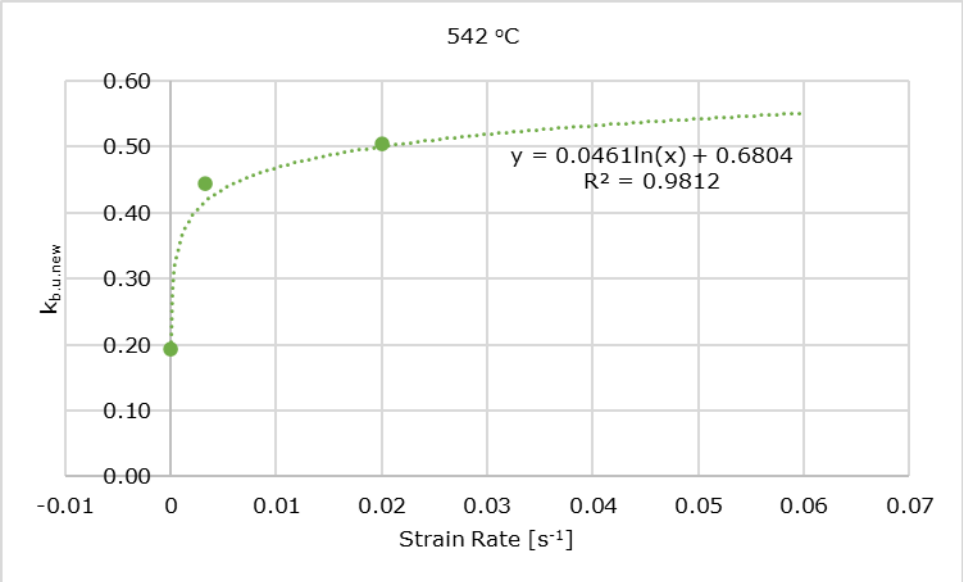

Figure 4. 83. New reduction factors for tensile strength with strain rate: for 542 °C.

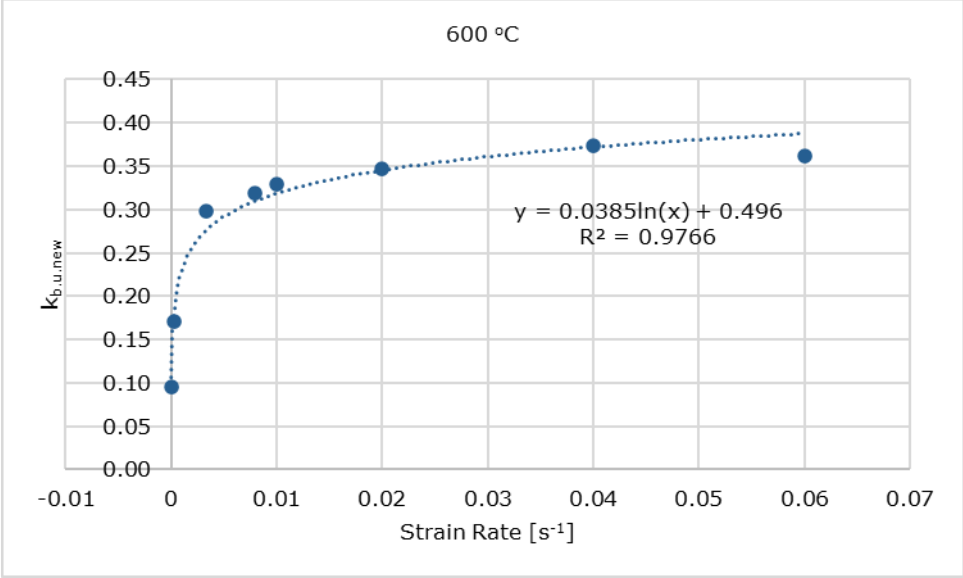

Figure 4. 84. New reduction factors for tensile strength with strain rate: for 600 °C.

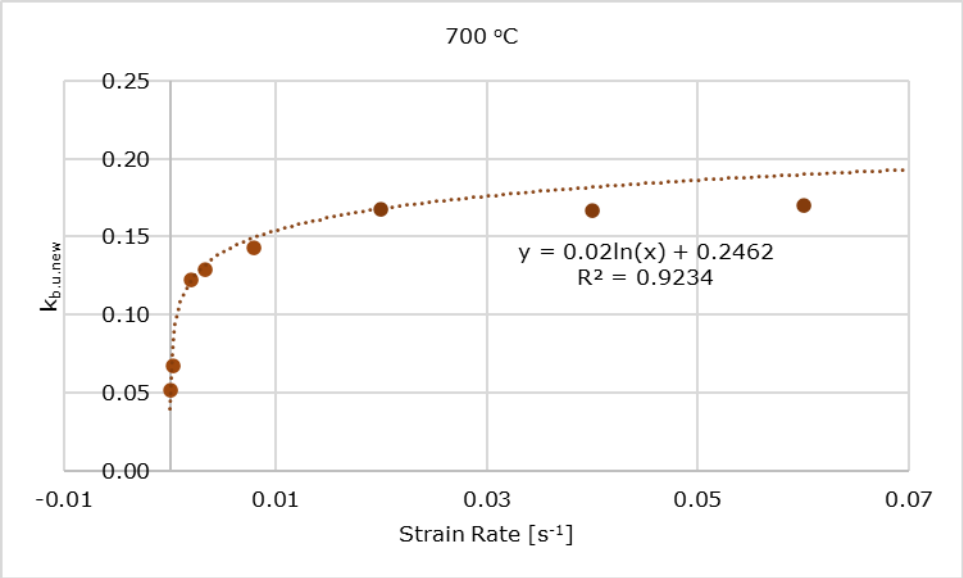

Figure 4. 85. New reduction factors for tensile strength with strain rate: for 700 °C.

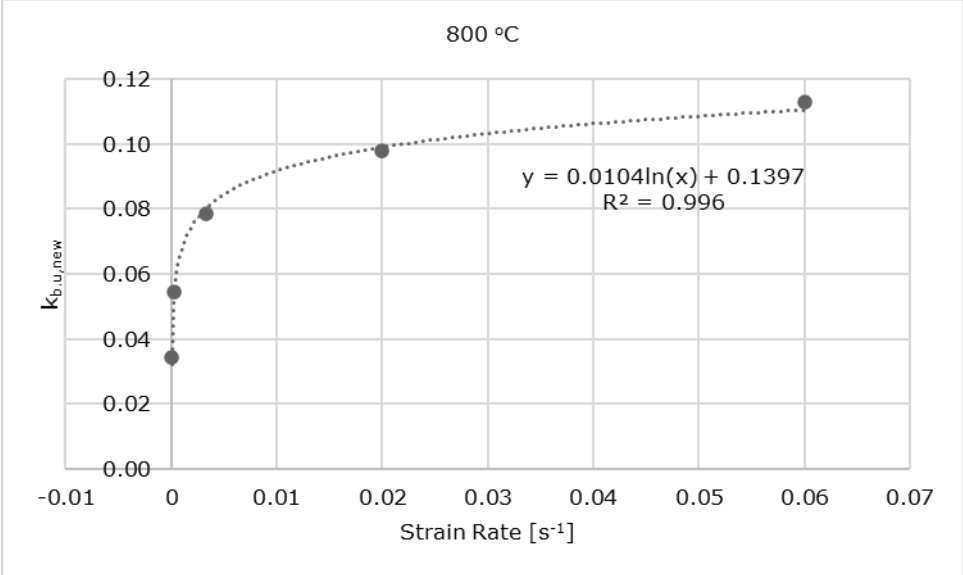

Figure 4. 86. New reduction factors for tensile strength with strain rate: for 800 °C.

The equations 4.13 until 4.18 were developed over the entire range of tested strain rates. As Figures 4.81-86 suggest, after the value of 0.02 s^{-1} the reduction factors increase slightly, while the largest variation is between 0.000033 s^{-1} and 0.02 s^{-1}. The equations will be corrected by assuming that the bolt strength reduction factor does not increase with the strain rate after 0.02 s^{-1}. By limiting the equations to this value, the results provided for the reduction factors in case of a higher strain rate will be underestimated, offering conservative results. Therefore, the final equations should be considered to be Eqs. 4.19 until 4.24, and presented in Figure 4. 87. until Figure 4. 92.

When θ = 400 °C $k_{b,u,new} = 0.0195 \ln(\dot{\varepsilon}) + 0.8955$, for $0.000033\ s^{-1} \leq \dot{\varepsilon} < 0.02$
and $k_{b,u,new} = 0.819$, for $\dot{\varepsilon} \geq 0.02$ [4.19]

When θ = 500 °C $k_{b,u,new} = 0.0422 \ln(\dot{\varepsilon}) + 0.7797$, for $0.000033\ s^{-1} \leq \dot{\varepsilon} < 0.02$
and $k_{b,u,new} = 0.615$, for $\dot{\varepsilon} \geq 0.02$ [4.20]

When θ = 542 °C $k_{b,u,new} = 0.0461 \ln(\dot{\varepsilon}) + 0.6804$, for $0.000033\ s^{-1} \leq \dot{\varepsilon} < 0.02$
and $k_{b,u,new} = 0.504$, for $\dot{\varepsilon} \geq 0.02$ [4.21]

When θ = 600 °C $k_{b,u,new} = 0.0385 \ln(\dot{\varepsilon}) + 0.496$, for $0.000033\ s^{-1} \leq \dot{\varepsilon} < 0.02$
and $k_{b,u,new} = 0.345$, for $\dot{\varepsilon} \geq 0.02$ [4.22]

When θ = 700 °C $k_{b,u,new} = 0.02 \ln(\dot{\varepsilon}) + 0.2462$, for $0.000033\ s^{-1} \leq \dot{\varepsilon} < 0.02$
and $k_{b,u,new} = 0.166$, for $\dot{\varepsilon} \geq 0.02$ [4.23]

When θ = 800 °C $k_{b,u,new} = 0.0104 \ln(\dot{\varepsilon}) + 0.1397$, for $0.000033\ s^{-1} \leq \dot{\varepsilon} < 0.02$
and $k_{b,u,new} = 0.099$, for $\dot{\varepsilon} \geq 0.02$ [4.23]

Where $\dot{\varepsilon}$ = the strain rate [s^{-1}].

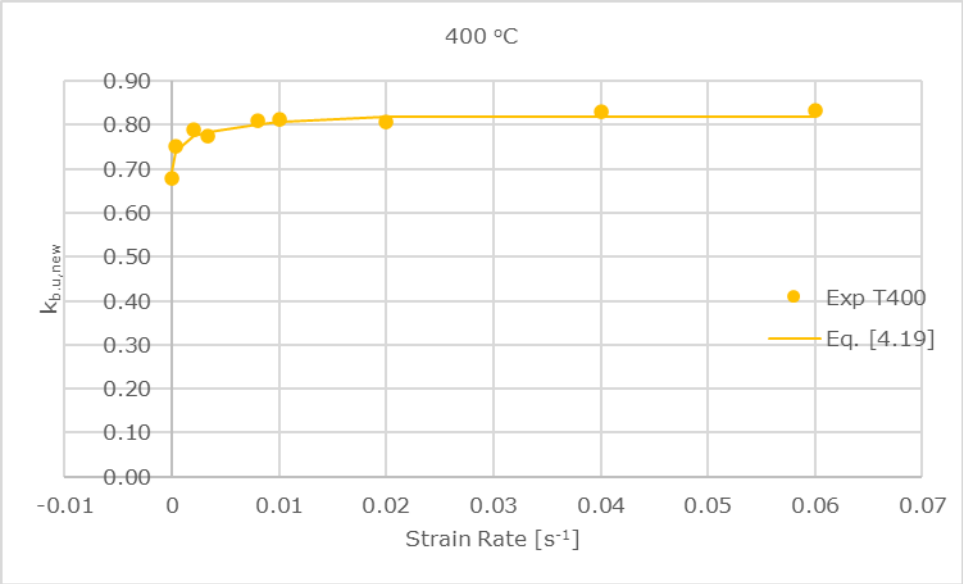

Figure 4. 87. Proposed reduction factors for tensile strength with strain rate: for 400 °C.

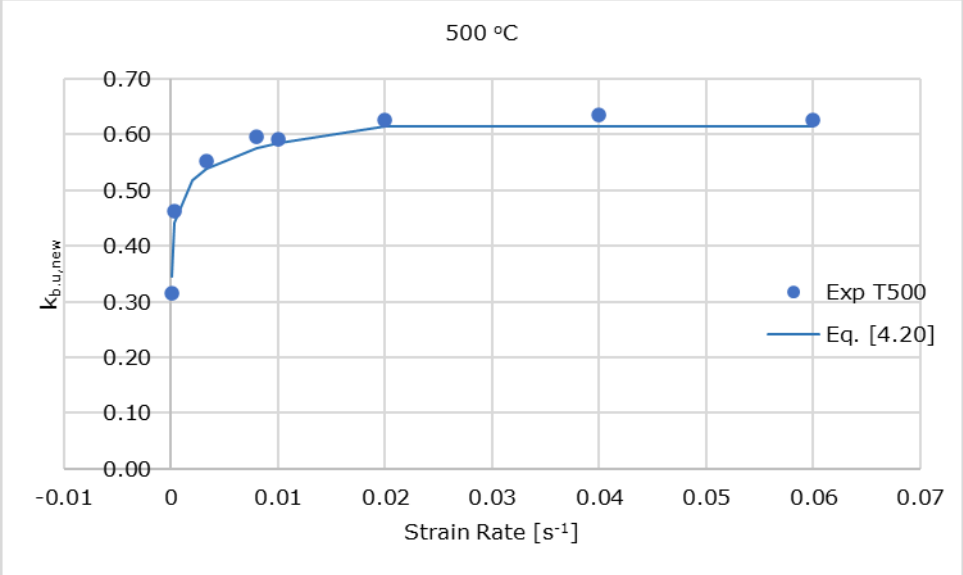

Figure 4. 88. Proposed reduction factors for tensile strength with strain rate: for 500 °C.

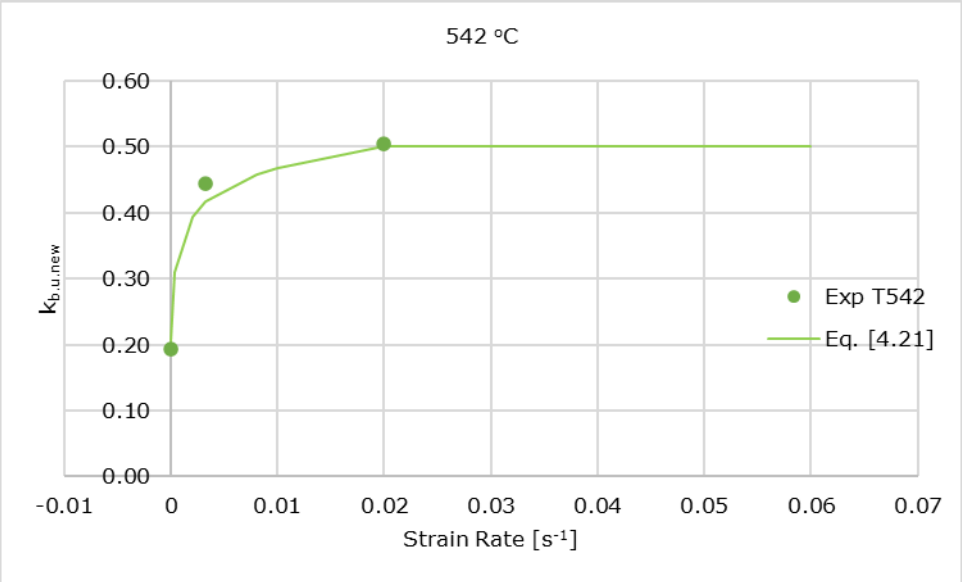

Figure 4. 89. Proposed reduction factors for tensile strength with strain rate: for 542 °C.

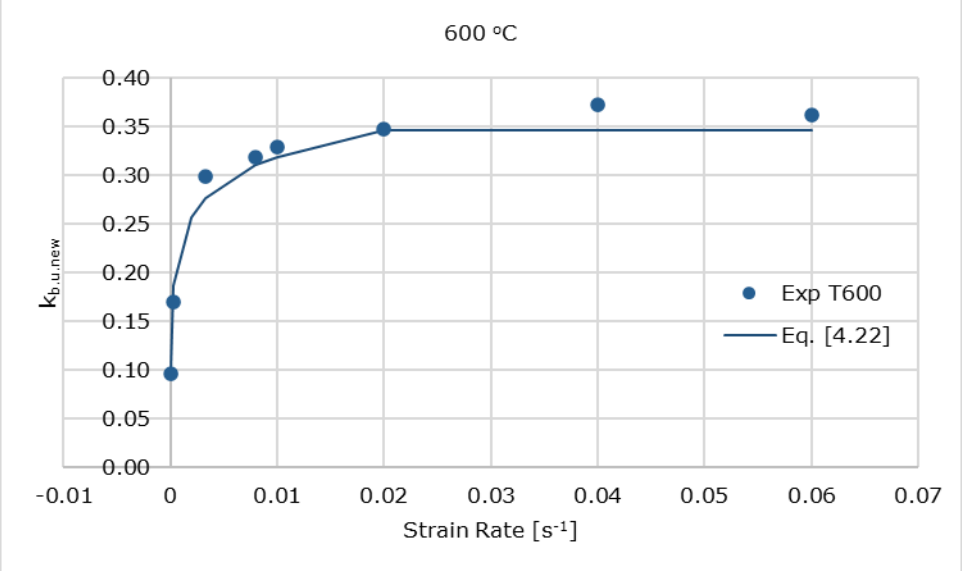

Figure 4. 90. Proposed reduction factors for tensile strength with strain rate: for 600 °C.

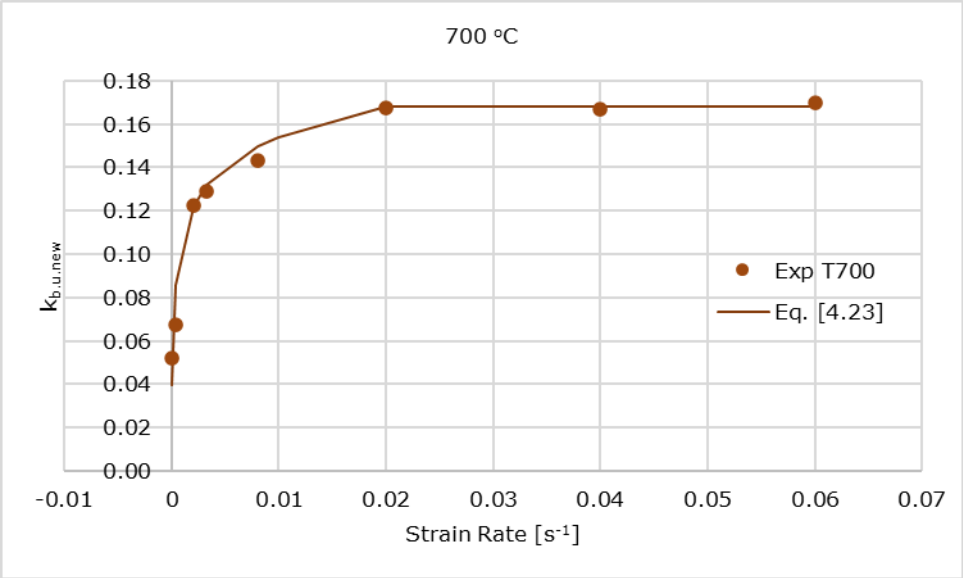

Figure 4. 91. Proposed reduction factors for tensile strength with strain rate: for 700 °C.

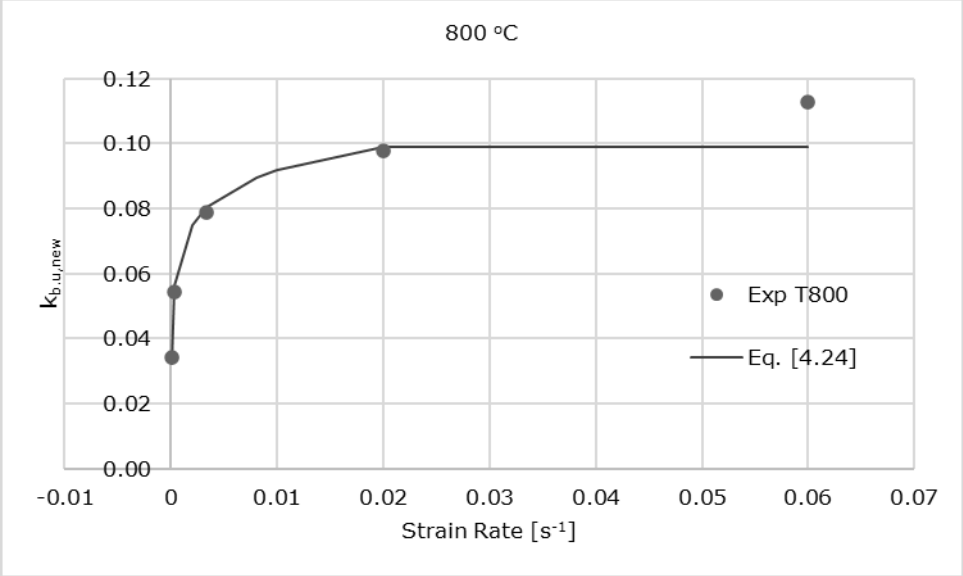

Figure 4. 92. Proposed reduction factors for tensile strength with strain rate: for 800 °C.

4.8.2 Proposed Method

Annex B of ISO 6892-2 mentions that some non-neglectable uncertainties appear due to strain rate in the computation of tensile strength.

Now, one can compute a range for the value of tensile strength based on the new reduction factors presented in Table 4. 7. The minimum factor, $k_{b,u,min}$, was considered for the slowest strain rate applied in this research. The maximum value, $k_{b,u,max}$, is considered to be the factor obtained for the 0.02 s^{-1} strain rate, as from this value up, the influence of the strain rate may be neglected. The proposed values of bolt strength reduction factors are quite similar with the values proposed by EN1993-1-2 (2005) for temperatures below 400 °C. For 0.000033 s^{-1} strain rate, the difference is below 5%, as shown in Table 4.7. For 0.02 s^{-1} strain rate, the difference is below 5%, even for temperature of 400 °C. In contrast for larger temperatures, the reduction factors from EN1993-1-2 (2005), overestimates the reduction factors in case of a 0.000033 s^{-1} strain rate, and underestimates them in case of 0.02 s^{-1} strain rate, with more than 50% in some cases.

Table 4. 7. Proposed reduction factors for grade 10.9 bolt tensile strength.

	$k_{b,u,min}$	**$k_{b,u,max}$**	$k_{b,ec3}$	Difference [%]	
T [°C]	**0.000033 [s^{-1}]**	**0.02 [s^{-1}]**		0.000033 [s^{-1}]	0.02 [s^{-1}]
20	**1**	**1**	1	0	0
100			0.968		
150	**0.979**	**0.936**	0.952	2.9	-1.7
200			0.935		
300	**0.891**	**0.941**	0.903	-1.3	4.2
400	**0.678**	**0.808**	0.775	-12.5	4.2
500	**0.316**	**0.625**	0.55	-42.5	13.6
542	**0.195**	**0.504**			
600	**0.096**	**0.347**	0.22	-56.4	57.7
700	**0.052**	**0.168**	0.1	-48.5	67.7
800	**0.034**	**0.098**	0.067	-49.3	46.0
900			0.033		

4.9 Conclusions

The experimental tests conducted in this study involved the use of tensile tests on grade 10.9 bolt material. The aim was to obtain a stress-strain curve that accurately describes the material behaviour. To achieve this, machined specimens were tested, and the influence of temperature and applied strain rate on the material was thoroughly investigated. In total, 81 testing configurations were analysed, each of which was repeated to ensure measurement accuracy. The results variability was

found to be under 5% for all configurations, except for one where the difference was approximately 6%.

Before any further assessment of the mechanical properties could be done, the raw data obtained from the laboratory was analysed.

One key area of assessment was the yield strength position. It was concluded that the yield strength value for grade 10.9 bolts should be taken at 0.5% strain on the stress-strain curve. This conclusion was verified by comparing the modulus of elasticity provided by the EN1993-1-2 (2005) for steel under elevated temperature with the modulus of elasticity obtained experimentally.

The Eurocode EN1993-1-2 (2005) provides reduction factors, $k_{b,\theta}$, that refer to the bolt strength reduction under elevated temperature. Therefore, a rigorous analysis of the tensile strength variation with temperature and strain rate was carried out. As expected, the tensile strength decreases with an increase in temperature. The strain rate has a small influence on tensile strength when the temperature is 400 ^{o}C or below, with a maximum standard deviation of 6% in these cases. However, a greater variability in the results was observed for temperatures of 500 ^{o}C and above, until 800 ^{o}C. The standard deviation reaches 20% for 500 ^{o}C, and it is around 40% for higher temperatures.

The results obtained from the experimental tests were used to propose a new table for the reduction factors for grade 10.9 bolt strength under elevated temperature. These new reduction factors are directly dependent on the strain rate that might develop in a bolt, during a fire event. This enables the computation of an interval of bolt strength values, when designing a connection under elevated temperature. This interval allowed for the coverage of a wide range of possible fire scenarios, whereby the strain rate developed in the bolt could range from very low, 0.000033 s^{-1}, to very high, 0.02 s^{-1}. Additionally, it was observed that the tensile strength increases negligibly when the strain rate is higher than 0.02 s^{-1}. Therefore this strain rate value can be considered as the limit when assessing the strength of the connections under elevated temperatures, within an extreme scenario as a local collapse of a structural element.

Overall, the proposed reduction factors are offered in the form of equations and in the tabular form as well, providing a practical tool for engineers when designing connections under elevated temperatures.

5 Numerical Simulations

This chapter describes the numerical analysis of the T-stub bolted connection in fire. The validation of the numerical model is made against experimental tests on T-stubs, under normal and elevated temperature, realized by Both et al. (2021), at the laboratory of the Department of Steel Structures and Structural Mechanics. The finite element model is presented, including characteristics such as geometry, materials, loads and contact interactions, mesh, and finite element type. The chapter emphasise the importance of the strain rate at elevated temperature in the behaviour of grade 10.9 bolt, which has a direct impact on the behaviour of T-stub connection.

5.1 Experimental Tests on T-stub Connection

An extensive experimental program was carried out at the Politehnica University of Timișoara, to assess the performance of T-stubs when exposed to extreme conditions of high temperature and high loading rate (Both et al., 2021). This program was an essential component of a larger research project (CODEC, 2012) focused on connection components, full-scale joints and sub-assemblies, with the primary goal of investigating the robustness of structures under extreme loadings. The experimental program consisted of 44 tests, with 11 different geometrical configurations, conducted under quasi-static and high loading rate protocols, both at normal and high temperature in a steady-state approach.

The T-stubs were positioned vertically in the Instron dynamic universal testing machine of 1000kN, as shown in Figure 5. 1. (Both et al., 2021), with the lower part of the specimen fixed into the device and the upper part clamped in the grips of the device's cross-head. Each T-stub was made up of an end plate (S235) and a web plate (S355) welded together (Figure 5. 2.). Each specimen was realized from a pair of identical T-stubs linked together with two Grade 10.9 bolts of 16 mm diameter. The tests under at high temperature were performed by introducing the specimens into the Zwick environmental chamber (see Figure 5.1).

One of the 11 geometrical configurations (Both et al., 2021) is used for numerical model validation. The specimen, originally referred to as T-12-16-100, consists of a pair of T-stubs with a 12 mm flange thickness, 10 mm web thickness, and 100 mm distance between the two M16 bolts. This configuration was used in four tests:

- two at normal temperature - one under quasi-static loading rate (labelled T-12-16-100-C), and one under high loading rate (labelled T-12-16-100-CS);
- two at 542 °C - one under quasi-static loading rate (labelled T-12-16-100-T) and one under high loading rate (labelled T-12-16-100-TS).

The specimens marked with the suffixes C/T were loaded at a displacement rate of 0.05 mm/s (quasi-static loading rate), while those marked with CS/TS were

loaded at 10 mm/s (high loading rate). The strain values were recorded using a crosshead displacement transducer.

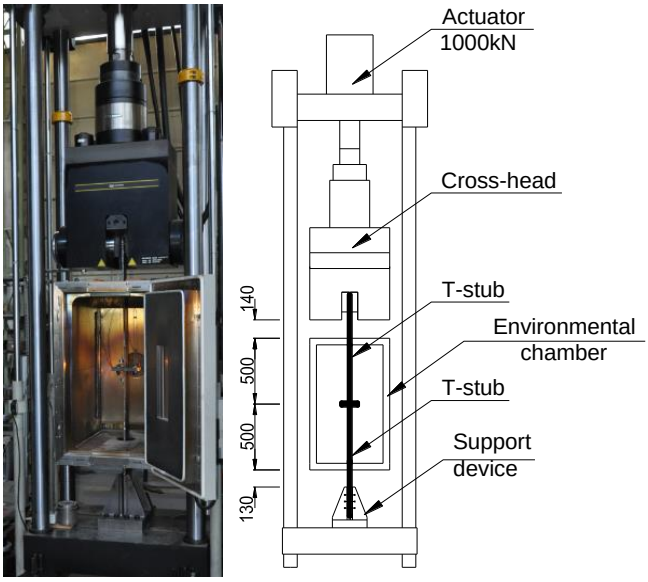

Figure 5. 1. Experimental set-up (Both et al., 2021).

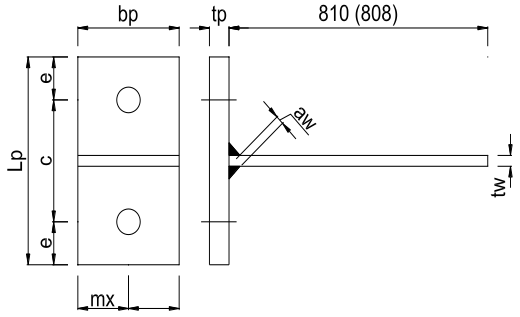

t_p=12 mm; b_p=90 mm; L_p=100 mm; e=30 mm.
Figure 5. 2. Experimental set-up: T-stub geometry (Both et al., 2021).

Both et al. (2021) found that at normal temperature, under quasi-static and high loading rate, in all cases, the ultimate force of the T-stubs was attained by the failure of the bolts. For the geometrical configuration T-12-16-100, due to reduced distance between the bolts, the failure mode is represented by Mode 2, close to Mode 3. It must be mentioned that according to EN1993-1-8 (2005), the T-stub connection can present three modes of failure:

- Mode 1: The plastic hinges are formed within the flange adjacent to the web, which is subsequently followed by the yielding and fracturing of bolts;
- Mode 2: the plastic hinges will emerge in the flanges located near the web and bolt lines, and this will ultimately lead to bolt yield and fracture;
- Mode 3: the bolt broke, while the flanges maintain their elasticity.

The typical modes of failure of a T-stub are represented in Figure 5. 3. Figure 5. 4. shows the T-12-16-100 specimen after was tested under quasi-static loading rate and under high loading rate, respectively.

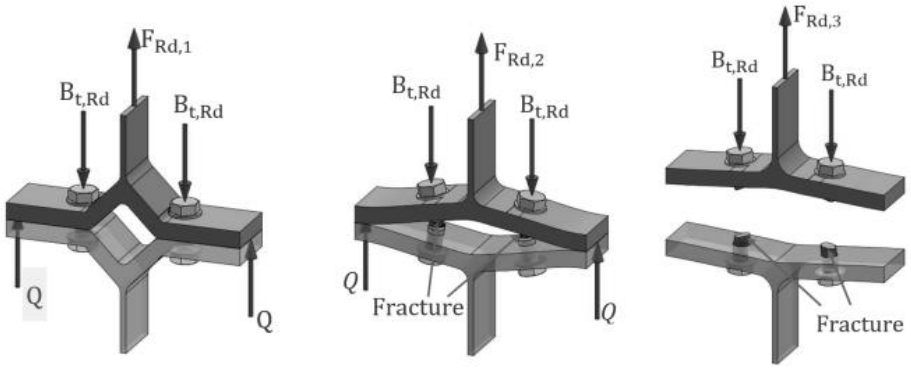

Figure 5. 3. T-stub failure modes : Mode 1, Mode 2, Mode 3 (Aquino et al., 2021).

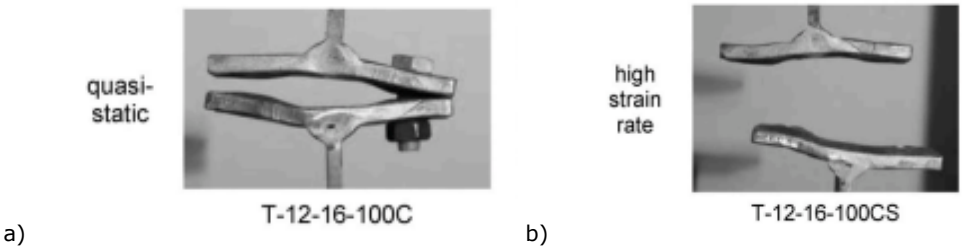

a) b)

Figure 5. 4. T-12-16-100 specimen after being tested at normal temperature, under a. quasi-static loading rate and b. high loading rate (Both et al., 2021).

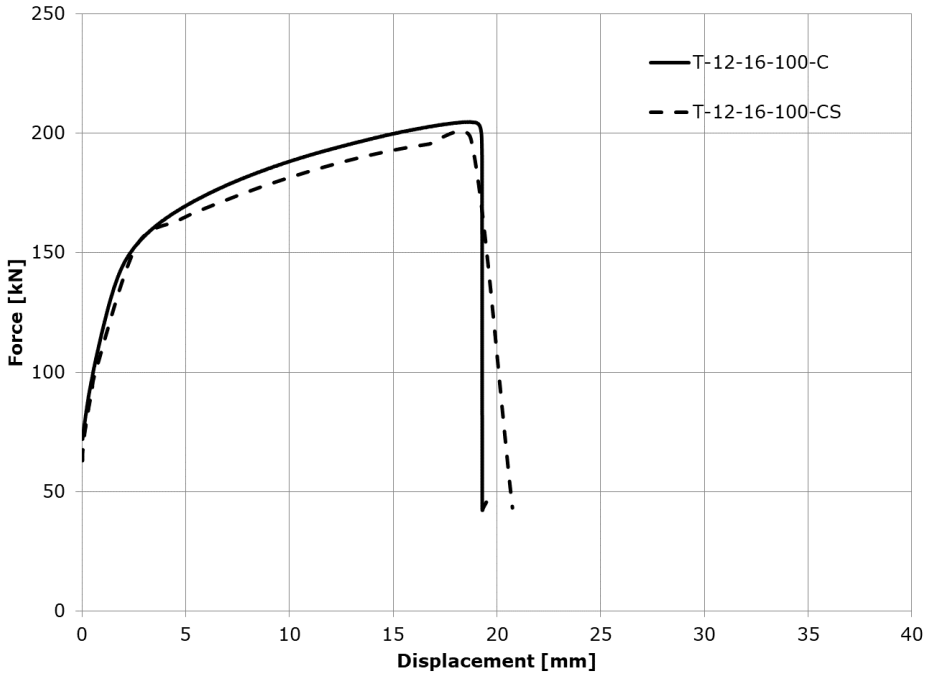

Figure 5. 5. The force – displacement curves of T-12-16-100 configuration, under normal temperature conditions (Both et al., 2021).

The force – displacement curves obtained in both tests (T-12-16-100C and T-12-16-100CS) conducted under normal temperature conditions show similar behaviour, as shown in Figure 5. 5. Based on similar results obtained for the other specimens, the authors (Both et al., 2021) concluded that the loading rate does not significantly affect the maximum strength and deformation capacity, and it does not influence the failure modes in case of tests under normal temperature.

The deformed shape of the configuration T-12-16-100 following experimental testing at a high temperature of 542°C is presented in Figure 5. 6. (Both et al., 2021). The specimens showed different failure modes, depending on the loading rate, with Mode 2 observed under high loading rate and a failure mode closer to Mode 3 under quasi-static loading. This is due to the relative increase in bolt strength when subjected to high loading rates, which allows for the development of plastic deformations in the flanges. Both et al. (2021) concluded that the strain rate plays a significant role in assessing the behaviour of bolted connections at elevated temperatures.

Figure 5. 7. displays the force-displacement curves obtained from the tests (T-12-16-100T and T-12-16-100TS) conducted under elevated temperature. It can be seen that the specimen presented different behaviour, for different loading rates:

a higher maximum force and displacement reached when subjected to a high loading rate.

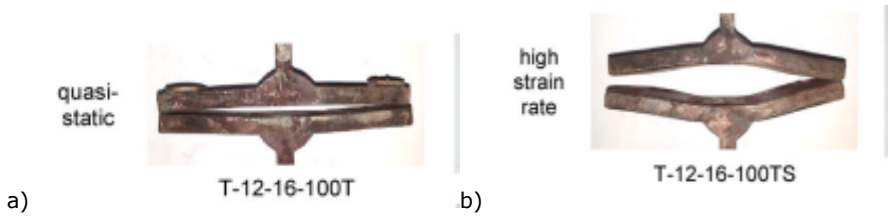

Figure 5. 6. T-12-16-100 specimen after being tested at elevated temperature, under a. quasi-static loading rate; b. high loading rate (Both et al., 2021).

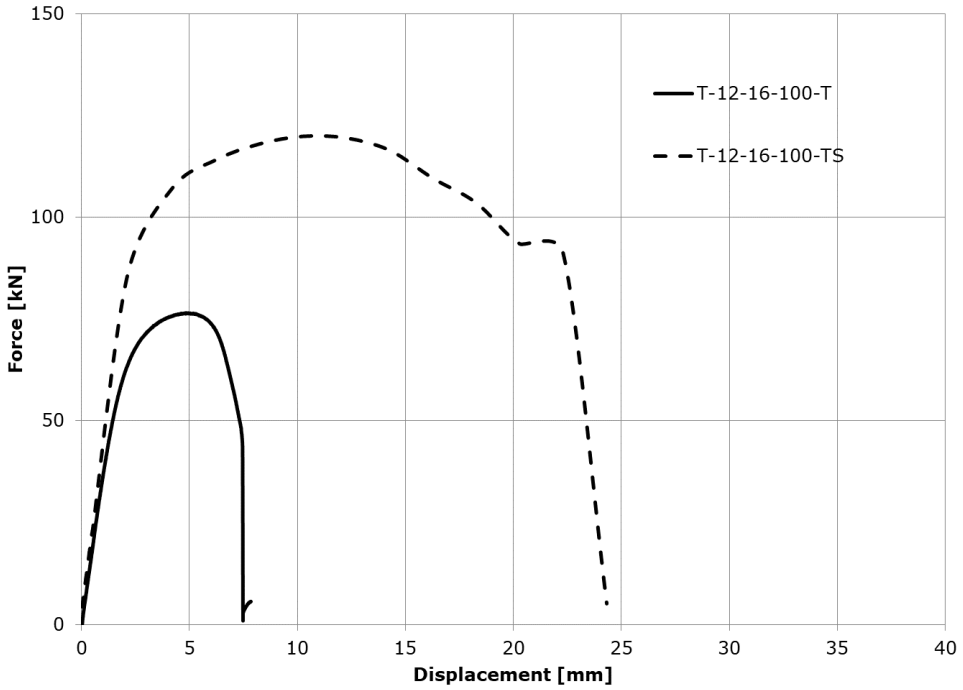

Figure 5. 7. The force – displacement curves of T-12-16-100 configuration, under elevated temperature conditions (Both et al., 2021).

5.2 The Finite Element Model

The geometrical configuration T-12-16-100 was modelled into Abaqus software (Abaqus, 2014), as shown in Figure 5.8. The T-stub components, such as plates and bolts, were created as 3D solid elements, through Extrude operation from the cross-section sketch.

The boundary conditions are assigned in the two reference points at the connection ends, labelled as RP-1 and RP-2. The model consists of two assemblies,

i.e. two T-stubs elements. Each assembly is formed of two plates, the web plate and the flange plate. The assemblies are connected with two M16 bolts.

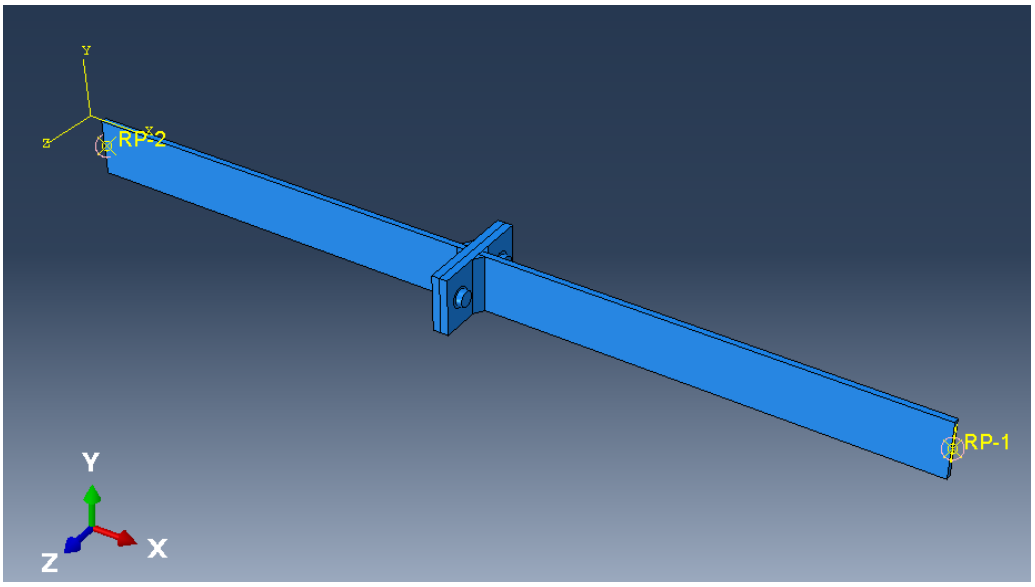

Figure 5. 8. 3D numerical model.

Figure 5. 9. presents the finite element model discretization, which is meshed using C3D8R finite elements (8-node linear brick, reduced integration). This type of element is a hexahedral solid element, named eight-node brick, composed of a single homogeneous material, with 3 displacement degrees of freedom (Abaqus, 2014). This element was considered for its ability to perform better for nonlinear problems, involving plasticity and contact phenomenon. In particular, the eight-node element leads to improved numerical solutions since they allow for a better representation of the discontinuities at element edges and of the strain field. In order to avoid the overlaps of the material during the simulations and deformation of the elements, the components of the assembly were given the "hard" contact properties, which aims to reproduce the real behaviour of solids.

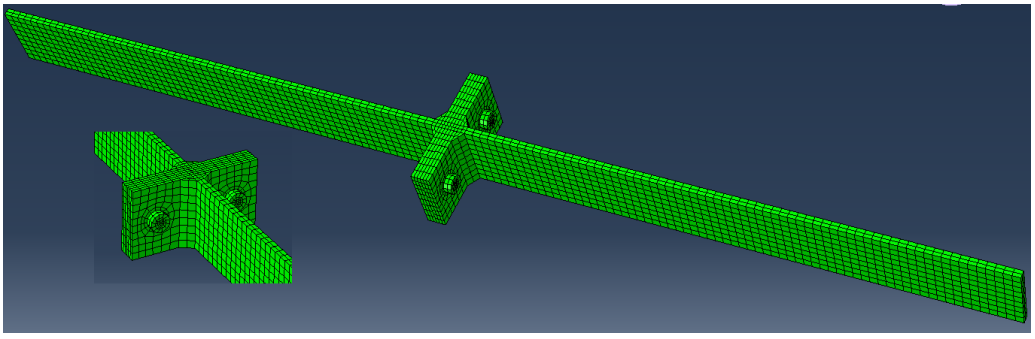

Figure 5. 9. Specimen discretization.

Geometry

The finite element (FE) models and the experimentally tested T-stub specimens were identical from geometrical point of view. The nominal and measured dimensions are presented in Table 5. 1. (Both et al., 2021). There were created 4 geometrical models, for each experimental tests:

- Numerical model 1: Labelled M1_20_Q, was meant to reproduce the experimental test T-12-16-100C, under normal temperature and quasi-static loading rate, of 0.05 mm/s;
- Numerical model 2: Labelled M2_20_H, was meant to reproduce the experimental test T-12-16-100CS, under normal temperature and high loading rate, of 10 mm/s;
- Numerical model 3: Labelled M3_542_Q, was meant to be compared with the experimental test T-12-16-100T, under elevated temperature (542 °C) and quasi-static loading rate, of 0.05 mm/s;
- Numerical model 4: Labelled M4_542_H, was meant to be compared with the experimental test T-12-16-100TS, under elevated temperature (542 °C) and high loading rate, of 10 mm/s;

Table 5. 1. Dimensions of the T-stubs (Both et all., 2021).

Specimen	Nominal					Measured / Modelled				
	t_p	b_p	c	e	m_x	t_p	b_p	c	e	m_x
T-12-16-100C	12	90	100	30	45	11.74	88.56	101.3	29.6	44.8
						11.7	89.19	101.4	28.6	43.5
T-12-16-100CS	12	90	100	30	45	11.77	88.9	102.7	27.9	44.7
						11.89	88.16	101.5	29.0	44.8
T-12-16-100T	12	90	100	30	45	11.8	88.9	101.5	29.1	44.1
						11.8	89.0	101.6	29.2	43.5
T-12-16-100TS	12	90	100	30	45	11.8	89.2	101.9	29.4	43.6
						11.8	89.2	101.0	29.1	43.9

Materials

Three materials were defined for each numerical model:

- S355, representing the web plate;
- S235, representing the flanges plate;
- B109, representing the bolts.

Samples of steel plates and bolt were tested to obtain the material behaviour at normal temperature.

During the process of conducting a tensile test on steel coupons, it is imperative to take into account any plastic deformation that occurs beyond the point of necking. This is because there may be a discrepancy in the critical cross-sectional area, which can lead to variations between the engineering and true stress-strain diagrams. If left unaddressed, this can ultimately affect the accuracy of numerical simulations that rely on the finite element method. In order to mitigate this risk, it is of high importance to establish a meticulously calibrated true stress-strain curve that can be relied upon for effective numerical investigations (Ene et al., 2022). Therefore, the following formulas are used for the derivation of trus stress – true strain curve (EN1993-1-5, 2005):

$$\sigma_{true} = \sigma_{engineering} (1 + \varepsilon_{engineering}) \quad [5.1.]$$

$$\varepsilon_{true} = \ln(1 + \varepsilon_{engineering}) \quad [5.2.]$$

The web plate's material S355 behaviour as introduced in Abaqus is shown in Figure 5. 10. The preliminary test realized by Both et al. (2021) was made at normal temperature, to obtain the stress-strain curve. Further the true stress – true strain curve was derived using the method presented above. In all 4 numerical models, this material was considered to be not influenced by the temperature, as it was mostly outside of the environmental chamber. Its deformations are considered to be negligible. The modulus of elasticity was considered 210000 kN/mm^2 and the Poisson's ratio equal with 0.3.

The T-stub flanges material behaviour, S235, is shown in Figure 5. 11. This curve was recorded in the laboratory using a sample of the material used for the T-stub (Both et al., 2021), at normal temperature, according to ISO 6298-1 (2009) requirements for material testing. In the numerical models at normal temperature (M1_20_Q and M2_20_H), this curve was transformed in true stress – true strain curve as it is represented in Figure 5. 11., with dark plain line. The modulus of elasticity was considered 210000 kN/mm^2 and the Poisson's ratio equal with 0.3.

For material S235 used in the numerical models at elevated temperature, firstly, the material engineering stress – engineering strain curve was developed based on the Eurocode EN1993-1-2 (2005) method for material behaviour at elevated temperatures (represented in Figure 5. 11. with dashed red line). Further, the true stress – true strain curve was calculated and introduced in the numerical models M3_542_Q and M4_542_H (represented in Figure 5. 11. with plain red line). The modulus of elasticity is 100422 kN/mm^2, as computed according to Eurocode EN1993-1-2 (2005), for 542 ^{o}C.

The material S235 includes the temperature influence, but not strain rate influence. In contrast, for the bolt material, the temperature and the strain rate influence are integrated through the material behaviour.

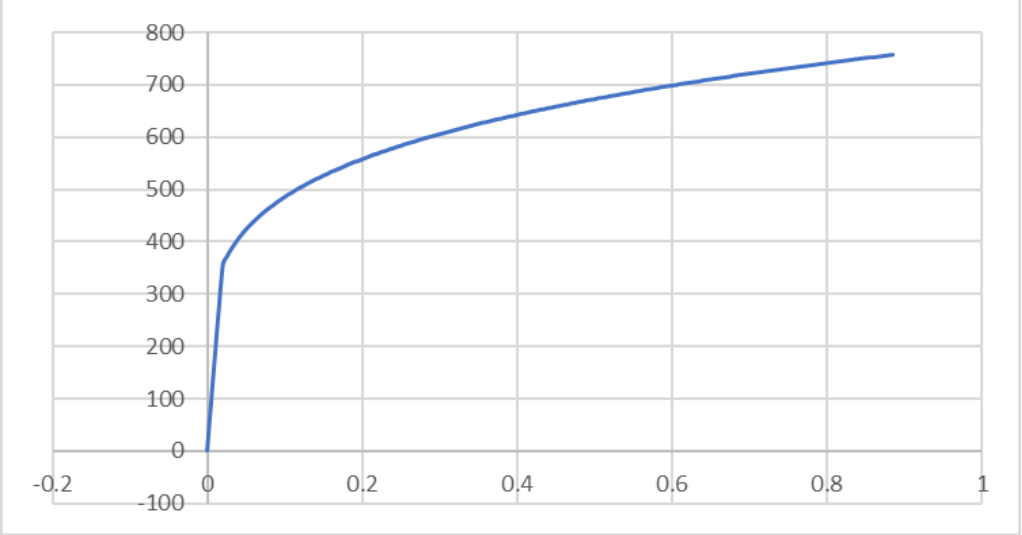

Figure 5. 10. The web plate's material S355: true stress – true strain curve.

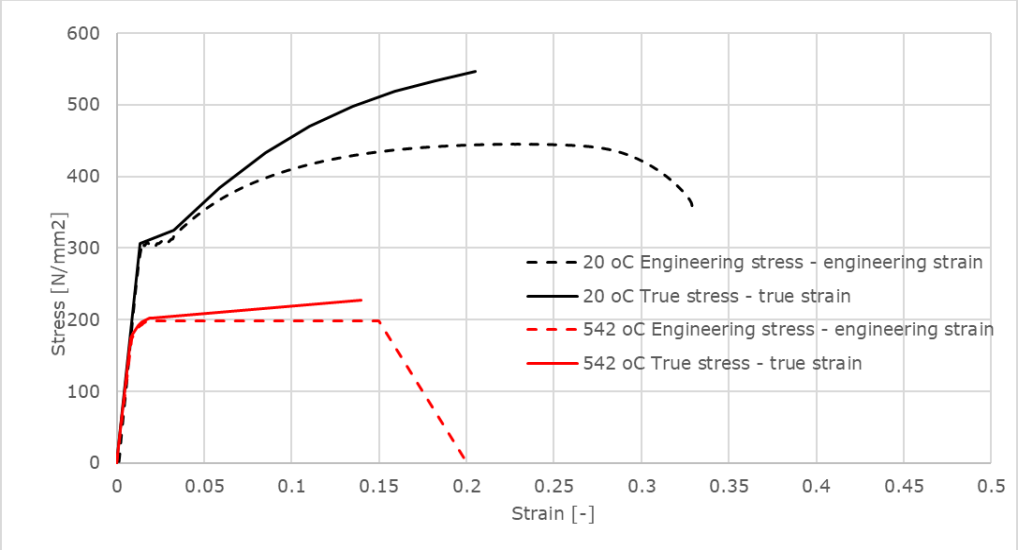

Figure 5. 11. The flanges' material S235.

Figure 5. 12. and Figure 5. 13. present the bolts' material behaviour. From the engineering stress -engineering strain curves obtained in the laboratory, under two strain rates, 0.000033 s^{-1} and 002 s^{-1}, the true stress – true strain curves were derived and modelled in the FE model M1_20_Q and M2_20_H (Figure 5. 12.). Therefore, for this material, a strain rate dependency was introduced. The modulus of elasticity was considered 210000 kN/mm^2 and the Poisson's ratio equal with 0.3.

For the FE models M3_542_Q and M4_542_H, the new proposed reduction factors were computed with equations 4.21 in order to develop the engineering stress

– engineering strain curves, for temperature of 542 °C. The values of $k_{b,u,new}$ considered were 0.276, the correspondent to the quasi-static strain rate test, and 0.504 for the high strain rate test, respectively. The strain rates considered here, are the ones expected to develop in the bolts, in the two experimental tests on T-stubs, under elevated temperature. These values were calculated through a preliminary numerical simulation, where the strain rate in the bolt was assessed and concluded to be 0.000156 s^{-1} for the quasi-static test, and 0.366 s^{-1} for the high strain rate test. As the proposed equations in Chapter 4 are designed to offer conservative results, the reduction factor for high strain rate is limited to the value of 0.504, for temperature of 542 °C, for all strain rates above 0.02 s^{-1}.

The material behaviour curves are presented in Figure 5. 13., together with the corresponding true stress – true strain curves. Therefore, for bolt material, under elevated temperature, a strain rate dependency was introduced. For the the FE models M3_542_Q and M4_542_H, the modulus of elasticity was computed according to Eurocode EN1993-1-2 (2005) to be 100422 kN/mm^2.

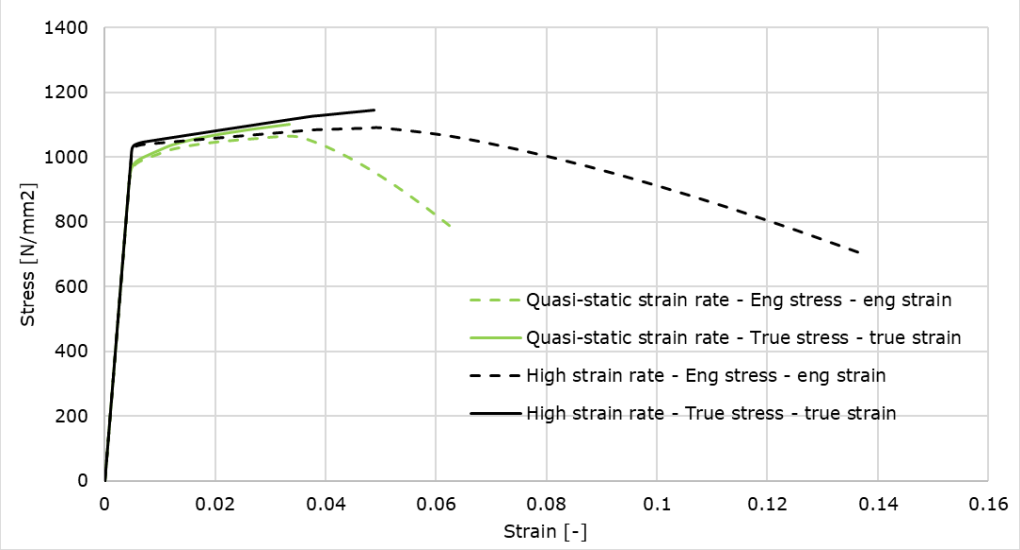

Figure 5. 12. The bolts' material for numerical models M1_20_Q and M2_20_H, strain dependent.

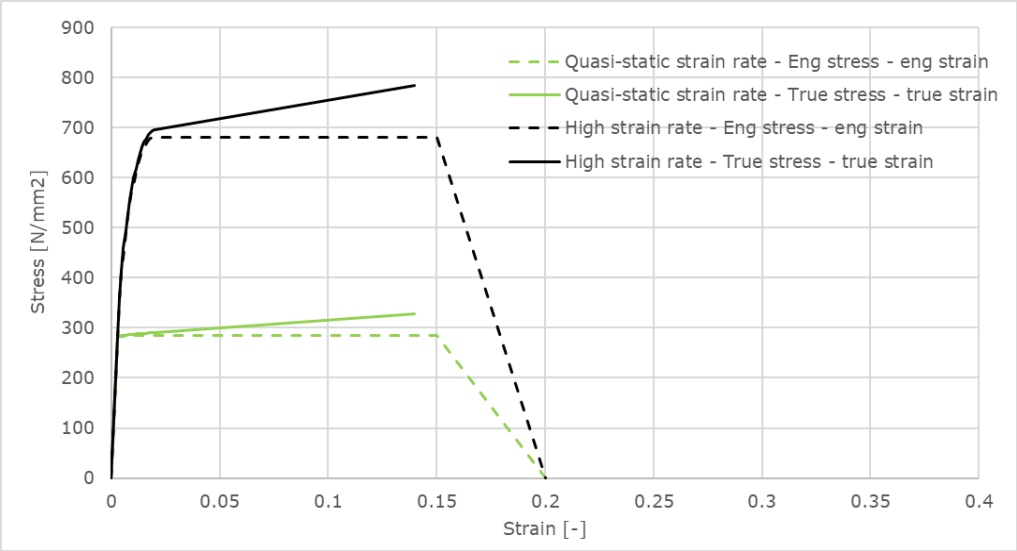

Figure 5. 13. The bolts' material for numerical models M3 and M4, strain dependent.

Boundary conditions

The boundary conditions were defined at the ends of the web plate, in the reference points RP-1 and RP-2, as shown in Figure 5.8. These points constrained all 6 degrees of freedom of the entire surface of the web thickness, through kinematic coupling. This allowed to define a pinned boundary condition (U1=U2=U3=0) in point RP-2 of the T-stub connection, and to apply a constant increasing axial displacement in point RP-1 along the X-axis, acting uniformly on the entire web thickness until the failure of the specimen (Figure 5. 14.).

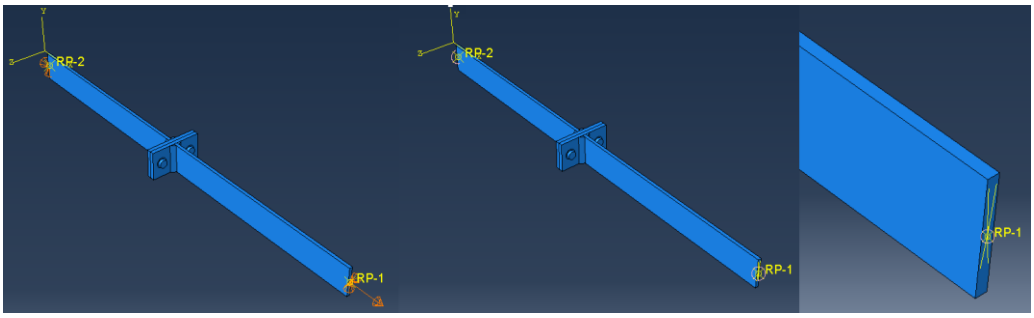

Figure 5. 14. Boundary conditions.

Numerical Analysis

The analysis was performed through a dynamic explicit solver, with a smooth step amplitude to reduce the dynamic effects and to reproduce the conditions of the quasi-static experimental test. The explicit dynamics procedure performs a large

number of small time increments efficiently. The use of small increments is advantageous because it allows the solution to proceed without iterations and without requiring tangent stiffness matrices to be formed. The explicit dynamics procedure is ideally suited for analysing high-speed dynamic events, but many of the advantages of the explicit procedure also apply to the analysis of slower (quasi-static) processes (Abaqus, 2014).

Summary

Based on the numerical models described above, it can be summarized that 4 models were created (Table 5. 2.), by changing the material's behaviour curves and the imposed displacement rate, as follows:

- numerical model 1, M1_20_Q: the S235 steel plate was modelled, using the true stress – true strain curve derived from the experimental material behaviour curve at 20 ^{o}C, as obtained in the laboratory. For the grade 10.9 bolt, the material behaviour curve true stress – true strain was derived from the results obtained in the laboratory, during the tensile test at normal temperature, under 0.000033 s^{-1} strain rate. Therefore, this material is considered as being strain rate dependent.
- numerical model 2, M2_20_H, which contains the same material definition as model M1_20_Q: the S235 steel plate was modelled, using the true stress – true strain curve derived from the experimental material behaviour curve at 20 ^{o}C, as obtained in the laboratory. For the grade 10.9 bolt, the material behaviour curve was derived from the results obtained in the laboratory, during the tensile test at normal temperature, under 0.02 s^{-1} strain rate. Therefore, this material is considered as being strain rate dependent.
- numerical model 3, M3_542_Q: the numerical analysis is realized for elevated temperature of 542 ^{o}C and is reproduced through material definition. The engineering stress – engineering strain curve for the S235 material used for the T-stub flanges was modelled based on the simplified method from the EN1993-1-2 (2005). For the grade 10.9 bolt, the material behaviour engineering stress – engineering strain curve was obtained with the new reduction factors computed with equation 4.15, proposed in the previous chapter, for a 0.000156 s^{-1} strain rate. Therefore, this material is considered as being strain rate dependent.
- numerical model 4, M4_542_H: the numerical analysis is realized for elevated temperature of 542 ^{o}C and is reproduced through material definition. The engineering stress – engineering strain curve for the S235 material used for the T-stub flanges was modelled based on the simplified method from the EN1993-1-2 (2005). For the grade 10.9 bolt, the material behaviour engineering stress – engineering strain curve was obtained with the new reduction factors computed with

equation 4.15, proposed in the previous chapter, for a 0.366 s^{-1} strain rate. Therefore, this material is considered as being strain rate dependent.

Table 5. 2. Overview of the numerical models

Nr	Model's Name	Temperature [°C]	Plate's material behaviour	Bolt's material behaviour	
				obtained	observation
1	M1_20_Q	20	experimentally	experimentally	0.000033 s^{-1}
2	M2_20_H	20	experimentally	experimentally	0.02 s^{-1}
3	M3_542_Q	542	EC3	New Method	0.000156 s^{-1}
4	M4_542_Q	542	EC3	New Method	0.366 s^{-1}

5.3 Numerical Model Validation against the Experimental Tests at Normal Temperature

The overall behaviour of the T-stub connection is represented by the force-displacement curve. The reaction force in the reference point RP-2 and the displacement of the reference point RP-1 were set as the output request. Figure 5. 15. shows a comparison of the force-displacement curve obtained from model M1_20_Q with the one recorded by Both et al. (2021) in the experimental test T-12-16-100C, at normal temperature, under quasi-static strain rate. The numerical results are compliant with the experimental response, validating the numerical procedure. As in the experimental test, the model reproduces well deformations in the T-stub connection, and its failure through bolt rupture (Figure 5. 16.).

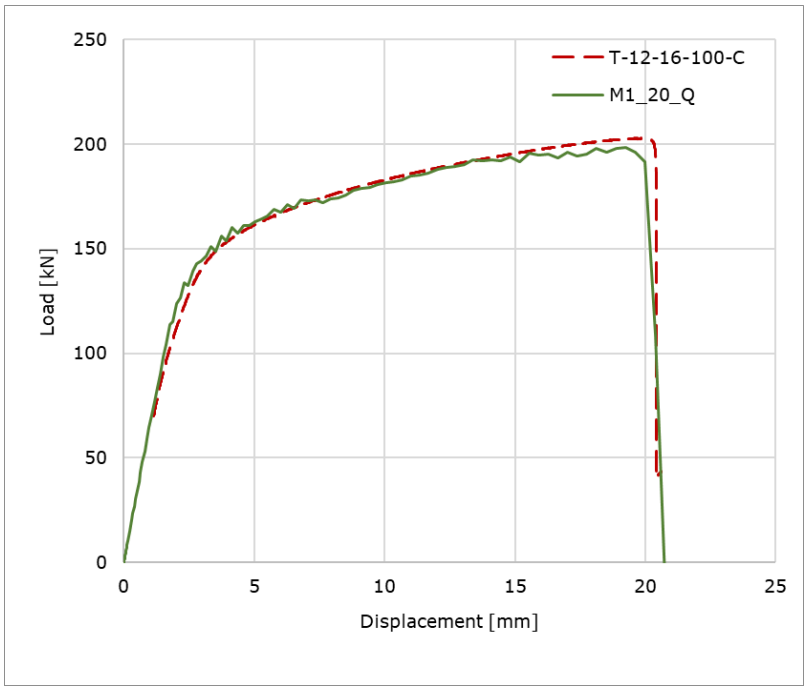

Figure 5. 15. Load-displacement curve: comparison of numerical model M1_20_Q and experimental test T-12-16-100C, at normal temperature, under quasi-static strain rate.

Figure 5. 16. Failure of T-stub specimen in the numerical model M1_20_Q, at normal temperature, under quasi-static strain rate.

Further, the results of numerical model M2_20_H are compared with the experimental tests T-12-16-100CS, at normal temperature, under high strain rate. Figure 5. 17. shows a comparison of between the force-displacement curve obtained numerically and the force-displacement curve recorded by Both et al. (2021) in the experimental test T-12-16-100CS. The numerical results are in accordance with the experimental response, validating the numerical procedure. As in the experimental test, the model reproduces well deformations in the T-stub connection, and its failure through bolt rupture (Figure 5. 18.). It can be seen that the numerical model reproduces very well the deformed shape of the specimen.

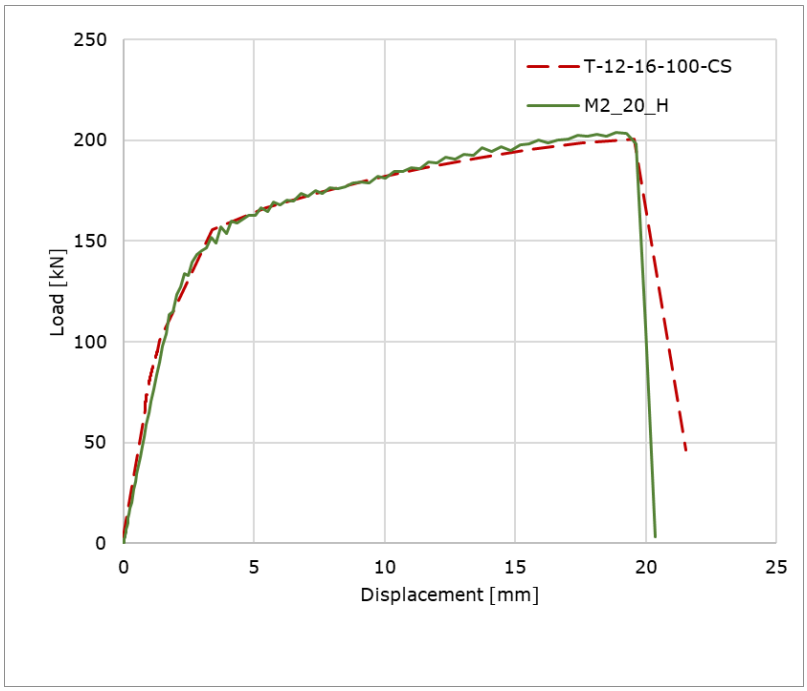

Figure 5. 17. Load-displacement curve: comparison of numerical model M2_20_H and experimental test T-12-16-100CS, at normal temperature, under high strain rate.

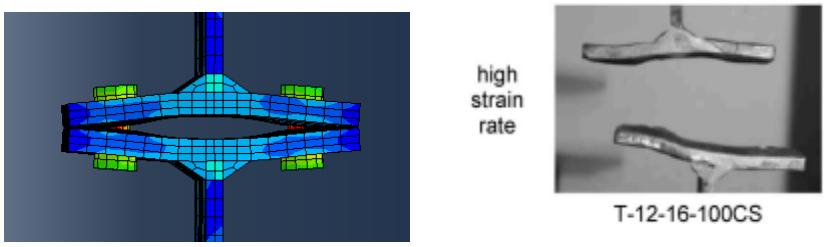

Figure 5. 18. Failure of T-stub specimen in the numerical model M2_20_H, at normal temperature, under high strain rate.

5.4 Numerical Model Assessment under Elevated Temperature, i.e. 542 °C

Using the same numerical procedure, validated in the previous section, the numerical models M3_542_Q and M4_542_H are compared with the experimental results, in terms of force-displacement curve. These models are realized under elevated temperature, of 542 °C. As described in the previous sections, the influence of the temperature is modelled through the material behaviour definition, for all

materials, S235 (flanges) and B109 (bolts). In contrast, only the material B109 considers also the strain influence.

Therefore, the force-displacement curve obtained numerically from model M3_542_Q, considering the value of 0.000156 strain rate for the bolt, is compared with the one obtained experimentally in the experimental T-12-16-100T, at elevated temperature, under quasi-static strain rate, in Figure 5. 19., represented with green lines. It can be seen that the numerical model reproduces very close the experimental curve.

The force-displacement curve obtained numerically from model M4_542_H, considering the value of 0.366 s^{-1} strain rate for the bolt, is compared with the one obtained experimentally in the experimental T-12-16-100TS, at 542 ^{o}C, under high strain rate, in Figure 5. 19., represented with red lines. This discrepancy between the numerical and the experimental curve are due to two factors. First, the S235 material of the flanges does not integrate the effect of high strain rate. Second, the reduction factor for the B109 material of the bolts is limited to the value corresponding to the strain rate of 0.02 s^{-1}, which was conservatively considered in Chapter 4 as being the limit for high strain rates. The real strain rate in the test is more than 18 times higher than the one considered in the numerical simulation. However, it must be underlined that the numerical model gives conservative results in these conditions, offering at the same time a qualitative prediction of the presence of the high strain rate, in comparison with the test / numerical simulation under quasi-static rate.

For comparison, another numerical model was created, in which the bolt material was described by a theoretically developed stress-strain curve, according to the simplified method from the Eurocode (EN1993-1-2, 2005):

- Numerical model 5, M5_EC3: the numerical analysis is realized for elevated temperature of 542 ^{o}C. The S235 material from the steel flanges and the bolts material were modelled using the simplified method from the EN1993-1-2 (2005), i.e. using the reduction factors k_y and $k_{b,\theta}$ from EN1993-1-2 (2005). Therefore, in this numerical model, the material is not strain rate dependent.

It can be seen that the model, which incorporates the material behaviour based on the new reduction factors is reproducing the real behaviour of the T-stub specimen, while the model based on the material developed with the EN1993-1-2 (2005) simplified method offers the same behaviour, no matter the loading conditions.

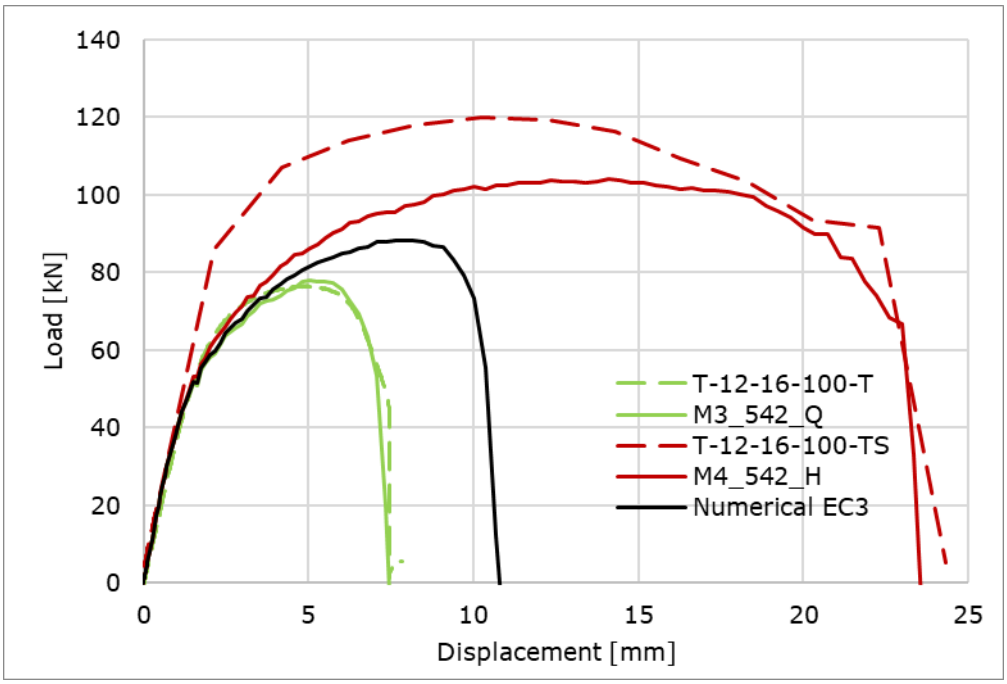

Figure 5. 19. Load-displacement curve: comparison of numerical models and experimental tests, at 542 °C, under quasi-static and high strain rate.

Figure 5. 20. shows the failure mode of the model M3_542_Q., and Figure 5. 21. shows the failure mode of the model M4_542_H. It can be seen that the numerical models reproduce very well the deformed shape of the tested specimens.

Figure 5. 20. Failure of T-stub specimen in the numerical model M3_542_Q, at 542 °C, under quasi-static strain rate.

Figure 5. 21. Failure of T-stub specimen in the numerical model M4_542_H, at 542 °C, under high strain rate.

5.5 Conclusions

In evaluating a bolted T-stub connection, the behaviour of the bolt plays a crucial role. Therefore, a T-stub bolted connection was assessed numerically. Thus, four experimental tests were taken from the literature (Both et al., 2021) and presented here. The tests consist in one geometrical configuration of a T-stub specimen, subjected to tension at normal and elevated temperature (542 °C). For each temperature, two loading conditions were applied: quasi-static loading rate and high loading rate, respectively.

In order to replicate the four experimental tests, the finite element analysis was conducted using Abaqus software. Four numerical models were initially established. The material true stress – true strain curves were derived and integrated into Abaqus models.

Under normal temperature, the material characteristics for both flanges and bolts, were obtained based on experimentally obtained stress-strain curves of the material. The stress-strain curve of S235 material was obtained in accordance with the ISO 6892-1 (2009) guidelines, using a recommended strain rate of 0.00033 s^{-1} for tensile testing. Similarly, the stress-strain curve of grade 10.9 bolt material was also obtained in accordance with the ISO 6892-1 (2009) guidelines. Two tests were performed for this material at low strain rate (0.000033 s^{-1}) and high strain rate (0.02 s^{-1}), respectively. It was observed that the strain rate had little effect on the behaviour of bolt material, with similar tensile strength but differences in material ductility. Therefore, the two numerical models considered the influence of strain rate on the material of the bolt but not on the material of the flanges, under normal temperatures. Although the S235 material did not include the strain rate influence, the model correctly reproduced the T-stub behaviour, as the strain rate influence is negligible at 20°C. The numerical model was successfully validated against experimental tests under both quasi-static loading rates and high loading rates at 20°C.

At 542 °C, the numerical models were compared with the experimental tests on T-stubs. The material's true stress-true strain curves were derived and integrated into Abaqus models. The S235 material behaviour at 542 °C was obtained using the simplified method from EN1993-1-2 (2005), which does not account for the influence of strain rate on material behaviour. However, the material behaviour of grade 10.9 bolt at 542 °C was obtained using the new reduction factors proposed in Chapter 4 of this thesis, which considers the applied strain rate. While the numerical simulations effectively reproduced the overall T-stub behaviour, a discrepancy in terms of maximum force was observed. This inconsistency can be attributed to the stress-strain curve of the S235 material, which does not consider the influence of strain rate under elevated temperatures, but also due to the reduction factor proposed for the bolt's material. This reduction factor was limited to the value corresponding to 0.02 s^{-1} strain rate, from conservative reasons.

A fifth numerical model was created to compare the new reduction factors for bolt material at elevated temperature with the values for the reduction factors from

EN1993-1-2 (2005). Material stress-strain curves were fully developed according to EN1993-1-2 (2005) for both flange and bolt materials, but they did not account for the influence of the strain rate. The numerical model based on material at elevated temperature according to EN1993-1-2 (2005), offers a mean value in terms of maximum force of T-stub. It overestimates the maximum force when the specimen is subjected to quasi-static strain rate and underestimates it when a high strain rate is applied.

In summary, the utilization of the new reduction factors has proven to be accurate in the evaluation the performance of grade 10.9 bolt material under fire conditions. This allows for a thorough analysis of the material's behaviour, providing valuable insights for engineers and other professionals in the field, in various applications that require high-strength bolts.

6 Conclusions and Personal Contributions

The aim of this research was to reveal more information and understanding on behaviour of high strength bolts for steel structures, in particular grade 10.9 bolts in fire conditions, under different loading rates.

The research work consists of two main parts:

- experimental study on mechanical properties of high strength bolts at elevated temperatures, concluded with new reduction factors for bolt strength, depending on the strain rate;
- numerical validation of the proposed new reduction factors, considering a T-stub assembly, experimentally tested under normal and high temperature and different strain rates.

The research work was conducted in the Steel Structures and Structural Mechanics Department of Politehnica University Timișoara. A large study on bolts used in constructions was put together, describing not only their type, but also their manufacturing processes, heat treatments, surface treatments, chemical composition of material, material and bolt assembly behaviour, and design under fire situations. The attention was focused on grade 10.9 bolts' material behaviour under elevated temperatures. From the state of the art, it was concluded that, the strain rate developed in a bolt during a fire scenario, represents an important parameter, as it affects the material's behaviour.

An extensive experimental work was undertaken in the laboratory of the same Department. Specimens, machined from grade 10.9 bolts manufactured according to EN 14399-4 (2005) guidelines, were subjected to tensile testing under 9 temperatures and 9 strain rates. The machined specimens were prepared for testing according to ISO 6892-2 (2011) guidelines. Therefore, 81 configurations were assessed. Each configuration was repeated in order to verify the measurements accuracy.

The temperature represents an important parameter in the study. Values ranging between 20 ^{o}C and 800 ^{o}C, were applied, more specifically: 20 ^{o}C, 150 ^{o}C, 300 ^{o}C, 400 ^{o}C, 500 ^{o}C, 542 ^{o}C, 600 ^{o}C, 700 ^{o}C, and 800 ^{o}C. In the frame of each test, the specimen was fixed in a Instron universal testing machine of 250 kN, and introduced in a MAYTEC HTO-08/01 round furnace. The temperature was increased gradually with a heating rate of 10 K/min. After the target temperature was reached in the oven, the temperature was maintained constant for 10 minutes, to ensure a consistent temperature over entire specimen. The temperature was further maintained constant during the whole test, until the failure of the specimen occurred.

For each temperature, the strain rate applied was in between 0.000033 s^{-1} and 0.06 s^{-1}. In this way the influence of strain rate was assessed at normal temperature and at elevated temperatures, respectively.

The stress-strain curves were recorded from the experimental tests as a description of the material behaviour. The raw data was carefully corrected for different errors, like specimen slippage or human errors.

Further, the yield strength and the tensile strength were found for each test. The yield strength was found to be at 0.5% strain, for almost all configuration, no matter the temperature or the strain rate. The modulus of elasticity was carefully analysed, and it was found to be reduced with the temperature according with the EN1993-1-2 (2005) recommendations.

An in-depth examination was conducted to study the impact of temperature and strain rate on the tensile strength. When the temperature is 400 °C or lower, the strain rate has a minor effect on the tensile strength, with a maximum variation of 6%. However, for temperatures above 500 °C and up to 800 °C, there was a greater variation in the results. The variation for 500 °C was 20%, and for higher temperatures, it was approximately 40%.

Based on experimental tests, a simplified method for calculating the strength of grade 10.9 bolts under high temperatures has been proposed. This method includes new reduction factors that are dependent on the strain rate that may occur in a bolt during a fire. By using this method, a range of bolt strengths can be calculated for designing connections under elevated temperatures, covering a wide range of potential fire scenarios from a very low strain rate of 0.000033 s^{-1} to a very high strain rate of 0.02 s^{-1}. It was also found that the tensile strength of the bolts increases minimally when the strain rate exceeds 0.02 s^{-1}.

In summary, the simplified method proposed is presented below in both equation and tabular forms. This serves as a practical tool for engineers who are designing connections under high temperatures.

The proposed series of equations for the computation of the tensile strength new reduction factors, for grade 10.9 bolts, function of the strain rate, for a given temperature, are:

When θ = 400 °C $k_{b,u,new} = 0.0195 \ln(\dot{\varepsilon}) + 0.8955$, for $0.000033\ s^{-1} \leq \dot{\varepsilon} < 0.02$
and $k_{b,u,new} = 0.819$, for $\dot{\varepsilon} \geq 0.02$ [6.1]

When θ = 500 °C $k_{b,u,new} = 0.0422 \ln(\dot{\varepsilon}) + 0.7797$, for $0.000033\ s^{-1} \leq \dot{\varepsilon} < 0.02$
and $k_{b,u,new} = 0.615$, for $\dot{\varepsilon} \geq 0.02$ [6.2]

When θ = 542 °C $k_{b,u,new} = 0.0461 \ln(\dot{\varepsilon}) + 0.6804$, for $0.000033\ s^{-1} \leq \dot{\varepsilon} < 0.02$
and $k_{b,u,new} = 0.504$, for $\dot{\varepsilon} \geq 0.02$ [6.3]

When θ = 600 °C $k_{b,u,new} = 0.0385 \ln(\dot{\varepsilon}) + 0.496$, for $0.000033\ s^{-1} \leq \dot{\varepsilon} < 0.02$
and $k_{b,u,new} = 0.345$, for $\dot{\varepsilon} \geq 0.02$ [6.4]

When θ = 700 °C $k_{b,u,new} = 0.02 \ln(\dot{\varepsilon}) + 0.2462$, for $0.000033\ s^{-1} \leq \dot{\varepsilon} < 0.02$
and $k_{b,u,new} = 0.166$, for $\dot{\varepsilon} \geq 0.02$ [6.5]

When θ = 800 °C $k_{b,u,new} = 0.0104 \ln(\dot{\varepsilon}) + 0.1397$, for $0.000033\ s^{-1} \leq \dot{\varepsilon} < 0.02$
and $k_{b,u,new} = 0.099$, for $\dot{\varepsilon} \geq 0.02$ [6.6]

Where $\dot{\varepsilon}$ = the strain rate [s^{-1}].

One can compute a range for the value of tensile strength based on the new reduction factors presented below. The minimum factor, $k_{b,u,min}$, was considered for the slowest strain rate applied in this research. The maximum value, $k_{b,u,max}$, is considered to be the factor obtained for the 0.02 s^{-1} strain rate, as from this value up, the influence of the strain rate can be neglected.

Table 6. 1. Proposed reduction factors for grade 10.9 bolt tensile strength.

	$k_{b,u,min}$	$k_{b,u,max}$
T [°C]	**0.000033 [s^{-1}]**	**0.02 [s^{-1}]**
20	**1**	**1**
150	**0.979**	**0.936**
300	**0.891**	**0.941**
400	**0.678**	**0.808**
500	**0.316**	**0.625**
542	**0.195**	**0.504**
600	**0.096**	**0.347**
700	**0.052**	**0.168**
800	**0.034**	**0.098**

The second part of this work consisted into validating the new reduction factors by numerical simulations. As the behaviour of the bolt plays a crucial role in evaluating a bolted T-stub connection, a finite element analysis was conducted using Abaqus software on this type of connection.

Therefore, four experimental tests were extracted from the literature, authored by Both et al. (2021), and briefly outlined. The tests involve a single geometric configuration of a T-stub specimen that is subjected to tension at normal and elevated temperatures (542°C). In each temperature scenario, two loading conditions were applied: quasi-static loading rate and high loading rate.

Numerical models were created to account for the four experimental tests in Abaqus software. Stress-strain curves for flanges and bolts were obtained through experimental testing at normal temperature. The models were validated against the experiments under quasi-static and high loading rates at 20°C.

At 542°C, the models were compared with T-stub tests. The behaviour of grade 10.9 bolt material at 542°C was obtained through the new simplified method proposed in this study, while the behaviour of the flange material was obtained through the simplified method from Eurocode EN1993-1-2 (2005). The numerical models effectively replicated the experiments, in terms of resistance and failure mode. A discrepancy was observed in the overall behaviour for the T-stub subjected to high strain rate, explained through the stress-strain curve of the flange material considered in the numerical model, which does not account for strain rate, as well as the reduction factor for the bolt material, which is conceived to offer conservative results.

An investigation was conducted to compare the new reduction factors for bolt material behaviour at elevated temperatures with the values of the reduction factors provided by EN1993-1-2 (2005). The comparison revealed that the EN1993-1-2

(2005) model overestimated the maximum force at low strain rates and underestimated it at high strain rates.

Further research

Further work could be carried out to enhance the modelling and expand the number of simulated cases. Since the T-stub behaviour is closely linked with the bolt behaviour, the thesis studied the influence of strain rate on the bolt behaviour when Mode 3 failure occurs. The strain rate also affects the structural steel behaviour during fire conditions, so it's response should be evaluated. This approach would allow the analysis of the T-stub behaviour in all three modes of failure.

The thesis proposes reduction factors for the strength of grade 10.9 bolts at elevated temperatures, considering the applied strain rate. Further research can expand the method's scope, including investigating the impact of thread stripping on bolt assembly failure and validating the new coefficients for various bolt grades.

A method of estimating the conditions to which a bolt was exposed during a fire can be established by conducting Vickers hardness measurements on fractured specimens that have failed at the same temperature, but different strain rates. This can be helpful in identifying the causes and mode of failure in the post-structural collapse expert evaluation.

The primary aim of the thesis was to conduct a thorough analysis of the impact of strain rate on bolt strength, paving the way for further research into bolt behaviour, as the strain rate influence also the bolt's ductility. Further research has the potential to enhance the knowledge in the field of complex numerical simulations of connections under extreme loading conditions.

A summary of personal contributions:

- a comprehensive literature survey regarding the bolt's tests at elevated temperature, which highlighted the gaps in the actual knowledge;
- experimental set-up for testing the bolts under 81 configurations (9 temperatures and 9 strain rates);
- setting the value of 0.000033 s^{-1} as being the correct conservative strain rate for quasi-static applications;
- setting the value of 0.02 s^{-1} as being the conservative strain rate for high strain rate applications;
- new reduction factors for the resistance under elevated temperature of grade 10.9 bolts, which correct the existing EN1993-1-2 (2005) values, taking also into account the influence of the strain rate;
- validation of the new reduction factors in comparison with existing tests on T-stubs sub-assemblies.

7 Annexes

7.1 Annex A – Laboratory Results

This Annex presents all the stress-strain curves recorded in the laboratory during this research.

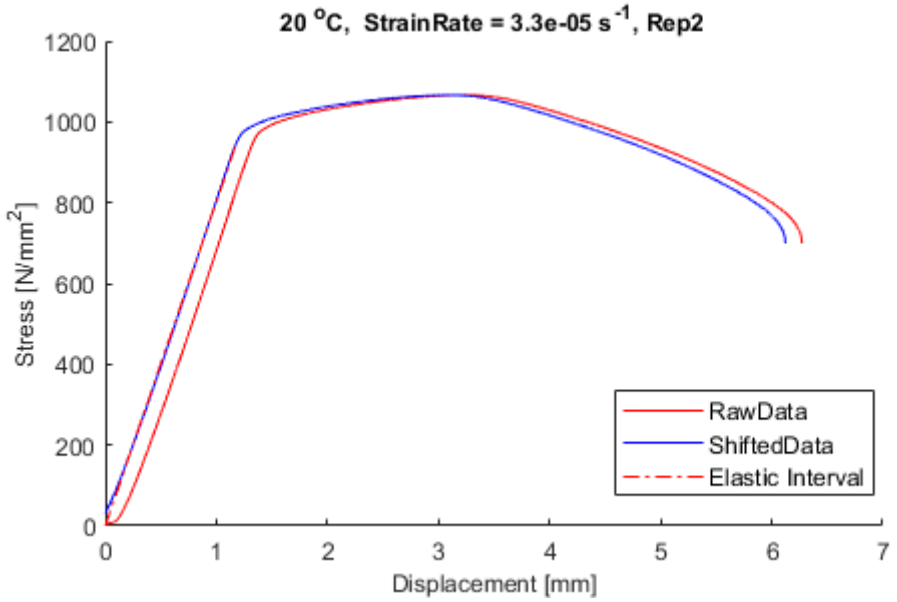

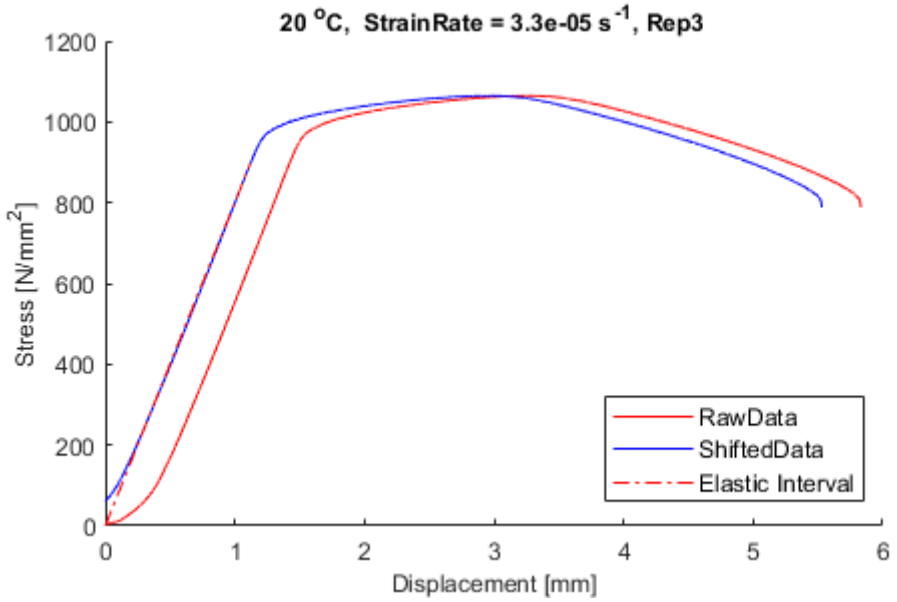

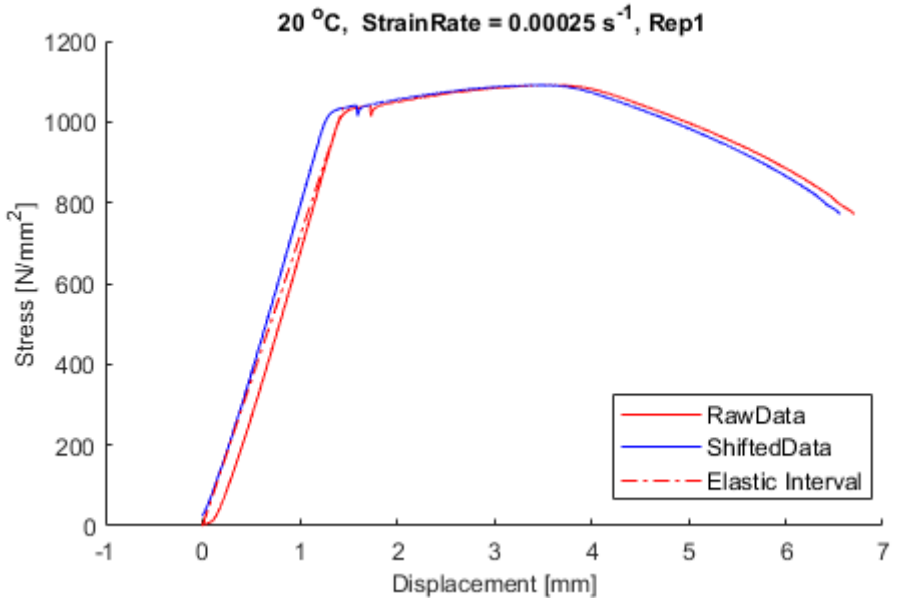
20 °C, StrainRate = 0.00025 s-1, Rep1
Stress [N/mm2]
Displacement [mm]
RawData
ShiftedData
Elastic Interval

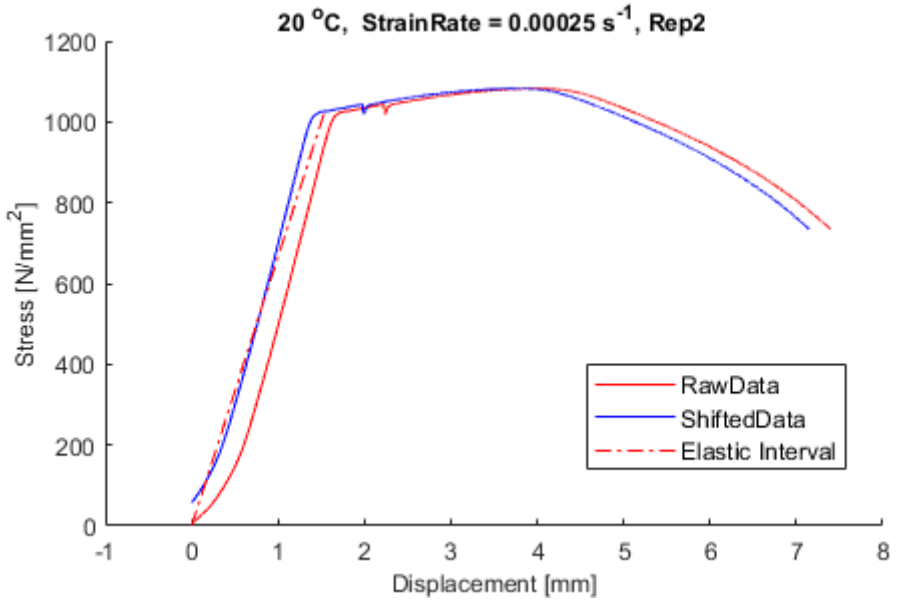
20 °C, StrainRate = 0.00025 s-1, Rep2
Stress [N/mm2]
Displacement [mm]
RawData
ShiftedData
Elastic Interval

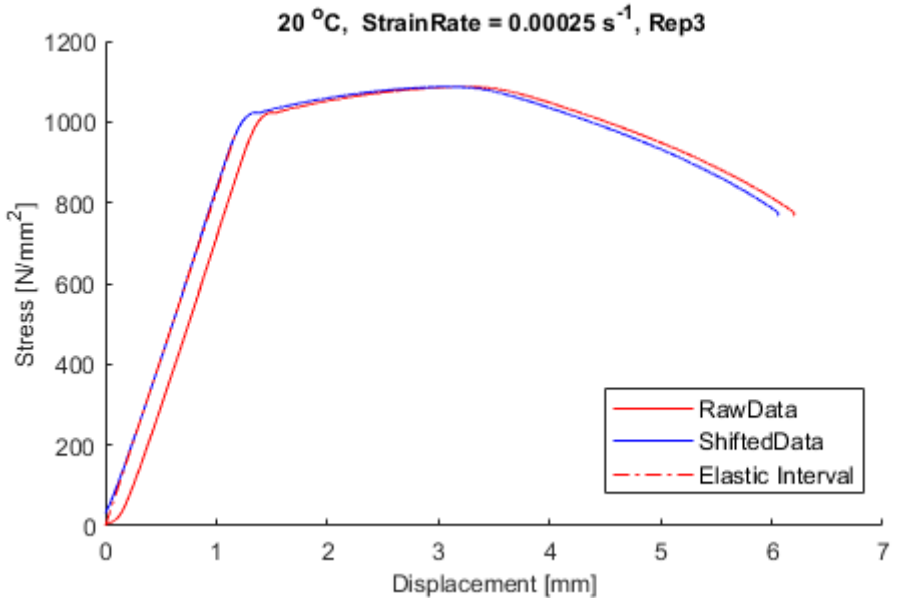
20 °C, StrainRate = 0.00025 s-1, Rep3
Stress [N/mm2]
Displacement [mm]
RawData
ShiftedData
Elastic Interval

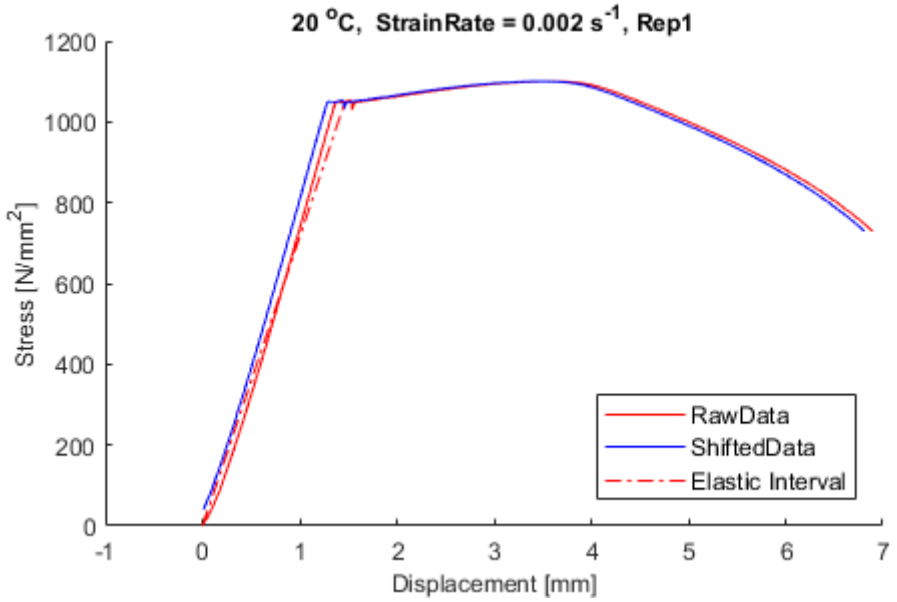
20 °C, StrainRate = 0.002 s-1, Rep1
Stress [N/mm2]
Displacement [mm]
RawData
ShiftedData
Elastic Interval

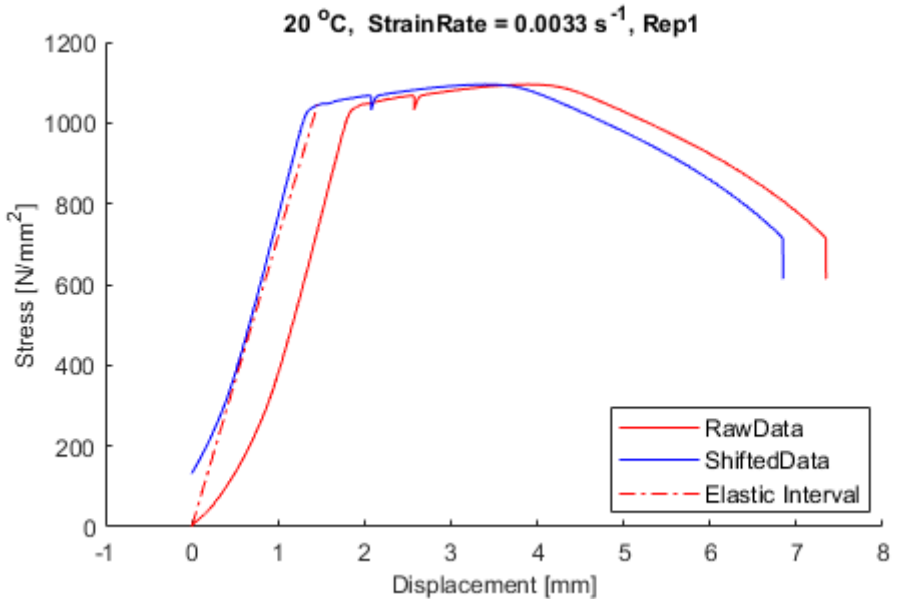
20 °C, StrainRate = 0.0033 s-1, Rep1
Stress [N/mm2]
Displacement [mm]
RawData
ShiftedData
Elastic Interval

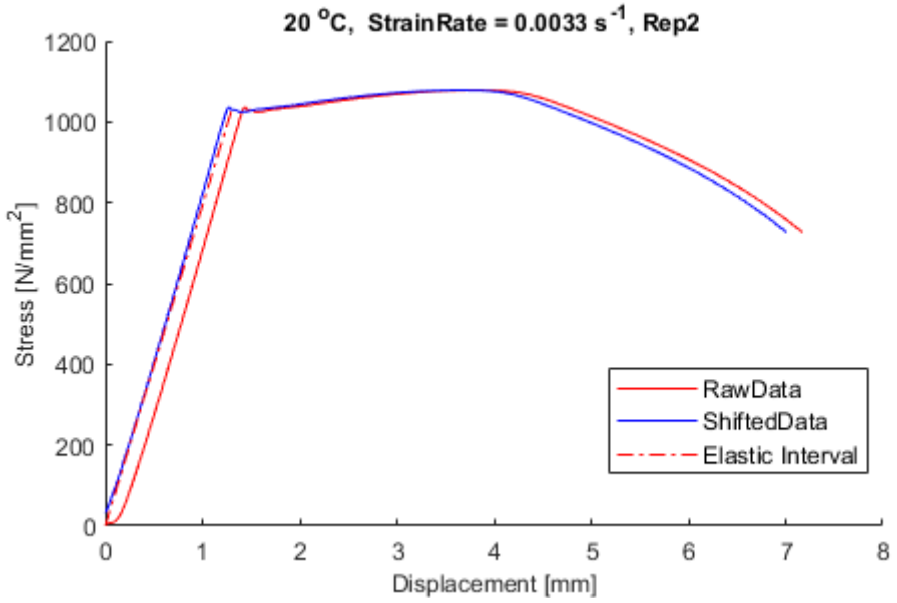
20 °C, StrainRate = 0.0033 s-1, Rep2
Stress [N/mm2]
Displacement [mm]
RawData
ShiftedData
Elastic Interval

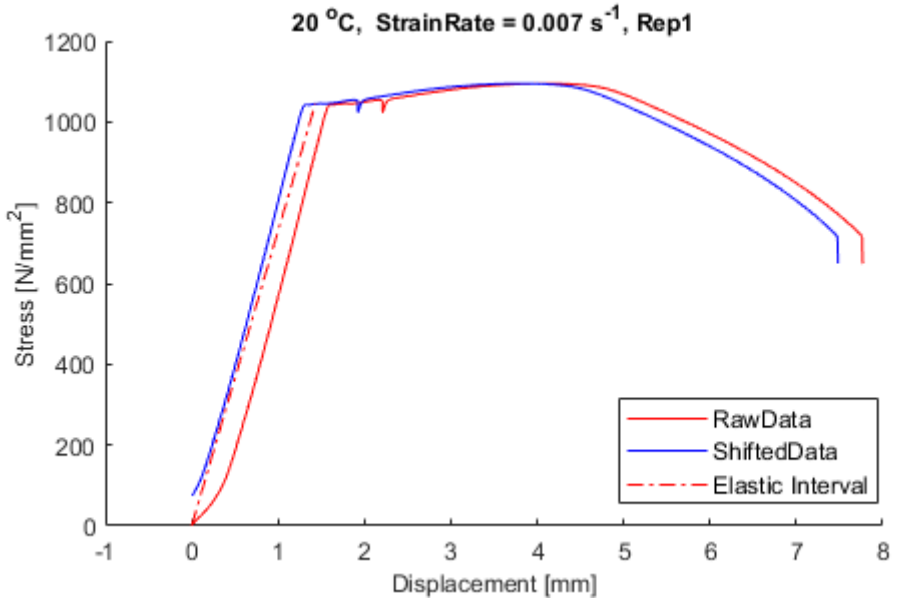
20 °C, StrainRate = 0.007 s-1, Rep1
Stress [N/mm2]
Displacement [mm]
RawData
ShiftedData
Elastic Interval

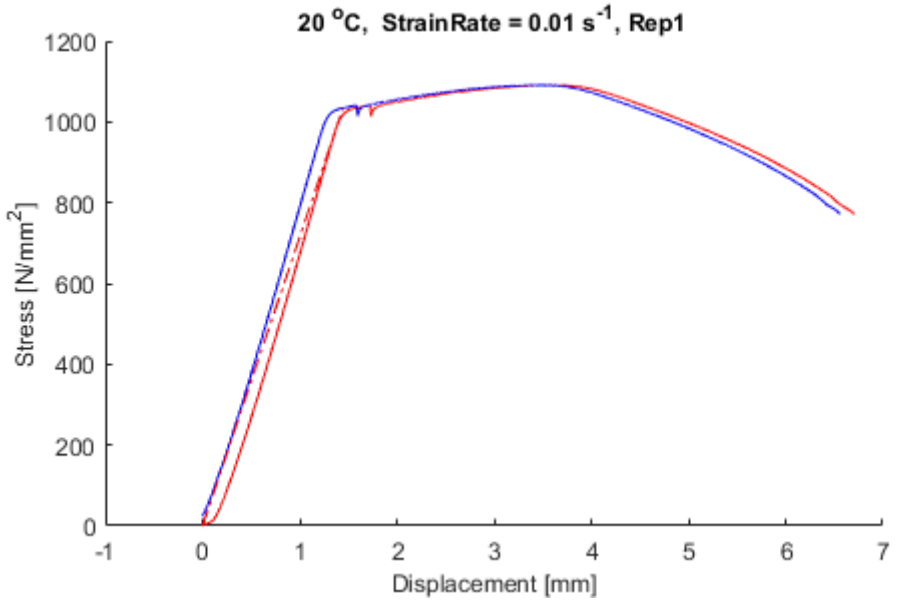
20 °C, StrainRate = 0.01 s-1, Rep1
Stress [N/mm2]
Displacement [mm]

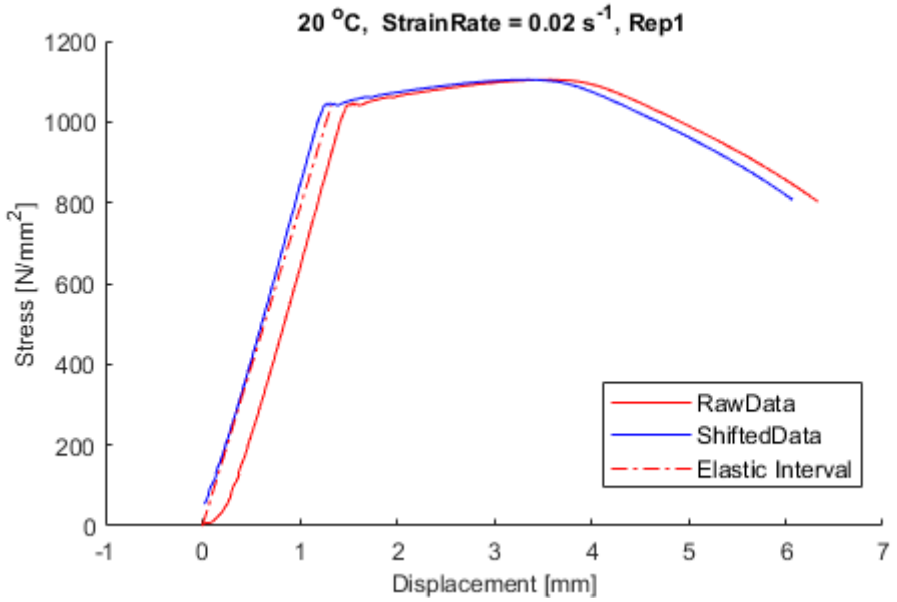
20 °C, StrainRate = 0.02 s-1, Rep1
Stress [N/mm2]
Displacement [mm]
RawData
ShiftedData
Elastic Interval

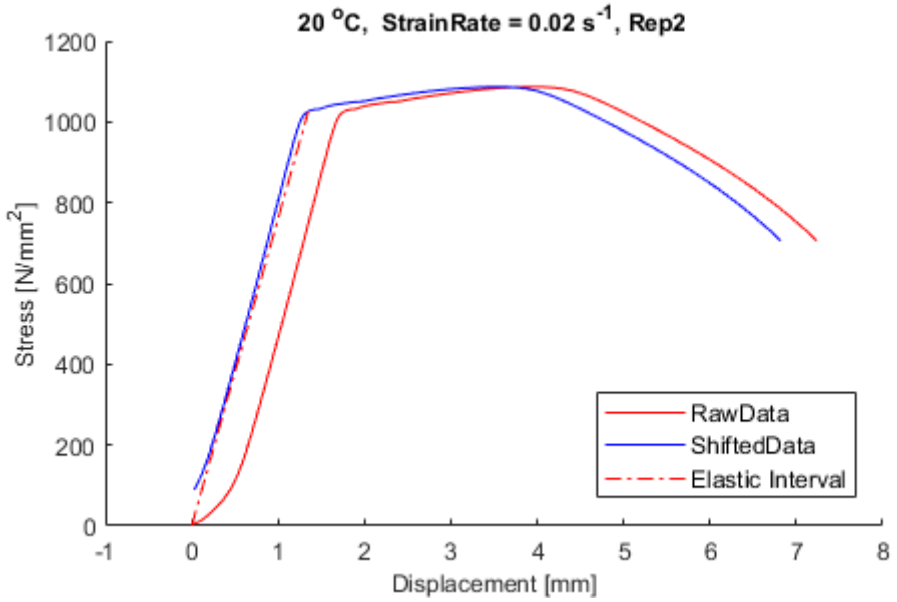
20 °C, StrainRate = 0.02 s-1, Rep2
Stress [N/mm2]
Displacement [mm]
RawData
ShiftedData
Elastic Interval

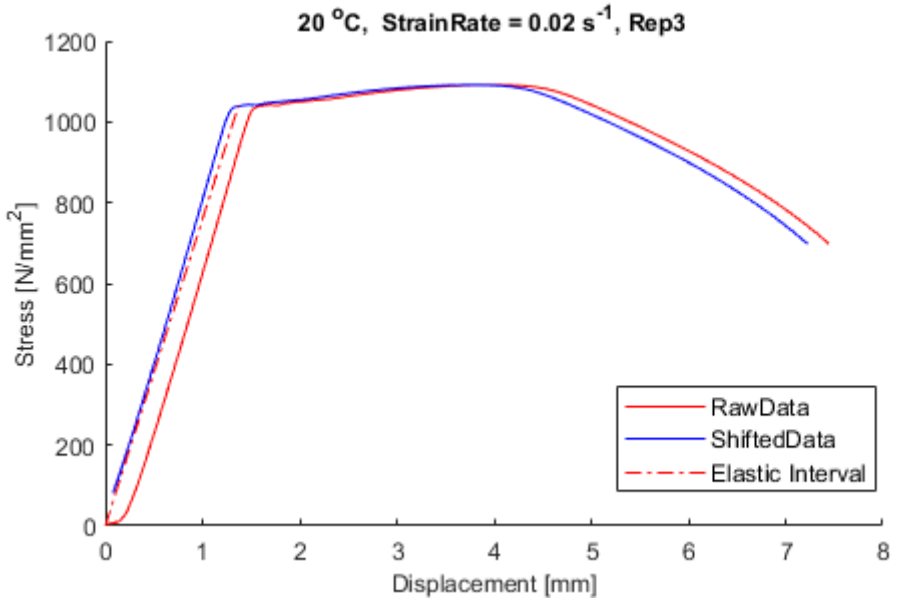
20 °C, StrainRate = 0.02 s-1, Rep3
Stress [N/mm2]
Displacement [mm]
RawData
ShiftedData
Elastic Interval

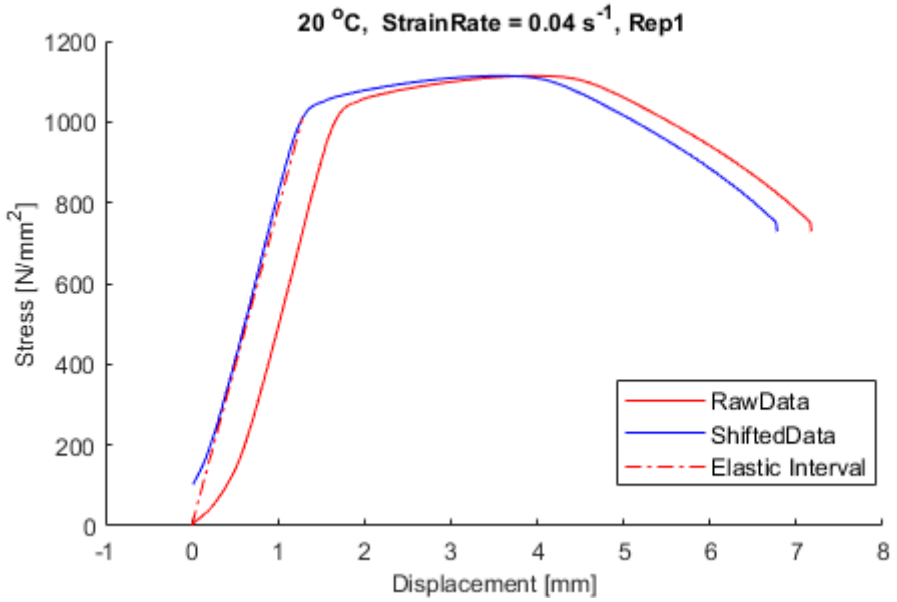
20 °C, StrainRate = 0.04 s-1, Rep1
Stress [N/mm2]
Displacement [mm]
RawData
ShiftedData
Elastic Interval

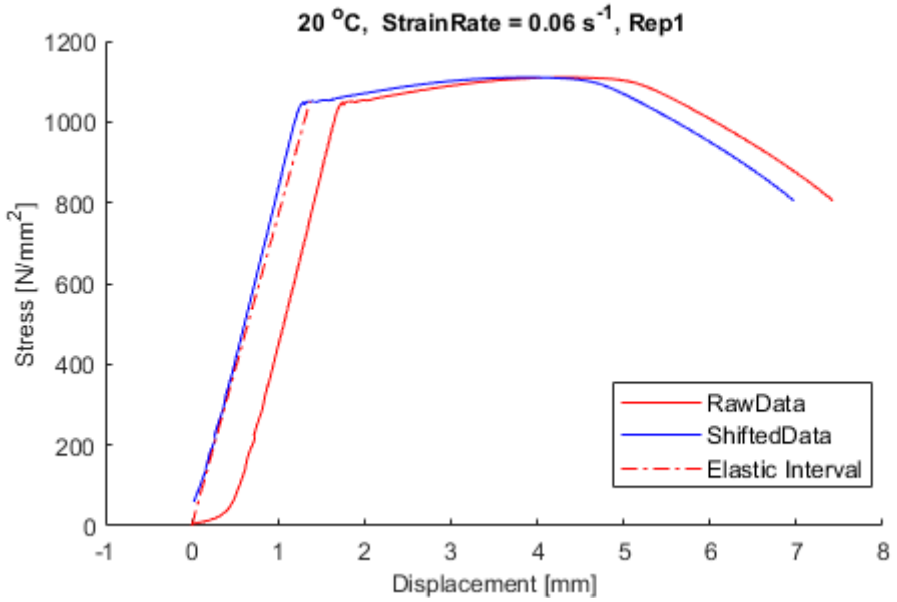
20 °C, StrainRate = 0.06 s-1, Rep1
Stress [N/mm2]
Displacement [mm]
RawData
ShiftedData
Elastic Interval

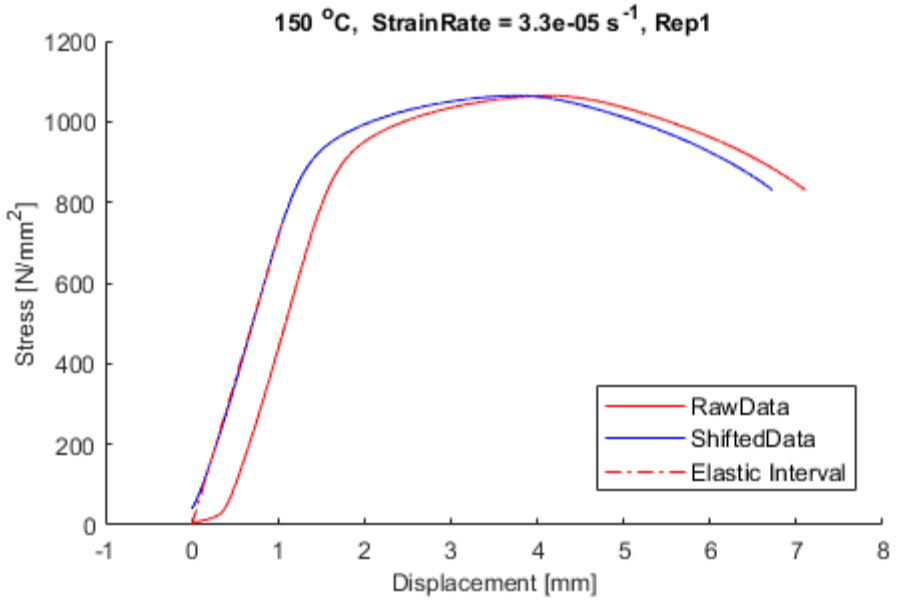
150 °C, StrainRate = 3.3e-05 s-1, Rep1
Stress [N/mm2]
Displacement [mm]
RawData
ShiftedData
Elastic Interval

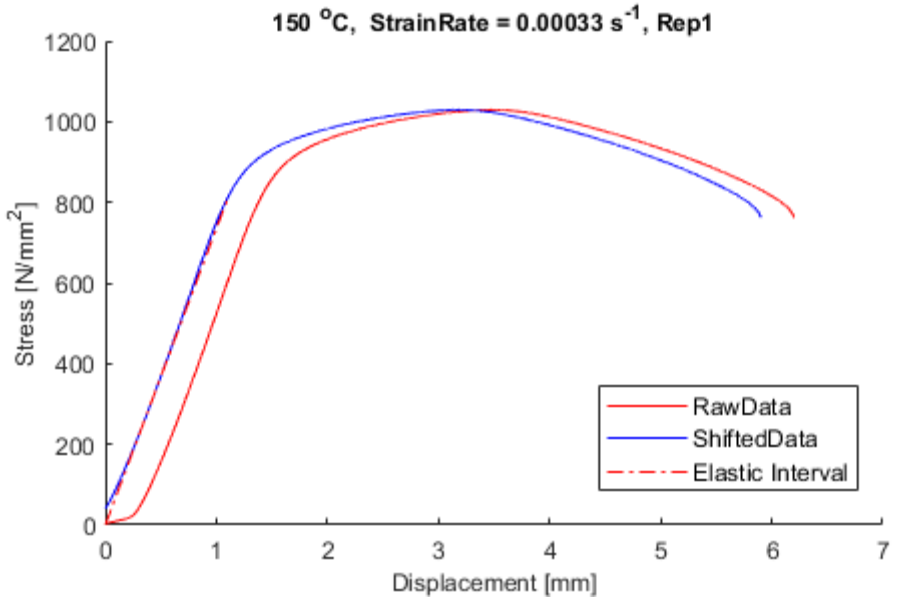
150 °C, StrainRate = 0.00033 s-1, Rep1
Stress [N/mm2]
Displacement [mm]
RawData
ShiftedData
Elastic Interval

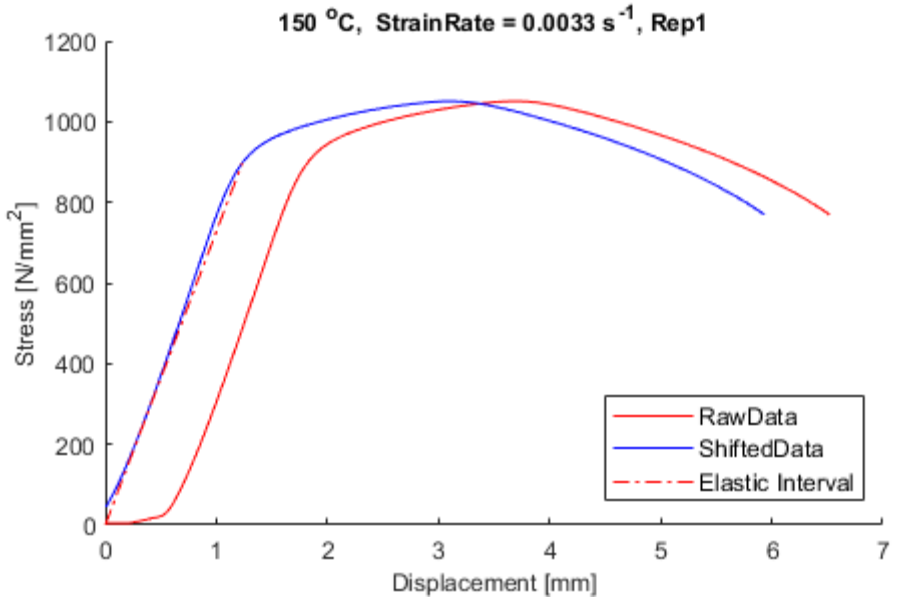
150 °C, StrainRate = 0.0033 s-1, Rep1
Stress [N/mm2]
Displacement [mm]
RawData
ShiftedData
Elastic Interval

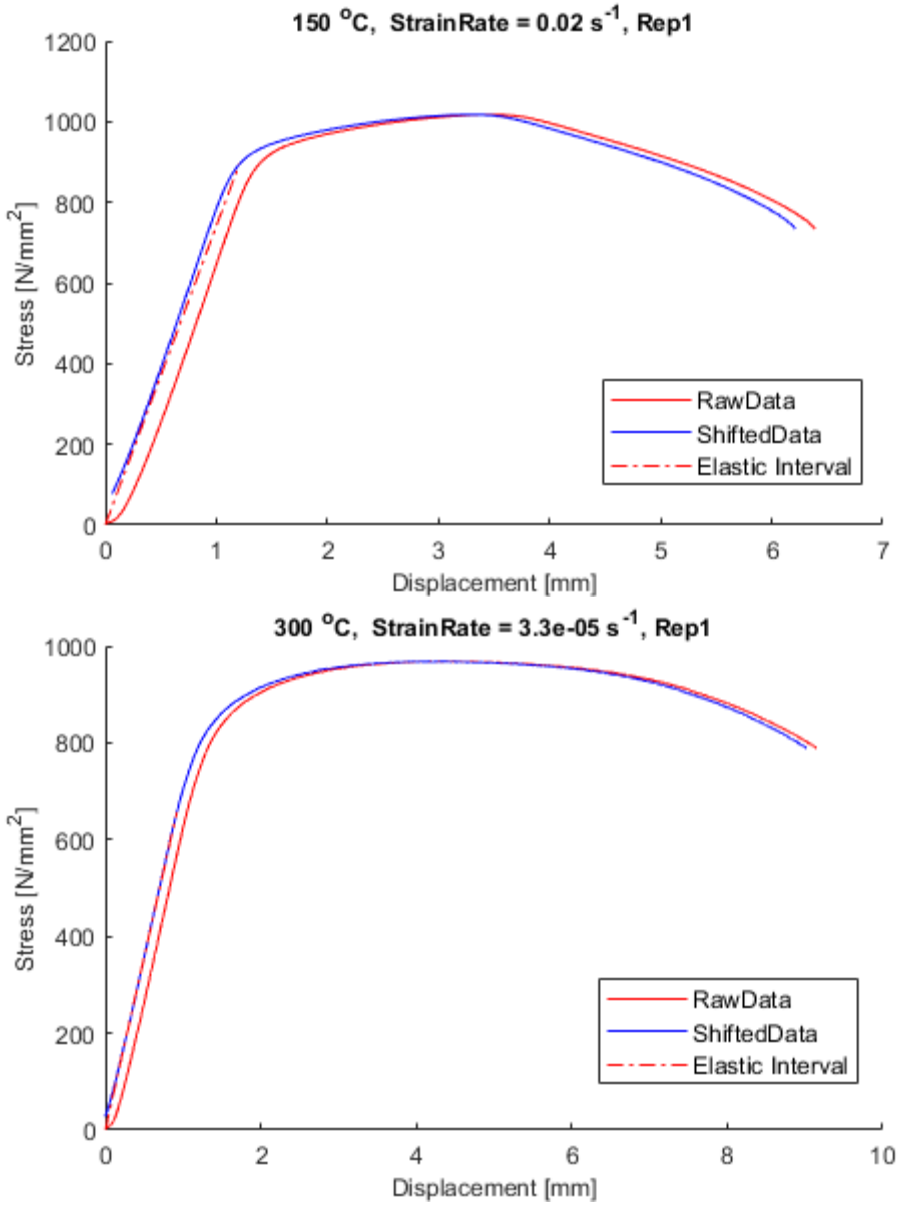
150 °C, StrainRate = 0.02 s-1, Rep1
Stress [N/mm2]
Displacement [mm]
RawData
ShiftedData
Elastic Interval
300 °C, StrainRate = 3.3e-05 s-1, Rep1
Stress [N/mm2]
Displacement [mm]
RawData
ShiftedData
Elastic Interval

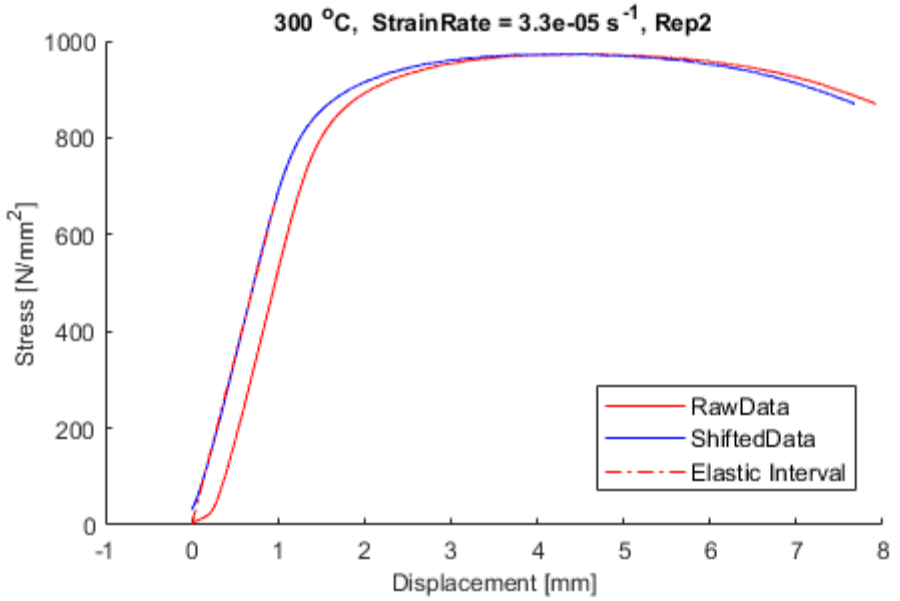
300 °C, StrainRate = 3.3e-05 s-1, Rep2
Stress [N/mm2]
Displacement [mm]
RawData
ShiftedData
Elastic Interval

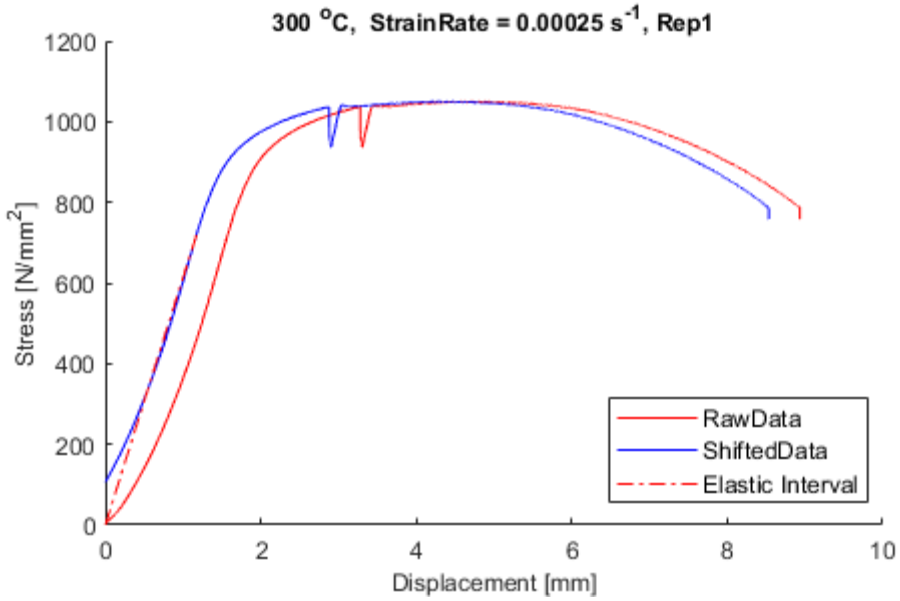
300 °C, StrainRate = 0.00025 s-1, Rep1
Stress [N/mm2]
Displacement [mm]
RawData
ShiftedData
Elastic Interval

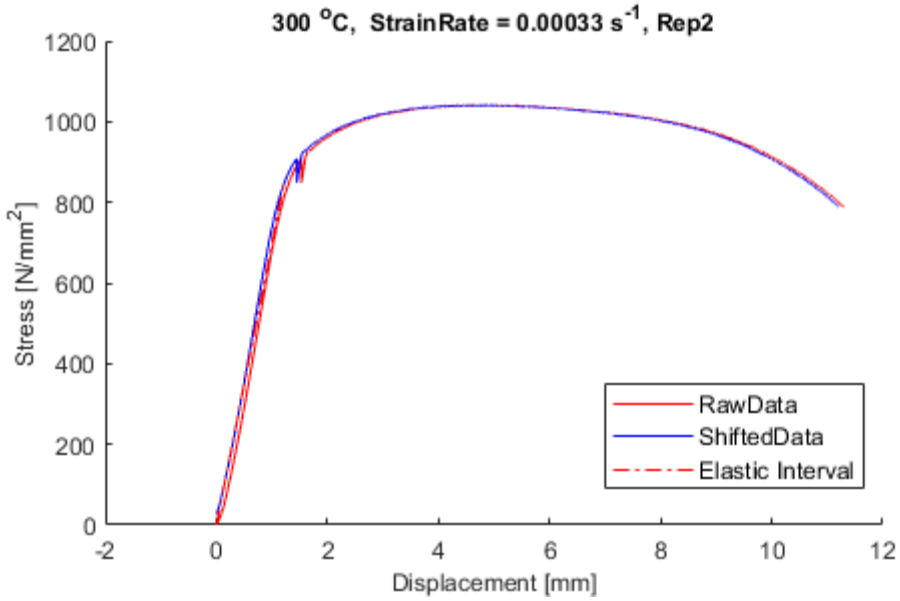
300 °C, StrainRate = 0.00033 s-1, Rep2
Stress [N/mm2]
Displacement [mm]
RawData
ShiftedData
Elastic Interval

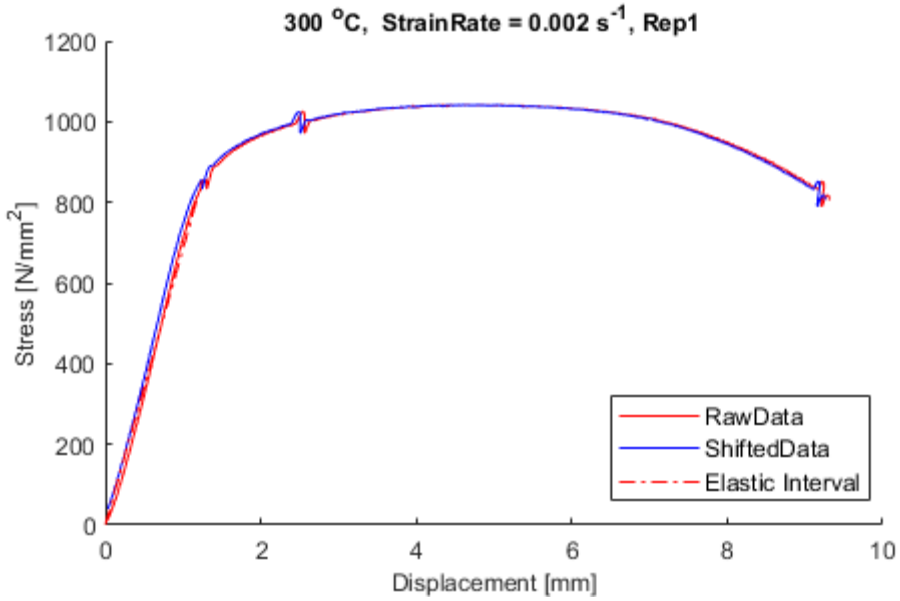
300 °C, StrainRate = 0.002 s-1, Rep1
Stress [N/mm2]
Displacement [mm]
RawData
ShiftedData
Elastic Interval

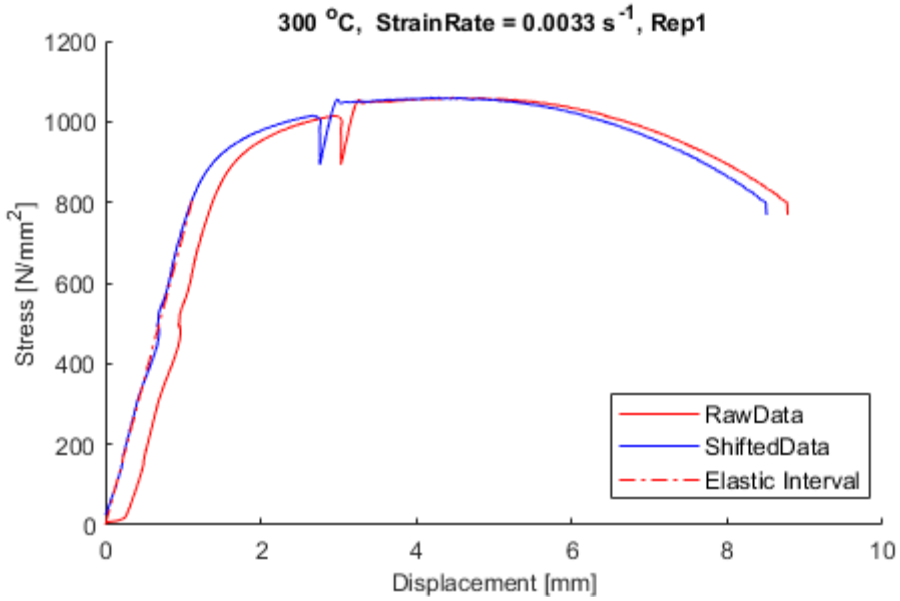
300 °C, StrainRate = 0.0033 s-1, Rep1
Stress [N/mm2]
Displacement [mm]
RawData
ShiftedData
Elastic Interval

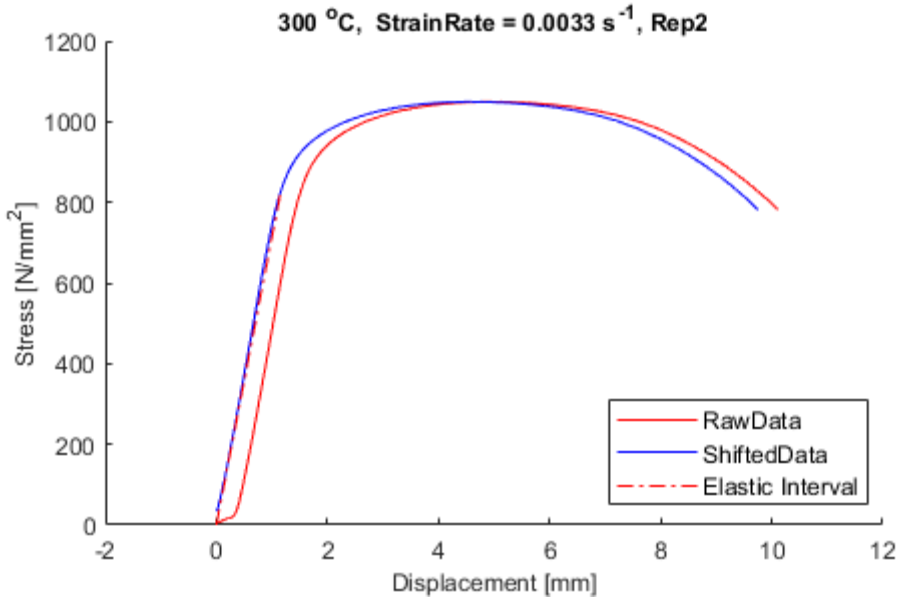
300 °C, StrainRate = 0.0033 s-1, Rep2
Stress [N/mm2]
Displacement [mm]
RawData
ShiftedData
Elastic Interval

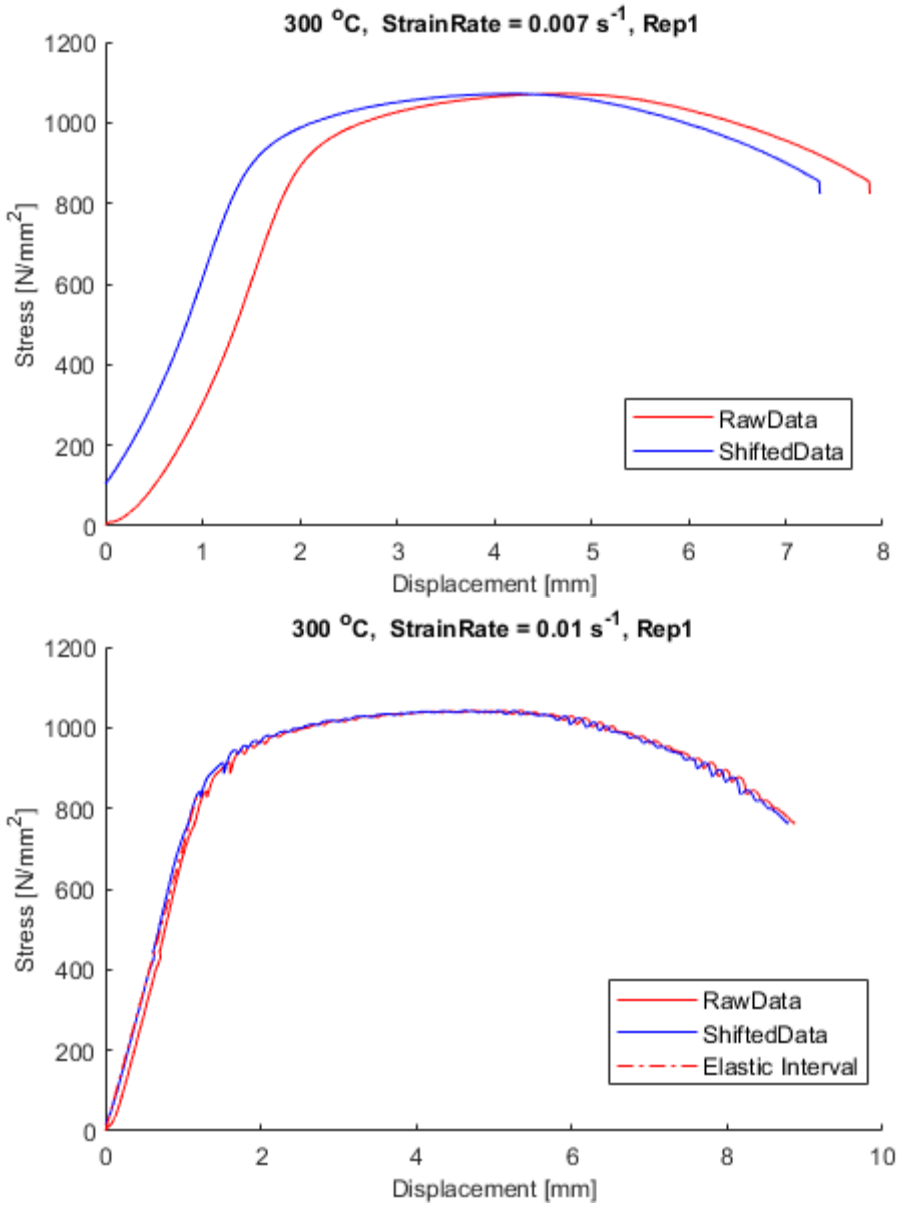
300 °C, StrainRate = 0.007 s-1, Rep1
Stress [N/mm2]
Displacement [mm]
RawData
ShiftedData
300 °C, StrainRate = 0.01 s-1, Rep1
Stress [N/mm2]
Displacement [mm]
RawData
ShiftedData
Elastic Interval

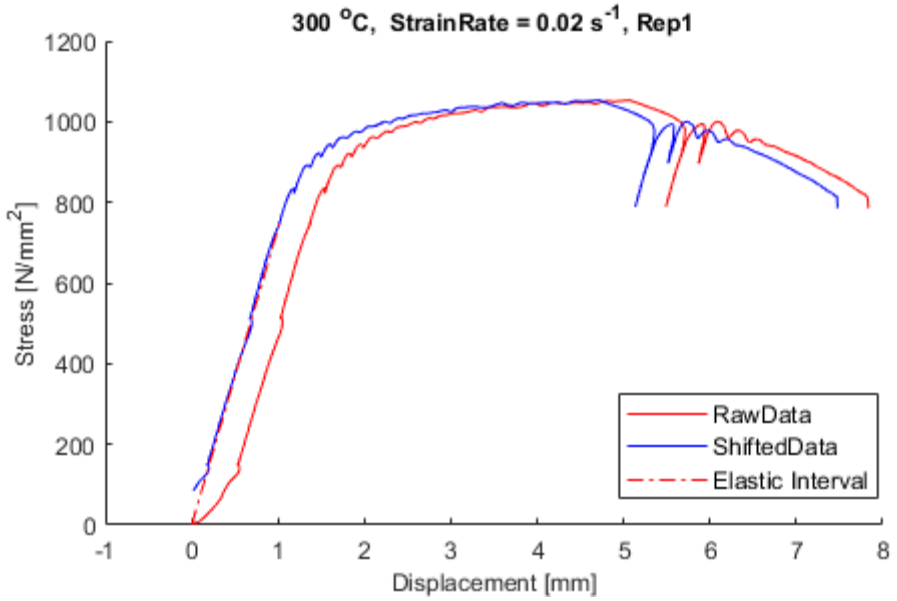
300 °C, StrainRate = 0.02 s-1, Rep1
Stress [N/mm2]
Displacement [mm]
RawData
ShiftedData
Elastic Interval

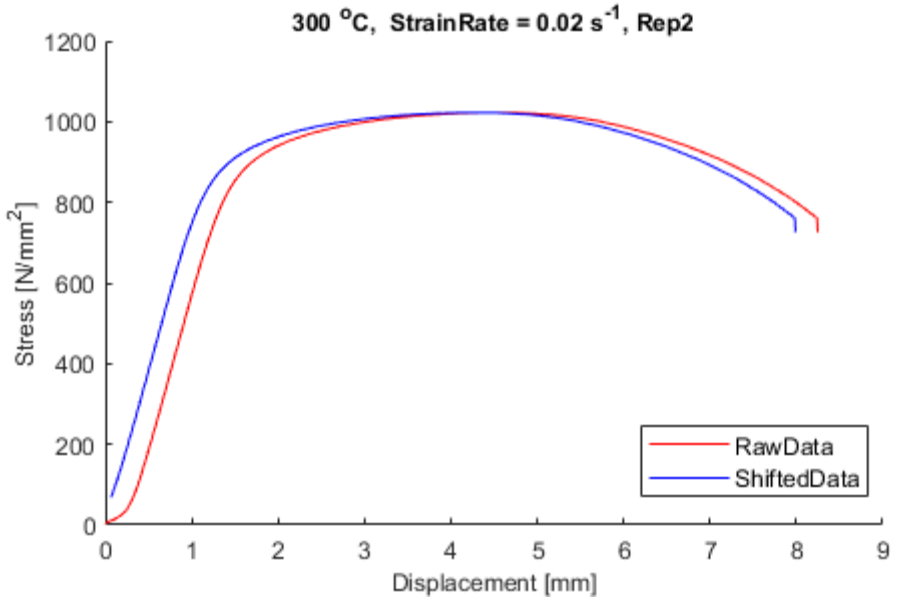
300 °C, StrainRate = 0.02 s-1, Rep2
Stress [N/mm2]
Displacement [mm]
RawData
ShiftedData

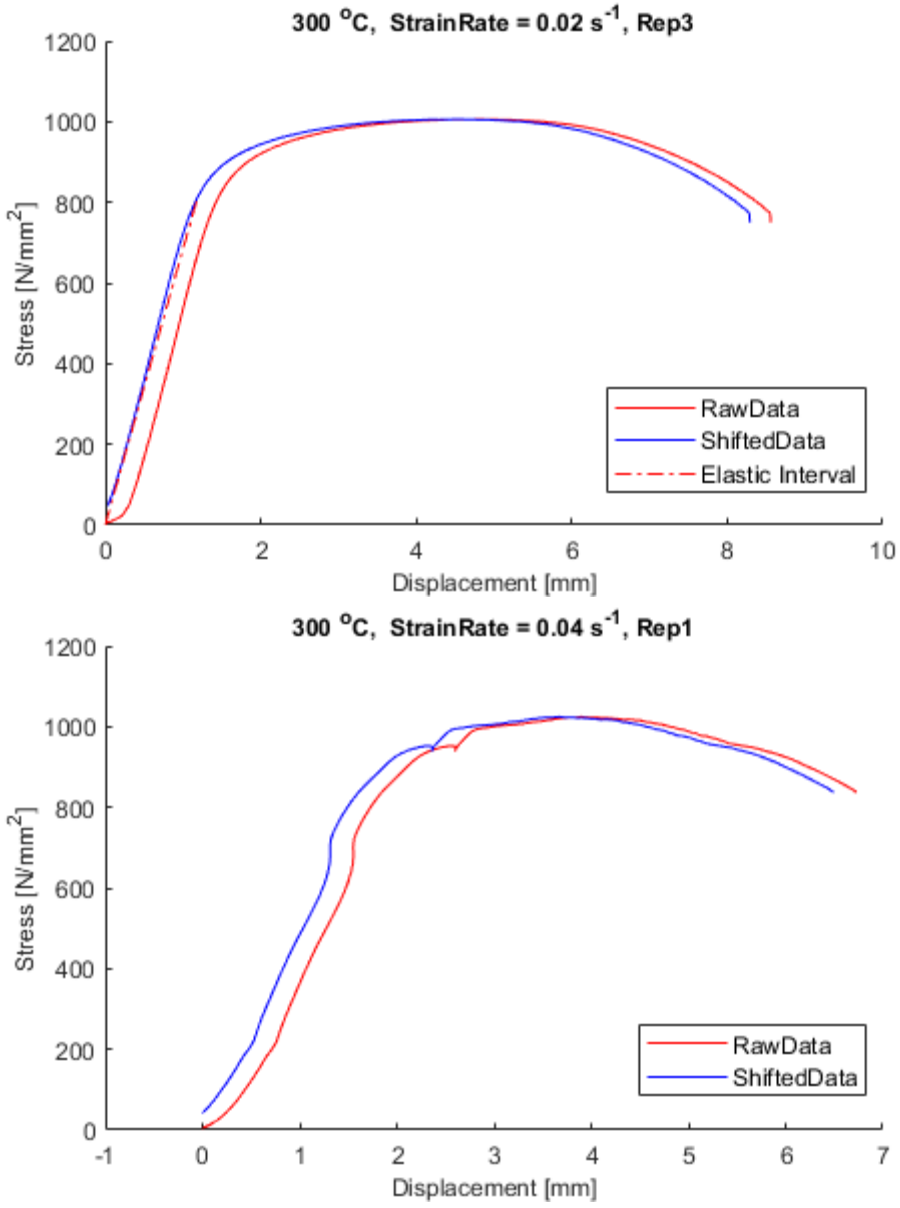
300 °C, StrainRate = 0.02 s-1, Rep3
Stress [N/mm2]
Displacement [mm]
RawData
ShiftedData
Elastic Interval
300 °C, StrainRate = 0.04 s-1, Rep1
Stress [N/mm2]
Displacement [mm]
RawData
ShiftedData

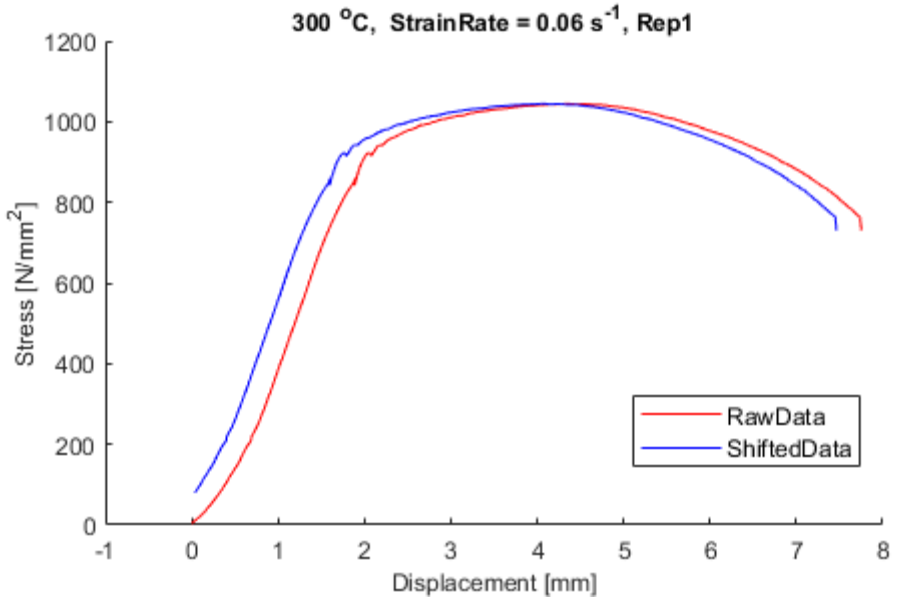
300 °C, StrainRate = 0.06 s-1, Rep1
Stress [N/mm2]
Displacement [mm]
RawData
ShiftedData

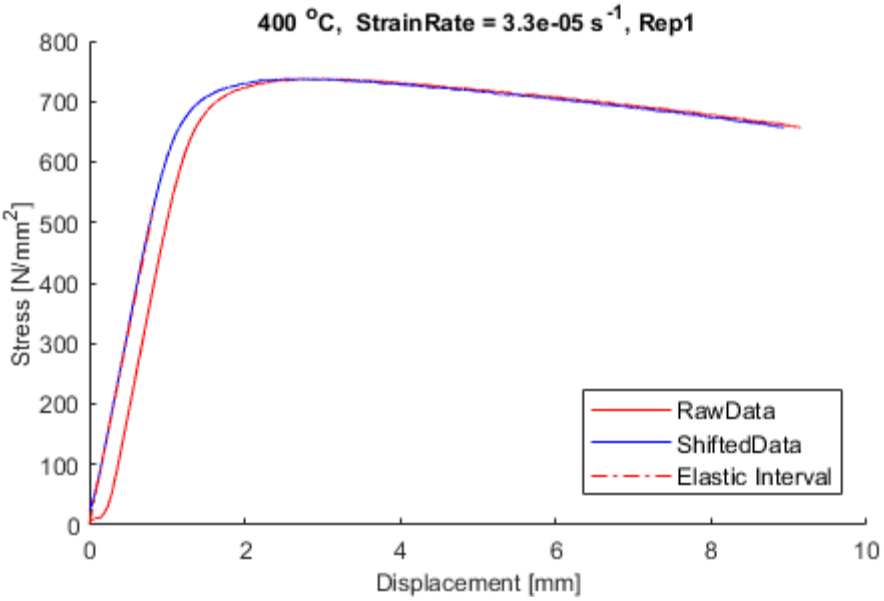
400 °C, StrainRate = 3.3e-05 s-1, Rep1
Stress [N/mm2]
Displacement [mm]
RawData
ShiftedData
Elastic Interval

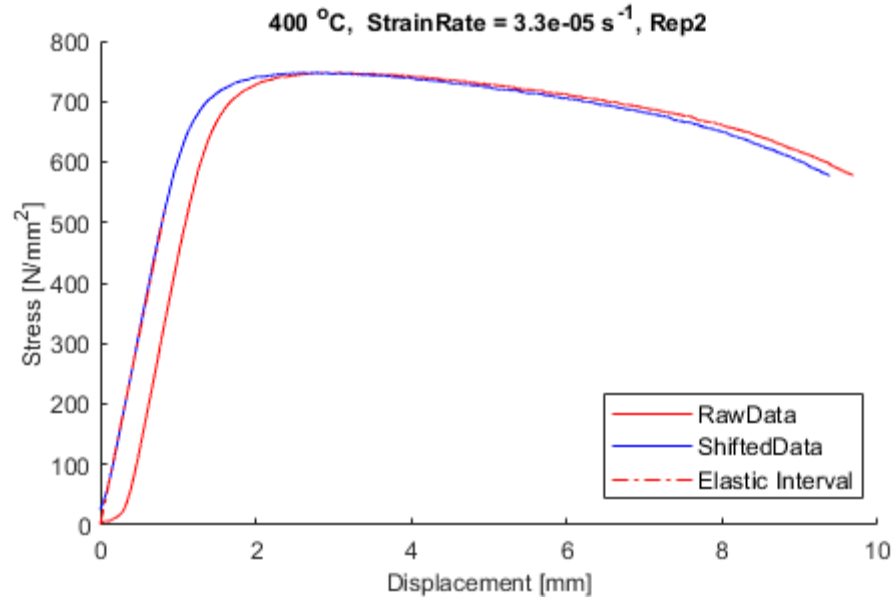
400 °C, StrainRate = 3.3e-05 s-1, Rep2
Stress [N/mm2]
Displacement [mm]
RawData
ShiftedData
Elastic Interval

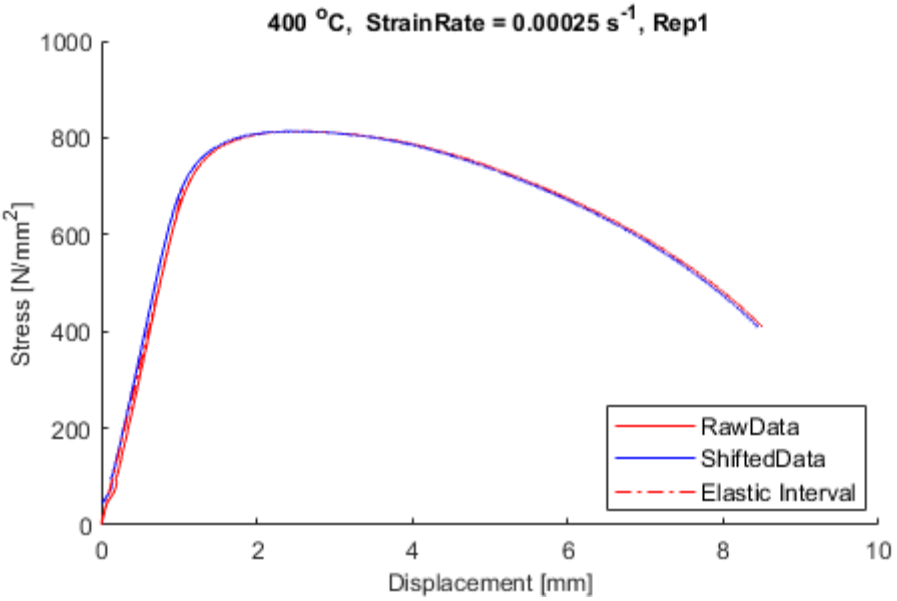
400 °C, StrainRate = 0.00025 s-1, Rep1
Stress [N/mm2]
Displacement [mm]
RawData
ShiftedData
Elastic Interval

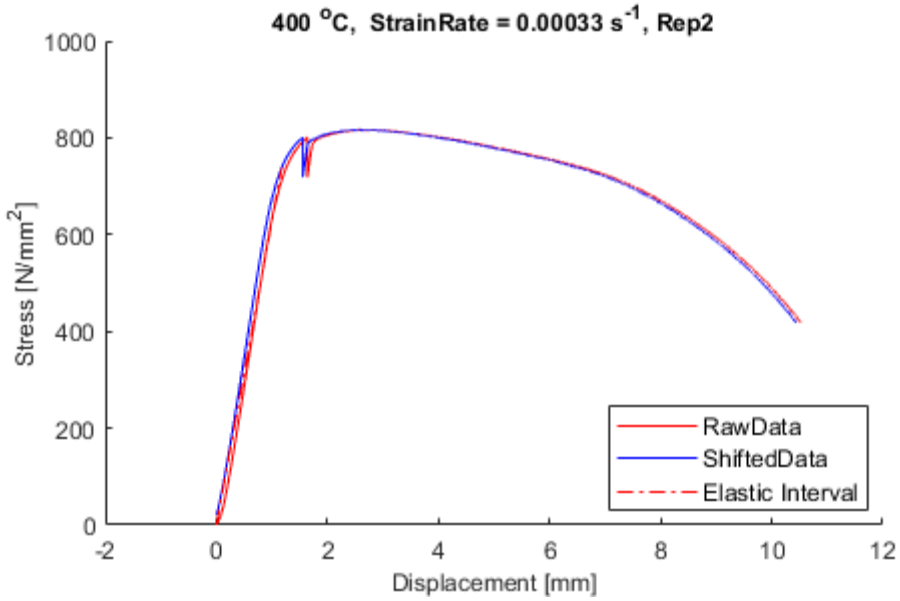
400 °C, StrainRate = 0.00033 s-1, Rep2
Stress [N/mm2]
Displacement [mm]
RawData
ShiftedData
Elastic Interval

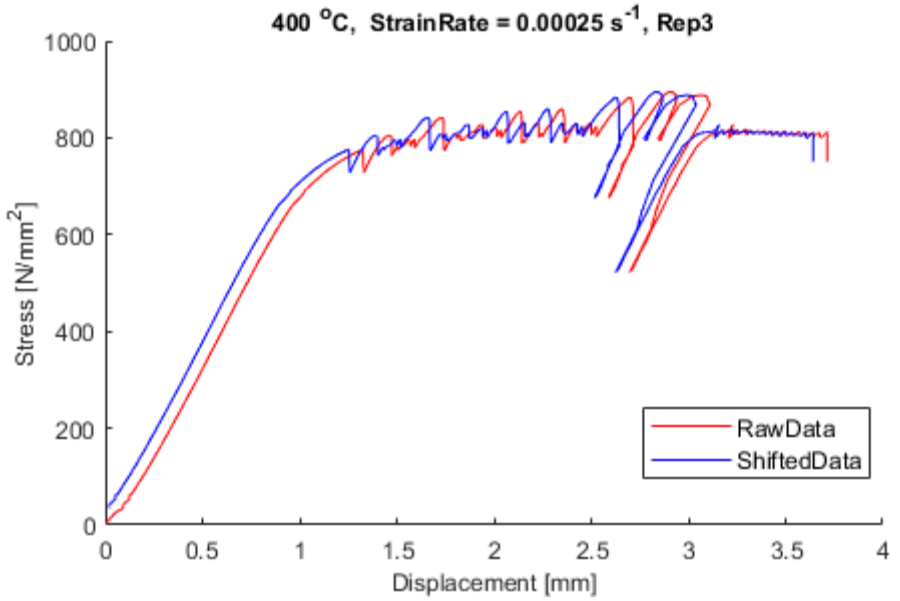
400 °C, StrainRate = 0.00025 s-1, Rep3
Stress [N/mm2]
Displacement [mm]
RawData
ShiftedData

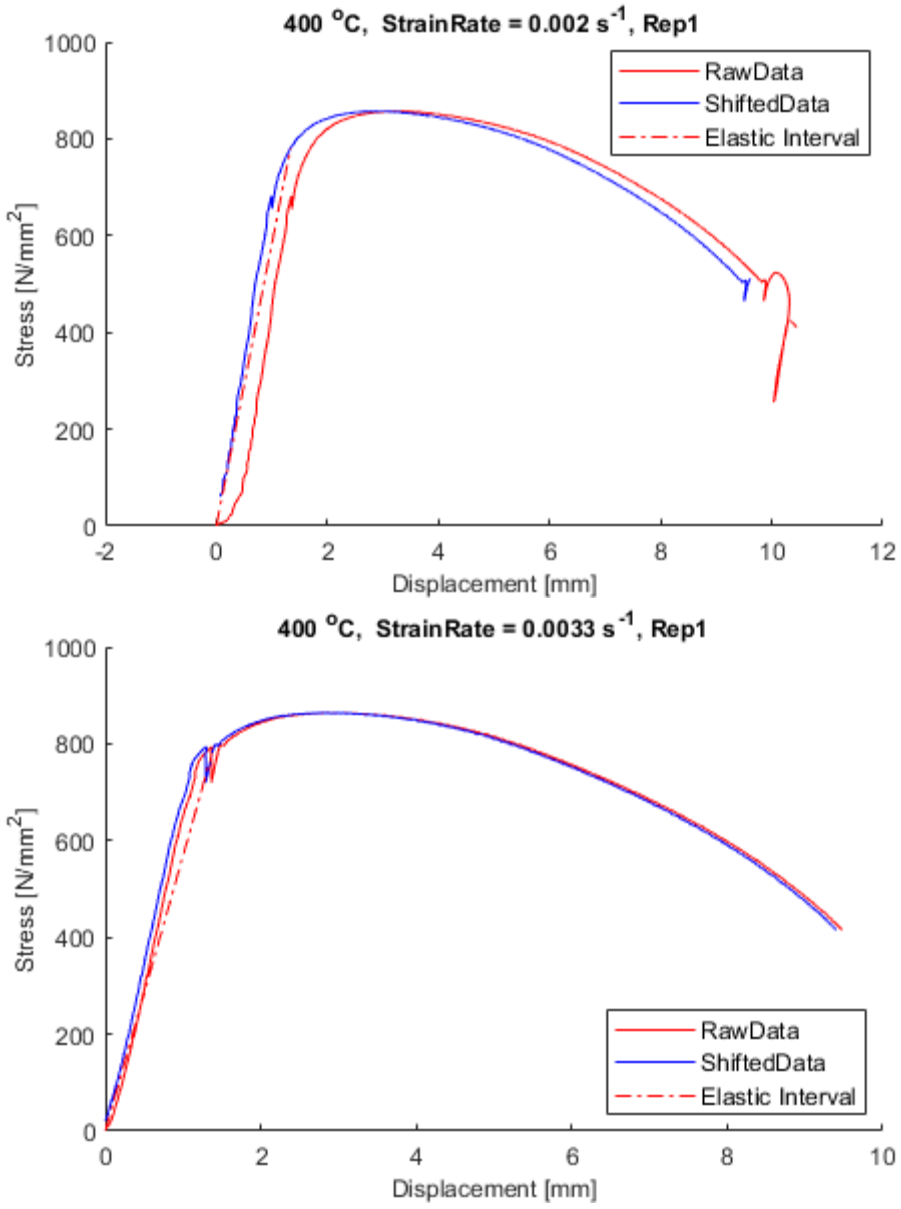
400 °C, StrainRate = 0.002 s-1, Rep1
RawData
ShiftedData
Elastic Interval
Stress [N/mm2]
Displacement [mm]
400 °C, StrainRate = 0.0033 s-1, Rep1
RawData
ShiftedData
Elastic Interval
Stress [N/mm2]
Displacement [mm]

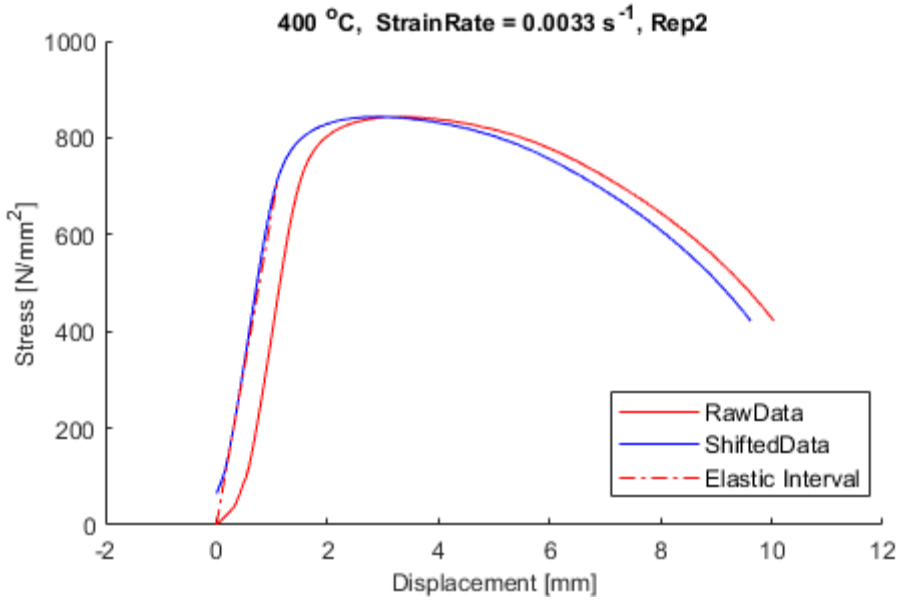
400 °C, StrainRate = 0.0033 s-1, Rep2
Stress [N/mm2]
Displacement [mm]
RawData
ShiftedData
Elastic Interval

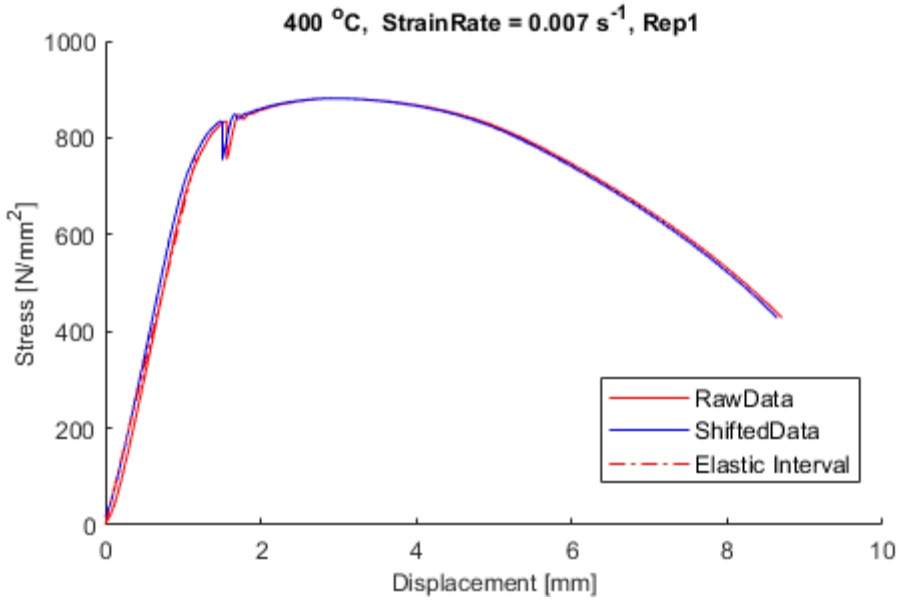
400 °C, StrainRate = 0.007 s-1, Rep1
Stress [N/mm2]
Displacement [mm]
RawData
ShiftedData
Elastic Interval

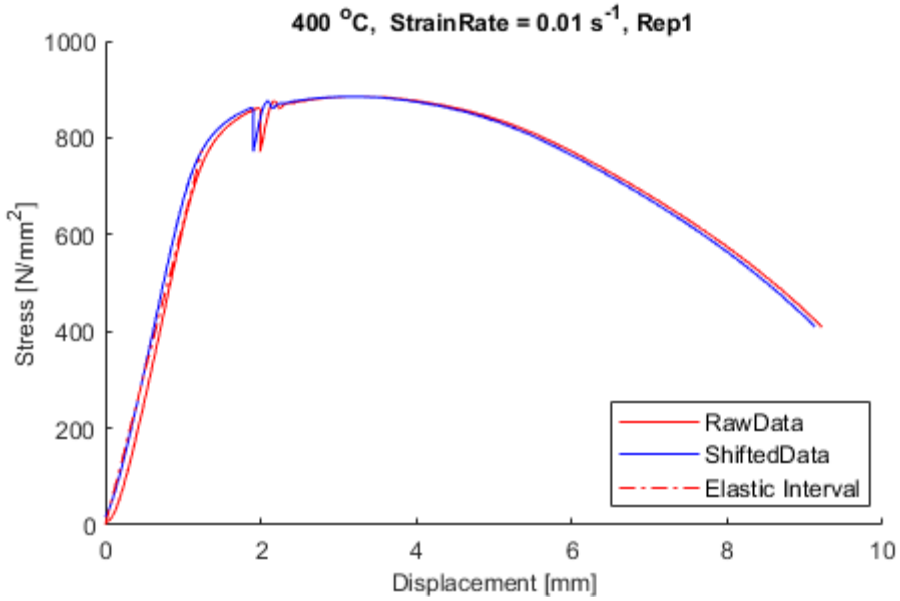
400 °C, StrainRate = 0.01 s-1, Rep1
Stress [N/mm2]
Displacement [mm]
RawData
ShiftedData
Elastic Interval

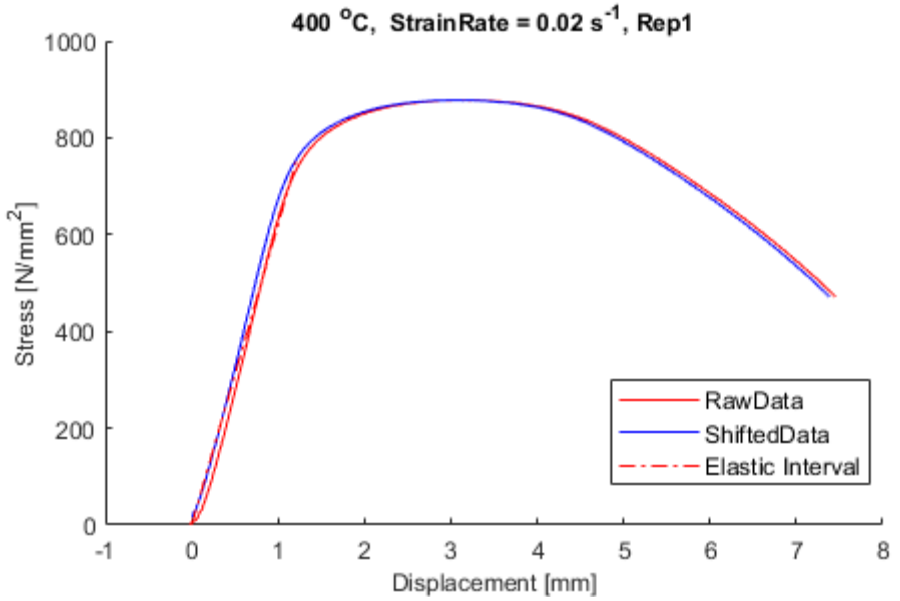
400 °C, StrainRate = 0.02 s-1, Rep1
Stress [N/mm2]
Displacement [mm]
RawData
ShiftedData
Elastic Interval

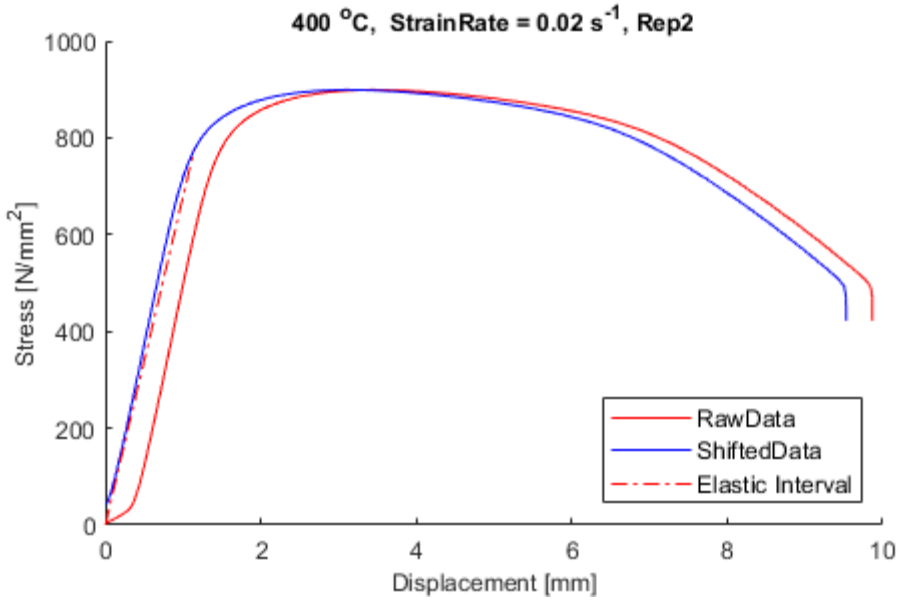
400 °C, StrainRate = 0.02 s-1, Rep2
Stress [N/mm2]
Displacement [mm]
RawData
ShiftedData
Elastic Interval

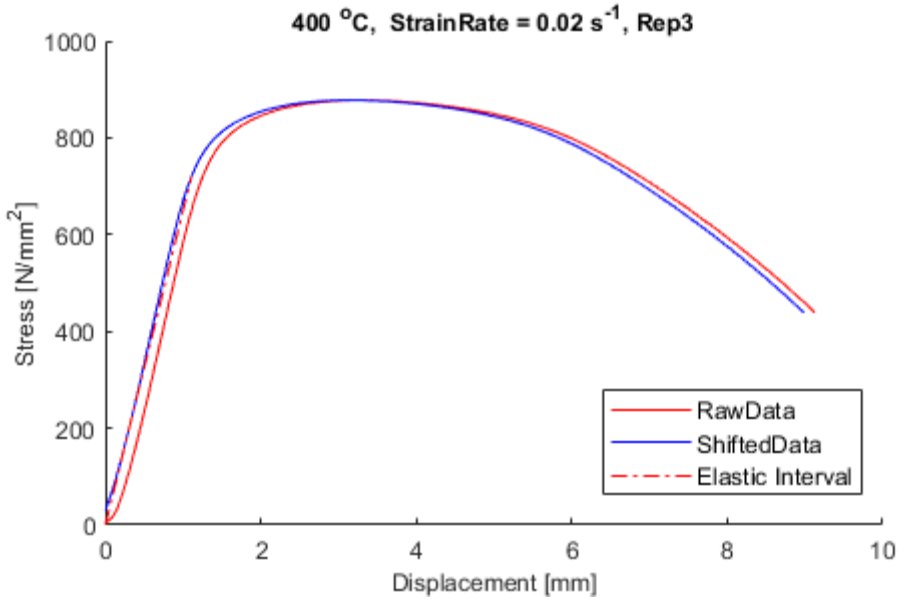
400 °C, StrainRate = 0.02 s-1, Rep3
Stress [N/mm2]
Displacement [mm]
RawData
ShiftedData
Elastic Interval

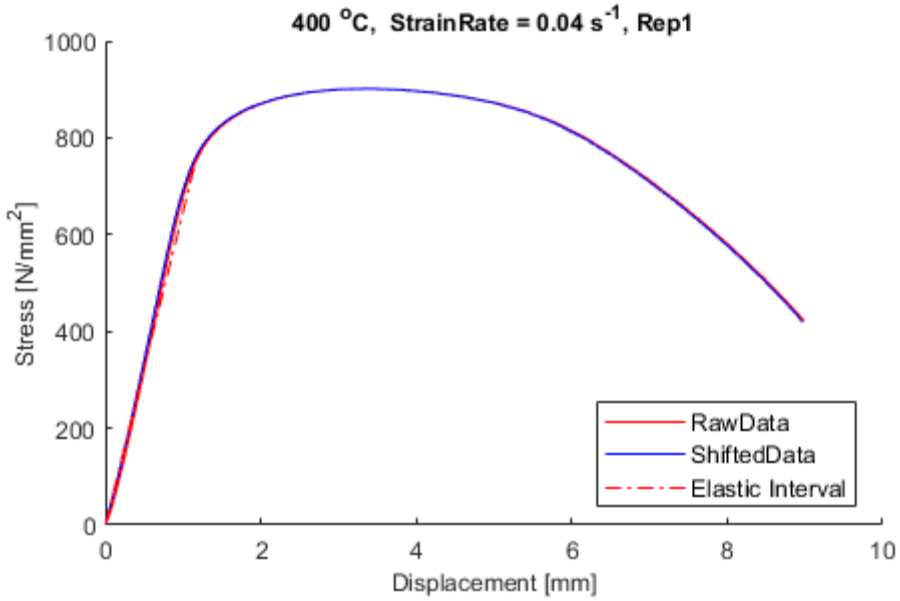
400 °C, StrainRate = 0.04 s-1, Rep1
Stress [N/mm2]
Displacement [mm]
RawData
ShiftedData
Elastic Interval

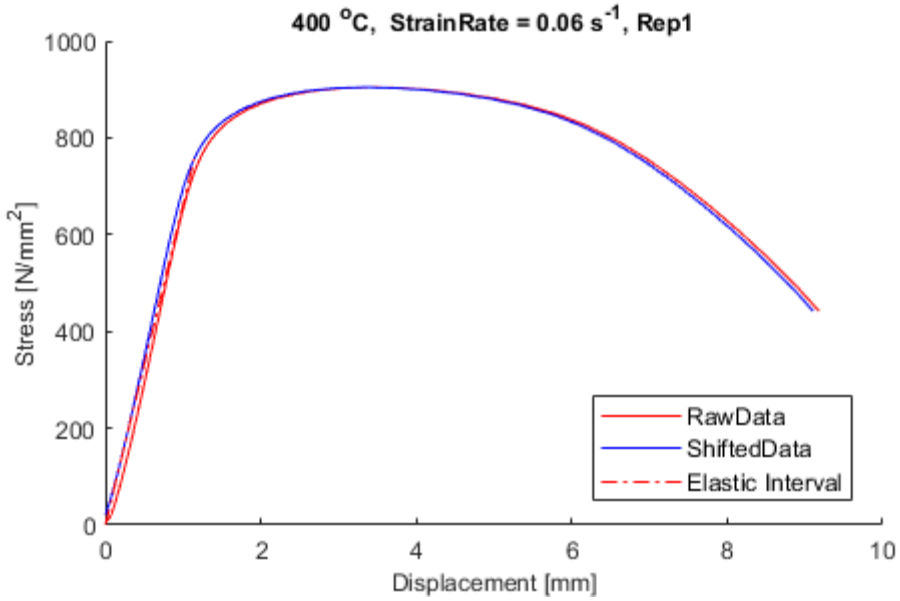
400 °C, StrainRate = 0.06 s-1, Rep1
Stress [N/mm2]
Displacement [mm]
RawData
ShiftedData
Elastic Interval

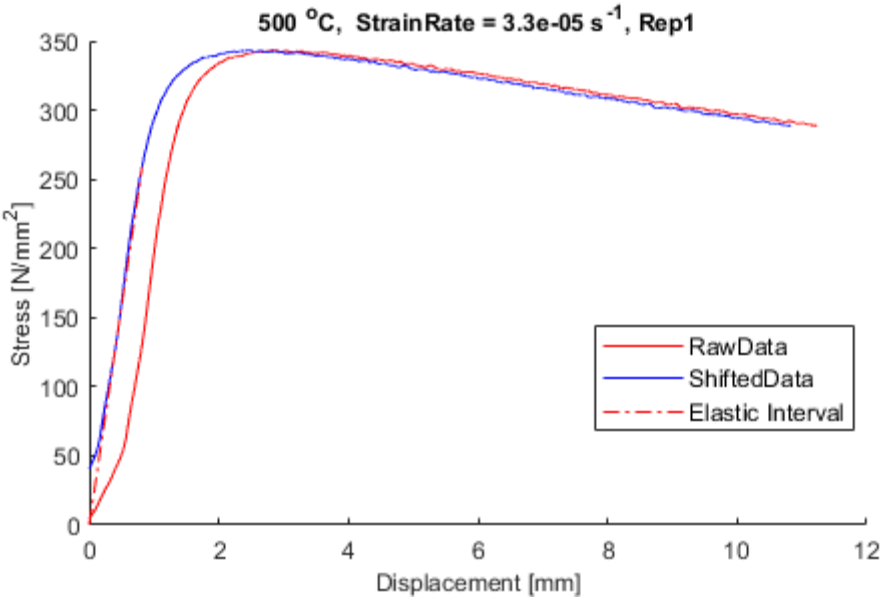
500 °C, StrainRate = 3.3e-05 s-1, Rep1
Stress [N/mm2]
Displacement [mm]
RawData
ShiftedData
Elastic Interval

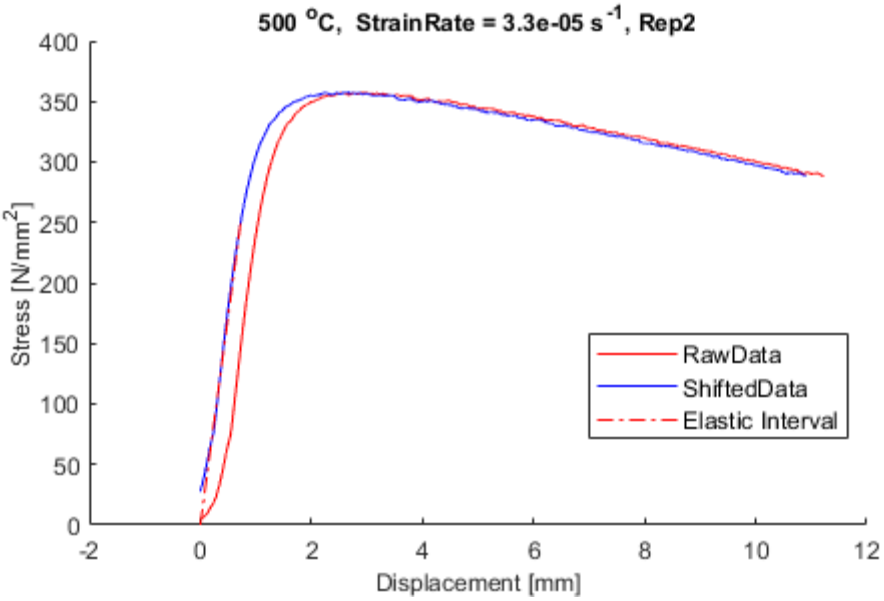
500 °C, StrainRate = 3.3e-05 s-1, Rep2
Stress [N/mm2]
Displacement [mm]
RawData
ShiftedData
Elastic Interval

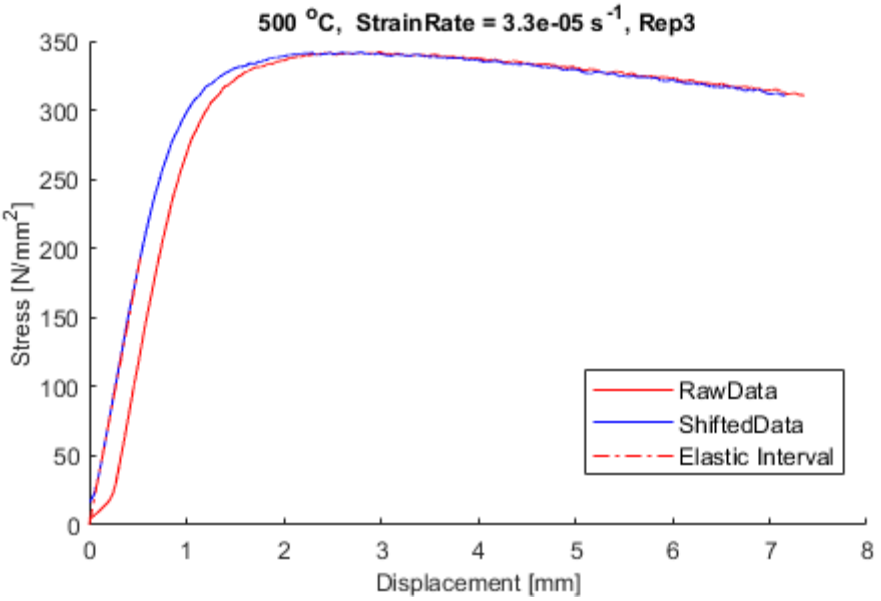
500 °C, StrainRate = 3.3e-05 s-1, Rep3
Stress [N/mm2]
Displacement [mm]
RawData
ShiftedData
Elastic Interval

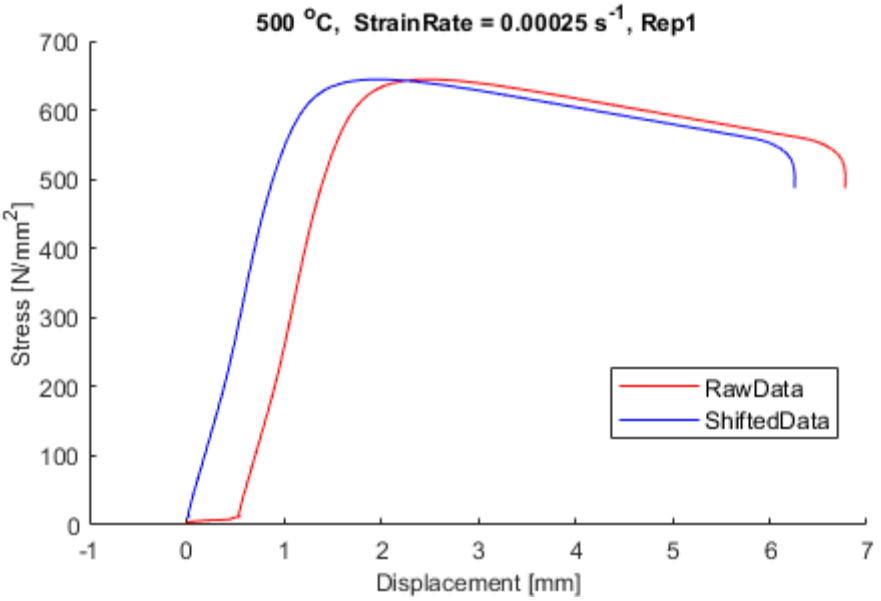
500 °C, StrainRate = 0.00025 s-1, Rep1
Stress [N/mm2]
Displacement [mm]
RawData
ShiftedData

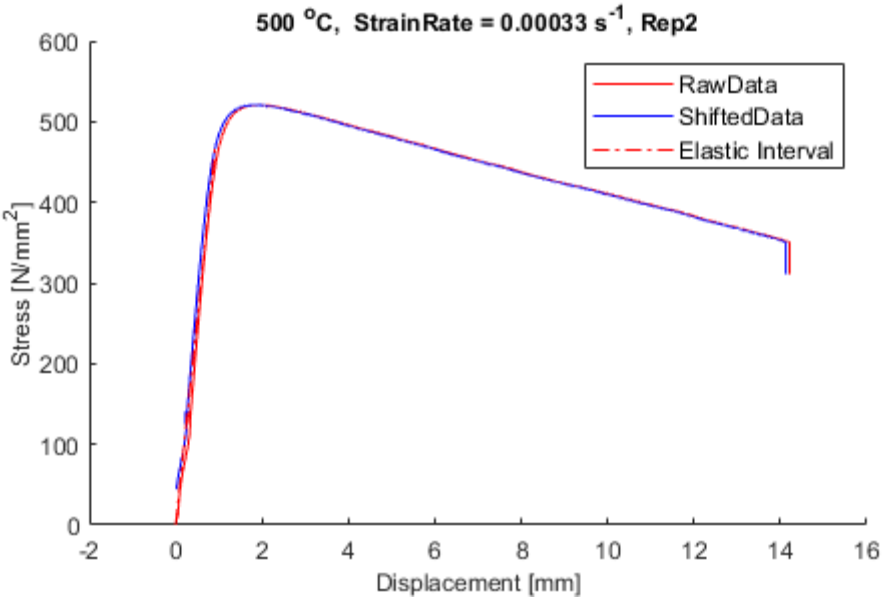
500 °C, StrainRate = 0.00033 s-1, Rep2
RawData
ShiftedData
Elastic Interval
Stress [N/mm2]
Displacement [mm]
0
100
200
300
400
500
600
-2
0
2
4
6
8
10
12
14
16

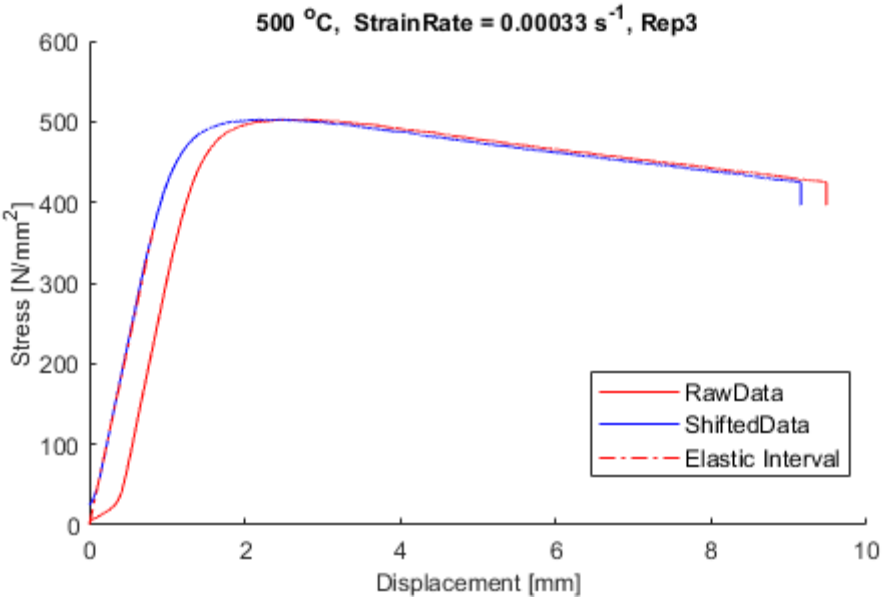
500 °C, StrainRate = 0.00033 s-1, Rep3
RawData
ShiftedData
Elastic Interval
Stress [N/mm2]
Displacement [mm]
0
100
200
300
400
500
600
0
2
4
6
8
10

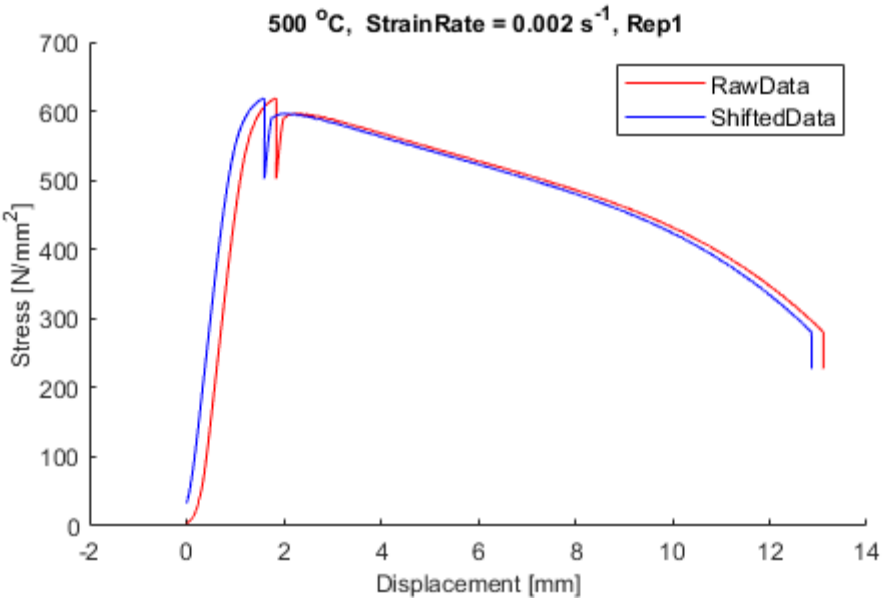
500 °C, StrainRate = 0.002 s-1, Rep1
RawData
ShiftedData
Stress [N/mm2]
Displacement [mm]
0
100
200
300
400
500
600
700
-2
0
2
4
6
8
10
12
14

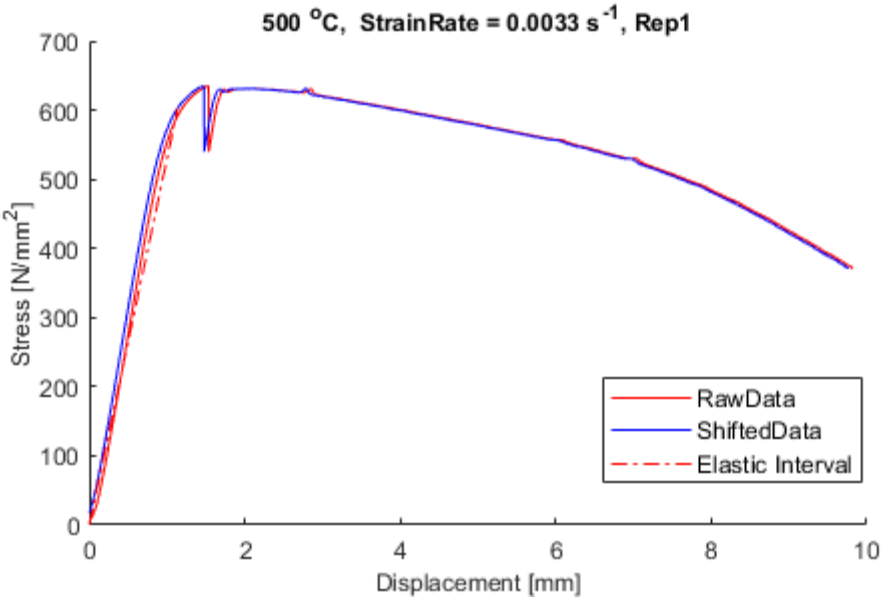
500 °C, StrainRate = 0.0033 s-1, Rep1
RawData
ShiftedData
Elastic Interval
Stress [N/mm2]
Displacement [mm]
0
100
200
300
400
500
600
700
0
2
4
6
8
10

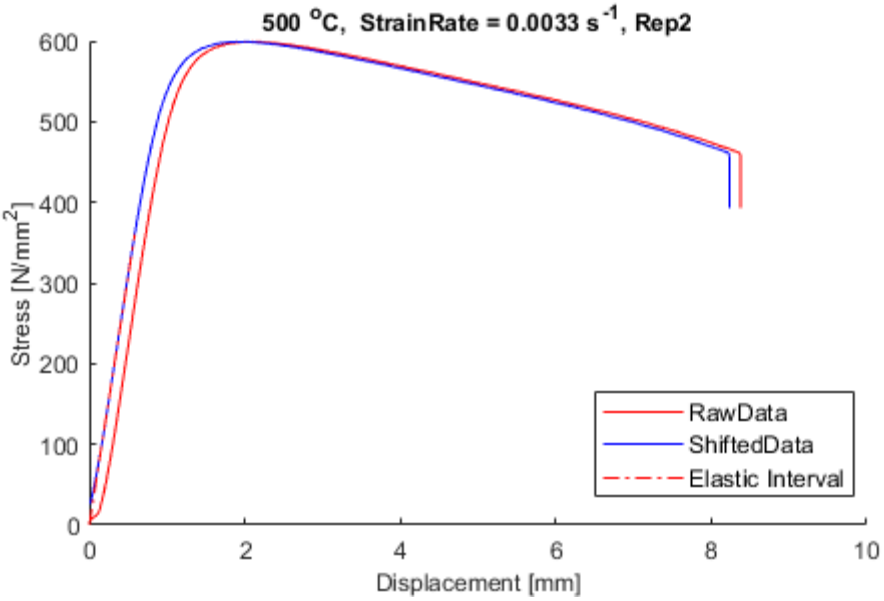
500 °C, StrainRate = 0.0033 s-1, Rep2
Stress [N/mm2]
Displacement [mm]
RawData
ShiftedData
Elastic Interval

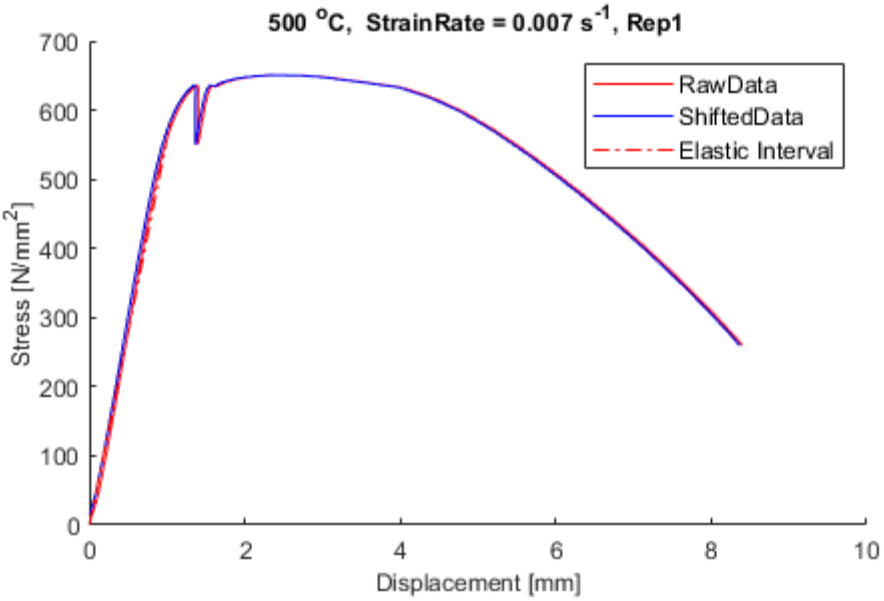
500 °C, StrainRate = 0.007 s-1, Rep1
Stress [N/mm2]
Displacement [mm]
RawData
ShiftedData
Elastic Interval

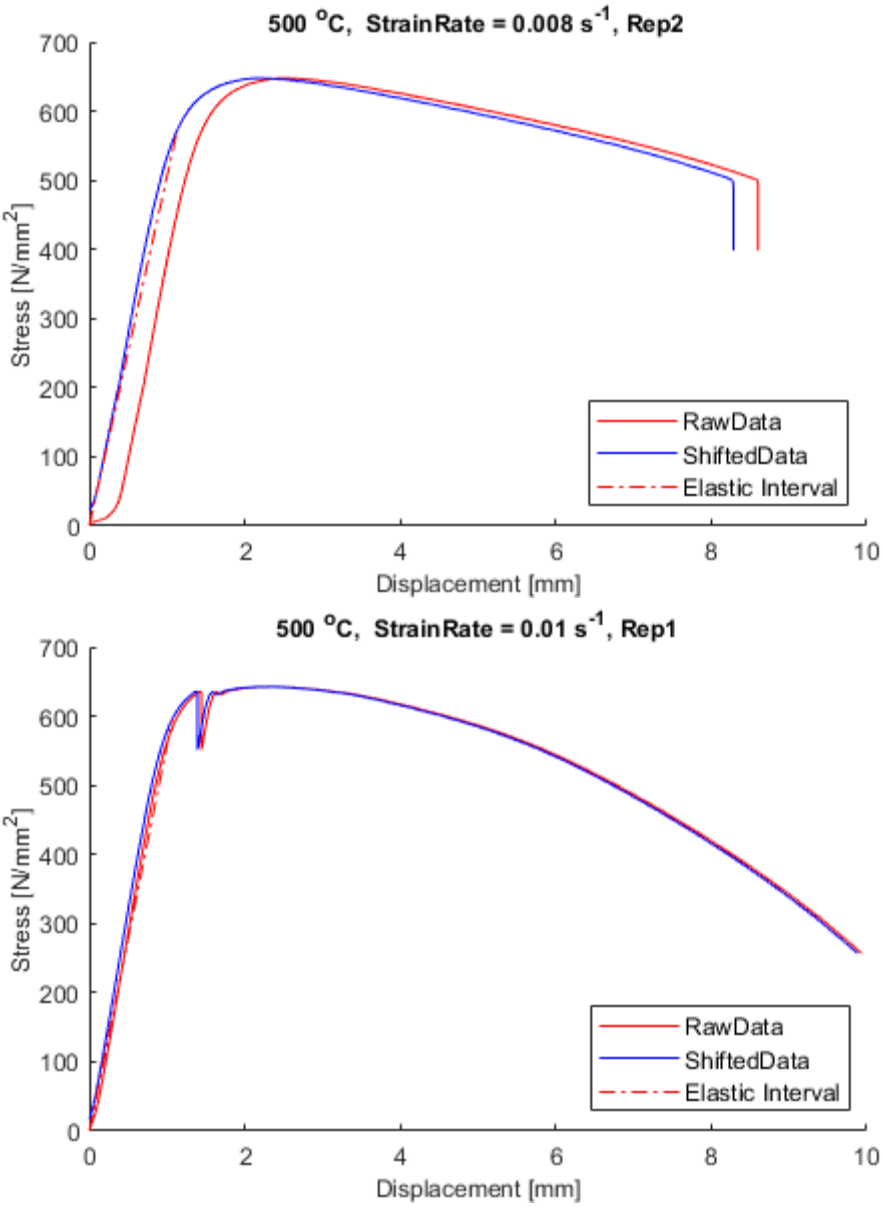
500 °C, StrainRate = 0.008 s-1, Rep2
Stress [N/mm2]
Displacement [mm]
RawData
ShiftedData
Elastic Interval
500 °C, StrainRate = 0.01 s-1, Rep1
Stress [N/mm2]
Displacement [mm]
RawData
ShiftedData
Elastic Interval

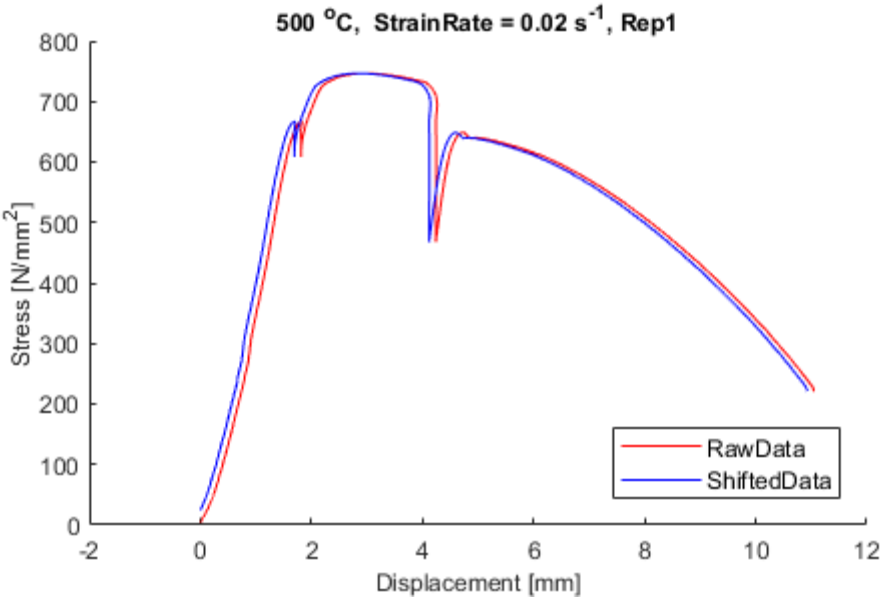
500 °C, StrainRate = 0.02 s-1, Rep1
Stress [N/mm2]
Displacement [mm]
RawData
ShiftedData

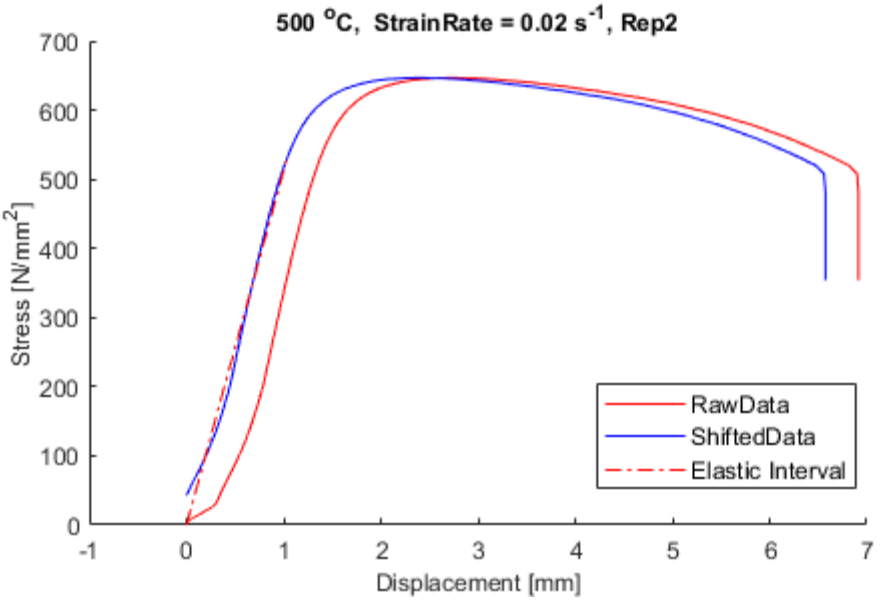
500 °C, StrainRate = 0.02 s-1, Rep2
Stress [N/mm2]
Displacement [mm]
RawData
ShiftedData
Elastic Interval

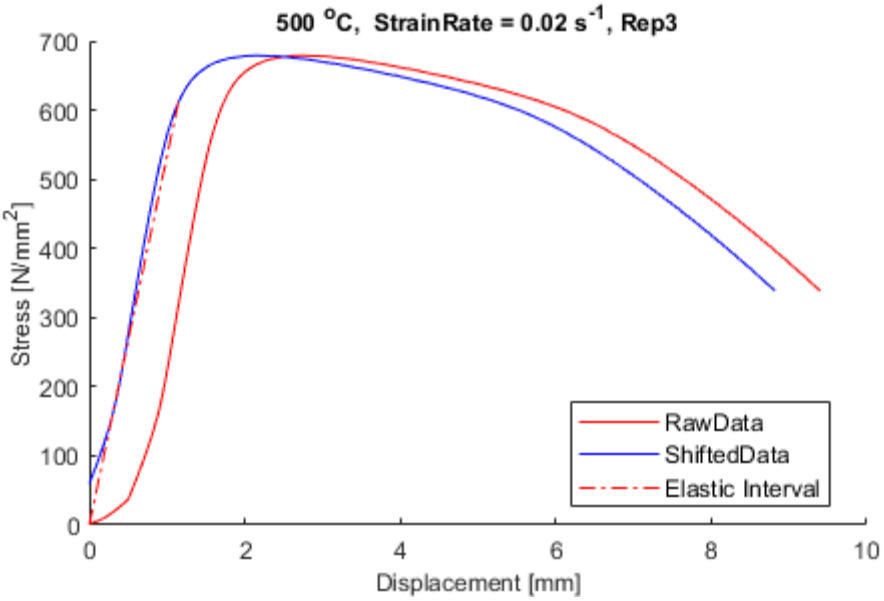
500 °C, StrainRate = 0.02 s-1, Rep3
Stress [N/mm2]
Displacement [mm]
RawData
ShiftedData
Elastic Interval

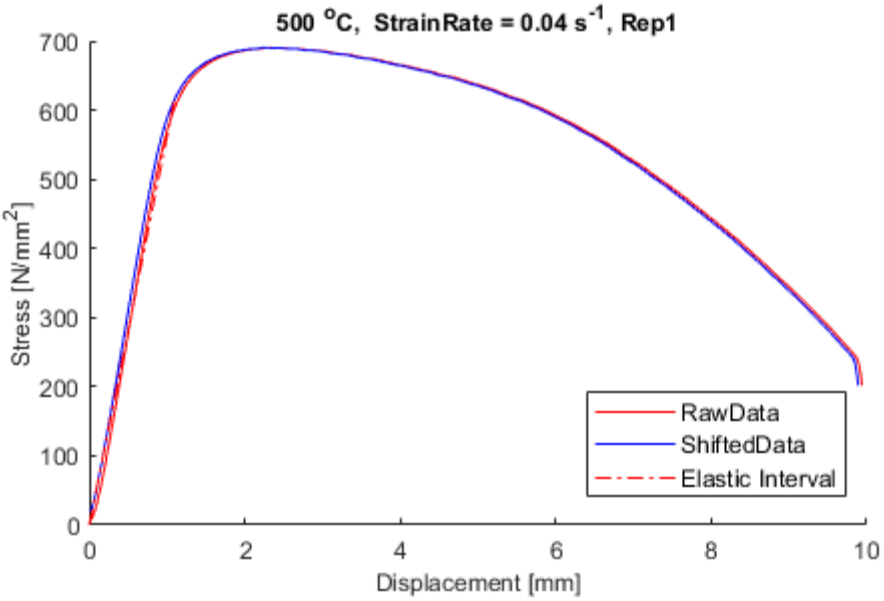
500 °C, StrainRate = 0.04 s-1, Rep1
Stress [N/mm2]
Displacement [mm]
RawData
ShiftedData
Elastic Interval

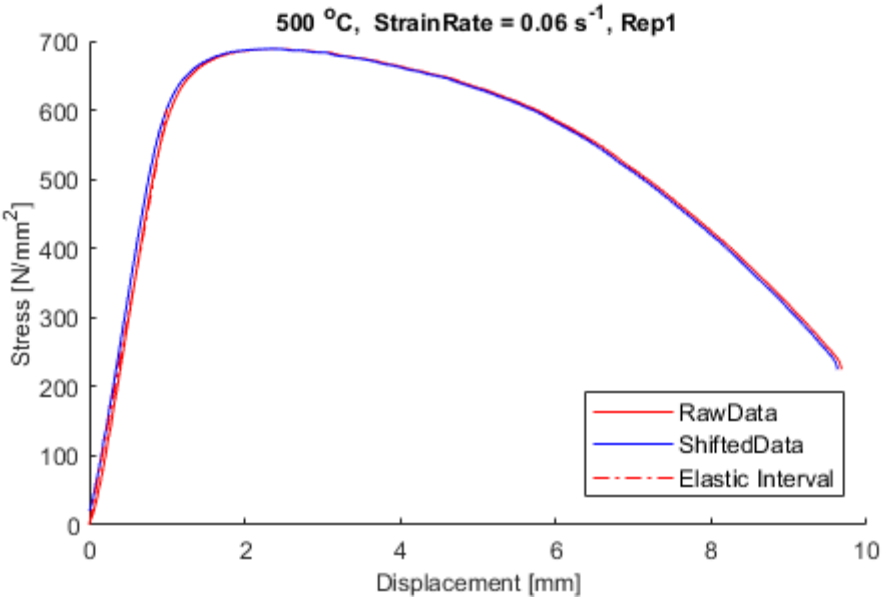
500 °C, StrainRate = 0.06 s-1, Rep1
Stress [N/mm2]
Displacement [mm]
RawData
ShiftedData
Elastic Interval

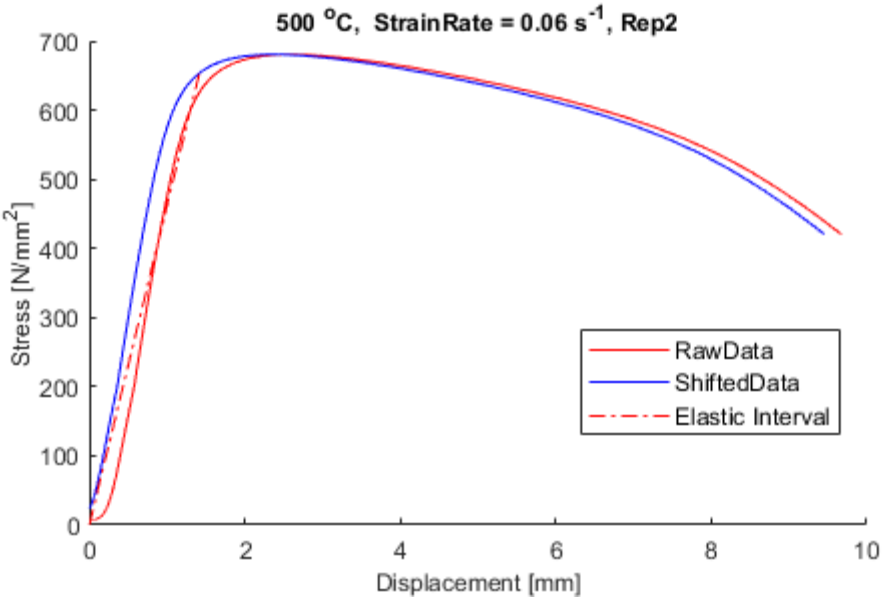
500 °C, StrainRate = 0.06 s-1, Rep2
Stress [N/mm2]
Displacement [mm]
RawData
ShiftedData
Elastic Interval

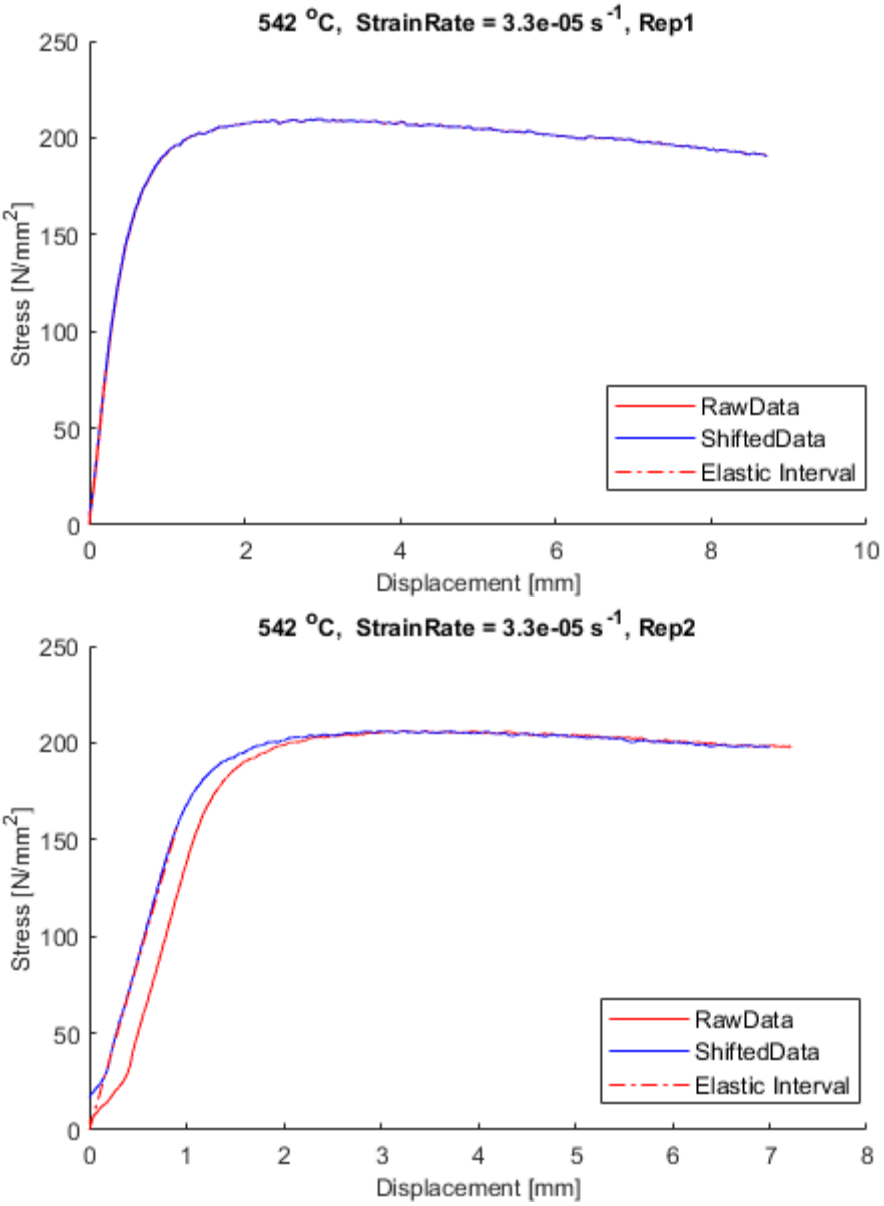
542 °C, StrainRate = 3.3e-05 s-1, Rep1
Stress [N/mm2]
Displacement [mm]
RawData
ShiftedData
Elastic Interval
542 °C, StrainRate = 3.3e-05 s-1, Rep2
Stress [N/mm2]
Displacement [mm]
RawData
ShiftedData
Elastic Interval

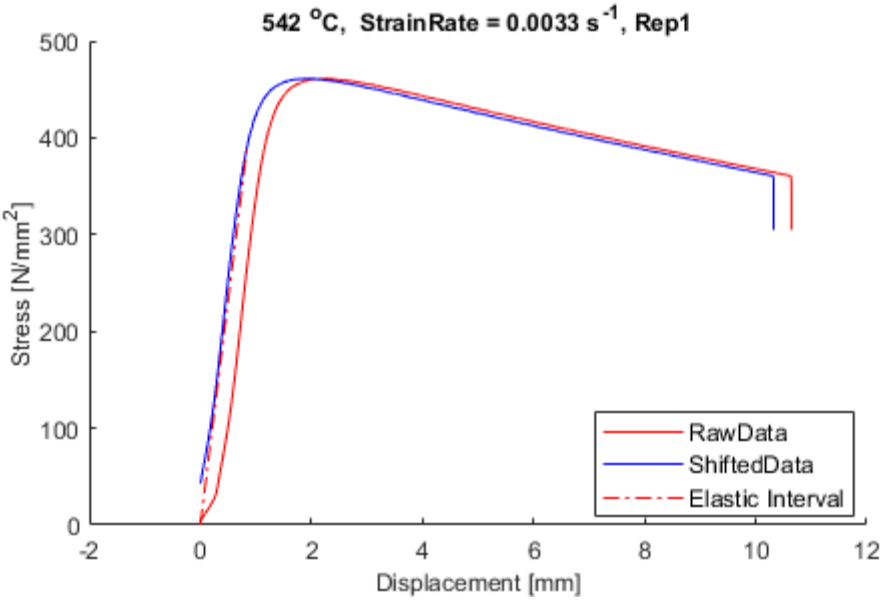
542 °C, StrainRate = 0.0033 s-1, Rep1
Stress [N/mm2]
Displacement [mm]
RawData
ShiftedData
Elastic Interval

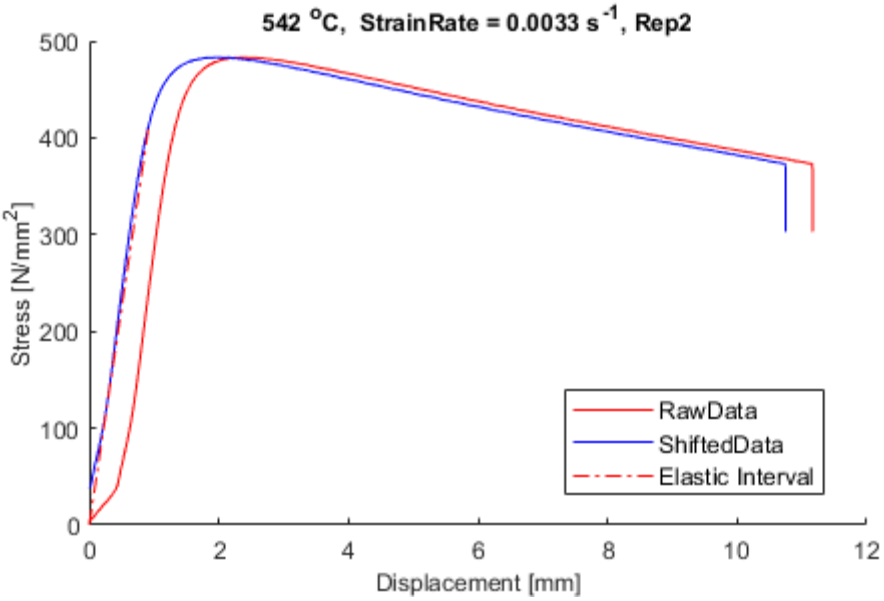
542 °C, StrainRate = 0.0033 s-1, Rep2
Stress [N/mm2]
Displacement [mm]
RawData
ShiftedData
Elastic Interval

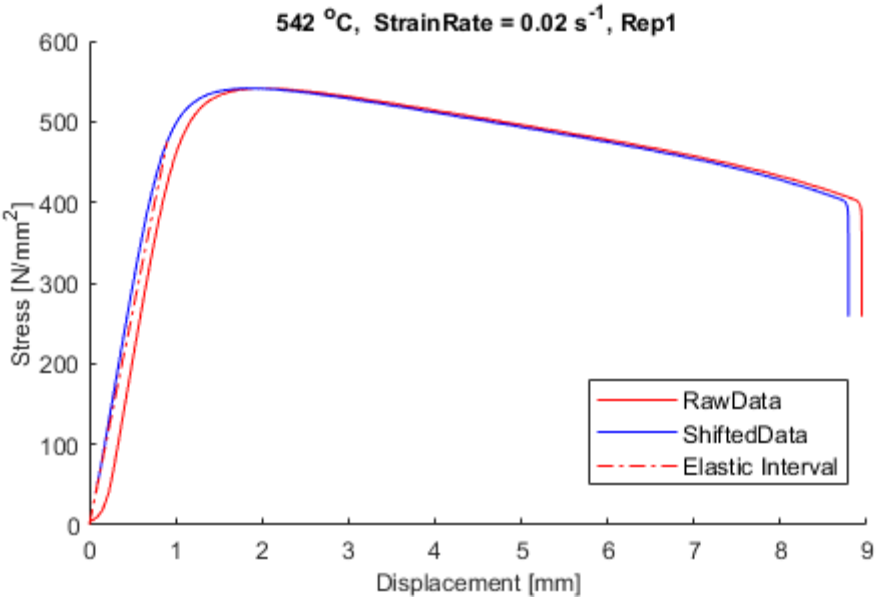
542 °C, StrainRate = 0.02 s-1, Rep1
Stress [N/mm2]
Displacement [mm]
RawData
ShiftedData
Elastic Interval

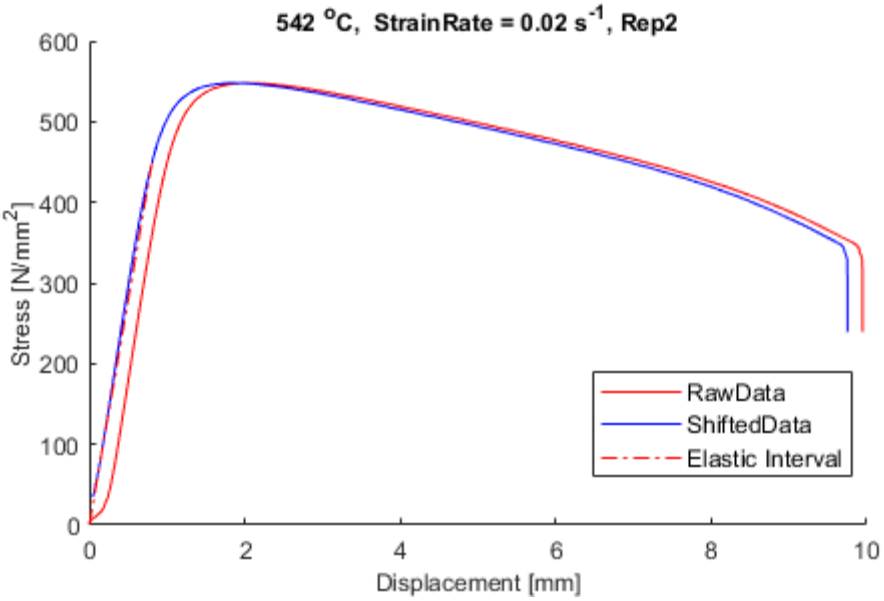
542 °C, StrainRate = 0.02 s-1, Rep2
Stress [N/mm2]
Displacement [mm]
RawData
ShiftedData
Elastic Interval

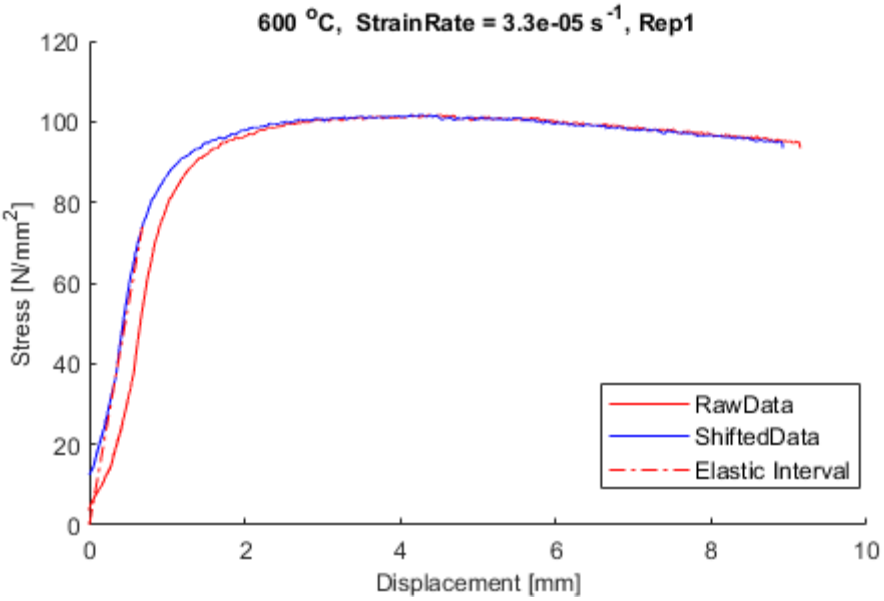
600 °C, StrainRate = 3.3e-05 s-1, Rep1
Stress [N/mm2]
Displacement [mm]
RawData
ShiftedData
Elastic Interval

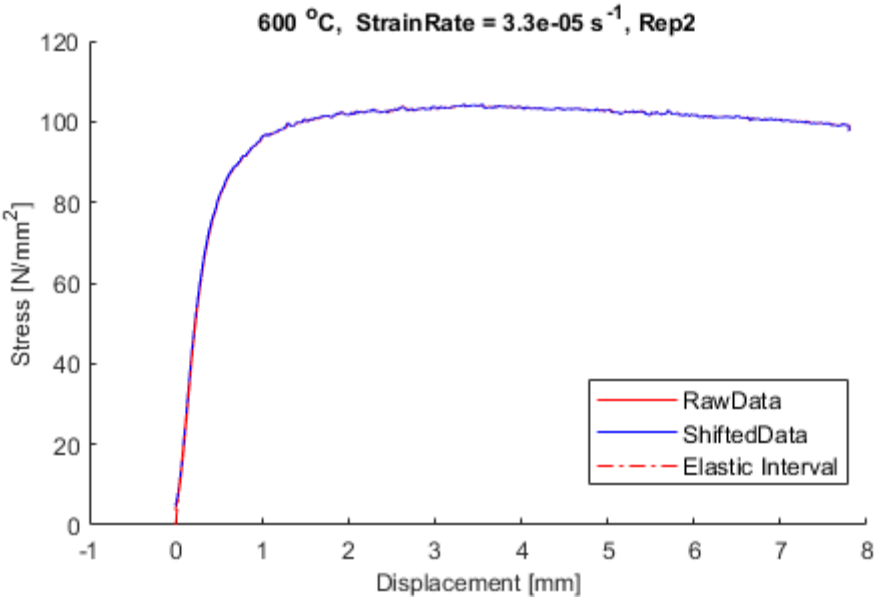
600 °C, StrainRate = 3.3e-05 s-1, Rep2
Stress [N/mm2]
Displacement [mm]
RawData
ShiftedData
Elastic Interval

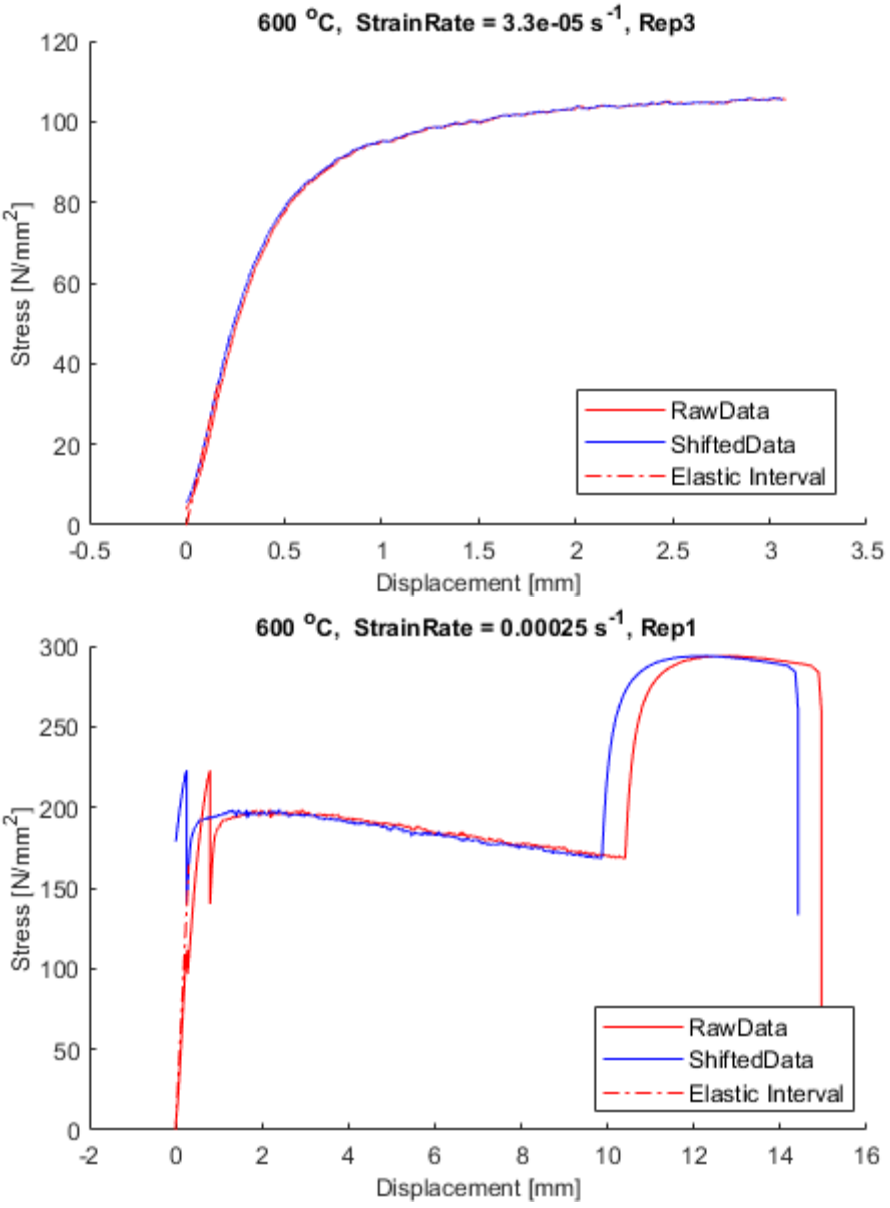
600 °C, StrainRate = 3.3e-05 s-1, Rep3
Stress [N/mm2]
Displacement [mm]
RawData
ShiftedData
Elastic Interval
600 °C, StrainRate = 0.00025 s-1, Rep1
Stress [N/mm2]
Displacement [mm]
RawData
ShiftedData
Elastic Interval

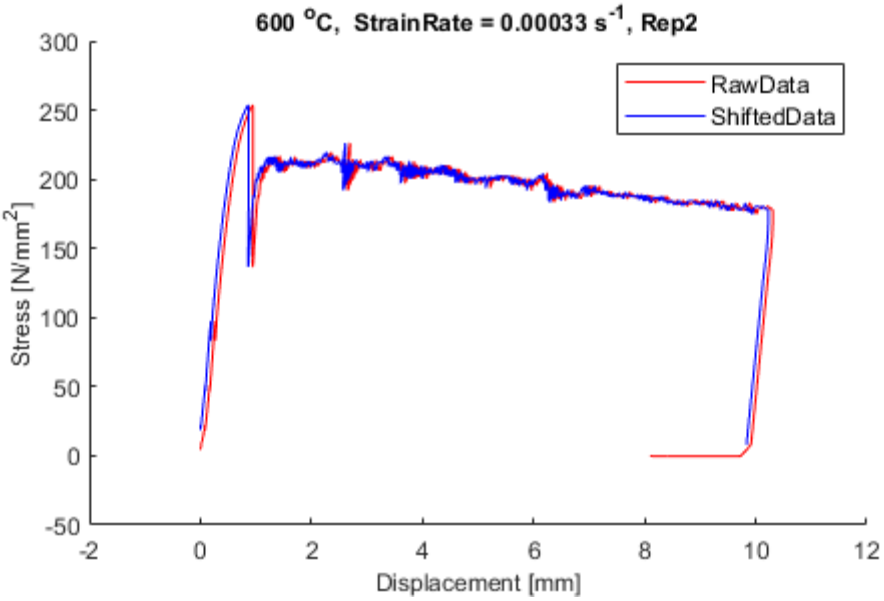
600 °C, StrainRate = 0.00033 s-1, Rep2
RawData
ShiftedData
Stress [N/mm2]
Displacement [mm]
300
250
200
150
100
50
0
-50
-2
0
2
4
6
8
10
12

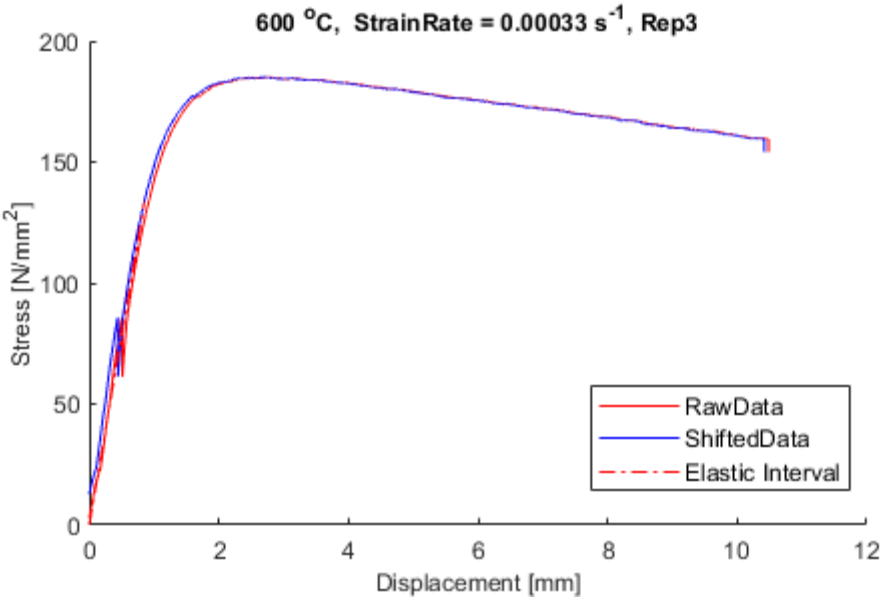
600 °C, StrainRate = 0.00033 s-1, Rep3
RawData
ShiftedData
Elastic Interval
Stress [N/mm2]
Displacement [mm]
200
150
100
50
0
0
2
4
6
8
10
12

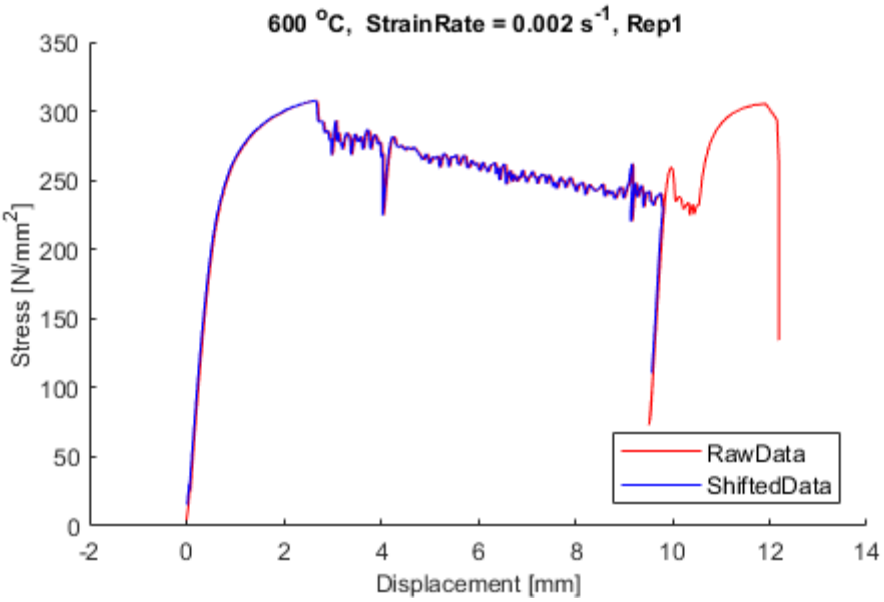
600 °C, StrainRate = 0.002 s-1, Rep1
Stress [N/mm2]
Displacement [mm]
RawData
ShiftedData

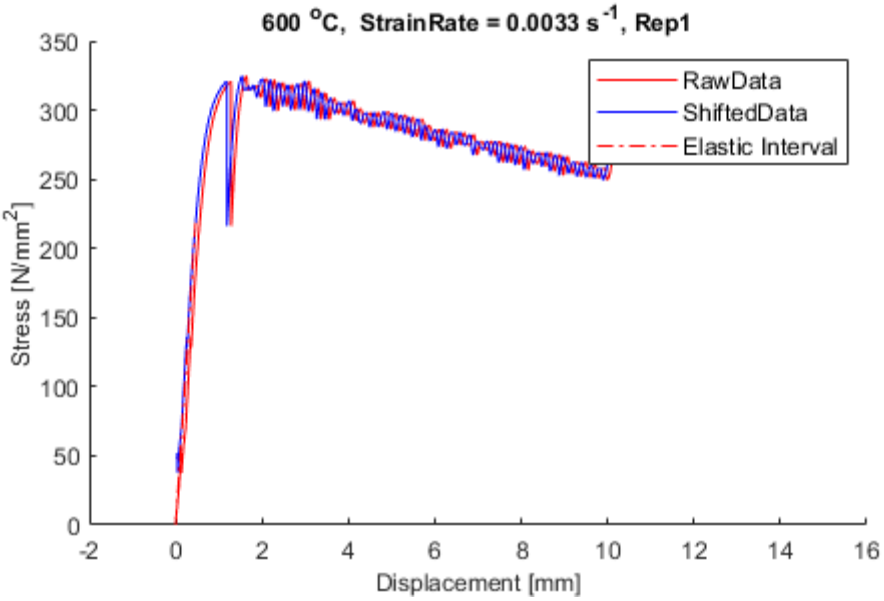
600 °C, StrainRate = 0.0033 s-1, Rep1
Stress [N/mm2]
Displacement [mm]
RawData
ShiftedData
Elastic Interval

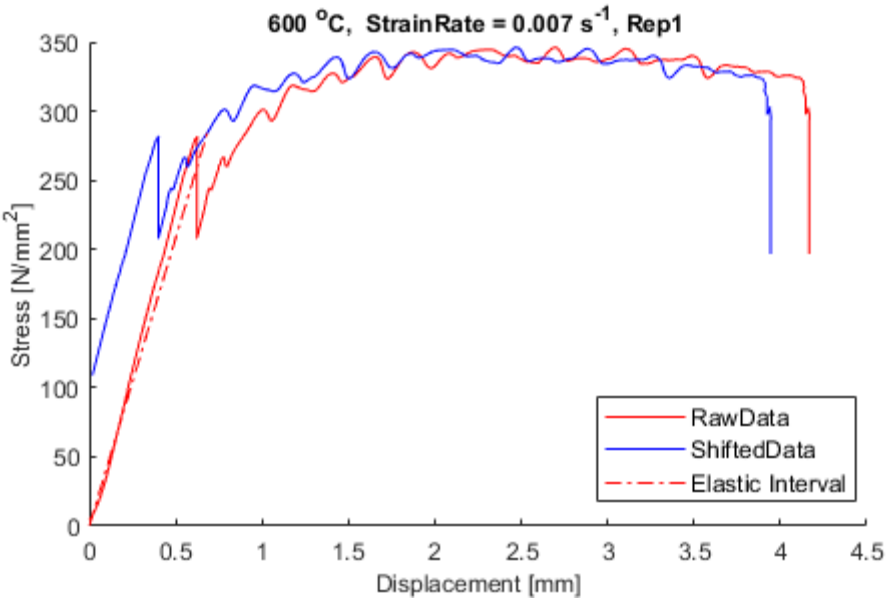
600 °C, StrainRate = 0.007 s-1, Rep1
Stress [N/mm2]
Displacement [mm]
RawData
ShiftedData
Elastic Interval

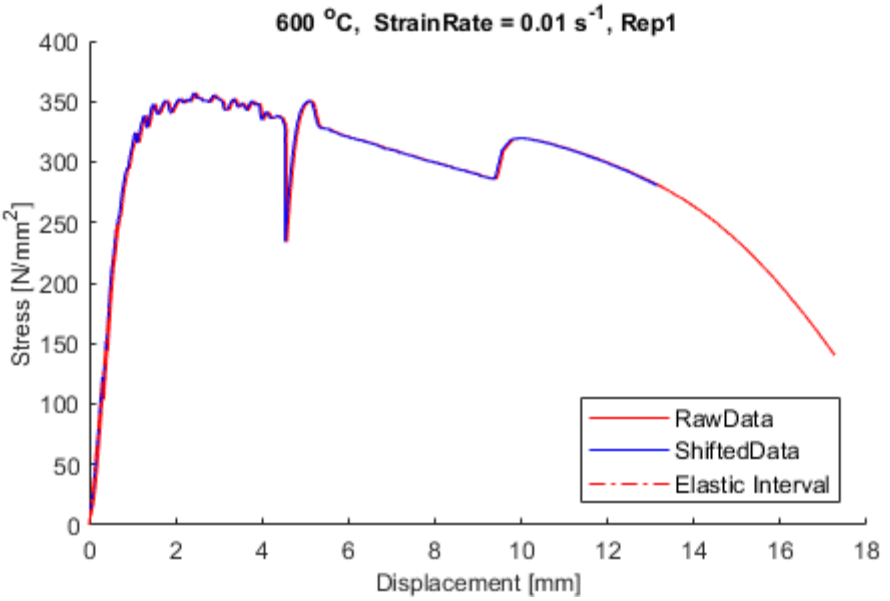
600 °C, StrainRate = 0.01 s-1, Rep1
Stress [N/mm2]
Displacement [mm]
RawData
ShiftedData
Elastic Interval

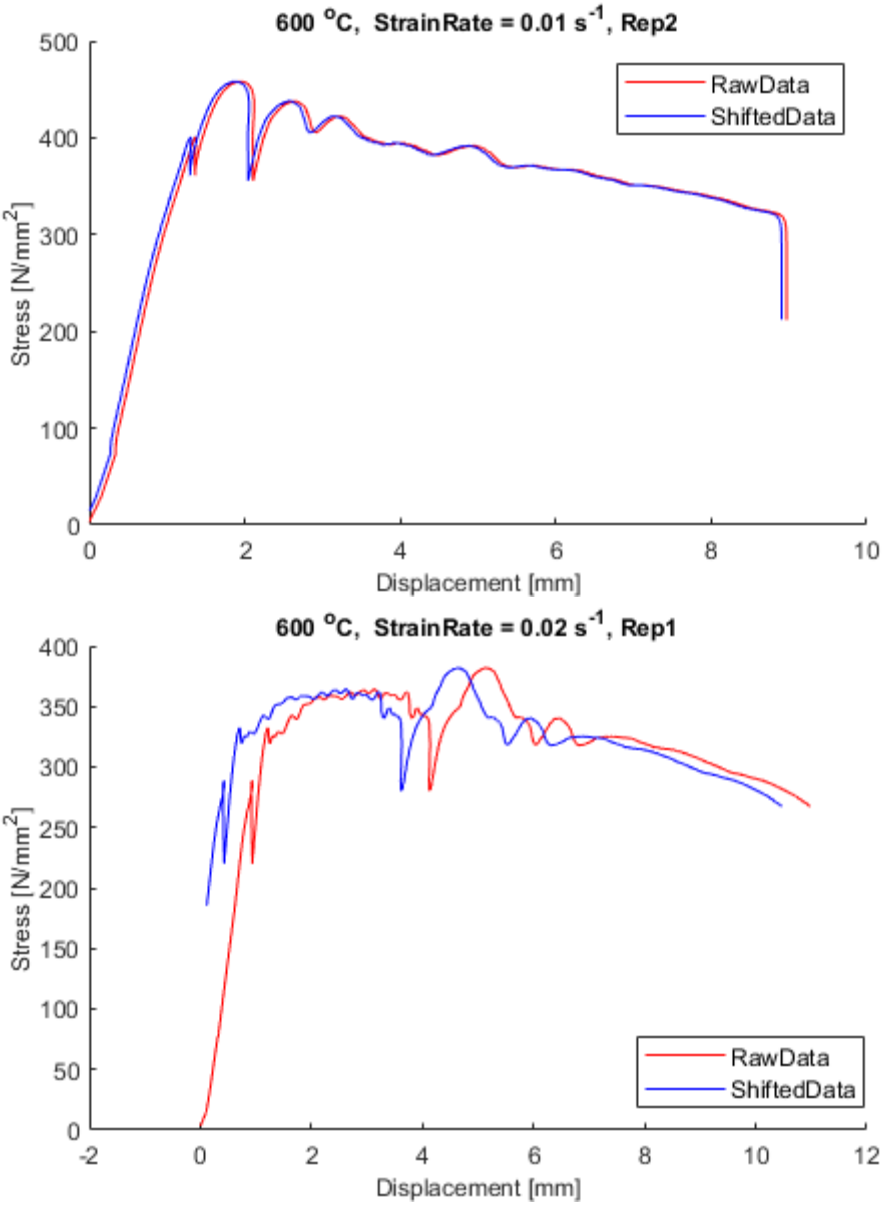
600 °C, StrainRate = 0.01 s-1, Rep2
RawData
ShiftedData
Stress [N/mm2]
Displacement [mm]
600 °C, StrainRate = 0.02 s-1, Rep1
RawData
ShiftedData
Stress [N/mm2]
Displacement [mm]

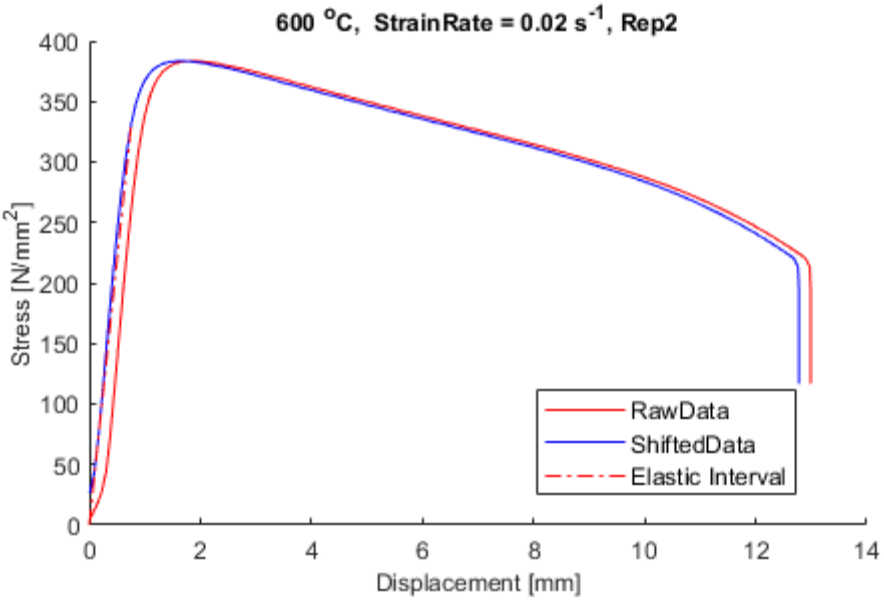
600 °C, StrainRate = 0.02 s-1, Rep2
Stress [N/mm2]
Displacement [mm]
RawData
ShiftedData
Elastic Interval

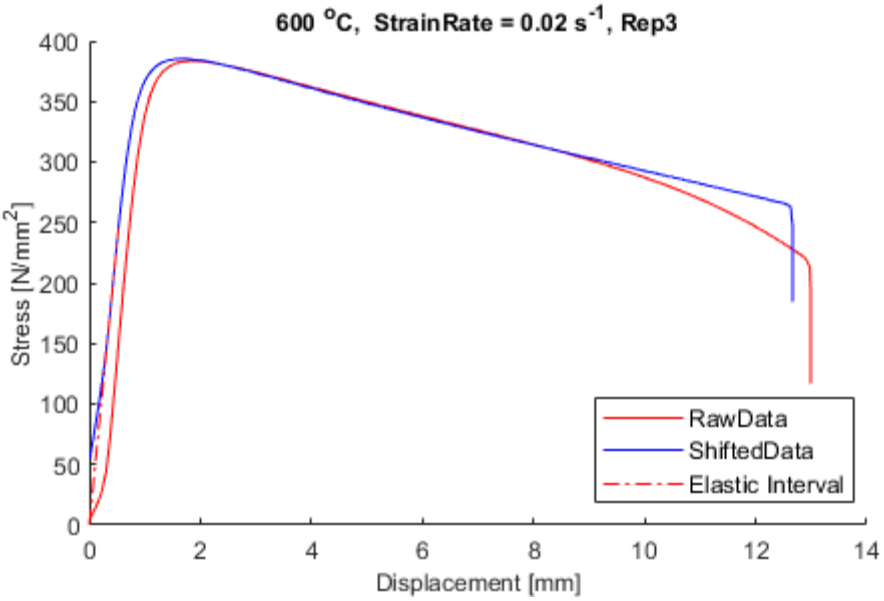
600 °C, StrainRate = 0.02 s-1, Rep3
Stress [N/mm2]
Displacement [mm]
RawData
ShiftedData
Elastic Interval

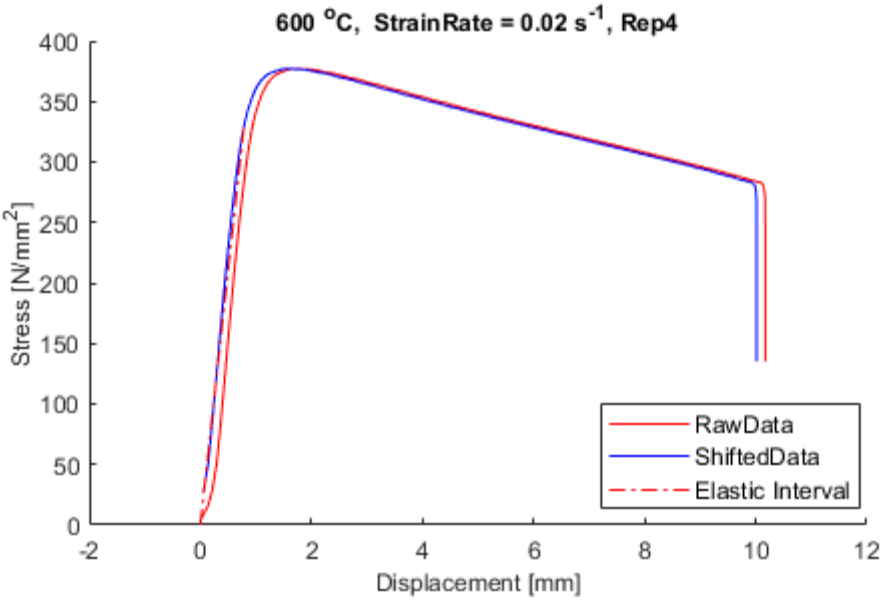
600 °C, StrainRate = 0.02 s-1, Rep4
Stress [N/mm2]
Displacement [mm]
RawData
ShiftedData
Elastic Interval

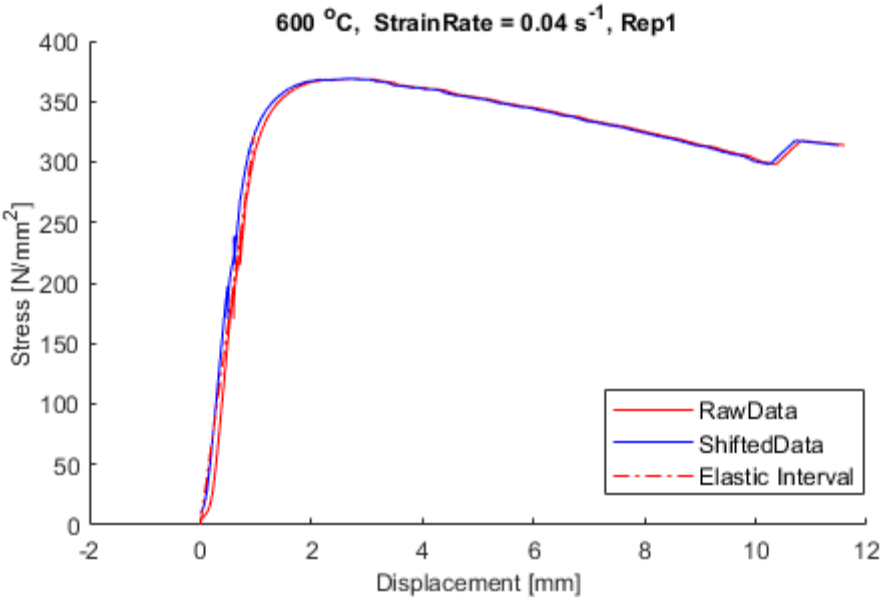
600 °C, StrainRate = 0.04 s-1, Rep1
Stress [N/mm2]
Displacement [mm]
RawData
ShiftedData
Elastic Interval

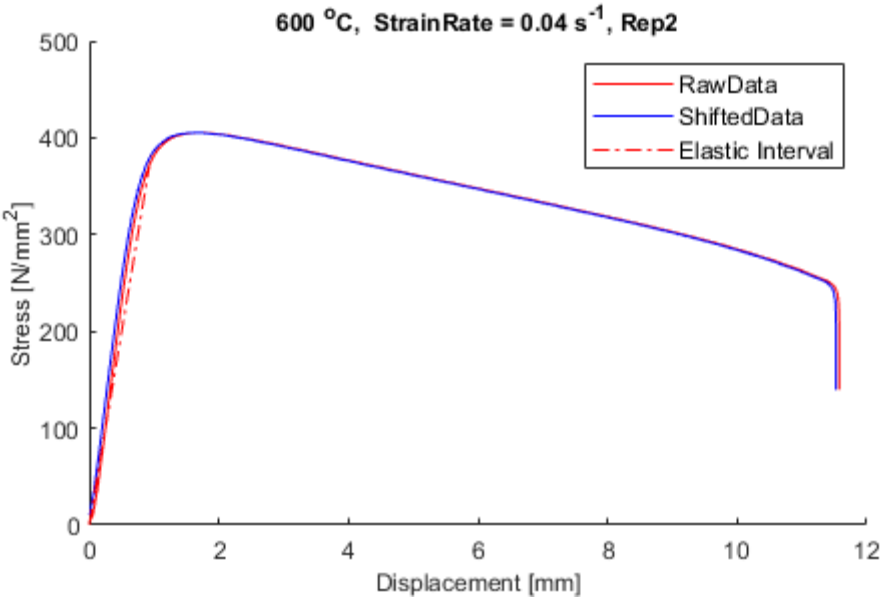
600 °C, StrainRate = 0.04 s-1, Rep2
RawData
ShiftedData
Elastic Interval
Stress [N/mm2]
Displacement [mm]
0
100
200
300
400
500
0
2
4
6
8
10
12

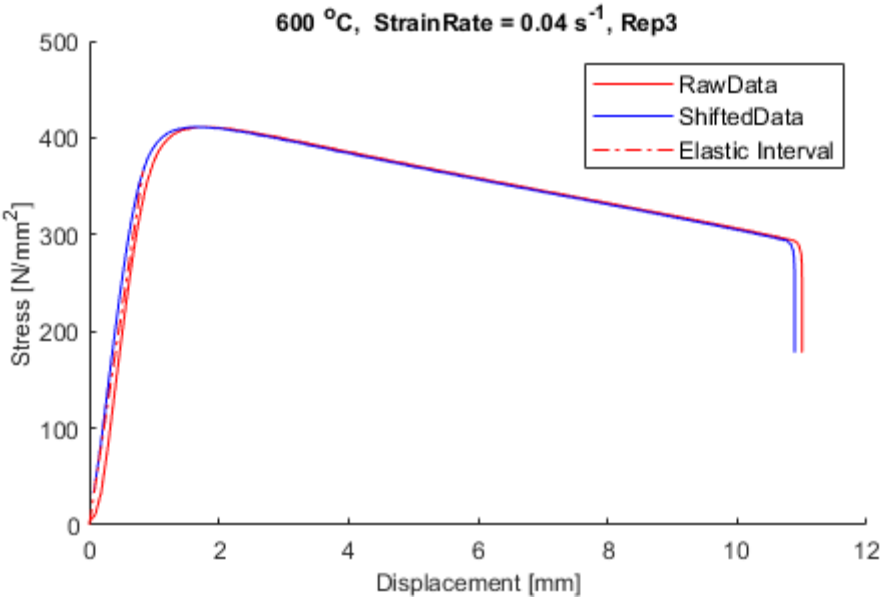
600 °C, StrainRate = 0.04 s-1, Rep3
RawData
ShiftedData
Elastic Interval
Stress [N/mm2]
Displacement [mm]
0
100
200
300
400
500
0
2
4
6
8
10
12

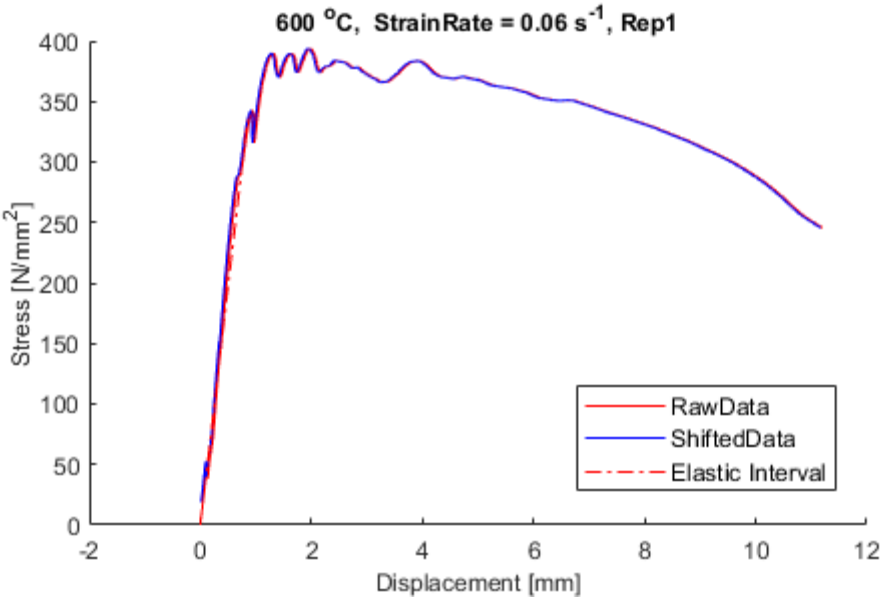
600 °C, StrainRate = 0.06 s-1, Rep1
Stress [N/mm2]
Displacement [mm]
RawData
ShiftedData
Elastic Interval

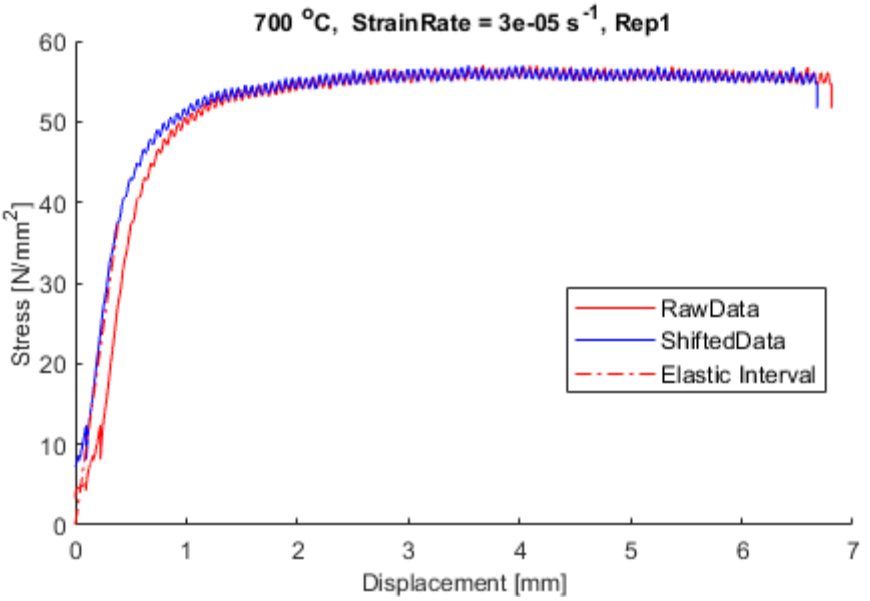
700 °C, StrainRate = 3e-05 s-1, Rep1
Stress [N/mm2]
Displacement [mm]
RawData
ShiftedData
Elastic Interval

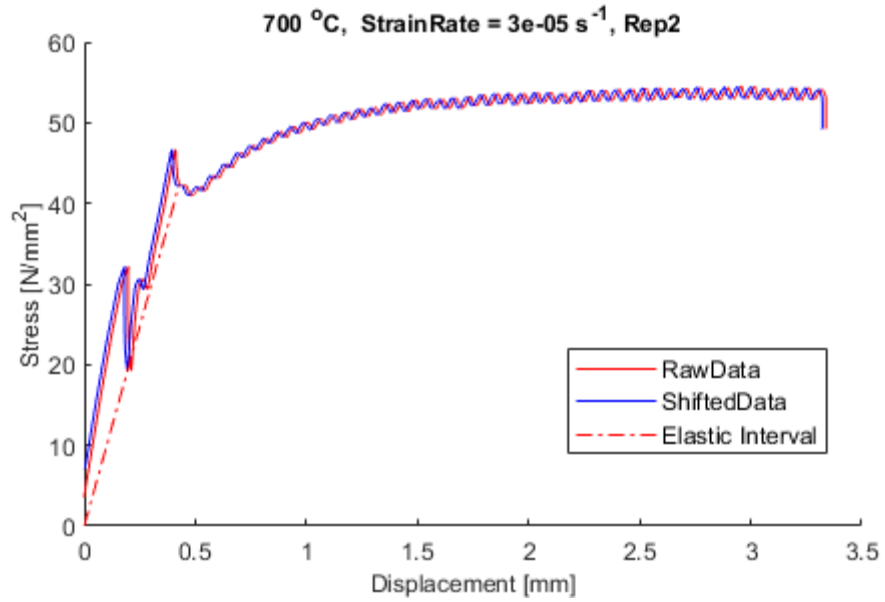
700 °C, StrainRate = 3e-05 s-1, Rep2
Stress [N/mm2]
Displacement [mm]
RawData
ShiftedData
Elastic Interval

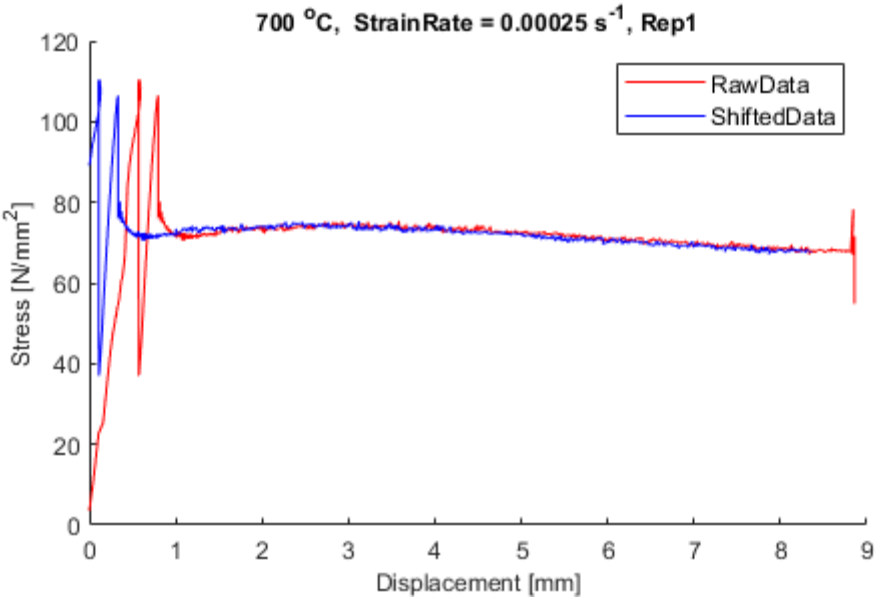
700 °C, StrainRate = 0.00025 s-1, Rep1
Stress [N/mm2]
Displacement [mm]
RawData
ShiftedData

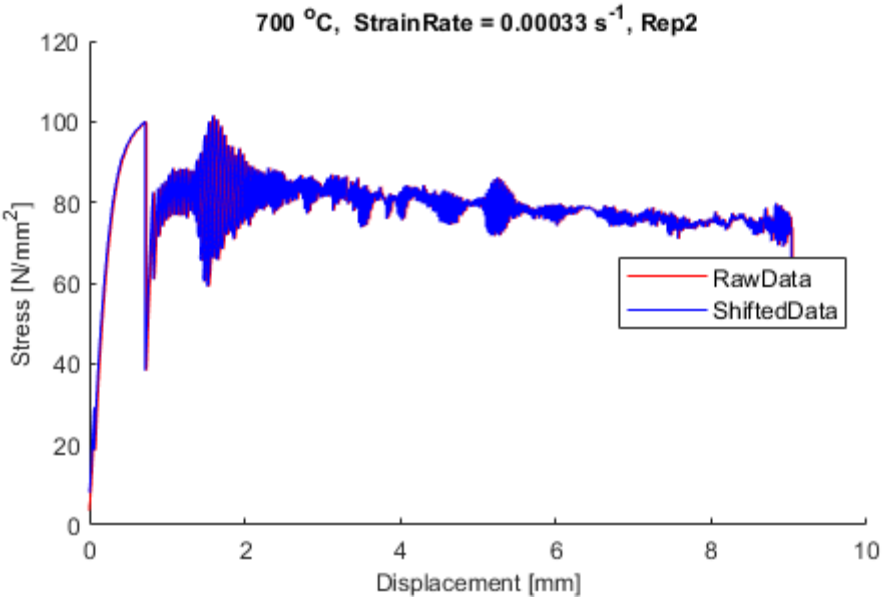
700 °C, StrainRate = 0.00033 s-1, Rep2
Stress [N/mm2]
Displacement [mm]
RawData
ShiftedData

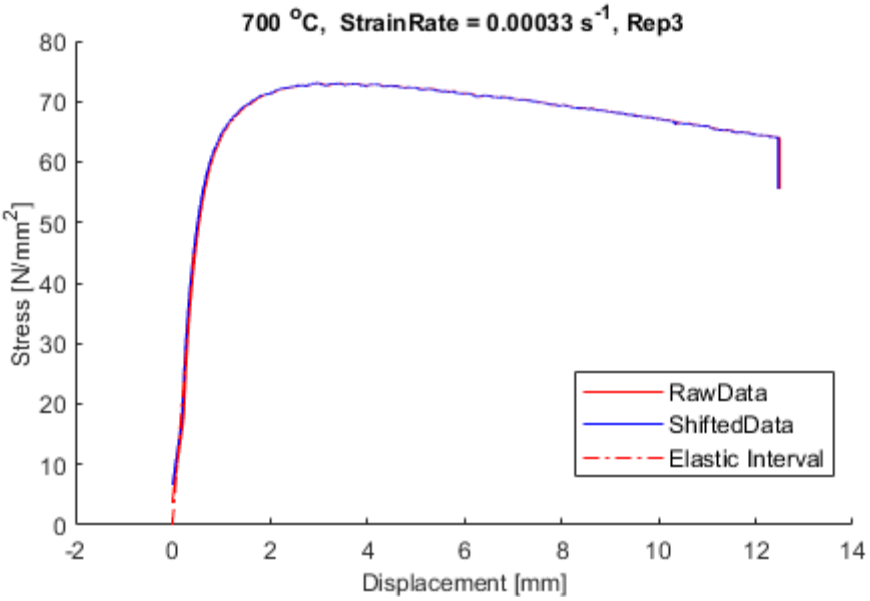
700 °C, StrainRate = 0.00033 s-1, Rep3
Stress [N/mm2]
Displacement [mm]
RawData
ShiftedData
Elastic Interval

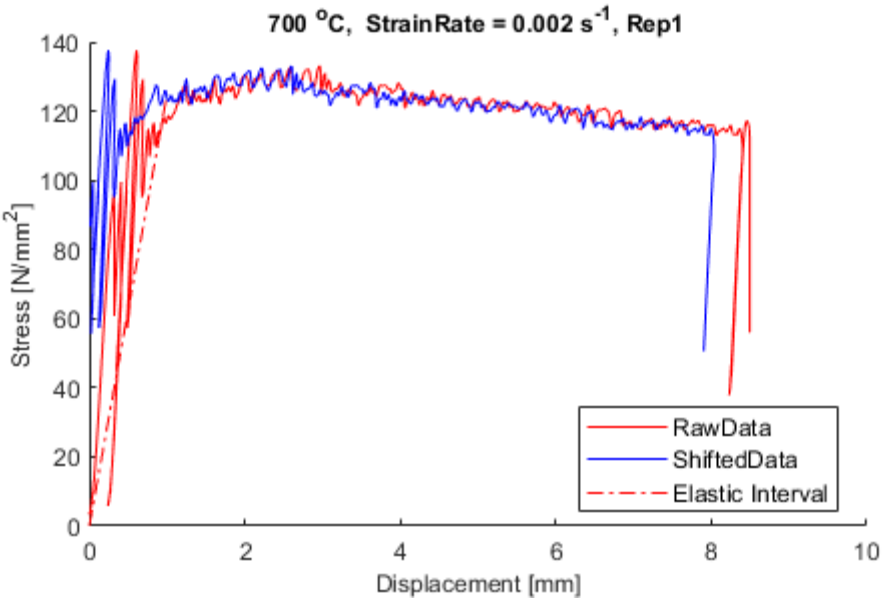
700 °C, StrainRate = 0.002 s-1, Rep1
Stress [N/mm2]
Displacement [mm]
RawData
ShiftedData
Elastic Interval

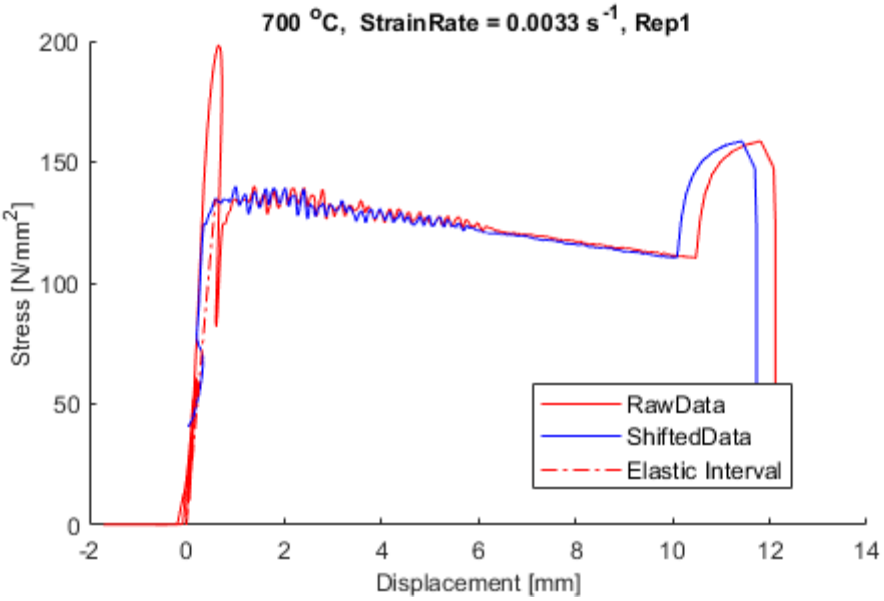
700 °C, StrainRate = 0.0033 s-1, Rep1
Stress [N/mm2]
Displacement [mm]
RawData
ShiftedData
Elastic Interval

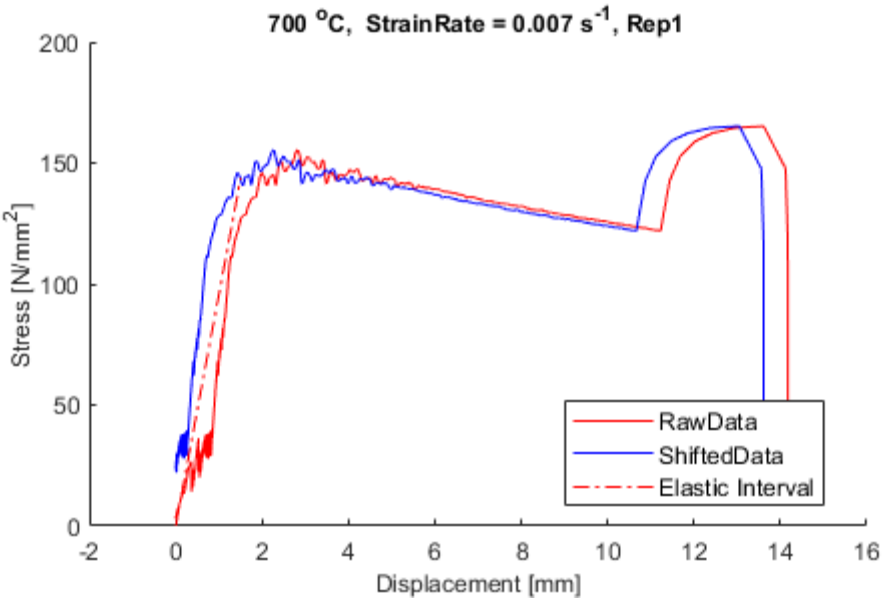
700 °C, StrainRate = 0.007 s-1, Rep1
Stress [N/mm2]
Displacement [mm]
RawData
ShiftedData
Elastic Interval

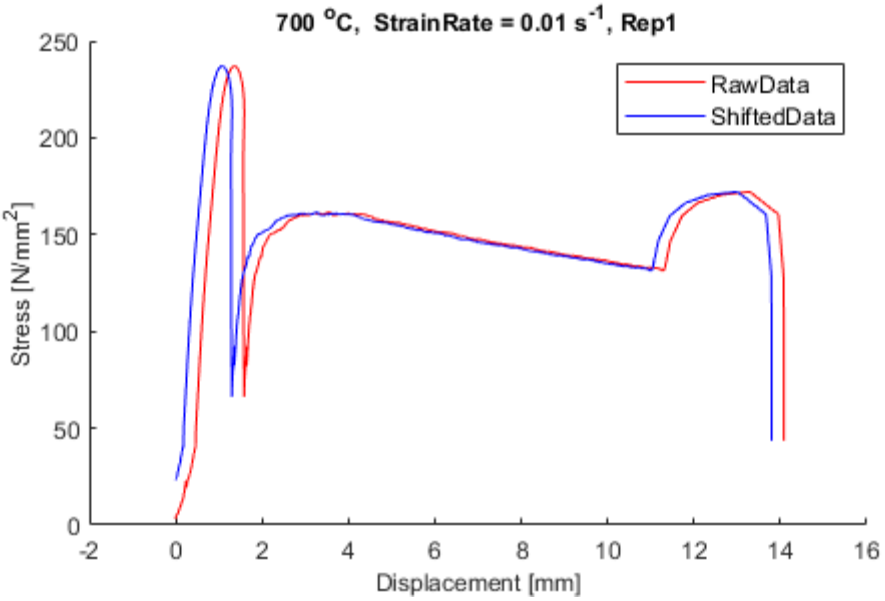
700 °C, StrainRate = 0.01 s-1, Rep1
Stress [N/mm2]
Displacement [mm]
RawData
ShiftedData

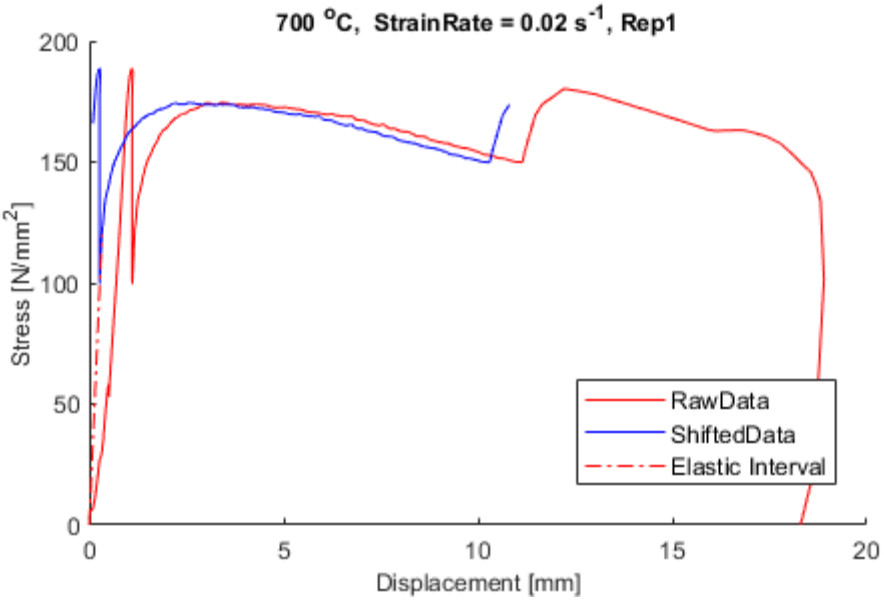
700 °C, StrainRate = 0.02 s-1, Rep1
Stress [N/mm2]
Displacement [mm]
RawData
ShiftedData
Elastic Interval

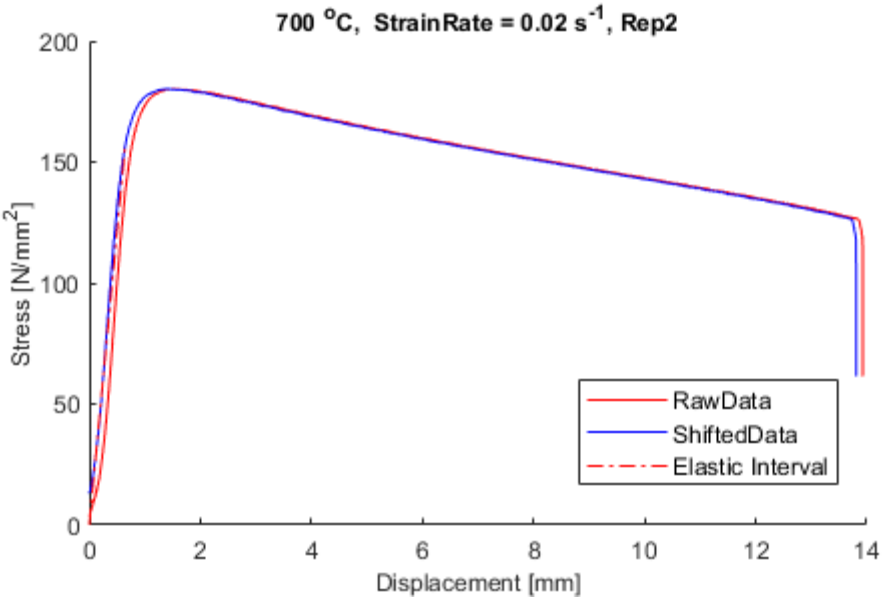
700 °C, StrainRate = 0.02 s-1, Rep2
Stress [N/mm2]
Displacement [mm]
RawData
ShiftedData
Elastic Interval

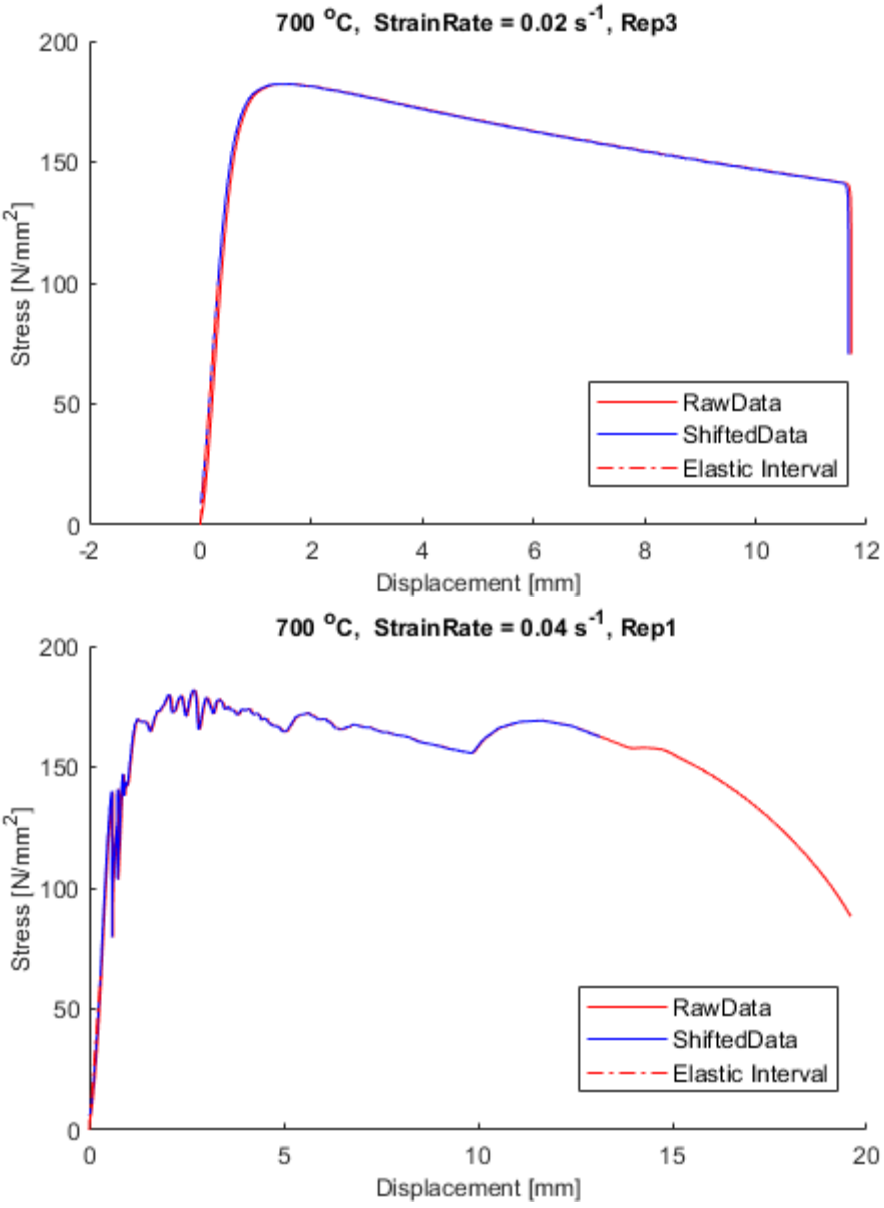
700 °C, StrainRate = 0.02 s-1, Rep3
Stress [N/mm2]
Displacement [mm]
RawData
ShiftedData
Elastic Interval
700 °C, StrainRate = 0.04 s-1, Rep1
Stress [N/mm2]
Displacement [mm]
RawData
ShiftedData
Elastic Interval

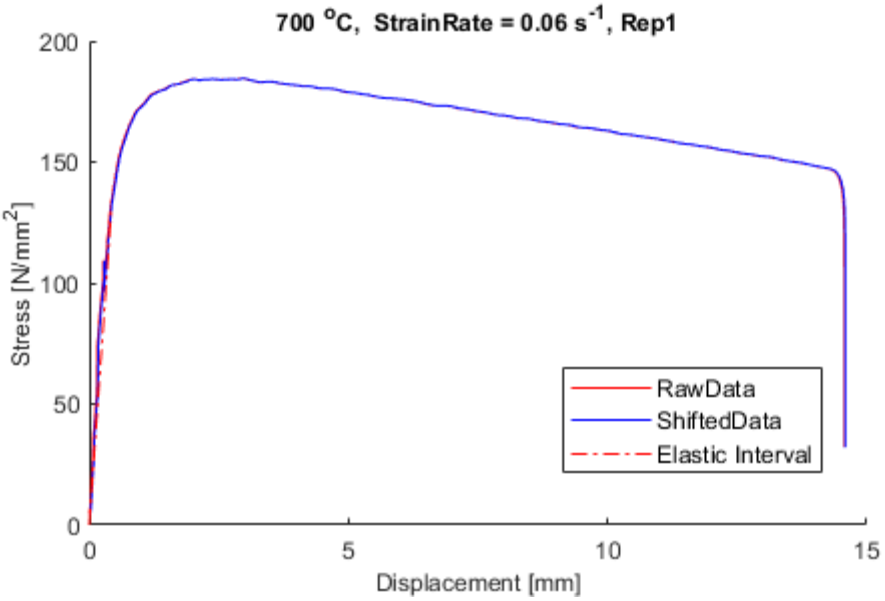
700 °C, StrainRate = 0.06 s-1, Rep1
Stress [N/mm2]
Displacement [mm]
RawData
ShiftedData
Elastic Interval

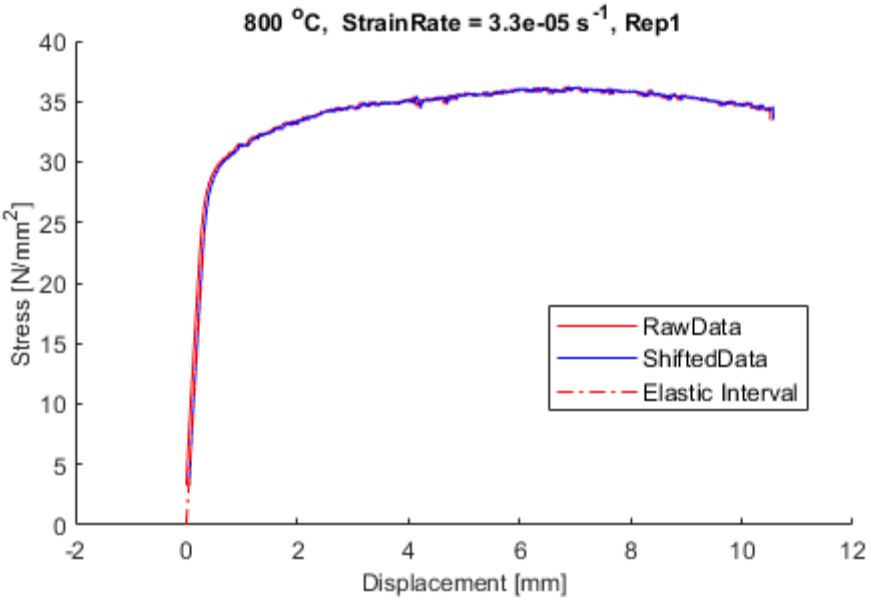
800 °C, StrainRate = 3.3e-05 s-1, Rep1
Stress [N/mm2]
Displacement [mm]
RawData
ShiftedData
Elastic Interval

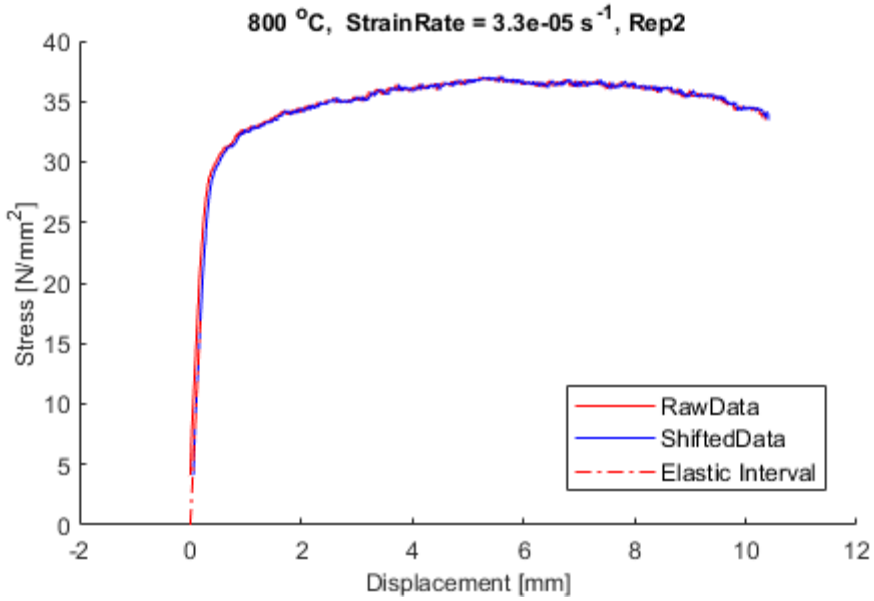
800 °C, StrainRate = 3.3e-05 s-1, Rep2
Stress [N/mm2]
Displacement [mm]
RawData
ShiftedData
Elastic Interval

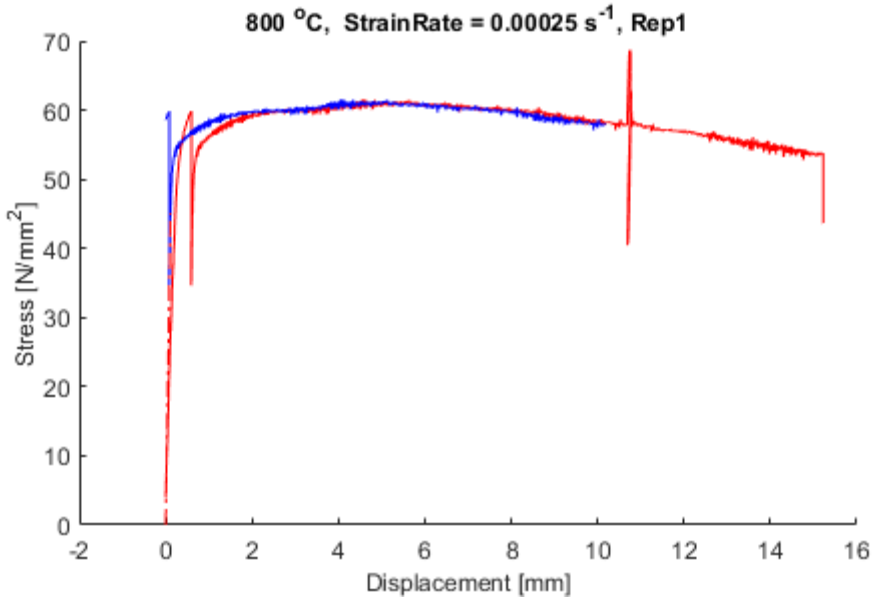
800 °C, StrainRate = 0.00025 s-1, Rep1
Stress [N/mm2]
Displacement [mm]

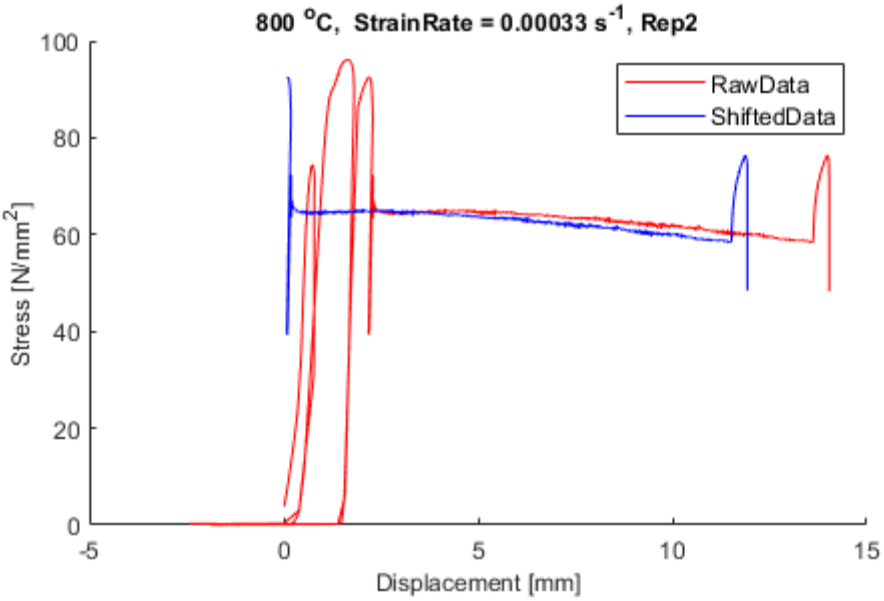
800 °C, StrainRate = 0.00033 s-1, Rep2
RawData
ShiftedData
Stress [N/mm2]
Displacement [mm]
0
20
40
60
80
100
-5
0
5
10
15

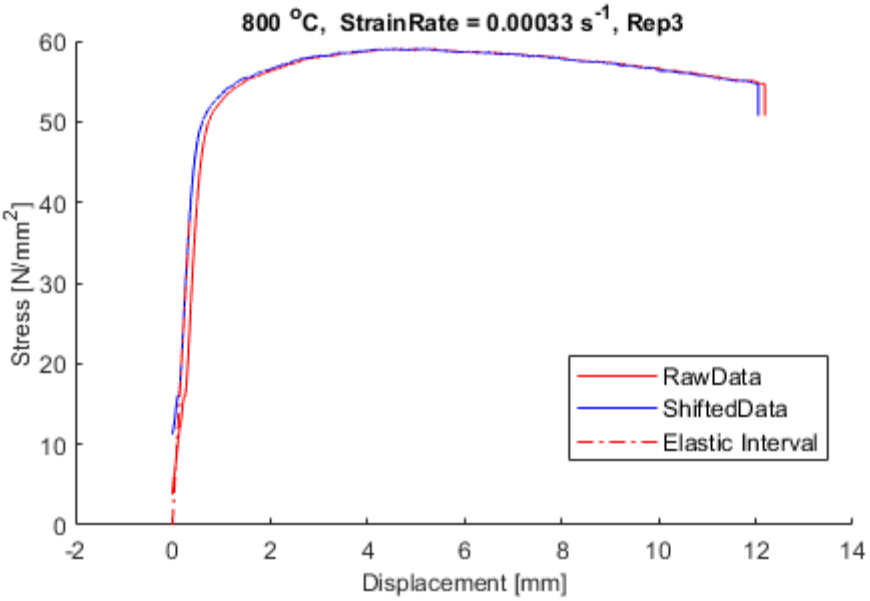
800 °C, StrainRate = 0.00033 s-1, Rep3
RawData
ShiftedData
Elastic Interval
Stress [N/mm2]
Displacement [mm]
0
10
20
30
40
50
60
-2
0
2
4
6
8
10
12
14

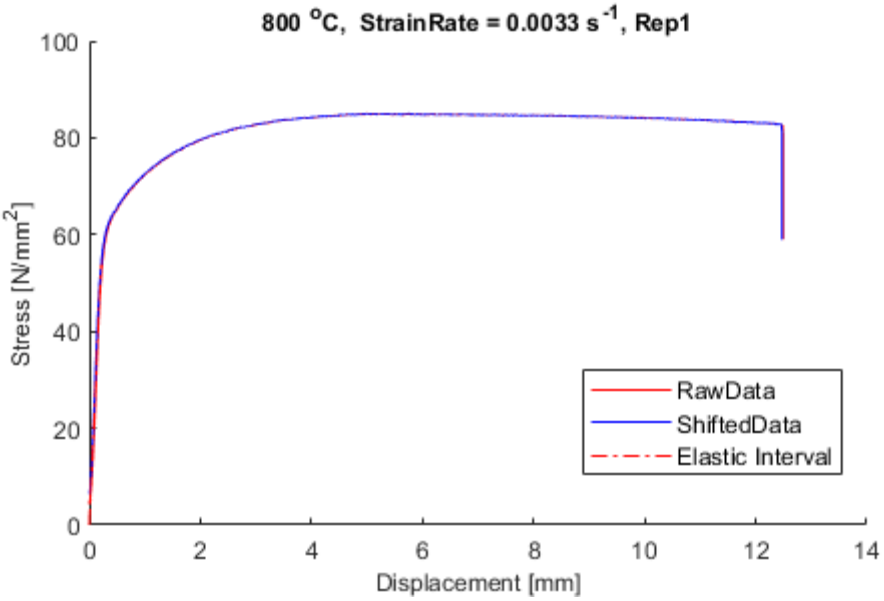
800 °C, StrainRate = 0.0033 s-1, Rep1
Stress [N/mm2]
Displacement [mm]
RawData
ShiftedData
Elastic Interval

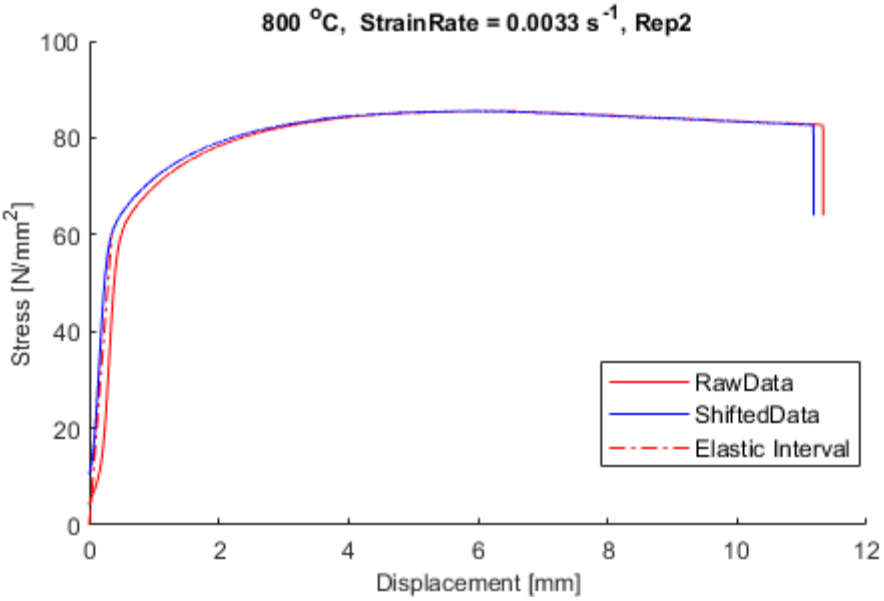
800 °C, StrainRate = 0.0033 s-1, Rep2
Stress [N/mm2]
Displacement [mm]
RawData
ShiftedData
Elastic Interval

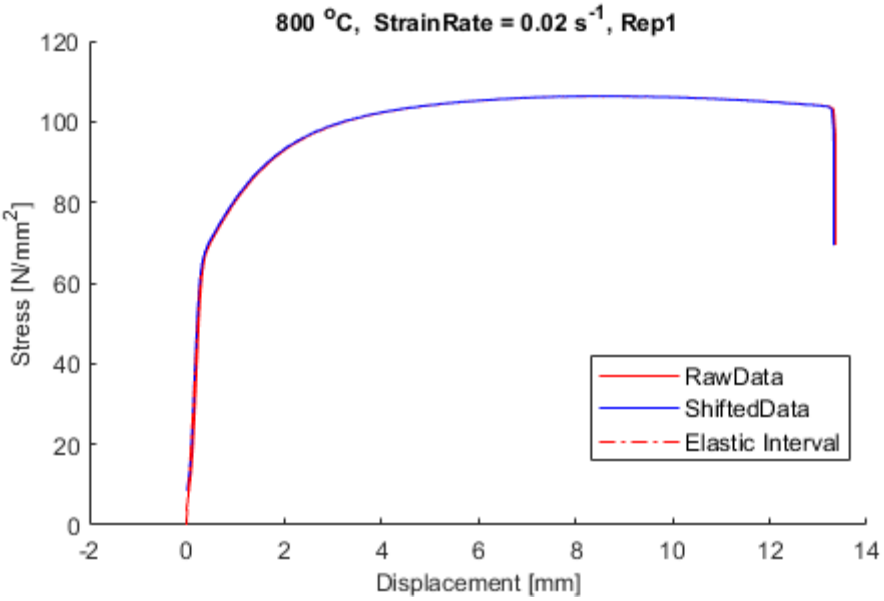
800 °C, StrainRate = 0.02 s-1, Rep1
Stress [N/mm2]
Displacement [mm]
RawData
ShiftedData
Elastic Interval

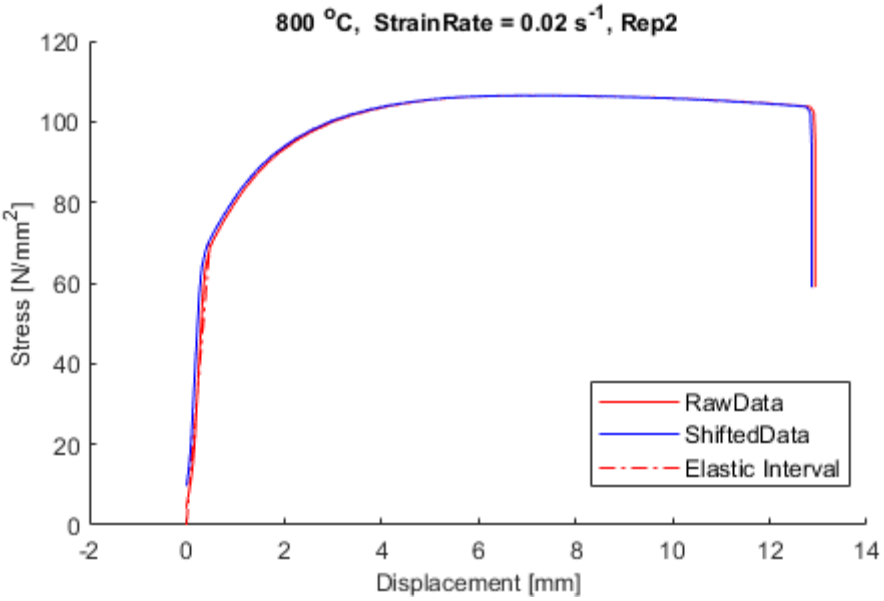
800 °C, StrainRate = 0.02 s-1, Rep2
Stress [N/mm2]
Displacement [mm]
RawData
ShiftedData
Elastic Interval

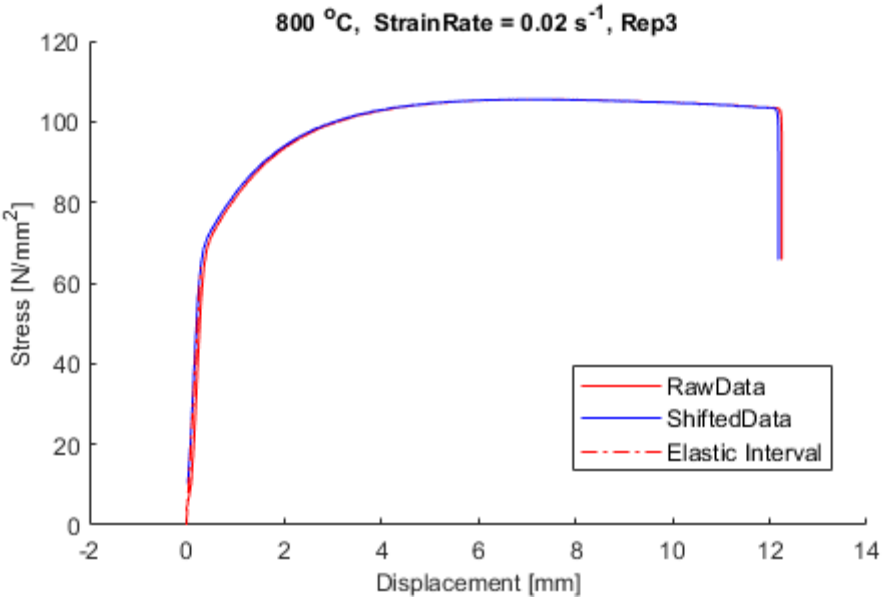

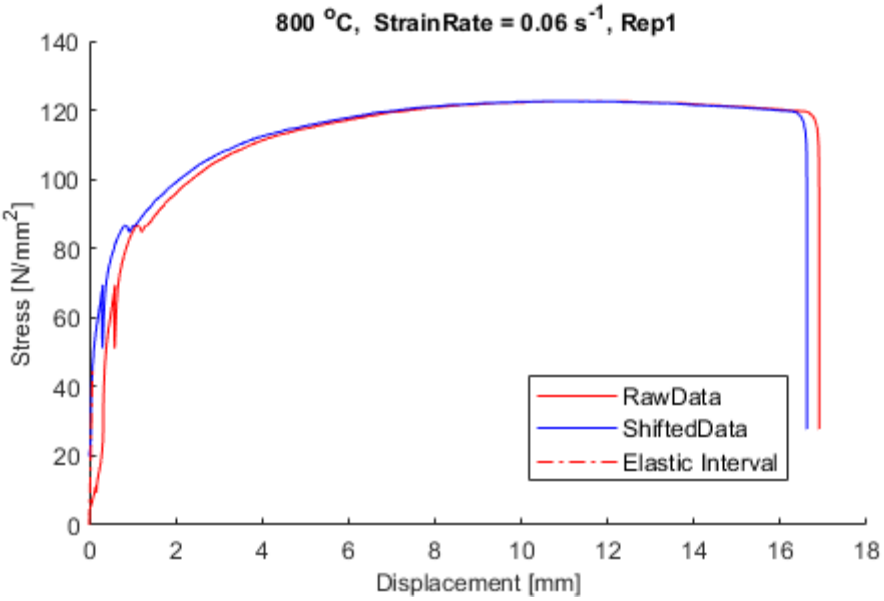

7.2 Annex B - MatLab Algorithms

Raw data treatment:

a. After the data was recorded in the laboratory, the following algorithm imports all data

b. Delete the ending part of the curve, where false values were recorded due to sudden rupture of the specimen or due to extensometer which reached its limits

c. The elastic range is computed

d. The curve is shifted in the left side, so that the sliding segment which appears at the beginning of the experiment is corrected

```
close all
clear all
clc

%% Import the Raw Data
    % matrix of results 9 (strain rates) x 9 (temperatures);
    % Each position is a vector of Structures;
    % the Structure is the experimental test, ...
    % and the vector comprises all the repetitions.
%%% The tests are arranged in folders per type of testing control mode
%%% Further tests are arranged per temperatures;
%%% Each folder contains all strain rates, and all repetitions.
%%% Lists of Folders are named "SeriesListCS.txt" and "SeriesListCD.txt"
pathdata = 'D:\UPT\Research\phD FIRE\scriere teza\Lab Data\CS - strain
control\';
fid = fopen('D:\UPT\Research\phD FIRE\scriere teza\Lab Data\CS - strain
control\SeriesListCS.txt');
SeriesList = textscan(fid,'%s');
%%% In each Temperature folder is a list of tests, named
"TestsList.txt".
for f=1:length(SeriesList{1,1})
    fid = fopen(['D:\UPT\Research\phD FIRE\scriere teza\Lab Data\CS -
strain control\',SeriesList{1,1}{f,1},'\TestsList.txt']);
    TestsList = textscan(fid,'%s %f %f %f %f %f %f %f %f %f %f'); %
'%f' for numbers and '%s' for string
    fclose(fid);
    for t=1:length(TestsList{1,1})
        i=TestsList{1,9}(t,1);
        j=TestsList{1,10}(t,1);
        k=TestsList{1,11}(t,1);
        clear RawData
        RawData                                                    =
importdata([pathdata,SeriesList{1,1}{f,1},'\',TestsList{1,1}{t,1},'.tx
t']);

Structura(i,j).Repetition(k)=struct('NameTest',TestsList{1,1}{t,1},...
```

```
            'Procedure','CS',...
            'diameter',TestsList{1,4}(t,1),... % diameter measured in
3 pct

'temperature',TestsList{1,2}(t,1),'strainRate',TestsList{1,3}(t,1),...
            'TestTime',RawData.data(:,1),...
            'NominalStrain',RawData.data(:,2),...% Nominal and Grip are
the same => NominalStrain is given by the machine
            'Strain',RawData.data(:,5)/100,...  % strain given by the
extensometer, in [-] units !!!!
            'Stress',RawData.data(:,6)); %[kN/mm2]
    end
end




%% shift the curve on the left in order to delete the starting slip

for i=1:9
    for j=1:9
        for r=1:length(Structura(i,j).Repetition)
            clear Slope Strain Stress StandardDeviation NominalStrain
            Strain=Structura(i,j).Repetition(1,r).Strain;
            Stress=Structura(i,j).Repetition(1,r).Stress;

NominalStrain=Structura(i,j).Repetition(1,r).NominalStrain;
            Temperature=Structura(i,j).Repetition(1,r).temperature;
            StrainRate=Structura(i,j).Repetition(1,r).strainRate;
            Slope=Strain./Stress;
            for k=2:length(Slope)
                StandardDeviation(k)=std(Slope(1:k));
            end
            clear x t x_ds t_ds
            ds = 10;  % Downsample factor
            dt = 1; % Time step
            ds_dt = ds*dt; % Time delta after downsampling
            t0 = 1;
            t = [1:length(StandardDeviation)];
            x = StandardDeviation;
            x(end) = min(x);
            x_ds = x(1:ds:end); % Downsample to test interpolation
            t_ds=t(1:ds:end);
```

```
            retainMAX=0;
            retainMIN=0;
            for k=(length(x_ds)-1):-1:2
                if (x_ds(k)<x_ds(k-1)) && (retainMIN==0)
                    retainMIN=t_ds(k-1);
                end
                if     (x_ds(k)>x_ds(k-1))     &&     (retainMAX==0)&&
(retainMIN>0)
                    retainMAX=t_ds(k);
                end
            end
            el_START=retainMAX;
            el_FIN=retainMIN;
            clear x

            figure
            hold on
            plot(NominalStrain,Stress,'-r')
            plot(NominalStrain(el_START),Stress(el_START),'dk');
            plot(NominalStrain(el_FIN),Stress(el_FIN),'dk');
            if (el_START>0) && (el_FIN>0)
                figure
                hold on
                plot(NominalStrain,Stress,'-r')
                clear C x y yfit yfitT P x0 Shifted
                x=NominalStrain(el_START:el_FIN);
                y=Stress(el_START:el_FIN);
                % x si y sunt coord val inregistrate in lab
                P = polyfit(x,y,1);
                CoefElastic=P;
                yfit = polyval(P,x);
                x0=-P(2)/P(1);
                if isnan(x0)
                    x0=0;
                end
                Shifted=NominalStrain-x0;

                NominalStrainShifted=Shifted(find(Shifted>=0));

Structura(i,j).Repetition(1,r).NominalStrainShifted=NominalStrainShift
ed;
                StrainShifted=Strain(find(Shifted>=0));

Structura(i,j).Repetition(1,r).StrainShifted=StrainShifted;

TestTimeShifted=Structura(i,j).Repetition(1,r).TestTime(find(Shifted>=
0));
```

```
Structura(i,j).Repetition(1,r).TestTimeShifted=TestTimeShifted;

                StressShifted=Stress(find(Shifted>=0));

Structura(i,j).Repetition(1,r).StressShifted=StressShifted;


yfitT=P(1)*NominalStrainShifted(1:length(NominalStrainShifted));


                plot(NominalStrainShifted,StressShifted,'-b');

plot(NominalStrainShifted(1:length(NominalStrainShifted)),yfitT,'-.r')

            end
        end
    end
end
       .
```

8 Bibliography

Abaqus, 2014: Analysis User's Guide, version 6.14.4. Dassault Systems Simulia Corp. (2014).

Aquino B., Jesus G., Gómez Amador A.M., Alencastre Miranda J.H., and Jiménez de Cisneros Fonfría J.J., 2021: "A Review of the T-Stub Components for the Analysis of Bolted Moment Joints" Applied Sciences 11, no. 22: 10731. https://doi.org/10.3390/app112210731.

Aspen, 2023: Surface finishing treatments [Accessed 15 Jul. 2023]. Available at: https://www.aspenfasteners.com/content/pdf/all_about_Coating.pdf

ASTM E21, 2020: Standard Test Methods for Elevated Temperature Tension Tests of Metallic Materials, 2020 Edition, September 1.

Both, I., Duma, D., Dinu, F., Dubina, D. and Zaharia, R., 2021: The influence of loading rate on the ultimate capacity of bolted T-stubs at ambient and high temperature. Fire Safety Journal, 125, p.103438.

Bull, L., Palmiere, E.J., Thackray, R.P., Burgess, I.W. and Davison, B., 2015: Tensile behaviour of galvanised grade 8.8 bolt assemblies in fire. Journal of Structural Fire Engineering, 6(3), pp.197-212.

Cod de proiectare seismică – partea I – Prevederi de proiectare pentru clădiri - indicativ p100-1/2013.

CODEC, 2012: Structural Conception and Collapse Control Performance Based Design of Multi-Story Structures under Accidental Actions, Executive Agency for Higher Education, Research, Development and Innovation Funding, Romania, 2012. PN II PCCA 55/2012.

D'Aniello, M., Cassiano, D. and Landolfo, R., 2016: Monotonic and cyclic inelastic tensile response of European preloadable gr10. 9 bolt assemblies. Journal of Constructional Steel Research, 124, pp.77-90.

Delia C.G., Faggiano B., Mazzolani F.M., 2005: On the structural effects of fire following earthquake, in: Improvement of Buildings, Taylor & Francis Group, London, UK.

DWIPUTRA, R., ANDO, S. and HIRASHIMA, T., 2016: Analytical Study on Critical Temperature of Bolted Splice Connections. Structures in Fire.

EN 1090-2, 2011: Requirements for the execution of steel structures.

EN 14399-1, 2005: High strength structural bolting for preloading Part 1: General requirements.

EN 14399-2, 2015: High-strength structural bolting assemblies for preloading Part 2: Suitability for preloading.

EN 14399-3, 2005: High-strength structural bolting assemblies for preloading Part 3: HR system.

EN 14399-4, 2005: High-strength structural bolting assemblies for preloading Part 4: HV system.

EN 1993-1-1, 2005: (English): Eurocode 3: Design of steel structures - Part 1-1: General rules and rules for buildings.

EN 1993-1-2, 2005 (English): Eurocode 3: Design of steel structures - Part 1-2: General rules - Structural fire design [Authority: The European Union Per Regulation 305/2011, Directive 98/34/EC, Directive 2004/18/EC].

EN 1993-1-5, 2005 (English):European Committee for Standardization, Eurocode 3: Design of steel structures - Part 1-5: Plated structural elements. Annex C.6. Brussels, Belgium: CEN, 2005.

EN 1993-1-8, 2005 (English): Eurocode 3: Design of steel structures - Part 1-8: Design of joints [Authority: The European Union Per Regulation 305/2011, Directive 98/34/EC, Directive 2004/18/EC].

EN 1998-1, 2004 (English): Eurocode 8: Design of structures for earthquake resistance – Part 1: General rules, seismic actions and rules for buildings [Authority: The European Union Per Regulation 305/2011, Directive 98/34/EC, Directive 2004/18/EC].

EN 20898-2, 1993: Mechanical properties of fasteners - Part 2: Nuts with special proof load values. Coarse thread (ISO 898-2: 1992).

EN IS0 4032, 2000: Hexagon nuts, style 1 - Product grades A and B (ISO 4032: 1999).

EN ISO 68, 1998: General purpose screw threads — Basic profile. Part 1: Metric screw threads.

EN ISO 6892-1, 2009: Metallic materials — Tensile testing — Part 1: Method of test at room temperature.

EN ISO 6892-2, 2011: Metallic materials — Tensile testing — Part 2: Method of test at elevated temperature.

EN ISO 888, 2012: Fasteners - Bolts and studs - Nominal lengths and thread length.

EN ISO 898-1, 1999: Mechanical properties of fasteners made of carbon steel and alloy steel Part 1: Bolts, screws and studs (ISO 898-1: 1999).

EN ISO 898-1, 2009: Mechanical properties of fasteners made of carbon steel and alloy steel. Bolts, screws and stud with specified property classes — Coarse thread and fine pitch thread.

Ene A., Stratan A., 2022: Monotonic and Cyclic Modelling of Structural Steel for Finite Element Analysis. The 13th International Conference "Innovative Technologies for Joining Advanced Materials" (TIMA 22), November 24-25, 2022, Timisoara, Romania. (accepted for publication).

Evans D.D., Walton W.D., Mowrer F.W., 1997: Progress Report on Fires Following the Northridge Earthquake, Thirtheen Meeting of the UJNR Panel on Fire Research and Safety, UJNR Panel on Fire Research and Safety.

Franssen, J.M., 2004: Numerical determination of 3D temperature fields in steel joints. Fire and materials, 28(2-4), pp.63-82.

Gadeanu L., Regep Z., Mercea Gh., 1989: Constructii Metalice 1, Institutul Politehnic "Traian Vuia", Timisoara.

Galvanizeit, 2023: http://www.galvanizeit.org/hot-dip-galvanizing [Accessed 15 Jul 2023].

Hanus, F., Zilli, G. and Franssen, J.M., 2011: Behaviour of Grade 8.8 bolts under natural fire conditions—Tests and model. Journal of Constructional Steel Research, 67(8), pp.1292-1298.

Izzuddin B.A., Vlassis A.G., Elghazouli A.Y., Nethercot D.A., 2008: Progressive collapse of multi-storey buildings due to sudden column loss — Part I: simplified assessment framework, Eng. Struct. 30 (2008) 1308–1318, https://doi.org/10.1016/j.engstruct.2007.07.011.

Jelenewicz, C., 2019: Course - History of Fire Protection Engineering, University of Maryland.

Kirby, B.R., 1995: The behaviour of high-strength grade 8.8 bolts in fire. Journal of Constructional Steel Research, 33(1-2), pp.3-38.

Kawohl, A.K. and Lange, J., 2016: Tests on 10.9 bolts under combined tension and shear. Acta Polytechnica, 56(2), pp.112-117.

Kodur, V., Kand, S. and Khaliq, W., 2012: Effect of temperature on thermal and mechanical properties of steel bolts. Journal of Materials in Civil Engineering, 24(6), pp.765-774.

Lange, J. (Prof. Dr.-Ing.) & González F. (Dr.-Ing.), 2012: Behavior of High-Strength Grade 10.9 Bolts under Fire Conditions, Structural Engineering International, 22:4, 470-475.

Lu, Y., Jiang, J., Chen, Q., Cai, W., Chen, W. and Ye, J., 2022: Fracture behavior of Grade 10.9 high-strength bolts and T-stub connections in fire. Journal of Constructional Steel Research, 199, p.107618.

MAYTEC HTO-08/1, 2023 – Manual of Utilisation: https://www.maytec-ht.de/page/products/HTO_Furnaces/HTO-08.php

MAYTEC PMA-12/V7-1, 2023: Manual of Utilisation https://www.maytec-ht.de/page/products/PMA_Measuring_devices/index.php

MatLab, 2021: MATLAB user manual. The MathWorks, Inc., Natick, MA.

Mushahary, S.K., Singh, K.D. and Jayachandran, S.A., 2022: Tensile and shear strength of 10.9 grade bolts in heating and cooling fire. Journal of Constructional Steel Research, 197, p.107503.

Pantousa D., Mistakidis E., 2016: Fire-after-earthquake Resistance of Steel Structures Using Rotational Capacity Limits. 1 10, 2016, pp. 867–891.

Riaux H., 1980 : Comportement à l'incendie des assemblages simples boulonnés. Ph.D. thesis. INSA of Rennes.

The Steel Construction Institute, 2015: Guidance Note: Protective Treatment of Fasteners. No 8.02/3.

Singla, Amneesh & Jangir, Ankit, Dinesh & Verma, 2018: Effect of Rolling and Galvanizing Process on Mechanical Properties of Mild Steel. International Journal for Research in Applied Science and Engineering Technology. Volume 6 Issue III , March 2018. 10.22214/ijraset.2018.3189.

Šmak, M., Kubíček, J., Kala, J., Podaný, K. and Vaněrek, J., 2021: The influence of hot-dip galvanizing on the mechanical properties of high-strength steels. Materials, 14(18), p.5219.

Sun R., Huang Z., Burgess I.W., 2012: Progressive collapse analysis of steel structures under fire conditions, Eng. Struct. 34 (2012) 400–413, https://doi.org/10.1016/j. engstruct.2011.10.009.

Uni-kiel.de., 2023: Cast Iron; 9.5.1 General Remarks. Available at: https://www.tf.uni-Kiel.de/matwis/amat/iss/kap_9/backbone/r9_5_1.html [Accessed 15 Jul. 2023].

Usmani, A.S., Rotter, J.M., Lamont, S., Sanad, A.M. and Gillie, M. 2001: Fundamental Principles of Structural Behavior under Thermal Effects, Fire Safety Journal, Vol. 36, Elsevier Science Ltd., p 721-744.

Wurth, 2023: https://www.wuerth-industrie.com [Accessed 15 Jul. 2023].

Zaharia R., Pintea D., 2009: Fire after earthquake analysis of steel moment resisting frames, Int J Steel Struct 9 (2009) 275–284, https://doi.org/10.1007/ BF03249501.